CHEMICAL REVIEWS

Review

Cite This: *Chem. Rev.* XXXX, XXX, XXX–XXX

pubs.acs.org/CR

Understanding Glass through Differential Scanning Calorimetry

Qiuju Zheng,[†,○] Yanfei Zhang,[†,○] Maziar Montazerian,[‡,○] Ozgur Gulbiten,[§] John C. Mauro,[†,∥] Edgar D. Zanotto,[‡] and Yuanzheng Yue*[,†,⊥,▽]

[†]School of Materials Science and Engineering, Qilu University of Technology (Shandong Academy of Sciences), Jinan 250353, China

[‡]Vitreous Materials Laboratory (LaMaV), Department of Materials Engineering (DEMa), Federal University of São Carlos (UFSCar), 13.565-905 São Carlos, SP, Brazil

[§]Science and Technology Division, Corning Incorporated, Corning, New York 14831, United States

[∥]Department of Materials Science and Engineering, The Pennsylvania State University, University Park, Pennsylvania 16802, United States

[⊥]State Key Laboratory of Silicate Materials for Architectures, Wuhan University of Technology, Wuhan 430070, China

[▽]Department of Chemistry and Bioscience, Aalborg University, DK-9220 Aalborg, Denmark

ABSTRACT: Differential scanning calorimetry (DSC) is a powerful tool to address some of the most challenging issues in glass science and technology, such as the nonequilibrium nature of the glassy state and the detailed thermodynamics and kinetics of glass-forming systems during glass transition, relaxation, rejuvenation, polyamorphic transition, and crystallization. The utility of the DSC technique spans across all glass-forming chemistries, including oxide, chalcogenide, metallic, and organic systems, as well as recently discovered metal−organic framework glass-forming systems. Here we present a comprehensive review of the many applications of DSC in glass science with focus on glass transition, relaxation, polyamorphism, and crystallization phenomena. We also emphasize recent advances in DSC characterization technology, including flash DSC and temperature-modulated DSC. This review demonstrates how DSC studies have led to a multitude of relevant advances in the understanding of glass physics, chemistry, and even technology.

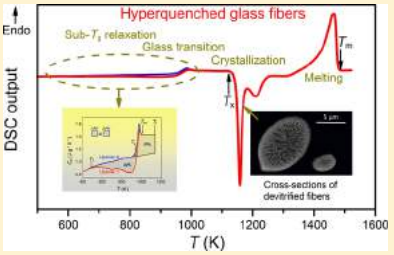

CONTENTS

Received: August 12, 2018

DOI: 10.1021/acs.chemrev.8b00510
Chem. Rev. XXXX, XXX, XXX–XXX

1. INTRODUCTION

Glass is everywhere; it is one of the most critical materials for the development of modern human civilization and is ubiquitous in our everyday lives. The oldest glasses are naturally occurring, many of which are nearly as old as the universe. Glass itself is a fascinating phase of matter, combining aspects of the liquid and solid states.[1−3] The key structural feature of any glass is its lack of the atomic long-range order (LRO) (e.g., periodic lattice arrangement over a length scale above 2 nm), in contrast to crystals, while the essential dynamic feature is the glass-to-liquid transition upon heating, during which a jump in configurational entropy occurs. Moreover, it is important to note that glass exhibits short-range order (SRO), e.g., identical interatomic arrangement within a polyhedral unit, and intermedium range order (IRO), e.g., identical interpolyhedral arrangement.

A diverse variety of glass-forming chemistries exist, having a wide range of structural building blocks from which a disordered glass network can be constructed. The detailed nature of these chemical building blocks and the manner in which they are connected depend on the particular nature of the chemical bonding in these systems. For example, traditional oxide glasses have network structures composed of tetrahedral and/or trigonal building blocks involving mixed covalent-ionic bonding. Chalcogenide glasses are built upon two-, three-, and four-coordinated building blocks, which are covalently bonded. Metallic glasses, including bulk metallic glasses (BMGs), consist mainly of icosahedral units with metallic bonding. Organic polymeric glasses are made from the cross-linked molecular chains involving covalent intramolecular bonding and van der Waals bonding between chains. The recently discovered metal−organic framework (MOF) glasses are composed of tetrahedral units with coordination bonds.[4] Water can also be quenched into a glassy state and is comprised of tetrahedral units connected via hydrogen bonds. It is these different types of bonds, resulting from the various electronic structures of the constituent atoms, that lead to different structures (short- and medium-range order) and properties in the glassy state.

Within the same family of glasses, the structure, topology, and properties also differ from one member to another, determined by the chemical composition. Some glass-forming systems, such as many silicates and polymers, are easily vitrified upon cooling, whereas others are more difficult to form glasses; for example, most metallic liquids can only be vitrified if they undergo extremely rapid quenching. This gives rise to a first important question: how can we quantify the "ease" of vitrification, i.e., the glass-forming ability (GFA), of a given system? A second equally important question is how a glass relaxes toward the supercooled liquid state and ultimately crystallizes to its thermodynamic equilibrium state. Differential scanning calorimetry (DSC) is perhaps the most useful and widely applicable of all characterization techniques for providing answers to these questions, which are of critical importance for both fundamental glass science and applied glass technology and engineering.

DSC equipment can be found in most chemical and materials science laboratories. DSC has become a universal standard tool for characterizing thermodynamic and kinetic properties, phase transitions, and property evolution in glasses. DSC is more than just a simple characterization tool: over the past two decades, it has been developed into an advanced and versatile set of techniques for many aspects of glass research. The widespread use of DSC is driven by its ultrahigh sensitivity to both small and large energy fluctuations caused by phase transitions and structural changes in glass during heating, cooling, annealing, and pressurization. With the emergence of Flash DSC (Section 2.3), the range of heating and cooling rates has been enormously broadened (up to a million degrees per second), allowing for measurements at ultrashort time scales. With the development of temperature-modulated DSC (TMDSC) (Section 2.4), scientists have been able to distinguish overlapping transitions and to detect weak and secondary transitions, due to the ability to separate the heat capacity and kinetic components of the DSC signal.

DOI: 10.1021/acs.chemrev.8b00510
Chem. Rev. XXXX, XXX, XXX−XXX

Several excellent review articles[5−7] and books[8,9] are available concerning the application of DSC in glass research. However, a comprehensive review is still lacking concerning the recent advances achieved through DSC and supplementary techniques in the study of both universal and unique thermodynamic and kinetic features of various glass families. Our motivation in the present review is, thus, to provide emphasis on glass transition, relaxation, and crystallization in different families of supercooled liquids and their corresponding glasses. In doing so, we give a comprehensive overview of the many roles of DSC in understanding the fundamental nature of glass. While many types of glasses exist, the majority of examples given in this review paper refer to oxide systems, which are by far the most important family of commercial glasses. Also, we describe the new DSC approaches that have been established over the past two decades.

Our review is structured as follows. We first briefly introduce the principles of DSC, Flash DSC, and TMDSC (Section 2) and then present a recent understanding of the calorimetric glass transition (Section 3). This new understanding originates from various studies of the effect of structure, pressure, and phase separation on the glass transition temperature (T_g) and configurational heat capacity ($C_{p,conf}$). We discuss the topological origin of the compositional trends of both T_g and liquid fragility (m), regarding the Gupta−Mauro temperature-dependent constraint model.[10] Another longstanding puzzle is how the heat capacity jump during the glass-liquid transition is linked to the IRO structure in glass. Part of the answer to this question is acquired by performing DSC and Raman spectroscopy measurements on a series of borosilicate glasses.[11] We also discuss the enhancement of the glass transition overshoot through increased pressure and include a recent finding on the rejuvenation of a metallic glass caused by nonaffine strain well below T_g. In the past two decades, some of the present authors have established new calorimetric approaches determining the fictive temperature (T_f), the cooling rate of hyperquenched or slowly quenched glasses, liquid viscosity, and liquid fragility. These approaches are reviewed in Sections 3.4 through 3.7 At the end of Section 3, we illustrate the recent understanding of polyamorphism, which is achieved by performing DSC and structural analyses on zeolites and MOFs and interpreting these results regarding the underlying potential energy landscape (PEL) of the system.[12]

In Section 4, we review recent major findings regarding the sub-T_g (below T_g) and sup-T_g (above T_g) enthalpy relaxation in glass. A variety of glasses have been used as the subjects of the present article, viz., from organic to inorganic, metallic to nonmetallic, and chalcogenide to MOF systems, including both strong and fragile glass-formers, and systems from both the bottom of the PEL (ultrastable molecular glasses) and those trapped in the upper part of PEL (e.g., hyperquenched or mechanically excited glass). Much space (Section 4.1) is allocated for describing the glass transition and the sup-T_g relaxation in thermodynamically ultrastable glasses, which are produced by molecular deposition since these glasses are one of the most significant discoveries in glass science over the last two decades.[13] In the opposite limit, the hyperquenching-annealing-DSC (HAD) approach is described to characterize the thermodynamic and structural features of glasses,[14] including highly out-of-equilibrium systems. Also, the atomic vibrational dynamics (e.g., the Boson peak) in HQ glasses during annealing can be traced using neutron scattering[15,16] or nuclear inelastic scattering[17] techniques in combination with the HAD approach. Using the HAD approach, scientists can adequately explore the primary and secondary relaxations in various families of MQ glasses or mechanically milled glasses in terms of PEL. We also discuss a calorimetric approach to identify the slow secondary relaxation, i.e., the Johari−Goldstein (JG) relaxation,[18,19] in metallic and oxide glasses. The striking differences in relaxation modes between strong and fragile systems are discussed in Section 4.2. Furthermore, the HAD approach enables monitoring of the energetic evolution of a HQ glass or a ball-milled or stretched glass well below T_g, by which the structural heterogeneity of these glasses can be reflected (Section 4.3). From there, one may also infer how the potential energy and structure of glass vary upon annealing or dynamic heating. In Section 4.4 we also describe the relationship between the anomalous relaxation behavior and the fragile-to-strong transition for some metallic glass systems.[20] Several Flash DSC studies of the glass transition and glass relaxation in ultrathin organic glassy films are reviewed in Section 5.

The recently developed TMDSC technique is reviewed in Section 6. This technique is based on the superposition of a sinusoidally varying signal on top of the usual linear heating path used in standard DSC. With TMDSC, the thermodynamic and kinetic effects can be separated through complex signal analysis. The TMDSC technique has led to the discovery of glass compositions where relaxation effects can be minimized. These so-called "intermediate phase" glasses have stirred significant controversy in the glass community. Evidence both for and against the existence of this intermediate phase will be reviewed in Section 6. The signal analysis techniques for TMDSC will also be discussed.

Nucleation, crystal growth, and overall crystallization in glass-forming supercooled (inorganic, organic, and metallic) liquids have been the subject of many studies. "Crystallization" is one of the most frequently used keywords in 200 years of glass history.[21] DSC has been extensively used as a fast, useful method to preanalyze crystallization processes, for instance, to detect good and poor glass-formers and to detect/control crystallization behavior. Furthermore, the results of DSC have been used to develop an important group of materials (glass-ceramics) via controlled crystallization of glasses. Numerous novel glass-ceramics have been commercialized for a variety of domestic, electronic, optical, dental, and biomedical applications.[22] As discussed by Davis and Zanotto, no other class of materials possesses such a valuable and unusual *combination* of properties advantageously and feasibly.[23] However, we found only a limited number of studies, reported in Section 7, dealing with the application of DSC to investigate and quantify the crystallization kinetics (e.g., nucleation and growth rates), glass-forming ability (GFA), glass stability (GS), and *liquidus* temperature (T_L) in inorganic MQ glasses. Therefore, we elaborate on the versatility and usefulness of several DSC techniques for examining this specific variety of dynamic processes spanning from nucleation to GS and GFA. We also intend to call attention to the advantages and problems related to the use of DSC and caution the reader against its "automatic" application. For example, while most DSC methods do not allow us to predict the crystallization kinetics quantitatively, some methods are beneficial for providing estimates of the temperature range where, for example, significant crystal nucleation and growth occur.

DOI: 10.1021/acs.chemrev.8b00510
Chem. Rev. XXXX, XXX, XXX−XXX

At the end of this review (Section 8), we give concluding remarks and perspectives regarding the application of DSC for glass research. As a powerful, sensitive thermochemical tool, DSC can provide profound insights into the thermodynamic and dynamic behavior of both supercooled liquids and the glassy state. Furthermore, new DSC methodology and instrumentation are being rapidly developed, particularly for use under extreme conditions. Emerging DSC approaches offer enormous potential to solve challenging problems in glass science and to contribute to understanding the intricate nature of glass. We believe that this review article will be highly beneficial for research activities and educational programs in the multidisciplinary fields of chemistry, physics, and materials sciences, particularly in glass chemistry and physics, and also to the glass and glass-ceramics industry.

2. PRINCIPLES OF DSC

DSC is the most common thermal analysis technique used for a wide range of applications, including fundamental research, development of new materials, and quality inspection in industrial production. It is an especially important characterization technique in the field of glass science and technology.[24] With DSC, a sample is scanned dynamically or held isothermally in the instrument, and the heat flow of both the sample and reference are monitored as a function of time and temperature.[25] Essentially, the calorimeter measures the heat/energy absorbed or released by the sample when it is subjected to the specific temperature path. As chemical reactions and physical transitions take place, there is an associated generation (exothermic reaction) or consumption (endothermic reaction) of heat. This process creates a heat flow that serves as the signal measured by the DSC instrument.[26]

There are two basic types of DSCs: the heat flux DSC and the power compensation DSC.[27−29] The design and measurement principles differ between these two kinds of DSC instruments. The characteristic common to both types of DSC is that the measured signal is proportional to a heat flow rate (J g^{-1} s^{-1}), Φ, which allows the time dependence of a transition to be analyzed based on the $\Phi(t)$ curve. In addition to these two standard types of DSC, we will describe the Flash DSC method, which can be operated at ultrafast scan rates. Finally, we will introduce the basic principles of TMDSC.

2.1. Heat Flux DSC

The heat flux DSC is a type of heat-exchanging calorimeter.[30] Through a well-defined heat conduction path with given thermal resistance, a defined exchange of the heat between a sample and its surroundings can be measured. The heat exchange path can be implemented in various ways, including the disk-type, the turret-type, and the cylinder-type measurement systems. Among them, the most frequently used type is the disk-type measurement system, where the heat exchange takes place via a disk that serves as a solid sample support. With this system, the DSC measurement can be conducted quickly and accurately over a wide temperature range. The heat flux DSC can generally be applied in the temperature range from −190 to 1600 °C depending on the instrument. The DSC measurements can be conducted in a certain atmosphere, e.g., in nitrogen or argon to avoid oxidation of the sample, in air or oxygen to oxidize the sample.

In the heat flux DSC with a disk-type measurement system,[31] the primary heat flows from the furnace to the sample crucible and reference crucible after passing symmetrically through a disk. The sample crucible and reference crucible are positioned on this disk symmetrical to the center, and the disk is located in the furnace chamber. The temperature sensors are integrated into the disk, which covers the area of support of sample crucible and reference crucible, respectively. The arrangement of the sample crucible and the reference crucible, as well as the temperature sensors attached to them, must be the same to reduce the uncertainty of the measurement. Following Fourier's law, the driving force (i.e., the thermodynamic affinity) for the heat flow is the difference in temperature. The heat flow into the sample itself corresponds to the difference between the flow into the sample chamber and that into the reference. Figure 1 shows the measurement cell of heat-flow DSC.

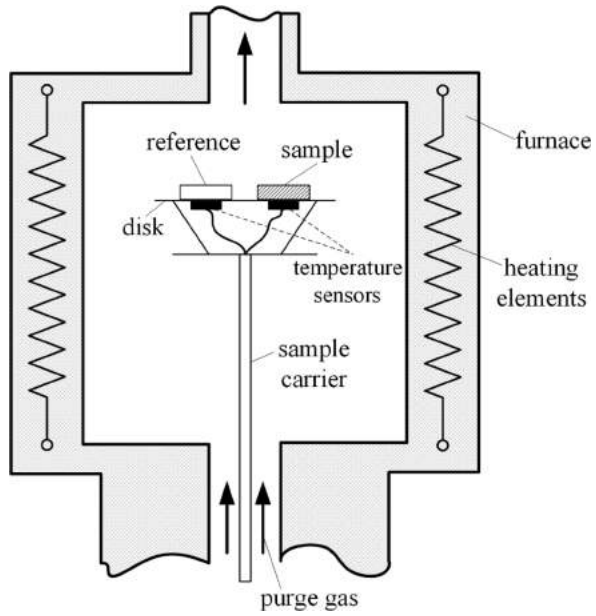

Figure 1. Schematic diagram of heat-flow DSC measurement cell.

When the furnace is heated, heat flows through the disk to the sample crucible and the reference crucible. If the sample crucible is empty, the heat flowing into the sample crucible and the reference crucible is the same. The differential temperature signal ΔT, which is usually expressed in the form of an electrical potential difference, is then zero. If any phase transition takes place in the sample, the steady-state equilibrium cannot be kept; a differential signal is generated. The signal is proportional to the difference between the heat flow rate to the sample crucible and that to the reference crucible.

Following Fourier's law, the DSC signal, Φ, the difference between the heat flow rates to the sample and the reference, is calculated by

$$\Phi = \Phi_S - \Phi_R = \frac{T_S - T_R}{R_{th}} = \frac{\Delta T}{R_{th}} \quad (1)$$

where Φ_S and Φ_R are the heat flux to the sample and reference crucibles, respectively. T_S and T_R are their respective temperatures, and R_{th} is the thermal resistance of the sensor. The temperature differences ΔT are measured by two thermocouples. By defining the sensitivity of a thermocouple S, we convert ΔT to a heat flux Φ (in W) by

DOI: 10.1021/acs.chemrev.8b00510
Chem. Rev. XXXX, XXX, XXX−XXX

$$S = \frac{V}{\Delta T}, \quad \Phi = \frac{V}{R_{th} S} \tag{2}$$

where V is the sensor signal in the thermoelectric voltage.

The caloric calibration must be done to ensure the accuracy of the DSC measurements. The heat flow rate Φ in eq 2 is the measured signal output by the DSC, and its relation with the true heat flow Φ_{true} consumed or produced by the sample must be calibrated. Caloric calibration involves the determination of the proportionality factor (K_Φ) between the measured heat flow rate Φ and the true heat flow rate $\Phi_{true,}$ as well as the proportionality factor (K_Q) between the measured exchanged heat, Q_{exch}, and the true exchanged heat, Q_{true}:[26]

$$\Phi_{true} = K_\Phi \Phi \tag{3}$$

$$Q_{true} = K_Q Q_{exch} \tag{4}$$

The calibration of K_Φ can be carried out by measuring the heat flow rate into a sample of known heat capacity C_p at a constant scan rate $q = dT/dt$.[32] The following relation is valid for the heat flow rate absorbed by the sample:

$$\Phi_{true} = C_p \cdot q \tag{5}$$

$$K_\Phi(T) = \frac{C_p(T) q}{\Phi_S(T) - \Phi_R(T)} \tag{6}$$

K_Q can be obtained by comparing the integral over a transition peak with the known heat of transition Q_{true}:[33]

$$Q_{true} = K_Q \int \{\Phi[T(t)] - \Phi_{bl}[T(t)]\}\, dt \tag{7}$$

where Φ_{bl} is the baseline signal, i.e., the heat flow rate curve measured with two empty crucibles, where no physical or chemical reaction occurs. Thus, both the heat flow rate and the transition heat can be calibrated separately.

2.2. Power Compensation DSC

The power compensated DSC is a type of heat-compensating calorimeter.[34−36] As shown in Figure 2, there are two identical microfurnaces, which are positioned inside a thermostatic chamber. The sample crucible is placed in one microfurnace, and the reference sample is in the other microfurnace. Each of the furnaces contains a temperature sensor and a heating resistor. With this setup, the sample and reference are entirely isolated from each other, and both the sample and reference crucibles have their heating element and temperature sensing element.

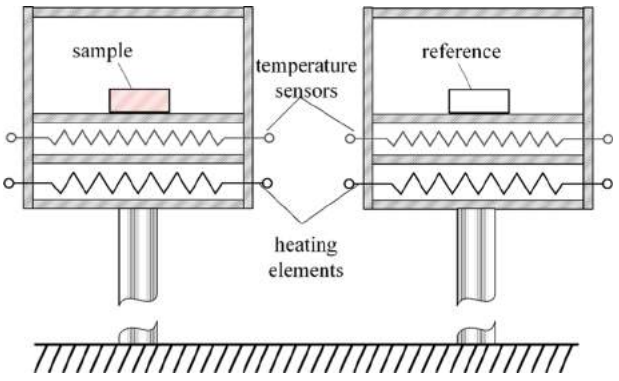

Figure 2. Schematic diagram of a power compensated DSC measurement cell.

During heat-up, the same electrical power is supplied to both microfurnaces. With the aid of separate temperature controllers, the sample and reference are heated and are always set at the same temperature. If any thermal reaction takes place on the sample, a temperature difference between the sample and reference occurs. The temperature difference is both the measured signal and the input signal of a second control circuit. The second circuit is used to compensate for the reaction heat flow rate of the sample, which is achieved by increasing or decreasing an additional heating power of the sample furnace. The compensating heating power ΔP is proportional to the remaining temperature difference ΔT. The integral of the compensating heating power corresponds to the consumed or released heat of the sample. The heating power compensation enables the microfurnace containing the sample to maintain the set temperature program and a zero-temperature difference between the sample and reference. Again, we need to convert the temperature difference ΔT measured by the thermocouple to the heat flow rate Φ. The output signal of power compensation DSC is also given as Φ. Following the relation $\Phi_{true} = K_\Phi \cdot \Phi$, K_Φ must also be determined by calibration.

Another type of DSC includes a combined heat flux and power compensation measuring system. This "hybrid system" has a pair of sensor−heater combinations on a disk. The temperature difference between the sample and reference is measured by temperature sensors and compensated by controlling the integrated heating elements. The prerequisite for short time constants and a negligible cross heat flow between the two sensor−heater elements is a good thermal coupling between the temperature sensor and its corresponding heater. This type of design combines the advantages of both the heat flux and the pure power compensation measuring system. For example, it has a stable baseline, short time constants, high resolution, low noise, and small temperature differences between the environment (furnace) and measuring system.

The operating modes of a DSC are normally divided into two types, viz., constant heating rate and varying heating rate. For the former type the temperature changes linearly with time following:

$$T(t) = T_0 + qt \tag{8}$$

where T_0 is the starting temperature and t is the time. The normal range of heating rates for a heat flux DSC could be 1 to 50 K/min (in some special case, up to 150 K/min).[26] In the isothermal mode, T_0 is constant, and q is zero.

2.3. Flash DSC

The scanning rate of a standard DSC is not sufficiently high for some studies, where physical and chemical processes occur much faster than the standard scan rate of 10 K/min. Many phenomena such as metastability, molecular reorganization, and various kinetic phenomena are difficult to probe using a standard DSC since they are easily hindered or suppressed as a result of the low scan rate. To solve these problems, ultrafast DSC instruments were invented by several research groups.[37−42] Such an instrument was often called nanocalorimetry[39] or Flash DSC.[43] The first high-speed calorimetry was developed by Pijpers et al.[37] The HyperDSC has been commercialized by PerkinElmer, which offers scan rates up to

DOI: 10.1021/acs.chemrev.8b00510
Chem. Rev. XXXX, XXX, XXX−XXX

750 K/min.[37] The advantage of the HyperDSC is that it can mimic temperature−time ramps that occur for the cooling rates used in realistic processing. Moreover, the increased sensitivity enables measurement of the signals with low heat flow rates for subtle transitions and small material mass. A further advance is the development of extremely fast-operating chip-based calorimeters, as described in refs 38 and 39. Some polymer liquids can be already vitrified by using Standard DSC and HyperDSC at a specific cooling rate.[40,41] However, other polymer liquids can be vitrified only by a chip-based fast scanning calorimeter, since it can provide much higher scan rates. In special cases, a chip-based ultrafast scanning calorimeter[42] is required to vitrify the extremely fast crystallizing glass-forming liquids.

To meet the need for fundamental research and industrial applications, the Mettler-Toledo Flash DSC 1 has been commercially developed.[43] The power compensation twin-type, chip-based fast scanning calorimeter (FSC) can be operated in a substantially broadened scan range, i.e., from very low scan rates to ultrahigh cooling and heating rates. The scan rates can reach 50,000 K/s in heating and 40,000 K/s in cooling. Thus, Flash DSC combined with the conventional DSC can cover more than 7 orders of magnitude of scan rates. The accuracy and reliability of the Flash DSC 1, e.g., concerning calibration, symmetry, repeatability, and scan rate control windows of operation, have been proven by various studies.[44,45] It should be mentioned that the temperature window for the Mettler-Toledo Flash DSC 1 is from −95 to 420 °C, suitable for research on most organic glasses and some metallic glasses. With the newly developed Mettler-Toledo Flash DSC 2+, the temperature window has been extended to a range from −95 to 1000 °C, which significantly widens the systems that can be studied concerning crystallization and melting. It is not currently possible to make an oxide glass sample ultrathin and tightly adhered to the chip of Flash DSC to get the correct signals of the enthalpy response to the ultrafast scans. However, it has been possible to achieve a submicron thick sample by blowing glass bubbles for soft extended X-ray absorption fine structure (EXAFS experiments).[46] This thin glass sample could be placed onto the surface of the sensor (i.e., sample holder) and then slightly melted to get a good contact to the sensor, so that accurate signals of the sample could be captured by the Flash DSC.

Flash DSC 1 applies a calorimeter chip with a twin sensor based on MEMS (Micro-Electro-Mechanical Systems) sensor technology.[47−51] As demonstrated in Figures 3 and 4, there are two identical thin silicon-nitride/oxide membranes on the chip, which are for the sample and reference sites. The membranes have a length of 1.6 mm and a thickness of 2 μm, which is suspended in a 300-μm thick silicon frame. The sample area of 0.5 mm is in the middle of the membrane and is coated with aluminum to ensure a homogeneous temperature profile. The sample and reference sides of the sensor each have two thermal resistance heaters. The primary heater is used to realize the general temperature program, and the other heater is used to compensate for temperature differences between the reference and the sample cell. The temperature of the sample is measured by a thermopile consisting of 8 p-type versus n-type poly silicon thermocouples, which acts as a heat sink. The thermal resistance (R_{th}) between the sample area and the surrounding is calculated by

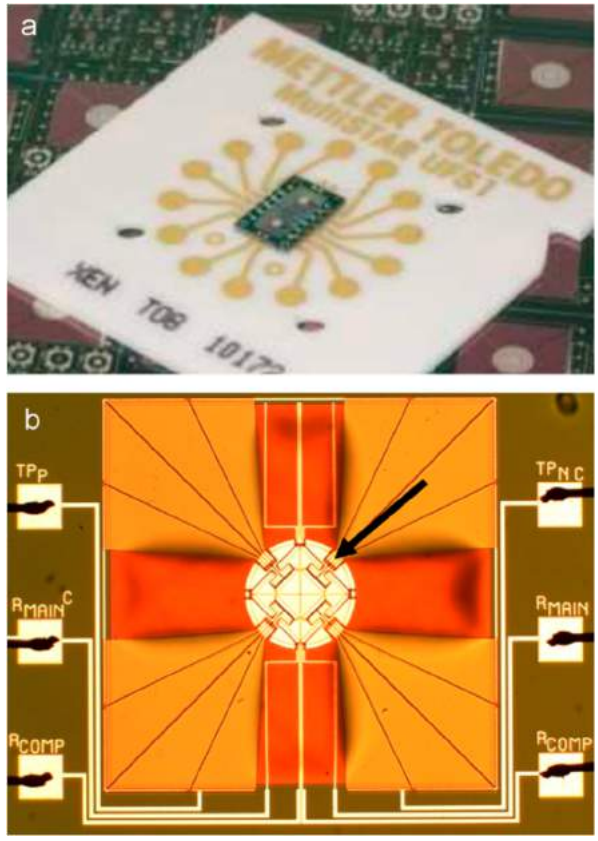

Figure 3. Photograph of device UFS1, internal design XI400: (a) device glued on a ceramic package, (b) close up of one of the two cells of the device: the heater covered with an aluminum layer in the center of the membrane makes up the sample area; the hot junctions of the 8 thermocouples (the arrow points 2 thermocouples) are inside the sample area. Reproduced with permission from ref 45. Copyright 2011 Elsevier B.V.

$$R_{th} = \frac{S_{DT}}{N'\alpha_S} \tag{9}$$

where S_{DT} is the device transfer, i.e., the ratio between the output voltage of the thermopile and the input power in the main heater resistance; N' is the number of thermocouples forming the thermopile, and α_s is the Seebeck coefficient of the thermopile.[45] For chip XI-400, the MultiSTAR UFS1 MEMS chip sensor is mounted onto a ceramic base plate, which is bonded by aluminum bonding wires. The sample is placed on and tightly connected to the membrane for the measurements. The sample mass usually is between 10 and 20 ng to 1−10 μg, and a stereo microscope is set to aid sample preparation and placement.

Dynamic power compensation is used in Flash DSC 1. Dynamic switching of the cell, to which the excess power is applied, enables the sign of the applied compensation power to be always positive.[52] This switching overcomes the drawbacks of conventional power compensation, with a reduction in noise and improvements in signal resolution and response time. With this method, the calorimetric accuracy is within 1−3% without any calorimetric calibration. The calorimeter chips need to be calibrated to quantify the relationship between the measured signals and the sample temperatures. Isothermal calibration of the main heater resistance and calibration of the thermopile sensitivity should be first conducted, and then the calibration

DOI: 10.1021/acs.chemrev.8b00510
Chem. Rev. XXXX, XXX, XXX−XXX

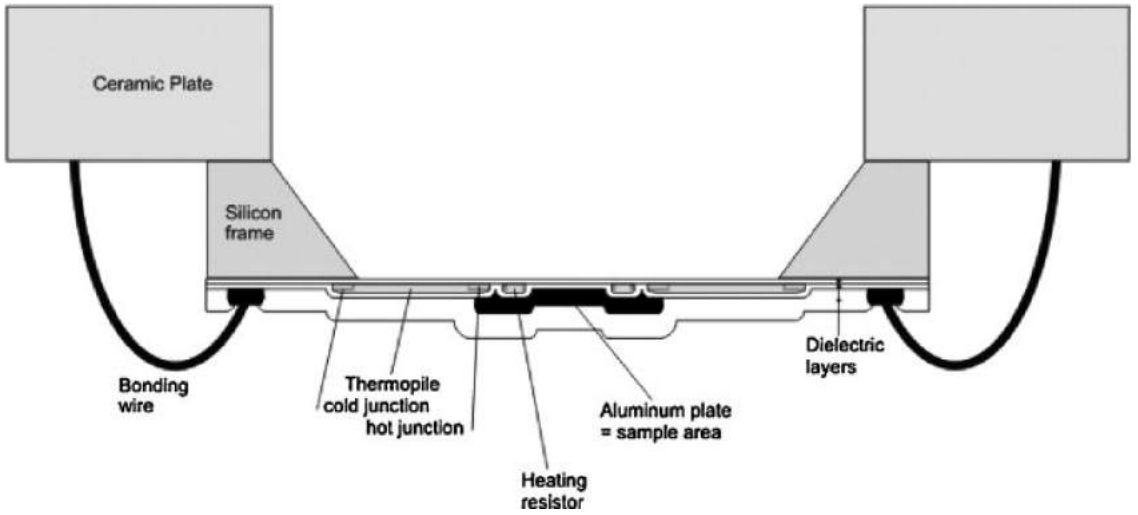

Figure 4. Schematic cross section (not to scale) of the UFS1 ceramic on the chip. Reproduced with permission from ref 44. Copyright 2011 Elsevier B.V.

accuracy is determined. A maximum temperature error of ±5 K is typically found for Flash DSC 1. In a first order approximation, the sample mass (m_s) is inversely proportional to scan rate (q) as described below:[53]

$$m_s = \frac{C(|CF|)}{|q|} \tag{10}$$

where $C(|CF|)$ is the proportionality as a function CF, the correction factor. |CF| should not be too high, to avoid high-temperature corrections, large thermal lags, and poor resolutions. Furthermore, sample masses and scan rates cannot be too low, to ensure detectable heat flow rate signals.

2.4. Temperature-Modulated DSC

DSC signals include a convolution of overlapping dynamic processes over the glass transition range. Peculiar features of supercooled glass-forming liquids such as dynamic heterogeneities lead to the complex nature of the temperature dependence of the heat capacity as a function of thermal history. However, the kinetic and thermodynamic contributions to the heat capacity cannot be deconvoluted using a conventional DSC with the standard linear heating rate. TMDSC was developed to overcome the limitations of standard DSC techniques.[54,55] In 1971, i.e., two decades before the commercialization of TMDSC, Gobrecht et al. introduced the principles of frequency dependent calorimetric measurements.[56] Birge and Nagel[57] subsequently demonstrated heat capacity spectroscopy, where the heat capacity is measured as a function of modulation frequency and temperature. Heat capacity is measured by applying a small sinusoidal temperature oscillation while the sample is held isothermally. The main idea is to use small perturbations away from equilibrium while linearity is preserved. This method provided further evidence for the definition of the glass transition as a breaking of the ergodicity[58,59] in a continuous fashion. Even though the mean temperature is constant with time, a glass transition occurs since the observation time changes inversely with the oscillation frequency. Therefore, the glass transition can be observed in any condition when the Deborah number[60] reaches unity. Following the development of frequency dependent measurements, Reading et al. introduced the first commercially available TMDSC, which involves a single frequency oscillation superimposed on a standard linear DSC heating rate.[54,61] The temperature profile of TMDSC can be shown as

$$T(t) = T_0 + qt + A_t \sin(\omega t) \tag{11}$$

where A_t and ω are the amplitude and the angular frequency of the sinusoidal oscillation, respectively. Differentiating eq 11 leads to the modulated heating rate

$$\frac{\partial T}{\partial t} = q + A_t\omega \cos(\omega t) \tag{12}$$

The system response can be defined in terms of a sinusoidal heat flow, as depicted in Figure 5. In a linearly responding material, the kinetic response is fast compared to the modulation period; that is, the two modulated functions are

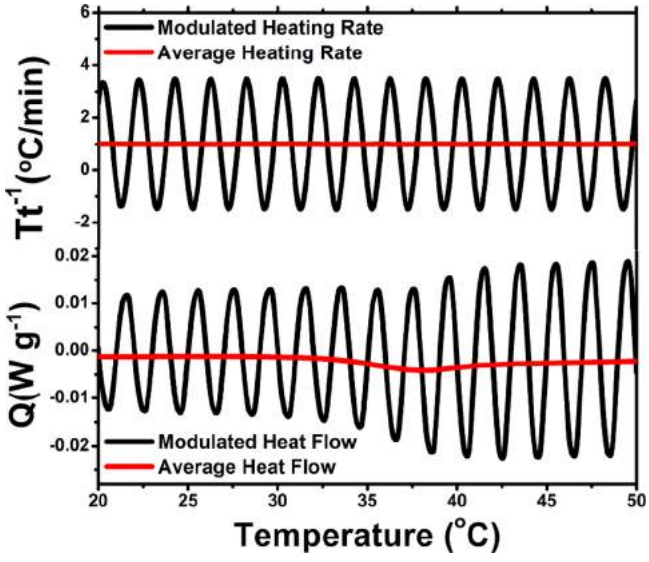

Figure 5. Modulated heating rate, Tt^{-1} (the top black curve), and the response function as modulated heat flow, Q_a (the bottom black curve), are superimposed on the temporal averages of the linear DSC heating rate (the top red curve) and linear DSC heat flow (the bottom red curve). Reproduced with permission from ref 62. Copyright 2013 AIP Publishing LLC.

DOI: 10.1021/acs.chemrev.8b00510
Chem. Rev. XXXX, XXX, XXX−XXX

in phase. In other words, they are two points moving in the complex plane with a constant angle. When a kinetic event occurs, which is on a time scale comparable to or slower than the modulation period, the phase angle between the two functions varies with the rate of the dynamic process. For instance, heat is transferred by atomic vibrations in the glass. The typical time scales of those vibrations are much shorter than the standard TMDSC oscillation periods. Therefore, the input (modulated heating rate) and output (modulated heat flow) functions are still in phase, and the phase angle is constant. In the supercooled liquid region, the heat capacity involves both vibrational and configurational contributions, and molecular motions dominate the heat flow process. The average molecular rearrangement time scale is again much shorter than the modulation period, and therefore the input and output functions are in phase. However, when the supercooled liquid approaches the glass transition region upon quenching, the structural relaxation times will drastically increase to a time scale similar to the modulation period of oscillation in the glass transition range. Hence, the phase angle between the two functions continuously changes in the vicinity of the glass transition.[62]

The phase angle can be linearly scaled with the distribution of relaxation times to investigate the dynamic processes and relaxation kinetics in glasses. The temperature sweep over the glass transition range represents the response of dynamic domains for a given observation time (or frequency) since the TMDSC technique relies on a single constant frequency. However, the same modulation can be repeated over a range of frequencies[63] to probe the frequency dependence of the heat flow (or enthalpy response) of the entire system or local domains. Stochastic methods have also been proposed[64] to investigate the frequency dependence of the enthalpy response by utilizing pulses controlled by a random number generator. A more detailed review of the interpretation of the TMDSC signals and their applications is provided in Section 6.

3. CLARIFYING GLASS TRANSITION VIA DSC

3.1. General Aspects of Glass Transition

Is glass a solid or liquid? This deceptively "simple" question is one of the longstanding mysteries of glass science and involves complex scientific consideration. Glasses appear solid on a typical human time scale, e.g., exhibiting elasticity and fracturing. This type of solid lacks LRO, in contrast to their crystalline counterparts. Also, they spontaneously relax and flow toward the supercooled liquid (SCL) state, even at low temperatures over a long time scale; such viscous flow is a liquid-state property. Also, the atomic structure of glass is noncrystalline and continuously connected to that of its parent SCL. In the limit of infinitely long time or given sufficiently long thermal treatments, glass will ultimately crystallize (i.e., become a thermodynamically stable solid). Given this combination of solid-like and liquid-like properties, glass can be considered as a special hybrid state of matter, where the solid-like properties are evident when probing its mechanical response on short time scale, but its noncrystalline structure, spontaneous relaxation, flow, and crystallization behavior make it more akin to a nonequilibrium "frozen" liquid.[65] Despite these similarities to the liquid and solid states, glasses also have unique properties that are determined by their nonequilibrium and nonergodic (frozen) nature. Based on these considerations, a new definition of glass has recently been proposed by Zanotto and Mauro: "Glass is a nonequilibrium, noncrystalline state of matter that appears solid on a short time scale but continuously relaxes towards the liquid state."[65] According to this definition, glass is a unique state of matter that combines features of both liquids and solids and also exhibits its unique characteristics. In addition to this short definition for a general audience, a more detailed scientific definition was proposed: "Glass is a nonequilibrium, noncrystalline condensed state of matter that exhibits a glass transition. The structure of glasses is similar to that of their parent SCL, and they spontaneously relax toward the SCL state. Their ultimate fate, in the limit of infinite time, is to crystallize".[65]

Glass has also been defined in other ways, e.g., "Any material that exhibits glass transition behaviour is a glass";[66] "Glass is a solid having a non-crystalline structure, which continuously converts to a liquid upon heating";[67,68] and "Glasses are disordered materials that lack the periodicity of crystals but behave mechanically like solids."[3] Regardless of the definition, all glasses share two common characteristics. First is that glasses lack long range, periodic atomic ordering; second is that glasses exhibit time-dependent glass transformation behavior in a certain temperature range, which is termed the glass transition range. The latter is the most important characteristic feature of glass. Any non-crystalline, nonequilibrium material that exhibits glass transition behavior is defined as a glass.[66]

"The deepest and most interesting unsolved problem in solid state theory is probably the theory of the nature of glass and the glass transition," as stated by Nobel Prize winner P. W. Anderson in 1995.[69] Despite substantial progress in understanding the glass transition, it remains one of the most challenging problems in condensed matter physics. The glass transition itself is the single key physical phenomenon defining the glassy state, which is of great scientific and technological importance.

Glass transition behavior is commonly described regarding enthalpy (or volume) versus temperature diagrams, as shown in Figure 6. When the temperature is above the melting point (T_m) for a pure system or *liquidus* temperature (T_L) for a multicomponent system, the liquid is in thermodynamic equilibrium. For any given composition, the *liquidus* temperature is the highest temperature of thermodynamic equilibrium between the solid and liquid phases, above which the crystals are unstable and dissolve in the liquid phase. T_L equals T_m for congruently melting compounds. The determination of T_L is described in Section 7.7. If the liquid is cooled down to T_m at a critical cooling rate (Section 7.5), it will start to undergo a first-order thermodynamic phase transition, namely, crystallization, leading to a discontinuous loss of enthalpy. However, for most glass-forming liquids, the crystallization is not the first-order thermodynamic phase transition under normal conditions (e.g., at a cooling rate above the critical rate) since it occurs in the supercooled region below T_m. Subsequent to crystallization, cooling will then follow the equilibrium path of the crystal. However, if the liquid is cooled quickly enough to avoid crystallization, a SCL is obtained. The structure of the liquid rearranges quickly to attain this metastable equilibrium state as the temperature decreases. Upon continued cooling, the relaxation time of the SCL increases at least exponentially, and the system eventually becomes frozen as the relaxation time exceeds the laboratory (observation) time. When this happens, the atoms have insufficient time to rearrange themselves to the metastable equilibrium state; that is, the

DOI: 10.1021/acs.chemrev.8b00510
Chem. Rev. XXXX, XXX, XXX−XXX

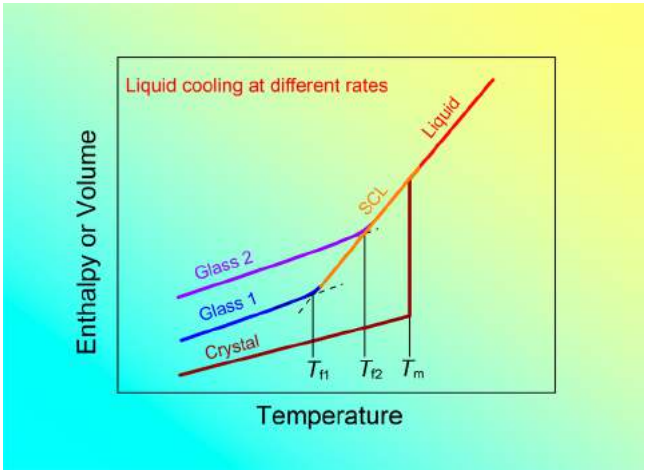

Figure 6. Schematic representation of the decrease in enthalpy/volume of an ideal one-component glass-forming liquid upon cooling. SCL: Supercooled liquid; Glass 1: transformed from SCL at a lower cooling rate, and hence, at a lower fictive temperature (T_{f1}); Glass 2: transformed at a higher fictive temperature (T_{f2}). Crystal: transformed from the liquid at the melting point (T_m) at a sufficiently low cooling rate (i.e., a critical cooling rate). The SCL−glass transition is a kinetic process, whereas the liquid-crystal transition is a thermodynamic one, i.e., a first-order transition.

structural rearrangement is kinetically arrested. As a result, the enthalpy deviates from the SCL line and follows that of the configurationally frozen system. This freezing of the system occurs continuously and results in a nonequilibrium material known as a "glass". Since the glass transition is a kinetic freezing process, the final enthalpy of glass depends on the cooling rate. When the cooling rate is high, the system has less time to relax into a lower energy structure, which leads to greater enthalpy in the final glass. This phenomenon is expressed in Figure 6, where it is seen that Glass 2 (e.g., fiberglass) has higher enthalpy or volume than Glass 1 (e.g., bulk glass), since the former is cooled more quickly than the latter. The temperature range between the equilibrium liquid and the frozen solid is defined as the "glass transition" range.[67] The temperature at the intercept between the two lines extrapolated from glassy and liquid enthalpies is the characteristic value of the glass transition, which is termed the glass transition temperature or fictive temperature (T_f). Due to its higher cooling rate, Glass 2 has a higher T_f value (T_{f2}), whereas Glass 1 has a lower value (T_{f1}). The T_f can be determined by a DSC as described in Section 3.4. Among the T_f values, there is a standard value called the standard calorimetric glass transition temperature (T_g), which is measured using a DSC at the heating rate of 10 K/min equal to the prior cooling rate (Section 3.4). T_g depends on composition, thermal history, and mechanical history. Whereas the crystallization of a liquid results in a discontinuity in extensive thermodynamic variables (e.g., volume and enthalpy), the glass transition is not a thermodynamic phase transition. A thermodynamic consequence of this kinetic transition is that configurational degrees of freedom in the glass are frozen, leading to a sharp loss in second-order thermodynamic properties such as heat capacity and thermal expansion coefficient.[70]

The glass transition is intimately connected to the notion of ergodicity. Ergodicity denotes a system where the time and ensemble averages of properties are equivalent and implies that the system explores a sufficient fraction of its configurational phase space to reach this equivalence.[59,71,72] However, a system that is initially ergodic can become nonergodic, i.e., if sufficient configurational degrees of freedom are lost.[73,74] This breakdown of ergodicity can occur either discontinuously or continuously, depending upon the details of the system. Whether or not a system is ergodic is a question of time scale. There are two relevant time scales involved when an experiment is taking place. One is the internal time scale (τ_{int}) on which the dynamics of the system occur, which is essentially a relaxation time over which a system loses "memory" of its preceding states. The other is the external time scale (τ_{ext}) on which properties are measured, which defines a measurement window over which the system is observed. The Deborah number[60] of an experiment is defined as the ratio of internal to external time scales,

$$D = \frac{\tau_{int}}{\tau_{ext}} \tag{13}$$

A large Deborah number ($D \gg 1$, $\tau_{int} \gg \tau_{ext}$) indicates that the system visits only a small subset of the available points in phase space during the external (i.e., observation) time scale. Hence, a system with a large Deborah number is nonergodic. On the contrary, a very small Deborah number ($D \gg 1$, $\tau_{int} \gg \tau_{ext}$) means that the system can explore a greater portion of phase space during the observation time, which leads to an ergodic system. Therefore, both the internal relaxation time of a system and the external observation time determine the ergodicity of the system.

Palmer[58] introduced the notion of "broken ergodicity," in which glass can be described as an ensemble of components of the phase space, where each component exhibits internal ergodicity, but transitions between components are not allowed. This breakdown of ergodicity occurs where the Deborah number of the system is near unity, i.e., $D \approx 1$. This breakdown is the most fundamental definition of the glass transition, i.e., where the internal relaxation time of a glass-forming system is equal to an external observation time scale ($t_{obs} = \tau_{system}$).[67] The transition between ergodic and nonergodic states, where $D \approx 1$ corresponds directly to the glass transition. For any realistic system, the loss of ergodicity is a gradual process; that is, the glass transition involves a continuous breakdown of ergodicity. Thus, the glass transition is fundamentally a process in which an equilibrium, ergodic liquid is gradually frozen into a nonequilibrium, nonergodic glassy state.[75] The glassy state can be observed only when the relaxation time scale of the system becomes much longer than the observation time scale; that is, the glass transition only takes place when a finite observation time is defined.

Given the above definition, what is a typical experimental observation time scale? The glass transition is defined as occurring at the temperature at which the relaxation time for the structural relaxation process reaches some critical value,[67,76−80] often taken as 100 s. The glass transition occurs over a range of temperatures, but it is convenient to define a single temperature as an indication of the onset of the glass transition range for a glass. This temperature is termed the glass transition temperature (T_g).[66,67] In most cases, T_g is determined from DSC measurements.[70,81,82] The calorimetric glass transition is characterized by "the change in heat capacity which occurs as the state of equilibrium is reestablished during warming after an initial cooling into the glassy state at a rate sufficiently high that no crystals have formed".[83] During the DSC upscan, the heat capacity of a glass increases rather

DOI: 10.1021/acs.chemrev.8b00510
Chem. Rev. XXXX, XXX, XXX−XXX

abruptly as the solid converts to the liquid, which is the enthalpy signal of the glass transition. The T_g of different glass systems can vary from below 50 K to above 1500 K.[83−89]

Another important concept is the Maxwell relation that connects the relaxation time with the shear viscosity;[90] the stress relaxation time τ is expressed in terms of viscosity and G_∞,

$$\tau(T) = \frac{\eta(T)}{G_\infty(T)} \tag{14}$$

G_∞ is the shear modulus measured at high frequency, which changes little with temperature, while both τ and η vary dramatically with temperature. The viscosity and stress relaxation time are roughly proportional since the temperature dependence of G_∞ is small. Building on the above definition and considering a typical shear modulus (in Maxwell's equation), Angell proposed an alternative definition of T_g as the temperature at which the viscosity of the supercooled liquid is equal to 10^{12} Pa s.[77] This definition was confirmed for many glass-forming systems.[81,91] At first sight, the definition is especially intriguing because it is defined for equilibrium; that is, it is a property of the supercooled liquid and does not depend on the cooling rate of the system. This is in contrast to the preceding definitions above, in which in the T_g is defined as a property of the nonequilibrium glassy state. However, this definition only holds for T_g measured at the normal heating rates of 5−20 K/min. If, instead, much lower or higher heating rates are used, the viscosity at T_g is not 10^{12} Pa s. Using Angell's definition, there is a single T_g value defined for each composition, which is not cooling rate dependent as it assumes a typical experimental relaxation time scale of 100 s.

To understand the nature of the glass transition, various theoretical models have been proposed, e.g., configurational entropy model,[92] free volume theory,[93] potential energy landscape,[94] mode-coupling theory,[95] frustration-based models,[96] the shoving model,[97] elastic model,[98] liquid fragility theory,[1] and temperature-dependent constraint theory.[99] On the one hand, these models have been applied in describing some aspects of the glass transition in different glass-forming systems from different perspectives. On the other hand, we should admit that a unified theory of glass transition has not been established.

Beyond these theoretical approaches, various experimental approaches have been developed to characterize and explain the glass transition. One of the most effective approaches is DSC, which is probably the most sensitive to the energy fluctuation during glass transition and relaxation among all the characterization approaches. The glass transition traced by DSC is termed the calorimetric glass transition, which is the focus of this section. It should be noted that to obtain a comprehensive understanding of the glass transition, DSC must be used in combination with other characterization techniques, such as dielectric spectroscopy, microscopic imaging, vibrational dynamics, and structural analysis. One of the main challenges in clarifying the origin of the calorimetric glass transition is the measurement of structural evolution during the glass transition and relaxation processes. Nevertheless, we recognize that important advances have, in recent years, been made in understanding the calorimetric glass transition. In the following section, we review these recent advances.

3.2. Calorimetric Glass Transition

3.2.1. Key Features and Parameters. The features and key parameters of the calorimetric glass transition are illustrated in Figure 7, where the changes of the isobaric heat capacity (C_p) with temperature are recorded for both the calcium metaphosphate glass during the DSC upscan (heating) and its corresponding liquid during the subsequent downscan (cooling) at the standard rate of 10 K/min.[81] Prior to this cycle of the DSC up and downscanning, the as-produced sample has undergone the first cycle of the DSC up and downscanning at 10 K/min. The onset of the glass transition during heating is defined as the standard glass transition temperature (T_g). The standard T_g value is determined as the crossing point temperature of the extrapolated C_{pg} line and the extrapolated line of the rapidly rising C_p line. This T_g value is equal to the temperature ($T_{g,infl}$) corresponding to the inflection point of the C_p drop line during cooling (see the blue filled circle in Figure 7). This standard T_g value is in coincidence with that determined by the enthalpy-matching method.[81,82,100] The glass-to-liquid transition during heating is manifested by $\Delta C_p(T_g)$, i.e., the C_p jump from glass C_p at T_g (denoted C_{pg}) to liquid C_p at the ending temperature of glass-to-liquid transition ($T_{g,end}$) (denoted C_{pl}).

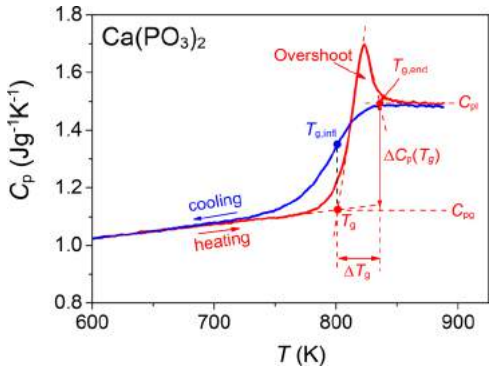

Figure 7. Temperature (T) dependences of the isobaric heat capacity (C_p) for calcium metaphosphate glass (CaP_2O_6), which were determined using DSC during the second heating−cooling cycle (rate: 10 K/min). The first scanning circle is not shown and its up and downscan rates were 10 K/min. The cooling rate of the as-produced glass sample was unknown. The glass−liquid transition during upscan is featured by the C_p jump, $\Delta C_p(T_g)$, whereas the liquid−glass transition is reflected by the C_p drop. The onset temperature of the glass−liquid transition, i.e., the intercept between the extrapolated glass C_p line and the line with the maximum tangent of the C_p rising curve, is defined as the standard glass transition temperature T_g. Reproduced with permission from ref 81. Copyright 2007 Elsevier B.V.

The width of the glass transition, ΔT_g, is the difference between $T_{g,end}$ and T_g, where $T_{g,end}$ is the offset of the glass transition, which is determined as the temperature of the intercept between the rapidly dropping line and the C_{pl} line (Figure 7). ΔT_g is inversely proportional to the liquid fragility quantified by the index $m = \mathrm{d}\log_{10}\eta/\mathrm{d}(T_g/T)_{T=Tg}$ (Section 3.6).[101] Figure 7 also shows that a C_p overshoot also occurs in the glass transition region during heating. The overshoot reflects the recovery of the enthalpy lost during annealing or cooling to that corresponding to the standard heating rate of 10 K/min.[100,102] The origin of this difference is that on the first upscan the glass starts in a much deeper minimum of the potential enthalpy surface[75] due to its higher degree of

DOI: 10.1021/acs.chemrev.8b00510
Chem. Rev. XXXX, XXX, XXX−XXX

annealing compared to the glass that is subjected to the second upscan. Theoretically, the enhancement of this overshoot is the direct consequence of the nonexponentiality and nonlinearity of the glass relaxation process.[103] The extent of the overshoot increases with a decrease of the prior cooling rate and with extending the prior annealing time around T_g.[104]

According to Angell,[77] for a typical heating rate of 5−20 K/min, T_g can be linked to the liquid viscosity of 10^{12} Pa s. This link was confirmed for oxide systems by Yue,[81,105] where the T_g was measured at the DSC upscan rate of 10 K/min, equal to the prior downscan rate. This T_g is defined as the standard calorimetric T_g as introduced in the next paragraph. T_g can also be measured by thermal expansion or relaxation time measurements.[66,67] The value of T_g for the same glass composition could be slightly different using various measurement methods, even at the same heating rate. It is known that T_g and T_f are dynamic characteristic values since each shifts to higher temperature with increasing heating rate or cooling rate.[100] In order to compare the dynamics and physical properties of different glass systems, a standard, unified approach for measuring T_g needs to be defined.

Yue compared the calorimetric glass transition temperature ($T_{g,DSC}$) directly measured by DSC at 10 K/min with the $T_{g,vis}$ indirectly determined at the viscosity of $\eta = 10^{12}$ Pa s (Figure 8).[81,105] $T_{g,DSC}$ is defined as the onset temperature of the calorimetric glass transition peak (Figure 7). As mentioned above, the C_p curve is measured at the standard upscan rate of 10 K/min (equal to the first downscan rate) during the second upscan. As shown in the inset of Figure 8, the two T_g values remarkably coincide for oxide glasses.[81,105] The agreement between $T_{g,vis}$ and $T_{g,DSC}$ measured can be used for assigning the standard T_g. This allows a direct comparison of the glass transition temperatures among different glass systems. In this article, T_g refers to the standard value unless otherwise specified.

3.2.2. Structure−Thermodynamics Relation. The connection between thermodynamic change and microstructural evolution during the glass−liquid transition is a longstanding problem. Much progress has already been made in understanding this problem.[106,107] In this section, we review some recent findings concerning the link between the configurational heat capacity at T_g ($C_{p,conf}(T_g)$) and the structure of glasses, which has been found by combining the DSC technique with Raman spectroscopy. Before doing so, we first explain the physical meaning of $C_{p,conf}$.

As is known, C_p is the sum of vibrational and configurational contributions arising from intrabasin and interbasin transitions, respectively; that is, $C_p = C_{p,vib} + C_{p,conf}$.[59,108] In the glassy state, the configuration space is partitioned into a set of metabasins with slow transitions between these metabasins due to the high activation barriers. The glassy state thus primarily contains vibrational degrees of freedom.[109] As it is heated through the glass transition region, the interbasin transitions begin to occur more frequently, and the supercooled liquid state thus contains both vibrational and configurational degrees of freedom in liquid state; that is, $C_{pl} = C_{p,vib} + C_{p,conf}$.[110−113] The vibrational component of C_p would change to a much lower extent through glass−liquid transition region compared to the configurational component, and hence, C_{pg} can be approximately regarded as the $C_{p,vib}$ component of C_{pl}, leading to the relation $C_{p,conf} \approx C_{pl} - C_{pg} = \Delta C_p$. This suggests that $C_{p,conf}$ may be indirectly obtained by measuring ΔC_p as a function of temperature through DSC. Thus, $C_{p,conf}$ is determined through

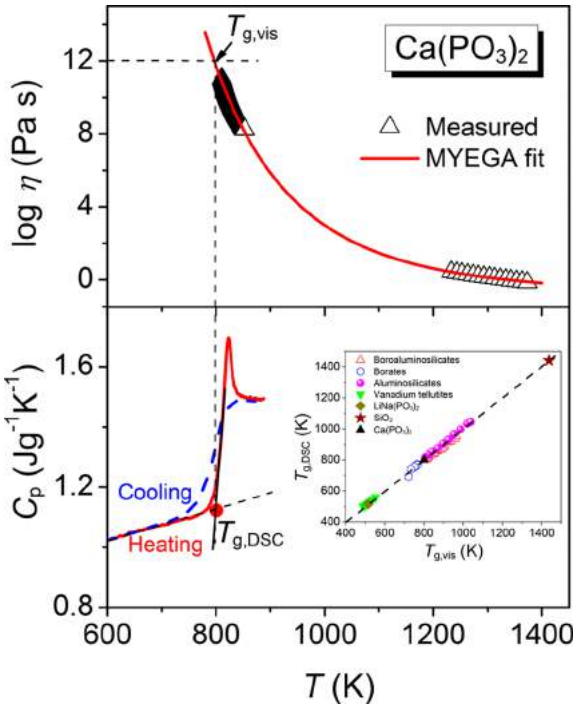

Figure 8. Correspondence between the temperature of the characteristic viscosity of 10^{12} Pa s and the calorimetric glass transition temperature (T_g) for calcium metaphosphate $Ca(PO_3)_2$. (a) The logarithm of the viscosity (log η) as a function of temperature. The solid curve was obtained by fitting the experimental data to the Mauro-Yue-Ellison-Gupta-Allan (MYEGA) equation (eq 32 in Section 3.7).[99] (b) The heat capacity (C_p) as a function of temperature. The solid red curve is the C_p curve recorded during the second upscan, whereas the dashed blue curve represents the second downscan C_p curve. Inset: Comparison between the glass transition temperatures measured by DSC at 10 K/min, $T_{g,DSC}$, and those obtained from the fit of viscosity data to the MYEGA equation[99] ($T_{g,vis}$) for oxide glasses. Reproduced with permission from refs 81, 91, and 105. Copyrights 2007, 2009, 2016 Elsevier B.V.

the relation $\Delta C_p = C_{pl} - C_{pg}$, where C_{pl} is accessible through DSC, and C_{pg} is obtained by extrapolating the C_{pg} curve to any T above T_g through a power law or a linear function (Section 3.4.1).[5,92,105] However, it should be stressed that ΔC_p deviates from $C_{p,conf}$.[112,113] In the present article, $\Delta C_p(T_g)$ and $C_{p,conf}(T_g)$ refer to the C_p jump through the glass transition region from T_g to $T_{g,end}$ (Figure 7), whereas ΔC_p and $C_{p,conf}$ represent the difference between C_{pl} and C_{pg} as a function of temperature in the entire liquid region that a DSC can access (Section 3.4.1).

As a supercooled liquid is quenched through the glass transition region, the structural degrees of freedom decrease, leading to a loss of the configurational entropy, i.e., to a drastic decrease of $C_{p,conf}(T_g)$. In a series of glasses, $C_{p,conf}(T_g)$ varies with the composition.[114] However, the structure of a glass is not sensitive enough to the dynamic slowing-down during the glass transition, so it is difficult to reveal the structural origin of the temperature dependence of $C_{p,conf}(T_g)$ during the glass transition. However, it is possible to detect the structure dependence of $C_{p,conf}(T_g)$ for a glass series with distinct structural difference and thereby to find the structural source of the change of $C_{p,conf}(T_g)$ with composition. An example for doing this is given in Figure 9, where we can see the composition dependences of both $C_{p,conf}(T_g)$ and T_g, and the

DOI: 10.1021/acs.chemrev.8b00510
Chem. Rev. XXXX, XXX, XXX−XXX

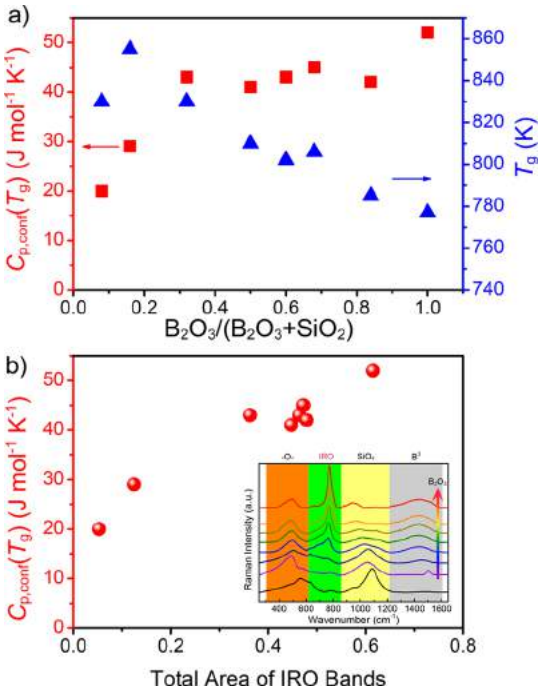

Figure 9. (a) Compositional dependence of both the configurational heat capacity $C_{p,conf}(T_g)$ and T_g for the borosilicate glass series with the composition (mol %) $(75q_r)B_2O_3-(75(1-q_r))SiO_2$-$15Na_2O$-$10CaO$, where $q_r = B_2O_3/(B_2O_3 + SiO_2)$. b) Intermediate-range order (IRO) structure dependence of $C_{p,conf}(T_g)$. The increase of the IRO structural units is indirectly expressed as that of the total area of IRO bands. Inset: Raman spectra, where the curves are shifted vertically for comparison. The colored stripes show the main bands originating from the vibration modes of different structural units. The total area of the IRO bands (see green stripe) is the algebraic sum of the area of each deconvoluted IRO band. Reproduced with permission from ref 11. Copyright 2016 the PCCP Owner Societies.

connection between the $C_{p,conf}(T_g)$ and IRO structure for the borosilicate glass series $15Na_2O$-$10CaO$-$75q_rB_2O_3$-$(75(1-q_r))$-SiO_2 (mol%), where $q_r = B_2O_3/(B_2O_3 + SiO_2)$. This glass series was chosen because it displays abundant structural features on both short and intermediate-range scales.

Figure 9a illustrates the evolution of T_g and $C_{p,conf}(T_g)$ with the substitution of B_2O_3 for SiO_2. T_g exhibits a nonmonotonic variation with composition. Specifically, initial addition of B_2O_3 leads to an increase of T_g from 830 to 855 K, while further increase in B_2O_3 results in a monotonic decrease of T_g to 777 K. It was reported that this nonmonotonic variation of T_g is mainly caused by the change of temperature dependent constraints and the short-range order structural evolution of boron.[108]

For $C_{p,conf}(T_g)$, in borate glasses, many researchers found that the boron speciation (i.e., 3- and 4-fold coordinated boron species) makes a significant contribution to the composition dependence of $C_{p,conf}(T_g)$ by using the Van't Hoff equation.[115−117] However, the boron speciation can account for only a minor change of $C_{p,conf}(T_g)$ in borate-silicate mixed glasses.[118,119] As shown in Figure 9a, $C_{p,conf}(T_g)$ exhibits a pronounced nonlinear increase with the substitution of B_2O_3 for SiO_2. Recently, it has been found that the intermediate range order (IRO) superstructures govern the major change of $C_{p,conf}(T_g)$ with the composition in the abovementioned system.[11]

The inset of Figure 9b shows Raman spectra of $15Na_2O$-$10CaO$-$75q_rB_2O_3$-$(75(1-q_r))SiO_2$ (mol%) glasses. By deconvoluting Raman spectra, various vibration modes of IRO superstructures are identified. As q_r initially increases, the B-O-Si network forms instead of boroxol rings, due to a lack of redundant B^3. Upon a further increase in the B_2O_3 content in the composition range of $0.32 < q_r < 0.84$, various IRO superstructures occur, i.e., ring- and chain-type metaborate, six-membered borate rings with 1 and 2 B^4, and boroxol rings. The two latter IRO superstructures become dominant with the further addition of B_2O_3.[11]

Based on the composition dependence of $C_{p,conf}(T_g)$ and that of IRO, the relation between IRO superstructures and $C_{p,conf}$ has been established (Figure 9b). Specifically, in the low-B_2O_3 glasses, the formation of B-O-Si network units and six-membered borate rings with B^4 (4-fold coordinated boron species) has a major contribution to the increase of $C_{p,conf}(T_g)$. As B_2O_3/SiO_2 ratio increases, the competition among disruption of metaborate groups and formation of other borate superstructures causes $C_{p,conf}(T_g)$ to be approximately unchanged. In the high-B_2O_3 glasses, the six-membered borate rings with B^4 and boroxol rings become dominant, leading to a further increase of $C_{p,conf}(T_g)$. The relation between IRO and $C_{p,conf}(T_g)$ reflects a close connection between the glass structure and the thermodynamic properties through the glass transition region, which is critical for understanding the nature of the glass transition.[11]

3.2.3. Topological Effect. T_g is mostly governed by the network connectivity and average bond strength for network glasses, and different glass systems possess different T_g values.[10,120−125] Within the same compositional family, the variation of T_g can be quantitatively determined by the variation in glass structure, which is a function of composition. Due to the nonequilibrium, noncrystalline nature of glass, it has been difficult to predict the composition dependence of T_g. While conventional atomistic modeling techniques, such as molecular dynamics, are limited by short time steps,[126,127] meta dynamic techniques have been developed to access longer time scales. Topological constraint theory has been proven to be an especially useful tool to predict the composition dependence of glass properties, as well as to provide insight into its structural and topological origins.[128−131] To reveal the nature of the calorimetric glass transition, temperature-dependent constraint theory has been successfully applied to predict the T_g values of numerous oxide glass formers. Here we briefly introduce this theory and compare the theory-predicted T_g values with those measured by DSC and thereby provide insights into the calorimetric glass transition.

Phillips and Thorpe[132,133] originally proposed treating glass as a network of bond constraints. Each atom in the glass network has three translational degrees of freedom, which can be removed by the presence of rigid bond constraints. According to their theory, the glass-forming ability is determined by comparing the number of atomic degrees of freedom with the number of constraints. While the original theory is formulated for zero temperature, Mauro and Gupta have incorporated the effect of temperature into the theory like the so-called "temperature-dependent constraint" theory. The glass properties are then quantitatively related to the number of constraints, and this enables calculation of the composition dependent on glass properties.

DOI: 10.1021/acs.chemrev.8b00510
Chem. Rev. XXXX, XXX, XXX−XXX

Based on the Adam–Gibbs theory,[92] the composition dependence of T_g is related to variations in the configurational entropy of a system. The Adam–Gibbs model considers that viscous flow is governed by cooperatively rearranging regions, and the size of these regions dictates the configurational entropy of the system. The size of the cooperatively rearranging regions is proposed to increase as the temperature of the system is lowered, requiring a greater number of atoms to flow together as thermal energy is removed from the system. According to the Adam–Gibbs model, a larger size of the cooperatively rearranging regions corresponds to a lower configurational entropy, since the total number of possible configurations decreases with decreasing temperature. More recent work by Naumis[134] linking energy landscapes with topological constraint theory has shown that the configurational entropy of a system is, in fact, largely proportional to the atomic degrees of freedom, $f(x)$, where x is the composition variable. Gupta and Mauro have combined the Adam–Gibbs model with Naumis's analysis to propose that T_g can be calculated via the following equation:[128−130]

$$\frac{T_g(x)}{T_g(x_R)} = \frac{f[T_g(x_R), (x_R)]}{f[T_g(x), x]} = \frac{d - n[T_g(x_R), (x_R)]}{d - n[T_g(x), x]} \quad (15)$$

where $d = 3$ is the dimensionality of the network and x_R is the reference composition. $n(T, x)$ is the average number of constraints per atom, which may include two-body linear, three-body angular, or higher-order constraints.[128−130] $n(T, x)$ can be calculated by averaging over all network-forming species i and each type of constraint α:

$$n(T, x) = \sum_i N_i(x) \sum_\alpha w_{i,\alpha} q_\alpha(T) \quad (16)$$

$N_i(x)$ is the mole fraction of network-forming species i, $w_{i,\alpha}$ is the number of α-type constraints associated with species i. $q_\alpha(T)$ is the temperature dependence of the constraints, which is a measure of rigidity for constraint α. In the limit of zero temperature, all constraints are fully rigid ($q_\alpha = 1$) since there is no thermal energy available to break a constraint. In contrast, constraints are easily broken in the limit of infinite temperature ($q_\alpha = 0$), i.e.

$$\lim_{T\to 0} q_\alpha(T) = 1 \quad \text{and} \quad \lim_{T\to \infty} q_\alpha(T) = 0 \quad (17)$$

At a finite temperature, some fraction of the constraints are broken while others are rigid. The temperature dependence of rigidity, $q_\alpha(T)$, can be expressed as either a continuous or discrete function. The discrete form of q_α is particularly useful for calculating the composition dependent on T_g since an analytical form for $T_g(x)$ can often be obtained.[128−130]

Temperature-dependent constraint theory has been applied to predict the T_g of various series of glass systems.[108,120,128,129,135,136] Here we consider a series of soda lime borate glasses as an example.[120] The borate glasses have been a particularly challenging system to predict properties due to the "boron anomaly". Four network-forming species (B^4, B^3, O, M^{NB}) and the associated constraints as a function of the composition are calculated based on Gupta's random pair model.[120] Then, the constraint onset temperature of each constraint is determined, and different constraints are ranked according to their relative bond strengths. The corresponding number of atomic degrees of freedom is determined according to the constraint counting. Finally, the analytical formulas are applied to calculate the composition dependence of T_g. As shown in Figure 10, the T_g calculated using the constraint model agrees with the experimental T_g values determined by DSC.[120,121]

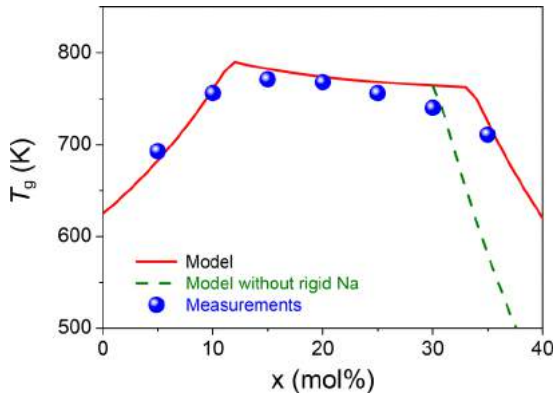

Figure 10. Comparison between the T_g values predicted by the topological constraint theory (red solid line) and those measured by DSC (blue filled spheres) for the glass composition (mol%): xNa$_2$O–10CaO–(89–x)B$_2$O$_3$–1Fe$_2$O$_3$). The changing trend of T_g with the Na$_2$O content (x), is indicated by the red solid line: both the constraints per network forming ions and the two rigid μ constraints per NBO-forming Na were considered during the topological prediction. Dashed line: the modifier constraints were not considered. Reproduced with permission from ref 120. Copyright 2010 American Chemical Society.

In addition to quantitative predictions of glass properties, topological constraint theory can also be used to explain the structural and topological origins of the property variations. For example, boroaluminosilicate glasses form the basis of many commercial glasses and have a wide variety of applications.[137,138] However, the structure and properties of such mixed network glasses are complicated due to the mixed network former effect, which yields nonlinear variation in several macroscopic properties.[139−142] Zheng et al. have studied the glass transition behavior of a series of sodium boroaluminosilicate glasses from peralkaline to peraluminous compositions by substituting Al_2O_3 for SiO_2.[10,143] The T_g values of the glasses determined by DSC and the composition dependence of T_g are displayed in Figure 11. A clear trend is seen in the inset: T_g increases with increasing the difference value of [Al_2O_3]–[Na_2O], but it increases faster in the peraluminous regime compared to the peralkaline regime.

Through multinuclear magnetic resonance spectroscopy, it was found that there were three structural roles of sodium, including charging compensation for Al^{IV}, converting boron from trigonal to tetrahedral coordination, and forming nonbridging oxygens, with competition among these three roles.[10] In the peralkaline regime, with the increase of [Al_2O_3], the concentration of Al^{IV} increases while the concentrations of NBOs and B^{IV} decrease. In the peraluminous regime, the concentration of Al^{V} increases with increasing [Al_2O_3], and there are essentially no B^{IV} or NBOs on silicon or boron.[143] The structural dependence of T_g can be explained based on the concept of topological constraints. In terms of constraint theory, T_g increases with the average number of network constraints per atom.[129,130] In the peralkaline regime, the decreased number of NBOs enhances the network connectivity, and the increased number of constraints with

DOI: 10.1021/acs.chemrev.8b00510
Chem. Rev. XXXX, XXX, XXX–XXX

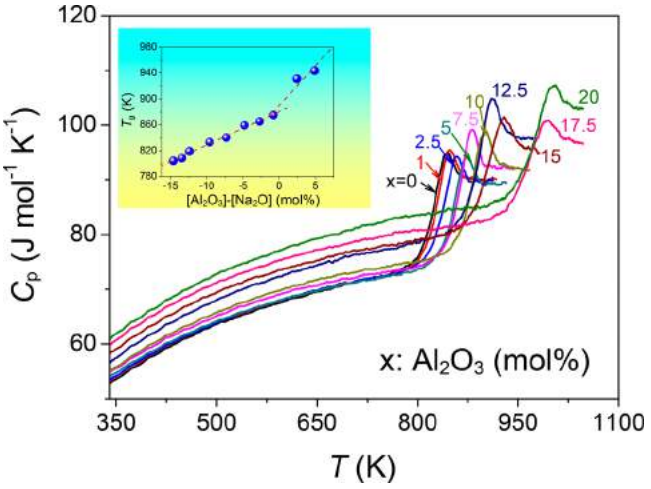

Figure 11. Impact of the substituted amount of Al_2O_3 for SiO_2 on the glass transition in the glasses with designed compositions (mol%) of $15Na_2O{\cdot}5B_2O_3{\cdot}xAl_2O_3{\cdot}(80-x)SiO_2$, where x = 0 to 20, as determined by DSC at the upscan rate of 10 K/min subsequent to a cooling rate of 10 K/min. The plot is shown as the isobaric heat capacity (C_p) against temperature (T). The measured compositions are given in ref 10. Inset: Composition dependence of T_g. The dashed lines are linear fits to the data in the $[Al_2O_3]-[Na_2O] < 0$ and $[Al_2O_3]-[Na_2O] > 0$ regimes. Reproduced with permission from ref 10. Copyright 2012 Elsevier B.V.

increasing $[Al_2O_3]$ leads to the increase of T_g. In the peraluminous regime, the five-coordinated aluminum contributes more constraints than four-coordinated silicon, which results in a higher value of T_g.[10,143]

Furthermore, to more accurately predict the dynamic properties of multicomponent glasses using temperature-dependent constraint models, additional topological factors must be taken into account. Here we mention some recent studies for improving the predictive ability of the topological constraint approach. First, Hermansen et al. proposed a temperature-dependent constraint model of alkali phosphate glasses considering the structural and topological role of the modifying ion subnetwork constituted by alkali ions and their nonbonding oxygen coordination spheres.[144] Second, they developed a topological model for binary phosphate glasses that builds on the previously introduced concepts of the modifying ion subnetwork and the strength of modifier constraints.[135] Third, Rodrigues and Wondraczek introduced cationic constraint effects into the theory.[145] In addition, it should be mentioned that other glassy dynamic properties (e.g., liquid fragility) can also be predicted by the topological temperature-dependent constraint theory. Interested readers are referred to several recent original papers[146,147] and review articles.[148,149]

In summary, the topological constraint approach is not yet fully developed, but it is capable of achieving the same results as can be obtained through DSC, e.g., determining dynamic properties (e.g., T_g and m) for several families of network glasses.

3.3. Mechanical and Thermal Effects

3.3.1. Pressure. Pressure and pressure history have a profound impact on the characteristics of the glass transition (including the C_p overshoot, and the T_f). Hence, the control of pressure history provides another avenue for understanding the nature of glass transition and designing novel materials with unique properties. The application of pressure can induce substantial structural changes in glass-forming systems, leading to changes in its vibrational density of states and macroscopic properties.[150−154] These effects can be illustrated with the simple $25Na_2O$-$10CaO$-$65\ B_2O_3$ (mol%) system, where pressure has a profound impact on both structure and physical properties.[155] Nuclear magnetic resonance (NMR) spectroscopy and DSC were two of the primary characterization tools for such study.

Figure 12a shows an enhancement of the C_p overshoot at temperatures above T_g as the isostatic pressure (p) increases. This overshoot is indicative of the nonexponentiality of the relaxation process,[102] i.e., a broadening of the relaxation time distribution. Hence, subjecting the glass to high hydrostatic pressure forces the glass into a deeper part of the enthalpy

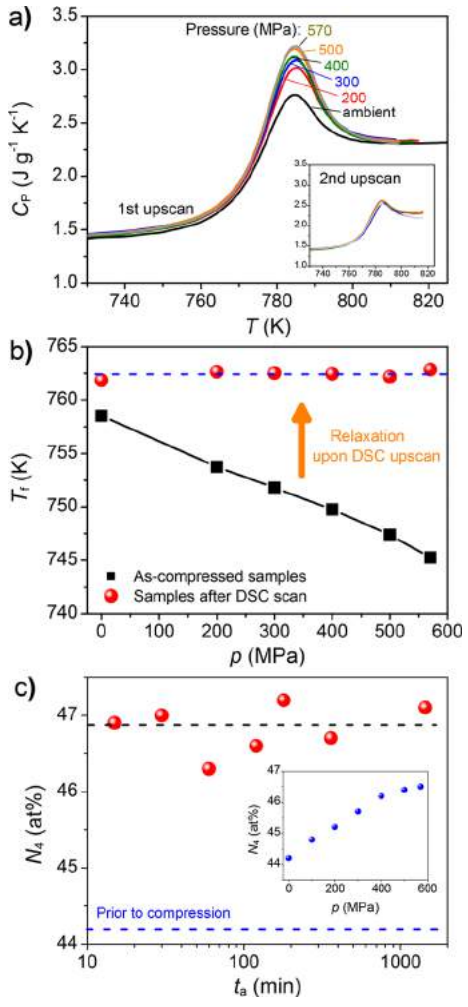

Figure 12. Isostatic pressure (p) effect on the glass transition for a $25Na_2O-10CaO-65\ B_2O_3$(mol%) glass. (a) Enhancement of the C_p overshoot of the glass transition with an increased p, which was applied to the samples during annealing at $0.9T_g$ and cooling prior to the first DSC upscans. The first and second DSC up and downscans were performed at 10 K/min at ambient pressure. Inset: C_p curves for the second DSC upscans at 10 K/min. (b) Fictive temperatures (T_f) as a function of p, which are determined from both the first and second DSC upscan, respectively. (c) Evolution of fraction of tetrahedral to total boron (N_4) with annealing duration. Inset: impact of isostatic pressure on N_4 in the absence of annealing. Reproduced with permission from ref 155. Copyright 2014 Macmillan Publishers Limited.

DOI: 10.1021/acs.chemrev.8b00510
Chem. Rev. XXXX, XXX, XXX−XXX

landscape compared to the system at ambient pressure. Note, however, that the enthalpy landscape itself is changing as a function of pressure. Consistent with prior work,[151,156] an increase in pressure enhances the nonexponentiality of the enthalpy relaxation process. Increasing pressure densifies the system, increasing the connectivity of the glass network due to BO_3−BO_4 conversion. As the glass is subsequently heated through the transition region, the systems compressed at higher pressure exhibit a greater jump in configurational entropy during the approach to equilibrium. This effect is shown in Figure 12b, where the pressure dependence of T_f is plotted. Changes in the IRO structure may also be playing an important role during the pressurization process.[157]

3.3.2. Non-Affine Strain. Recently, it was demonstrated that melt-quenched metallic glasses could be energetically excited, i.e., rejuvenated by thermal cycling in the temperature range well below room temperature (RT).[158,159] This rejuvenation is opposite to structural relaxation, and the latter occurs toward states of higher density and lower enthalpy (Section 3.4.3). In this case, the thermal cycling leads to non-affine strains (homogeneous stains) in metallic glasses, which enhance the structural heterogeneity and hence cause the excitation of potential energy in glasses. This is the so-called "non-affine strain effect," which can be quantified by DSC as shown in Figure 13. The effect is found to greatly increase the plasticity of melt-quenched metallic glasses, which is a crucial mechanical property for their engineering applications.

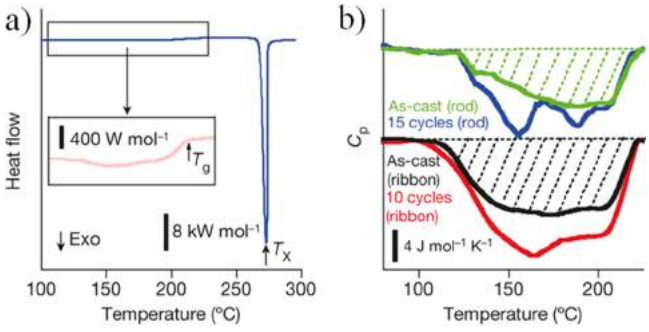

Figure 13. DSC traces of melt-spun ribbons of $La_{55}Ni_{20}Al_{25}$ and bulk rods of $La_{55}Ni_{10}Al_{35}$ metallic glasses. (a) Heat flow (in arbitrary unit) for the ribbon during heating, where a broad exothermic enthalpy relaxation is seen before T_g. (b) C_p curves showing the excitation of potential energy induced by room temperature to 77 K thermal cycling, i.e., rejuvenation. Shaded area: the released enthalpy (ΔH_{rel}) of as-produced glasses, which is obtained by integrating the difference of successive traces of C_p over the temperature range of the exotherms. The ΔH_{rel} areas of the rejuvenated glasses are shown, which are larger than those of the as-produced glasses. In both a and b, vertical bars give units and scales for the y axis. Reproduced with permission from ref 158. Copyright 2015 Macmillan Publishers Limited.

Figure 13a shows a typical DSC upscan of the melt-spun ribbon glass of $La_{55}Ni_{20}Al_{25}$, where a broad sub-T_g relaxation peak is seen prior to the glass transition and the subsequent crystallization. The enthalpies of relaxation (ΔH_{rel}) in both rod and ribbon samples were calculated from the corresponding heat capacity curves, as illustrated by the shaded areas in Figure 13b. Interestingly, a considerable increase in ΔH_{rel}, i.e., rejuvenation, was observed for both the rod and the ribbon samples after they underwent 15 and 10 cycles of thermal cycling, respectively, between RT (293K) and liquid-nitrogen temperature (77 K). For melt-spun ribbons, ΔH_{rel} reaches a maximum at ∼10 cycles, whereas, for bulk glass, ΔH_{rel} is smaller and approaches the maximum after ∼15 cycles. In each case, the maximum increase of ΔH_{rel} is ∼50% relative to the as-cast sample.

3.3.3. Liquid−Liquid Phase Separation. Some glass-forming systems contain multiple glassy phases that exhibit different glass transition responses. To identify these multiple glass transitions, DSC may be used as a sensitive method, while other advanced characterization techniques such as transmission electron microscopy (TEM), electron diffraction, and X-ray diffraction (XRD) can be used to detect the chemical identity of those phases. To demonstrate the effect of phase separation on the glass transition, here we take the fluoroaluminosilicate Fuji G338 ionomer glass system used as an example. The G338 glass is used as the glassy powder component of glass ionomer cement (GIC) in dental applications. In two recent studies,[160,161] both the as-received G338 glass and the heat-treated G338 glass were characterized using DSC and XRD. As shown in Figure 14, three glass

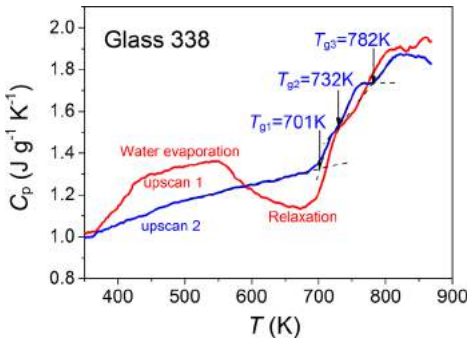

Figure 14. DSC upscan curves for both fresh G338 glass (red) and the glass subjected to upscan 1 (blue). Red curve: water-loss endothermic response followed by an exothermic enthalpy-release response, and then by triple glass transition responses. Blue curve: revealing three glass transitions represented by T_{g1}, T_{g2}, and T_{g3}, which are associated with three glass phases GP1, GP2, and GP3, respectively. Reproduced with permission from ref 160. Copyright 2015 Macmillan Publishers Limited.

transitions were identified in the as-received G338 glass from DSC upscan curve 2, implying the coexistence of three noncrystalline phases. To determine the chemical identity of the three phases, XRD analyses were conducted on samples subjected to dynamic heating, while further DSC and XRD analyses were performed on samples subjected to isothermal treatment. The results suggest that the three noncrystalline phases in G388 are Ca/Na-Al-Si-O, Ca-Al-F, and Ca-P-O-F phases, respectively. However, the exact chemical compositions of the three phases are hard to be acquired. The results shown in Figure 14 are important for understanding the impact of phase separation within ionomer glasses on the glass transition and on setting behavior of GIC by optimizing the glass production conditions.

3.4. Determination of Fictive Temperature

The fictive temperature (T_f) of a glass is a crucial parameter to describe its thermal history and a measure of the estimated average level of its corresponding liquid on the potential energy landscape. The accurate determination of T_f is critical to study the glass transition and glass relaxation and to control glass production processes. Here we review the enthalpic

DOI: 10.1021/acs.chemrev.8b00510
Chem. Rev. XXXX, XXX, XXX−XXX

approaches based on DSC measurements to determine T_f for slowly cooled glasses[82] and hyperquenched glasses,[162] and we introduce a combined approach to determine T_f of a glass with arbitrary thermal history.[100]

The properties of glass-forming systems depend not only on temperature and composition but also on thermal history. At temperatures above the glass transition range, the system is in a stable or metastable equilibrium state. As the system is cooled through the glass transition regime, the liquid is gradually frozen into a nonequilibrium glassy state. The nonequilibrium properties of the glass are of great importance and are generally considered to be a function of both the physical temperature T and the fictive temperature T_f.[163] The description of the nonequilibrium glassy state by means of T_f has drawn significant attention for several decades. There are various definitions of T_f used in the literature. The concept of fictive temperature was originally conceived by Tool and Eichlin,[164] who proposed a description of glass in terms of an equivalent equilibrium liquid state at a fictive temperature. This makes it possible to investigate complex glassy problems in terms of their corresponding equilibrium state. Nevertheless, based on his pioneering crossover experiments, Ritland[165] found that the glassy state cannot be described using just a single fictive temperature. To overcome this problem, Narayanaswamy[166] has introduced multiple fictive temperatures in his phenomenological model of glass relaxation, and his approach "indicates that any nonequilibrium state is actually a mixture of several equilibrium states." However, Mauro et al.,[167] based on the enthalpy landscape approach and nonequilibrium statistical mechanics, have proved that the configurational space distribution of the nonequilibrium glassy state cannot be described in terms of a mixture of equilibrium liquid states.

Moynihan et al.[168] stated that the values of fictive temperature calculated from different properties are not necessarily identical. Against the structural interpretation of fictive temperature using a macroscopic, property-based interpretation, he defined T_f as "simply the structural contribution to the value of the macroscopic property of interest expressed in temperature units.".[6] Instead of considering fictive temperature in terms of a mapping of the glass structure to an equivalent equilibrium structure, this definition bypasses the microscopic physics of the glass and is the definition that will be now be adopted, with T_f being determined by enthalpy. In other words, the fictive temperature is defined as the temperature at which the configurational enthalpy of the glass equals that of the corresponding liquid state.[167] T_f is a parameter to account for the thermal history dependence of glass structure and properties. The cooling rate and pressure are major factors in determining T_f of a glass-forming liquid. The DSC approach is usually used to determine T_f. In the following sections, we review the well-established methods for determining T_f for slowly cooled glasses[82] and hyperquenched glasses.[162] Moreover, a unified approach to determine T_f of a glass with arbitrary thermal history has been introduced.[100]

3.4.1. Slowly Cooled and Aged Glasses. Moynihan et al.[82] proposed an area-matching (i.e., enthalpy-matching) method for determining the fictive temperature (T_f) of slowly cooled glasses using DSC. This approach is based on C_p measurement of the glass as illustrated in Figure 15.

Figure 15 shows that after cooling at the standard rate of 10 K/min, the basaltic glass is reheated at 10 K/min to a temperature above the glass transition region to get the C_p upscan curve. The T_f value of the 10 K/min cooled glass can be calculated based on this C_p curve using the following equation:

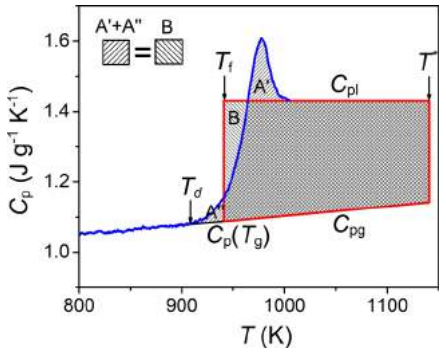

Figure 15. Heat capacity as a function of temperature for a basaltic glass determined at a heating rate of 10 K/min following a cooling rate of 10 K/min through the transition region. Replotted with permission from ref 162. Copyright 2002 Elsevier B.V.

$$\int_{T_f}^{T^*} (C_{pl} - C_{pg})\, dT = \int_{T_d}^{T^*} (C_p - C_{pg})\, dT \quad (18)$$

where C_{pg} is the glass heat capacity obtained by extrapolating the heat capacity below the glass transition, C_{pl} is the equilibrium liquid heat capacity, T' is the temperature at which C_p begins to deviate from C_{pg} and enters the glass transition region, and T^* is any temperature above the glass transition region. The T_f value derived in Figure 15 coincides with the standard onset glass transition temperature T_g (corresponding to the viscosity of 10^{12} Pa s shown in Figure 8). Furthermore, the area-matching method can be applied to determine the T_f values of any glasses that are cooled at a rate of $\leq$10 K/min.

Moynihan[6,169] found that when the prior cooling (q_c) and reheating rates (q_h) are the same, the T_f obtained using the area-matching method from the C_p reheating curve is very close to the onset glass transition temperature, $T_{g,onset}$. $T_{g,onset}$ is defined as the temperature at the intersection point between the extrapolated straight line of the glass C_p curve and the tangent line at the inflection point of the sharp rising C_p curve. Thus, $T_{g,onset}$ can be regarded as the T_f value calculated by the area-matching method, when the reheating rates are equal to the preceding cooling rates.

3.4.2. Fast-Quenched and Hyperquenched Glasses. However, when the prior cooling rate of a glass is higher than the subsequent reheating rate (typically 10 or 20 K/min), its T_f should be determined using another approach described in ref 162 (Figure 16). In other words, the approach illustrated in Figure 15 is not applicable to the T_f determination of fast-quenched and hyperquenched (HQ) glasses by a conventional DSC. Hyperquenched glasses here refer to the glasses that are cooled at an ultrafast rate, e.g., >10^5 K/s.[14,162,170−176] Moynihan's approach cannot be used to determine T_f of hyperquenched glasses.[82] His method requires that the DSC reheating rate should be the same as or higher than the cooling rate of the originally formed glass. In particular, it is not possible for a conventional DSC to reach a high scan rate comparable to hyperquenching rates (Section 3.4.2). In this circumstance, Yue et al.[162] and Velikov et al.[176] proposed a simple energy-matching method to determine the T_f value of a hyperquenched glass. According to Yue et al.,[162] hyper-

DOI: 10.1021/acs.chemrev.8b00510
Chem. Rev. XXXX, XXX, XXX−XXX

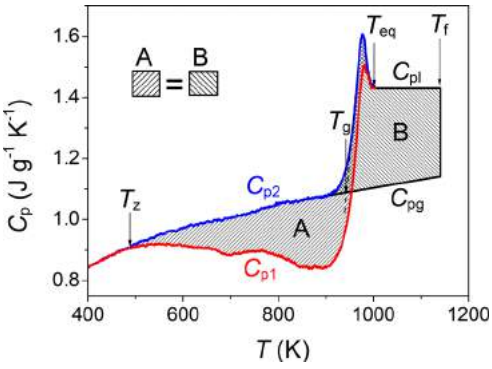

Figure 16. Determination of the fictive temperature (T_f) of a hyperquenched glass (stone wool glass fibers) by using the energy-matching method. The heating and cooling rates in the DSC measurements were 0.167 K/s. Replotted with permission from ref 162. Copyright 2002 Elsevier B.V.

quenching was achieved by a stone wool fiber spinning process. The fresh fibers were subjected to a DSC upscan at 10 K/min, which was followed by 10 K/min cooling downscan. Afterward, a second DSC upscan was performed on this relaxed glass using the same scan rate as the previous cooling. The T_f of the fibers can be calculated using the following equation:

$$\int_{T_c}^{T_{eq}} (C_{p2} - C_{p1})\, dT = \int_{T_g}^{T_f} (C_{pl} - C_{pg})\, dT \quad (19)$$

On the left-hand side of the equation, C_{p1} and C_{p2} are the heat capacity curves obtained from the first and second DSC upscans. The C_{p1} curve reflects the thermal history of the fibers experienced during hyperquenching, while the C_{p2} curve reflects the thermal history of the fibers determined by 10 K/min. The difference between C_{p2} and C_{p1} equals the enthalpy released during the entire DSC heating process. The release of enthalpy starts from T_c and ends at the temperature T_{eq} where $C_{p2} = C_{p1}$. The released enthalpy can be treated as the excess energy stored in the glass due to hyperquenching, which can be calculated by the integration of the difference between C_{p2} and C_{p1} curves from the onset temperature of the energy release (T_z) to the offset temperature of the glass transition, i.e., the starting temperature of the equilibrium liquid (T_{eq}). This released energy corresponds to the difference in the energy of the system's changing microstate as it explores its potential energy landscape.[171,172] It is also equal to the energy calculated by the integration of the difference between the liquid and glass heat capacities, $C_{pl} - C_{pg}$, from T_g to T_f, which is the right-hand side of eq 19. This correlation yields the thermodynamic basis on which the area A can match the area B in Figure 16. T_f is determined to be 1155 K by the right borderline of area B.[173]

3.4.3. Unified Approach. Theoretically, Yue's method of determining fictive temperature can be applied to any fast-cooled glass.[162] However, this approach breaks down for glasses having a fictive temperature T_f lower than T_{eq} (the onset temperature of the liquid equilibrium). That is because the integration of the right and left sides of eq 19 is not interchangeable in this case. Moreover, the reheating rate of the second DSC upscan must be equal to the previous cooling rate of the first downscan. Guo et al. have proposed a generalized approach to determine the fictive temperature of a glass with arbitrary thermal history under isobaric conditions.[100]

This generalized approach to determining T_f includes three area-matching steps, as illustrated in Figure 17.[100] The first

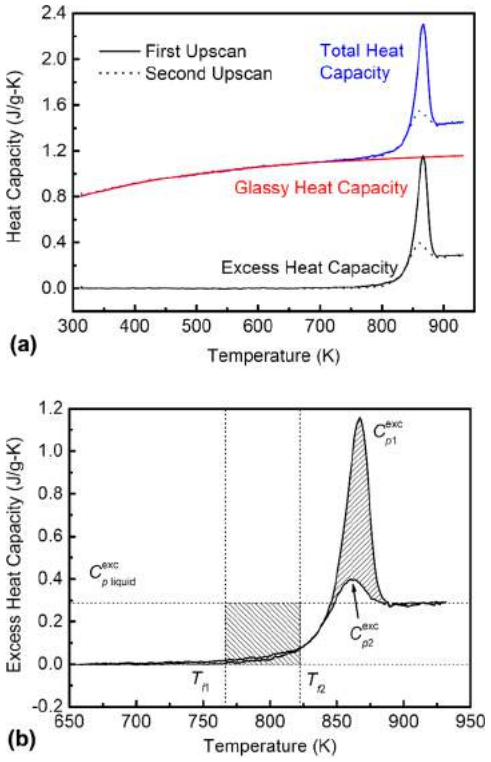

Figure 17. Measured heat capacity curves of annealed NIST SRM 710A soda lime silicate glass using a DSC upscan rate of 10 K/min. (a) Decomposition of the heat capacity signal into glassy and excess contributions. (b) Application of the area-matching procedure to determine T_{f1} and T_{f2}. Reproduced with permission from ref 100. Copyright 2011 Elsevier B.V.

step is to calculate the fictive temperature of the rejuvenated glass (T_{f2}) as shown in Figure 17a, which is similar to Moynihan's approach.[82] The second step is to calculate the difference between the enthalpies of initially formed and rejuvenated glasses, which is equal to the area between the two DSC upscan curves in Figure 17. This part is identical to the enthalpy released during DSC heating as described by Yue et al.[162] The third step is to calculate the fictive temperature of the initially formed glass (T_{f1}), where the area-matching is based on the following equation:

$$\int_{T_{f2}}^{T_{f1}} (C_{pl} - C_{pg})\, dT = \int_{0}^{\infty} (C_{p2} - C_{p1})\, dT \quad (20)$$

This unified, three-step area-matching method can be applied to determine T_f of hyperquenched glasses, annealed glasses, as well as annealed hyperquenched glass fibers, i.e., glasses of any thermal history. It should be noted that fictive temperature is independent of the DSC scan rate. In order to confirm this, Guo et al. used this method to calculate the fictive temperature of the same glass with four different DSC scan rates, all of which gave the same T_f values.[100] Therefore, this unified approach is able to isolate the T_f values from the kinetic effects during DSC measurements. The heating rate of the second DSC upscan does not need to be the same as the

DOI: 10.1021/acs.chemrev.8b00510
Chem. Rev. XXXX, XXX, XXX−XXX

previous cooling rate. The new approach is validated using numerical simulations, which are performed based on the Mazurin−Startsev algorithm.[174] It is found the fictive temperature determined by the calorimetric area-matching technique agrees very well with the modeled data, which is independent of the upscan rate used in the DSC measurement. This generalized approach for determining fictive temperature unifies both Moynihan's and Yue's methods. Yue's method is actually a special case of this approach when $T_f > T_{eq}$.[100]

3.5. Determination of Cooling Rate

The dependence of the fictive temperature (T_f) on the cooling rate q_c is of great importance for both the glass-forming processes and fundamental research.[175−177] For example, the fiber properties strongly depend on the cooling rate during the fiber forming process.[178] Knowing the cooling rate of a glass is crucial for any glass relaxation study. To determine the cooling rate of a glass, Yue et al. established the correlation between the fictive temperature dependence of the cooling rate and the temperature dependence of the equilibrium viscosity by performing DSC and viscometry measurements.[173] The MYEGA equation (eq 32) can be used to describe the temperature dependence of the equilibrium viscosity of glass.[99]

The $T_f \sim q_c$ relation in the low cooling rate range can be determined by DSC since low cooling rates are controllable in DSC. However, it is not easy to determine the $T_f - q_c$ relation in the high cooling rate range (>10^2 K/s) of a quenching process. Thus, finite element simulations were used to determine the cooling rate of a glass fiber during drawing and quenching.[179] The fictive temperature (T_f) of a hyperquenched glass can be determined using the method introduced in refs 162,173 By introducing the parallel shift factor of log K_c = 11.35, the log $\eta \sim T_g/T$ curve can be superimposed on the $\log(1/q_c) \sim T_g/T_f$ curve (Figure 18).[173] This parallel shift is reasonable since the activation energy for structural relaxation determined by DSC is the same as that for viscous flow.[82,180] The resulting dependence of T_f on q_c agrees with that found in a previous study.[177]

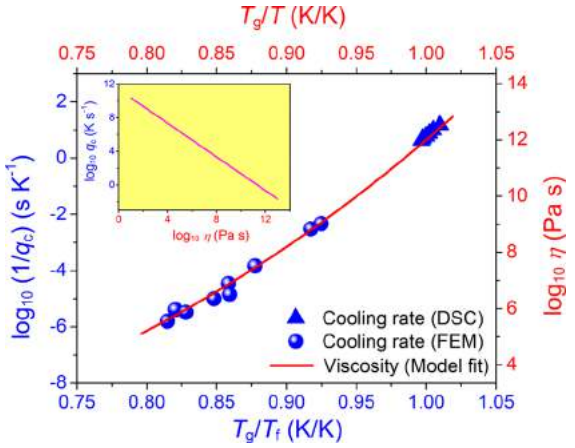

Figure 18. Overlapping correlation between the reciprocal cooling rate ($1/q_c$) and the viscosity ($\log_{10}\eta$) for a basalt glass in the case of $T = T_f$. Red solid curve: the T_g/T dependence of the $\log_{10}\eta$, which was determined by fitting the viscosity data to the MYEGA equation (eq 32). The filled triangles and spheres represent the $\log_{10}(1/q_c)$ versus T_g/T_f data, which were obtained by DSC and by finite element simulation (FEM), respectively. Inset: the linear relation between $\log_{10}\eta$ and $\log_{10} q_c$. Note that the viscosity curve in ref 173 was acquired by fitting the measured data to the Avramov equation.[181] Reproduced with permission from ref 173. Copyright 2004 American Institute of Physics.

Thus, the cooling rates of the fiber drawing process or other hyperquenching processes of different glass systems can be estimated from the viscosity−temperature relation through the shift factor log K_c.[173] In Section 3.4, we have demonstrated how to determine the T_f of both slowly cooled[82,180] and fast-quenched and hyperquenched[173] glasses by DSC. Therefore, the approach introduced here is a simple, effective one for determining the cooling rate of glasses, since it requires only a conventional viscometer and a DSC.[173]

3.6. Liquid Fragility Determined by Calorimetry and Viscometry

The liquid fragility index (m) describes the rate of viscosity change of a glass-forming liquid with temperature at T_g. In the so-called Angell plot, the logarithm of viscosity, $\log_{10}\eta$, is plotted against the T_g-scaled inverse temperature, T_g/T.[182−189] As shown in Figure 8, T_g corresponds to the viscosity of 10^{12} Pa·s. Liquid fragility itself is defined as the slope of the $\log_{10}\eta$ versus T_g/T curve at T_g:

$$m \equiv \left.\frac{\partial \log_{10}\eta}{\partial(T_g/T)}\right|_{T=T_g} \tag{21}$$

Angell classified supercooled liquids as either "strong" or "fragile," depending on whether they exhibit an Arrhenius or super-Arrhenius scaling of viscosity with temperature, respectively.[182−189] Strong liquids exhibit a near-Arrhenius dependence of viscosity on temperature, which normally exhibits small property changes during the glass transition. On the contrary, fragile liquids show a significant departure from Arrhenius behavior, which displays dramatic changes in properties in the glass transition. The fragility index of a perfectly strong liquid equals 14.97 according to the MYEGA equation,[99] with the $\log_{10}\eta_\infty$ (Pa s) average value of −2.93 determined in ref 190. The liquid fragility index is a useful scaling parameter for comparing the viscous flow behavior of all glass-forming liquids.

Given that it is such an important parameter, a method is needed for accurate determination of fragility.[191,192] Liquid fragility can be determined directly using viscosity measurements and eq 21. However, crystallization and volatilization of some glass-forming liquids make high-temperature viscosity measurements difficult, and the low-temperature viscosity experiments are time-consuming.[193,194] Therefore, alternative approaches are needed to quantify fragility indirectly. DSC has proven to be a useful tool for determining liquid fragility. Here the liquid fragility determined by DSC is denoted as the calorimetric fragility index (m_{DSC}), while that determined by viscosity measurements is defined as the kinetic fragility index (m_{vis}).[91] Moynihan et al. found that the activation energy for structural relaxation determined by DSC is in good agreement with the shear viscosity activation energy.[82,180] The activation energy for structural relaxation in the glass transition region can be calculated from the cooling rate (q_c) dependence of T_f measured using DSC.[195]

$$\frac{d \ln q_c}{d(1/T_f)} = -\frac{E_g}{R} \tag{22}$$

where E_g is the activation energy for equilibrium viscous flow in the glass transition region and R is the gas constant.

DOI: 10.1021/acs.chemrev.8b00510
Chem. Rev. XXXX, XXX, XXX−XXX

Kissinger proposed another equation to calculate the activation energy for the glass transition using DSC analysis at different scan rates:[196]

$$\ln\left(\frac{q}{T_f^2}\right) = -\frac{E_g}{RT_f} + \text{constant} \quad (23)$$

The calorimetric liquid fragility can then be determined from E_g and T_g through the following relation:

$$m = -\frac{E_g}{2.303RT_g} \quad (24)$$

Wang et al.[197] have introduced another equation to calculate calorimetric fragility:

$$\log\left(\frac{q_c}{q_{c,s}}\right) = m - m\frac{T_g}{T_f} \quad (25)$$

where q_c is the DSC downscan rate and $q_{c,s}$ is the standard downscan rate, typically 10 K/min. According to Yue et al., the dependence of the fictive temperature on the cooling rate can be well described using a viscosity model.[162,173] The slope of $\log(1/q_c) \sim T_g/T_f$ near T_g can be approximated as the calorimetric liquid fragility (m_{DSC}) over a rather small range of the cooling rates. All of the abovementioned methods assume the correlation of $\log(1/q_c) \sim 1/T_f$ to be Arrhenian near T_g. However, the actual scaling is non-Arrhenius across the whole temperature range, which may lead to a deviation of m_{DSC} from m_{vis}.[91]

The connection between the kinetic and calorimetric liquid fragility values for several series of glass-forming systems has been investigated over a wide range of m from 26 to 108.[91] The m_{DSC} was determined as the slope of the $\log(1/q_h) \sim T_g/T_f$ curve around T_g,[162,173] i.e., the changing rate of fictive temperature (T_f) with heating rate (q_h) in a small T_f range around T_g. The kinetic fragility (m_{vis}) is obtained by fitting the measured viscosity data to the MYEGA equation.[99] As shown in Figure 19, the calorimetric fragility (m_{DSC}) deviates systematically from the kinetic fragility (m_{vis}) for all the studied glasses, and the offset between the two kinds of fragility indices becomes larger with an increase of the fragility value. The deviation of m_{DSC} from m_{vis} is due to the Arrhenian approximation of the $\log(1/q_c) \sim T_g/T_f$ relation in the glass transition range. Zheng et al. developed an empirical model to quantify the deviation and accurately calculate liquid fragility from DSC measurements. Based on a correction factor to account for the non-Arrhenius scaling of the relaxation time, the empirical model is developed as follows:

$$m_{vis} = 1.289(m_{DSC} - m_0) + m_0 \quad (26)$$

where m_0 is 14.97. With this model, m_{vis} can be well predicted from m_{DSC} across a large range of fragilities, as demonstrated by the dashed line in Figure 19. Thus, a quantitative link between kinetic and calorimetric fragilities is reestablished.[91]

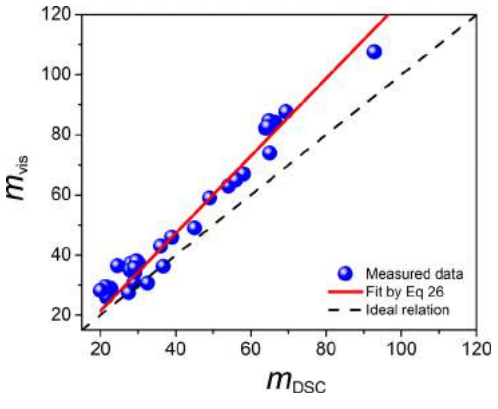

Figure 19. Correlation between the calorimetric and kinetic liquid fragility indices (m_{DSC} vs m_{vis}) for 20 boroaluminosilicate glasses, 6 soda-lime borate glasses, two fiber glass compositions, and 6 vanadium tellurite glasses. Blue Spheres: experimental m_{vis} data; Red solid line: modeled m_{vis} data; Dashed black line: $m_{vis} = m_{DSC}$. Reproduced with permission from ref 91. Copyright 2016 Elsevier B.V.

As discussed in Sections 3.2.1 and 3.2.2, several thermodynamic properties, e.g., $\Delta C_p(T_g)$ and ΔT_g, which reflect the liquid fragility, can be determined by DSC. Also, $(dC_p/dT)_{inflect}$ is another measure of liquid fragility, which is the slope of the rising C_p curve at the inflection point during the glass transition.[10] There have been many studies attempting to connect the kinetic fragility (m) determined by viscosity with thermodynamic quantities at the glass transition determined using DSC.[101,106,195,197−199] Zheng et al. investigated the glass transition behavior of two series of boroaluminosilicate glasses. They found that $\Delta C_p(T_g)$ increases with the increase of kinetic fragility (m). Furthermore, they have also studied the correlation between kinetic fragility and ΔT_g, $(dC_p/dT)_{inflect}$. A higher fragility value means a sharper breakdown of ergodicity and a more well-defined glass transition.[167] Thus, it is expected that ΔT_g[101,106] is inversely correlated with m, whereas $(dC_p/dT)_{inflect}$ is positively correlated with m. The experimental findings confirm those statements.[10] It should be clarified that not all glass-forming liquids follow the qualitative correlations discussed above, which are just commonly observed trends.[1,124]

Huang and McKenna have compared the kinetic fragility (m) with the ratio of the liquid to glassy heat capacities at T_g, C_{pl}/C_{pg}, for several glass families covering small molecule organic, polymeric, and inorganic glass-forming liquids.[198] The impact of fragility within each glass family is somewhat different and may be classified into three groups. Those authors found a negative correlation between kinetic fragility and C_{pl}/C_{pg}; that is, m decreases as C_{pl}/C_{pg} increases for the polymeric glass formers. No large dependence of m on C_{pl}/C_{pg} has been observed for small molecule organics and hydrogen bonding small molecules. Only inorganic glass formers exhibit a clear positive correlation between m and C_{pl}/C_{pg}, which agrees with the original statement of Angell that m increases with increasing C_{pl}/C_{pg}.[200] Angell has suggested that the anomalous fragility behavior of polymers is related to chain length or entanglements. The glass transition is possibly postponed, which could result in the decreasing change in heat capacity.[201−204] The correlation of m and C_{pl}/C_{pg} as a function of the molecular structure should be further investigated to gain a broader picture.

While the discussion of kinetic fragility and thermodynamic quantities starts with a simple, direct correlation, there have been several models proposed to quantify the correlation in a more comprehensive manner.[205−211] Recently, a model used to predict $C_{p,conf}(T_g)$, i.e., $\Delta C_p(T_g)$, based on m and T_g has been derived using a combined topological and thermodynamic approach.[108] In the derivation of the model, $C_{p,conf}(T_g)$ is defined in terms of configurational enthalpy and entropy, and

DOI: 10.1021/acs.chemrev.8b00510
Chem. Rev. XXXX, XXX, XXX−XXX

the Adam−Gibbs (AG) model for equilibrium viscosity is combined with the definition of fragility. Based on the enthalpy landscape approach and temperature-dependent constraint theory, the model is derived as follows:[108]

$$\Delta C_p[x, T_g(x)] = \frac{A(x_R)}{T_g(x)}\left(\frac{m(x)}{m_0} - 1\right) \quad (27)$$

where $A(x_R)$ is a proportionality constant for the reference composition x_R, m_0 is the fragility of an ideal strong liquid, and x is a composition variable.

The advantage of the Adam−Gibbs model lies in connecting kinetics (via the viscosity, η) with a thermodynamic variable S_{conf} as a function of temperature, which leads to the successful connection of $C_{p,conf}(T_g)$ with m. $\Delta C_p(T_g)$ can be predicted using the measured values of T_g and m.[108] Good agreement has been found between measured and predicted values of $\Delta C_p(T_g)$ for several inorganic glass systems, including borosilicate[108] and calcium aluminosilicate glasses.[125] The predictive ability of the model indicates that thermodynamic changes during the glass transition are indeed connected to the kinetic fragility index.

As discussed above, the simple linear relation between the kinetic fragility and $C_{p,conf}(T_g)$ is not always valid for polymeric glass formers. However, Martinez and Angell,[106] and Cangialosi et al.[212] connected the kinetic fragility to the excess entropy and heat capacity of a large number of glass-forming polymers. The liquid entropy in excess to the corresponding crystal is termed excess entropy, which is found to be proportional to S_{conf}.[186,213] The S_{conf} term in the AG model can be replaced by excess entropy S_{ex}. By introducing the Adam−Gibbs equation into eq 27, the following relation is obtained.[213]

$$m = 1 + \frac{\Delta C_p(T_g)}{S_{ex}(T_g)} \quad (28)$$

Wang et al. have developed an empirical correlation that connects kinetic fragility to thermodynamic variables for more than 50 nonpolymeric supercooled liquids, mainly including organic small molecules and hydrogen bonded liquids:[214]

$$m = 56\frac{T_g \Delta C_p(T_g)}{\Delta H_m} \quad (29)$$

where ΔH_m is the melting enthalpy, and all the thermodynamic variables can be determined calorimetrically. The correlation has also been derived from the random first-order transition theory.[215,216] The kinetic fragility has been well correlated to the thermodynamic properties for the studied compositions. By combining the empirical "2/3 rule" between the melting point and average glass transition temperature ($T_g/T_m = 2/3$) with eq 29, it yields the following form:

$$m = 40\frac{\Delta C_p(T_g)}{\Delta S_m} \quad (30)$$

The plot of scaled excess entropies of glasses and liquids as a function of the reduced temperatures, i.e., $\Delta S(T)/\Delta S_m$ vs T/T_m is often viewed as the thermodynamic equivalent of the kinetic fragility plot.[101] The slope in the $\Delta S(T)/\Delta S_m$ vs T/T_m plot can be derived as

$$\left.\frac{d(\Delta S(T)/\Delta S_m)}{d(T/T_m)}\right|_{T=T_g} = \frac{\Delta C_p^{ex}(T_g)}{\Delta S_m}\frac{T_m}{T_g} \quad (31)$$

The above equation means that the slope in the thermodynamic plot of $\Delta S(T)/\Delta S_m$ vs T/T_m can be determined by $\Delta C_p(T_g)/\Delta S_m$. Based on this correlation, $\Delta C_p(T_g)/\Delta S_m$ can be defined as a thermodynamic gauge for fragility. The measured kinetic fragility agrees well with the calculated values using eq 31,[214] which validates the quantitative correlation of thermodynamic and kinetic fragilities.

3.7. Determination of Viscosity by DSC

Viscosity is a key factor in all stages of glass industry production. It is also critical for understanding the crystallization kinetics and glass formation, the glass transition, and the nonexponential relaxation of liquids and their corresponding glasses.[163,217] Due to the technical complications of determining viscosity in many cases,[193,194] it is useful to find an alternative way of determining the viscosity−temperature curve. In this context, an approach combining DSC and a viscosity model has recently been proposed to derive the viscosity−temperature relation in the entire liquid and supercooled liquid range of temperature. The question is which model best suits this approach. As is known, numerous viscosity models exist to describe the temperature dependence of shear viscosity.[92,99,181,218] Three-parameter viscosity models can be expressed in terms of three common parameters: T_g, m, and the extrapolated high temperature limit of viscosity η_∞. One of these models is the MYEGA model, which is based on the temperature dependence of configurational entropy and gives a better fit to the experimental data compared to other 3-parameter models.[99] The model can be written as

$$\log_{10}\eta(T) = \log_{10}\eta_\infty + (12 - \log_{10}\eta_\infty)\frac{T_g}{T} \times \exp\left[\left(\frac{m}{12 - \log_{10}\eta_\infty} - 1\right)\left(\frac{T_g}{T} - 1\right)\right] \quad (32)$$

As reported in ref 190, the analysis of the viscosity data of 946 silicate liquids and another 31 nonsilicate liquids by the MEYGA model yields a universal high-temperature viscosity limit of $10^{-2.93}$ Pa·s. Thus, there are only two parameters left in the MYEGA model, namely, T_g and m. As mentioned in Section 3.6, m_{vis} can be calculated through m_{DSC} across the full range of fragilities.[91] Moreover, as shown in Figure 8, the calorimetric T_g can be used as the kinetic T_g. Thus, both T_g and m can be determined solely by performing DSC measurements. By combining the high-T viscosity limit ($10^{-2.93}$ Pa·s), we are able to obtain the entire viscosity curve of a glass-forming liquid only by DSC.[91] An example is shown in Figure 20, where the viscosity−temperature relation of a borate melt is obtained by introducing the calorimetric T_g, m_{DSC}, and $\log_{10}\eta_\infty = -2.93$ Pa·s into the MYEGA model, which excellently agrees with that measured directly by a viscometer across the full temperature range. But the DSC method is simpler and more effective compared to direct viscosity measurements.[91]

3.8. Polyamorphic Transitions

3.8.1. Definition and General Aspects. Polyamorphism refers to the existence or transformation of two noncrystalline

DOI: 10.1021/acs.chemrev.8b00510
Chem. Rev. XXXX, XXX, XXX−XXX

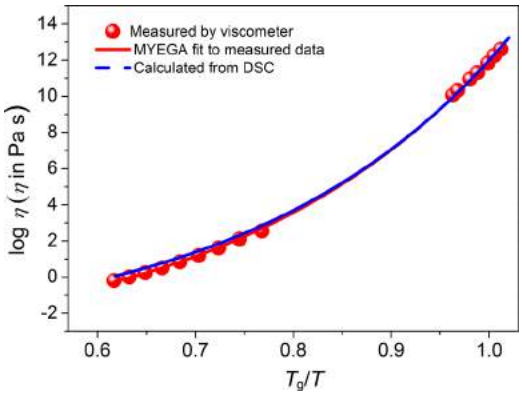

Figure 20. Logarithmic viscosity ($\log_{10}\ \eta$) as a function of the T_g scaled inverse temperature, (T_g/T), for a borate glass composition. Red filled circles: measured viscosity data; Red solid line: MYEGA fit to the measured viscosity data. Blue dashed line: viscosity data determined by introducing m_{DSC}, T_g, and $\log_{10}\ \eta_\infty = -3$ into the MYEGA equation. Reproduced with permission from ref 91. Copyright 2016 by Elsevier B.V.

phases of a given material system under certain temperature and pressure conditions. The two phases have the same chemical composition, but with different density, enthalpy, and entropy.[219] The phase boundary $dT/dP = dV/dS$ typically has a negative slope. Polyamorphism is different from phase separation, which refers to the coexistence of two phases with different chemical compositions (Section 3.3.3). Polyamorphism is a physical phenomenon applying to noncrystalline states such as glasses, amorphous solids, supercooled liquids, and equilibrium liquids. However, a liquid−liquid transition must occur only in a thermodynamically stable equilibrium state, whereas the polyamorphic transition can also take place in a nonequilibrium, nonergodic state. *Amorphous ice* is a typical example of a polyamorphic transition.[220,221] Some of these transitions (including that in water) are expected to end in a second critical point. Understanding of polyamorphism is important for obtaining a comprehensive picture of the glass transition.

Experimental detection of a possible phase transition between two supercooled liquid states in water has been a longstanding challenging problem due to the difficulty in avoiding crystallization of water. However, a major breakthrough in addressing this problem was achieved in 2018 by Woutersen et al.[222] They applied DSC, infrared spectroscopy, and molecular dynamics simulations to investigate a water-rich hydrazinium trifluoroacetate solution in which the local hydrogen bond structure surrounding a water molecule resembles that in neat water at elevated pressure, but which does not crystallize upon cooling. For the first time, they observed in this solution a sharp, reversible phase transition between two homogeneous liquid states. The hydrogen-bonded structures of these two states are similar to those of high density liquid (HDL) and low density liquid (LDL) water. Such structural similarity supports theories[223−225] that predict a sharp transition in pure water under pressure if ice crystallization could be suppressed. It should be noted that the terms of high density amorphous (HDA) and low density amorphous (LDA) solid phases are encountered in some glass forming systems.[226−229] These two solid phases can be transformed into each other, depending on temperature and pressure.[227−229] It is worth mentioning that liquid−liquid transitions in yttria-alumina liquids were first discovered by Aasland and McMillan[230] and Greaves et al.[231] They observed the coexistence of the HDA and LDA phases in the yttria−alumina system.

However, whether or not transformations between polyamorphic phases are of the first order is controversial.[226−229,232,233] In addition to LDA and HDA ice,[227,228] polyamorphism has been reported in many tetrahedral liquids or glasses.[219] For silica under pressure, Si−O polyhedra can transform from tetrahedral coordination eventually to octahedral coordination.[234] New densified HDA phases can be obtained from crystalline precursors.[2,235] Creating LDA phases by this route is challenging since it is hard to achieve decompression without cavitation. An alternative approach involves the amorphization of microporous crystalline materials, such as zeolites,[226,236] and metal−organic frameworks.[4,237] These two types of microporous materials are selected as the objects of this article to describe the current understanding of polyamorphism. To identify and follow the polyamorphic transition, DSC is utilized as a powerful and sensitive technique. However, DSC alone cannot tell the structural evolution during polyamorphic transition, and it must be used in combination with structural characterization techniques.

3.8.2. Zeolites. Pressure- and temperature-induced amorphization of crystals well below melting points is an exciting subject of glass science.[235,238] Here we take zeolite as an example to show the pressure-induced amorphization and polyamorphic transitions. The speed and extent of amorphization can be followed by DSC. Zeolite amorphization is accompanied by a sharp asymmetric exotherm followed by a smaller endothermic step.[239,240] Around 6 kJ per $NaAlSiO_4$ mole is released, and comparable to very-low-energy acoustic modes or floppy modes.[241] It has been argued that the floppy modes in zeolites create the extra-framework sites for charge-compensating cations.[242] Soft phonon modes might also be involved in the destabilization of the low-density anhydrous crystalline structure.

Figure 21 shows the direct comparison between DSC and X-ray diffraction (XRD) results. It is seen that the initial rise of the DSC exothermic curve with temperature coincides with the initial fall in the volume fraction of zeolite (x_{zeo}). The DSC exothermic peak appears at the temperature of the fastest crystal collapse (T_A) corresponding to $x_{zeo} = 0.5$, whereas the high-temperature endothermic drop follows the high temperature section of the x_{zeo} curve. This suggests that additional floppy modes may be created as constraints are lost during the collapse, and they disappear when the rigid amorphized phase recovers.

Figure 21 also shows the small-angle X-ray scattering invariant, Q_{SAXS}, which measures differences in local density. Q_{SAXS} increases as the XRD peaks become lower and the DSC output becomes exothermic, indicating that amorphization begins. However, the maximum in Q_{SAXS} occurs at a lower temperature than the DSC peak. X-ray scattering continues for a further 500 s and until 100 °C above the disappearance temperature of the crystalline phase, providing evidence for density variations in the amorphized material before the final homogeneous phase is obtained. Evidence for heterogeneity is also found in the later stages of zeolite amorphization by examining the linear thermal expansion coefficient, α_{Expan}, of the residual zeolite (Figure 21). α_{Expan} has a sharp maximum when most zeolite has amorphized. Many zeolites, however,

DOI: 10.1021/acs.chemrev.8b00510
Chem. Rev. XXXX, XXX, XXX−XXX

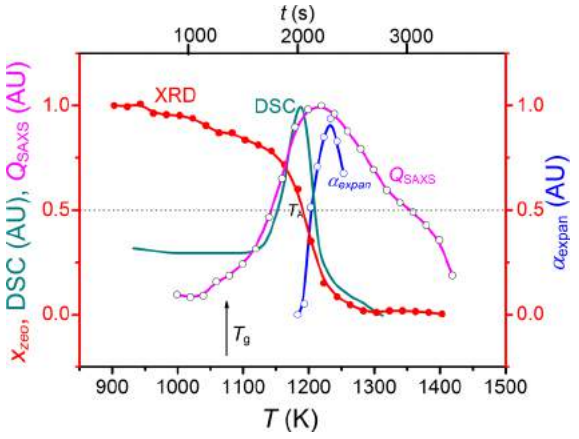

Figure 21. Direct comparisons between DSC output (heat flow), small-angle X-ray scattering (SAXS), and XRD during the collapse of zeolite Y. The peak and the half-width of the DSC exotherm coincide with the collapsing temperature (T_A) and the collapsing time (τ_A). The SAXS invariant, Q_{SAXS}, increases at a similar rate to the DSC exotherm but reaches a maximum at a higher temperature or a long time, and persists long after $x_{zeo} = 0$. In the final stages of collapse, residual zeolite crystals exhibit a peak in the thermal expansion coefficient, α_{Expan}, indicating the development of negative pressure within the amorphizing material before a homogeneous phase is obtained. Reproduced with permission from ref 245. Copyright 2003 Nature Publishing Group.

exhibit negative thermal expansion; for example, anhydrous crystals shrink considerably at lower temperatures.[243] This behavior has been found for zeolite A and zeolite Y before collapsing. However, from the rapid rise in α_{Expan} when $T > T_A$ (Figure 21), it is inferred that the crystalline fraction is temporarily in tension. Negative pressure is expected if amorphization occurs randomly and spontaneously within individual crystals. As an HDA phase forms, internal tension will be created and disappears when the collapse is complete.[244] In the framework of liquid fragility, the LDA phase is even stronger than SiO_2, whereas the HDA phase is relatively fragile.[4,245]

3.8.3. ZIF-4. Recently, a completely new family of melt-quenched glasses has emerged, chemically different from existing (i) organic, (ii) inorganic, and (iii) metallic glasses, which involve covalent bonds, ionic/covalent mixed bonds, and metallic bonds, respectively. This new family of glasses is obtained by melting and vitrifying zeolitic imidazolate frameworks (ZIFs), a subset of metal−organic frameworks (MOFs), upon quenching.[4,246−255] The ZIF glasses involve coordination bonds, which connect each metal node to four organic ligands, constituting the disordered tetrahedral network, in contrast to the long-range ordered network of their corresponding crystals. The ordered cagelike structure of ZIF crystals is lost in their glassy state. It should be noted that only some MOFs can be vitrified into a glassy state due to chemical decomposition that can occur during heating; that is, only those which fulfill certain structural conditions can be melted and quenched. The same applies to the lower melting point coordination polymers and hybrid perovskites.[257] The primary building unit in ZIF glasses is analogous to that in the SiO_2 glass, viz., the $[SiO_4]$ tetrahedron. According to the radial distribution function data, the short-range order in ZIFs is far greater than that in silica glass, since imidazolate linkers are much larger than the bridging oxygen results.[256] These melt-quenched ZIF glasses present a new opportunity to explore one of the most challenging problems in condensed matter science, i.e., glass transition and glass formation.[221,256,258−261] In addition to melting and glass formation, one particular ZIF, ZIF-4 $[Zn(Im)_2]$ (Im = imidazolate, $C_3H_3N_2^-$), exhibits a remarkable feature, namely, polyamorphic transitions, when it undergoes a DSC upscan. In the following, we review the findings about the polyamorphic transitions in ZIF-4, which were achieved by using DSC.

The DSC upscan curves of ZIF-4 are shown in Figure 22a, where it is seen that the endotherm at point A occurs due to

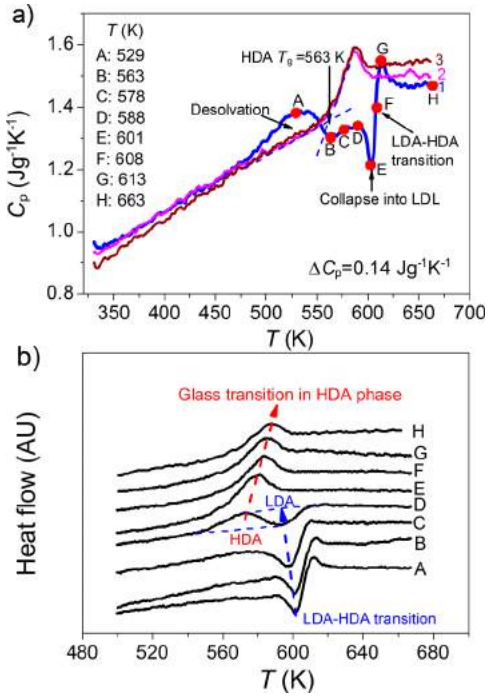

Figure 22. (a) DSC upscans on ZIF-4 at 10 K/min. Upscan 1: the successive events—solvent release, crystal collapse to low-density amorphous (LDA) phase, and LDA to HDA transition. Upscans 2 and 3: glass transition peaks. (b) DSC upscans to 673 at 10 K/min on ZIF-4 samples preheated to temperatures A (529 K), B (563 K), C (578 K), D (588 K), E (601 K), F (608 K), G (613 K), and H (673 K) and cooled back. Red arrow: increase in the T_g of HDA phase with the preheating temperature (D to H in Figure 22a); Blue arrow: increase in the temperature of ZIF-4 collapse into LDA with the preheating temperature (A to D in Figure 22a). Sample D (588 K): coexistence of LDA and HDA captured by the DSC upscan curve (Figure 22b). Reproduced with permission from ref 4. Copyright 2015 Macmillan Publishers Limited.

the release of the framework template (*N*,*N*-dimethylformamide). Subsequently, an exothermic feature is observed (D−F), which is attributed to the collapse of ZIF-4 into the low density amorphous phase (LDA) (confirmed by SAXS experiments[262]). Above this temperature, LDA converts to a high-density amorphous phase (HDA) (Figure 22a F−H), and the glassy nature of HDA after cooling is confirmed by the glass transition peak at T_g = 565 K during DSC upscans 2 and 3) (Figure 22a). The LDA−HDA transition is similar to polyamorphic transitions in inorganic zeolites[226,240,245] and glass-forming liquids.[2] HDA is a highly viscous liquid phase above its T_g, which crystallizes to ZIF-zni upon further heating, and ZIF-zni has different topology compared to the as-synthesized ZIF-4.[4] The T_g of HDA (Figure 22a) is

DOI: 10.1021/acs.chemrev.8b00510
Chem. Rev. XXXX, XXX, XXX−XXX

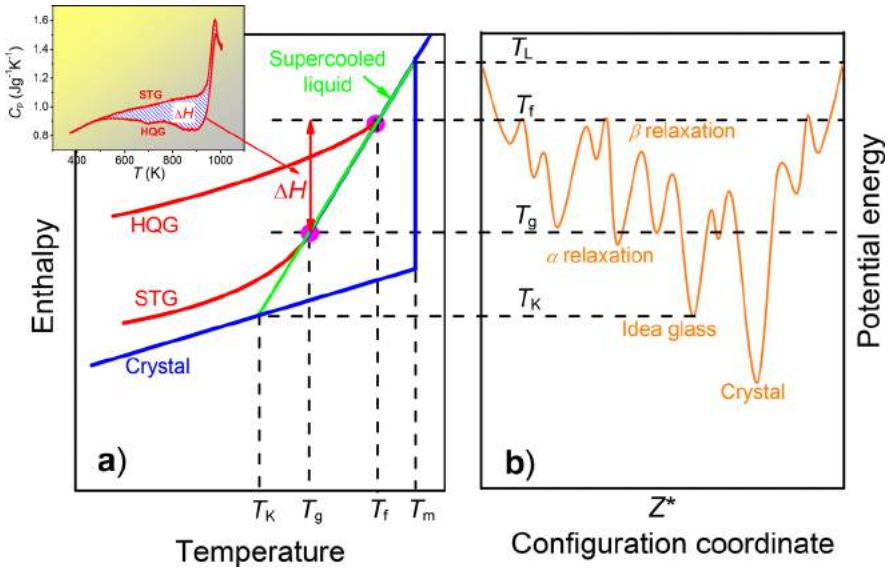

Figure 23. Schematic representation of the enthalpy relaxation from a hyperquenched glass (HQG) toward a standard glass (STG) (i.e., a glass cooled at the standard rate of 10 K/min) (left panel) and the reflection of such relaxation on the potential energy landscape (PEL) (right panel). (a) Enthalpy decrease upon cooling a supercooled liquid to the HQG with higher fictive temperature (T_{f2}) and to the STG with lower fictive temperature ($T_{f1} = T_g$), and also enthalpy drop during crystal formation at the *liquidus* temperature (T_L). Inset: A typical isobaric heat capacity (C_p) diagram for sub-T_g relaxation in a HQG, e.g., stone wool fibers.[14,15] The hatched area is the enthalpy released during the DSC first upscan, which is equal to the enthalpy drop of the glass from T_f to T_g. (b) Different relaxation modes depending on the level of the glass on the PEL. Primary (α) and secondary (β) relaxations occur around T_g and T_β, respectively.[274] Different states (liquid, supercooled liquid, ideal glass, and crystal) of a glass-forming system are indicated on the PEL. T_K is the Kauzmann temperature corresponding to a hypothetical ideal glass state.

significantly lower than the LDA onset temperature (589 K) (Figure 22b). It should be mentioned that the HDA−LDA reversible transition (H−C in Figure 22a) during the DSC downscan was not observed even at the lowest cooling rates (1 K/min) that DSC can reach.

Remarkably, LDA and HDA can coexist in the ZIF-4 sample heated to temperature D (Figure 22a), which is captured by DSC curve D (Figure 22b), where the endothermic response is followed by an exothermic one. It is also seen that the glass transition peak of HDA shifts to higher temperature with increasing the preheating temperature from D to H (red arrow in Figure 22b), whereas the exothermic peak for ZIF-4 collapsing into LDA shifts to lower temperature (blue arrow). The former shift is expected since the HDA structure is densifying with increasing the preheating temperature, while the latter opposite shift suggests some increase in atomic degrees of freedom as collapse advances. For the sample showing the HAD−LDA coexistence (Curve D in Figure 22b), there is a 24 K difference between the HDA and LDA glass transitions.

As mentioned above, the polyamorphic transition in ZIF-4 (Figure 22a) is not reversible under the laboratory conditions. This is similar to the case of the ultrastable glass[13] obtained by molecular deposition, which also has a higher T_g than that of its "normal" glass counterpart.[263] Upon reheating, the ultrastable glass is transformed into a standard glass state, i.e., not into an ultrastable state at laboratory cooling rates, even though it would be thermodynamically favorable. This is also the same scenario observed in long-time aged amber.[264] In contrast, LDA coexists with the HDA phase in ZIF-4 (Figure 22b). When ZIF-4 has fully released its solvent, its structural skeleton becomes looser but remains ordered with unchanged potential energy.[4] Upon further heating, the structure of solvent-free ZIF-4 relaxes toward a lower enthalpy state, leading to LDA (Figure 22a). This behavior is also common to anhydrous zeolites,[226,240,245] the enthalpies of which all exceed those of conventional oxide glasses with the same composition,[265] reflecting the metastable nature of zeolitic crystals. When the temperature rises above its T_g, LDA spontaneously transforms into the highly viscous liquid HDA. With further heating, this liquid phase is turned to a more stable ZIF-zni crystal phase, and subsequently to a melt before decomposition. When this melt is quenched, the ZIF-4 glass is obtained.

The apparent irreversibility for the phase transition in ZIF-4 is in contrast to the reversibility reported in *ab initio* molecular dynamics simulations of volume vs pressure in zeolite systems.[266] With increasing pressure, zeolite−LDA followed by LDA−HDA first order transitions could also be reversed by reducing pressure. Some evidence for phase transition reversibility was found experimentally during the initial zeolite collapsing process[226] and over protracted periods at room temperature.[240] The irreversibility of the transition in ZIF-4 on a laboratory time scale might be due to the inherent structural differences between ZIF-4 and inorganic systems, in particular, the difference in rigidity of the intertetrahedral bridging unit.[267] Compared to oxide melts and zeolites, for example, the floppy bridging oxygen is replaced by the rigid bridging imidazolate in ZIF-4. This could influence differences in conformational changes involved in the LDA−HDA transition that determine the HDA topology and may not be kinetically symmetric.[4] The coexistence of HDA and LDA in the ZIF-4 subjected to heating to D (588 K) (Figure 22b) implies that the entropy of the HDA phase is close to that of LDA.

4. EXPLORING ENTHALPY RELAXATION VIA DSC

The most common method for glass formation is by cooling a liquid from high temperature at a rate fast enough to avoid

DOI: 10.1021/acs.chemrev.8b00510
Chem. Rev. XXXX, XXX, XXX−XXX

crystallization. During cooling, the supercooled liquid gradually falls out of thermodynamic equilibrium and enters into the glassy state, passing through the glass transition region.[1,2] Due to the nonequilibrium nature of glass, one of its most intriguing phenomena is the spontaneous structural relaxation that occurs when approaching the metastable supercooled liquid state. Specifically, when the glass is subjected to a sub-T_g annealing process (i.e., annealing below T_g), almost all of the important relaxation mechanisms occur from atomic vibrations, the fast β relaxation process, the secondary slow β relaxation process (Johari−Goldstein relaxation), and finally the cooperative α (primary) relaxation process, evolving with time within the nonequilibrium region.[2] DSC has proven to be a powerful technique for studying the enthalpy relaxation behavior of different glass systems because of its high sensitivity, high accuracy, practicality, and direct access to thermodynamics. This section reviews recent advances in investigating enthalpy relaxation in glass by using DSC in combination with structural characterization techniques such as NMR, neutron scattering, total X-ray diffraction, and nuclear inelastic scattering. We describe both the α and β relaxation features in melt-quenched glasses such as oxide, metallic, organic, chalcogenide, and metal−organic framework glasses. Furthermore, we discuss how to detect the structural heterogeneity in both normal and poor glass formers by studying sub-T_g enthalpy relaxation. To understand the structural origin of the enthalpy relaxation effects, it is necessary to combine the hyperquenching-annealing-DSC (HAD) approach with structural characterization techniques. Sub-T_g relaxation behavior is also discussed in terms of a potential energy landscape description. Finally, we introduce a recent understanding of the origin of the fragile-to-strong transition with the help of the DSC approach.

4.1. Sub- and Sup-T_g Relaxation

4.1.1. Potential Energy Landscape. The potential energy landscape (PEL) description of liquids and glasses[3,94,171,176,209,268,269] is a useful approach for relating the complex sub-T_g relaxation processes, in particular, the α and β relaxations, to molecular-scale events of the glasses. Simply speaking, the PEL refers to a multidimensional surface generated by a system's potential energy as a function of molecular coordinates. In this regard, Goldstein suggested that there should be a temperature below which the molecular motions can be detected by transitions over certain potential barriers in the energy landscape.[270] This temperature is similar to the fictive temperature T_f in some sense. Figure 23 illustrates a schematic connection between the enthalpy drop (Figure 23a) of a glass-forming liquid during cooling and annealing and the PEL of this liquid (Figure 23b). Note that in Figure 23b the PEL with multidimensional nature is schematically constructed by plotting the potential energy against the one-dimensional configurational coordinate (Z^*) for simplicity. In 1995, Stillinger proposed that the relaxation of glass in its configuration space of the PEL conceptually corresponds to a combination of fast motion between inherent structures within a metabasin (β relaxation) and a slower diffusive motion among metabasins (α relaxation).[271] In other words, during relaxation, the configuration of the glass system gradually samples the rugged topography of the landscape in order to reach the deeper basin by crossing the saddle points between the basins[272] (Figure 23b).

The depth of the basins sampled by the system in the energy landscape varies as a result of sub-T_g annealing.[273] The DSC is a rather sensitive tool to detect the changes of the potential energy in liquid, supercooled liquid, and glass states, and to probe the changes in their degrees of atomic freedom, i.e., from migration to vibration, upon cooling of a liquid or vice-versa on reheating a glass.[273] Relaxation is a process of approaching equilibrium by traversing the PEL. Figure 23 schematically depicts the energy level of the trapped state obtained at different cooling rates.[273] It is obvious that a higher cooling rate corresponds to a higher energy level of the basin, where the liquid is located and trapped at a higher T_f (HQG). With sub-T_g annealing, the depth of the basins occupied by the glass gradually decreases, and the system recovers to the standard glass state. The enthalpy loss (ΔH) of HQG during dynamic heating from room temperature to the onset temperature of the supercooled liquid or isothermal annealing can be precisely determined by two runs of C_p measurements as shown in the inset of Figure 23a.

The higher potential energy configurations trapped by hyperquenching relax more rapidly than those trapped by slow quenching, and hence, the former one is involved in the β relaxation as shown in Figure 23b. All the potential energy states over the temperature range from T_f of the HQG to that of the STG could be observed in a real-time window during the subsequent enthalpy recovery procedure. Thus, we may find the characteristics of β relaxation in glasses. The HAD approach makes the β relaxation more visible and more separable from the α relaxation. The potential energy of a glass can be excited or rejuvenated via different ways such as hyperquenching, ball-milling, and mechanical stretching, and the excited glass can relax again upon sub-T_g annealing. The path of the enthalpy relaxation is different from one system to another, thus providing thermodynamic, dynamic, and structural information on a glass system. The bottom part of the PEL can be accessed by extremely slow cooling or by molecule-by-molecule deposition. Fabrication of ultrastable glasses by molecular deposition can suppress the potential energy of a glass to a level corresponding to thousands of years of annealing or cooling. In addition, the question about whether an ideal glass state (Figure 23b) exists at finite temperature is still under debate.[2−4,94,239,240,245,271,275] According to the MYEGA model, the configurational entropy vanishes only when the temperature approaches zero. The crystal state is seen at the lowest level of the PEL (Figure 23b).

A systematic study of the heterogeneous relaxation dynamics of a glass system was carried out by Diezemann et al. based on the PEL picture.[276−279] Their investigations concentrated on linking the molecular reorientation by means of transitions among an extensive number of free energy minima in PEL to both α and β relaxations. First, by studying the heterogeneity of α relaxation in glass-forming liquids, a free energy landscape model was proposed in which the molecular reorientation rates (rotational relaxation) were intrinsically linked to the time scale of the α relaxation (structural relaxation).[276] The model was further improved by including the translational dynamics of the supercooled liquids.[277] The simulated aging of a nonequilibrium state by quenching from infinitely high temperature to low temperature was investigated based on a qualitative description of the physics inherent in the free-energy model.[278] They found that the time scale for re-equilibration is solely determined by that of the α relaxation. Although the proposition of the free energy landscape model has brought our understanding of the heterogeneous dynamics of the α relaxation significantly forward, the β relaxation

DOI: 10.1021/acs.chemrev.8b00510
Chem. Rev. XXXX, XXX, XXX−XXX

process has been largely ignored.[280−282] Diezemann et al.[279] improved the abovementioned free energy landscape model by including β relaxation. Their modeling results agreed well with the experimental results of dielectric relaxation and spin−lattice relaxation. An analytically solvable PEL model of α and β relaxation was reported by Mauro and Smedskjaer,[283] showing a natural decoupling of the dynamics into intra-metabasin (β) and intermetabasin (α) relaxation processes.

The quantitative energy landscape model for a glass-forming system with a realistic chemistry was established by Mauro and Loucks[284] using *ab initio*-derived interatomic potentials for selenium.[285] Their approach enabled calculation of glass transition and relaxation behavior on laboratory time scales, taking advantage of the broken ergodic nature of the glassy state.[109] Since the landscape was calculated under isobaric rather than isochoric conditions, it is actually an enthalpy landscape[286] rather than a PEL. A detailed review of the enthalpy landscape description of the glass transition is given elsewhere.[75] The enthalpy landscape or PEL in a real liquid system may be partially mapped by HAD measurements as displayed in Figure 23 and described in a recent paper.[4]

In the following section, we review some studies of the sub-T_g enthalpy relaxation behavior of several glass systems by HAD and describe the relaxation dynamics of the glasses within the PEL framework.

4.1.2. Hyperquenched Glasses. *4.1.2.1. Sub-T_g Annealing.* Hyperquenched (HQ) glasses are those that form using an extremely high cooling rate (>10^5 K/s) via different routes such as the melt spinning process[15,162,287] and electrospray quenching process.[288] Such a high cooling rate causes the liquid structure to be frozen at a high T_f in a high potential energy region of the PEL and, hence, create a glassy state far from equilibrium.[273] During sub-T_g annealing, the trapped energy will be gradually released, resulting in a decrease in the T_f.[289] Structural and energetic heterogeneities can also be detected during this relaxation process.

Enthalpy relaxation in HQ glasses has received much attention.[175,288,290] Over the past two decades, Yue et al. have conducted systematic and detailed calorimetric studies on the sub-T_g enthalpy relaxation in different kinds of HQ glasses including oxide glass fibers, metallic glasses, organic glasses, and water by using the hyperquenching-annealing-DSC (HAD) strategy.[14,15,162,287,291,292] The HAD method explores the thermodynamics, kinetics, and structural evolution of glasses and supercooled liquids in the temperature region between T_g and T_f. Here we demonstrate several intriguing features regarding the enthalpy relaxation of the HQ glasses relative to that of the standard glass (i.e., a glass cooled at the standard rate of 10 K/min to 20 K/min),[162,175] which provides insight into the evolution process of a HQ glass relaxing from a high to low energy state in the PEL.

Figure 24 shows a typical sub-T_g enthalpy relaxation pattern of a HQ glass system (namely, stone wool fibers with aluminosilicate composition) cooled at a rate of about 10^6 K/s; the pattern was obtained during the first and second DSC upscans (C_{p1} and C_{p2}), respectively.[162] The exothermic peak on the C_{p1} curve indicates the release of the excess enthalpy of the HQ glass relative to the standard glass upon dynamic heating.[14,15,162,287,288,291,292] The enthalpy release is also considered to be an enthalpy recovery process, i.e., a recovery from the enthalpy of HQ glass to that of the standard glass. The inset of Figure 24 displays the rate of the excess energy release of the HQ glasses, $d\Delta E/dT$,[291] which is equal to the

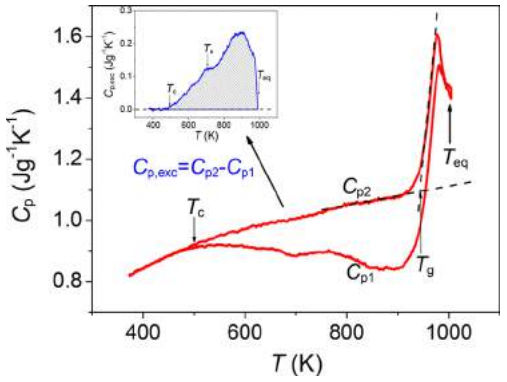

Figure 24. Isobaric heat capacity of HQ stone wool fibers against temperature (T), measured at 20 K/min during the first (C_{p1}) and the second DSC upscan (C_{p2}), respectively. Inset: the excess of the heat capacity ($C_{p,exc} = C_{p2} - C_{p1}$) versus T. T_{re} stands for the onset temperature for the release of enthalpy, and T_{eq} is the equilibrium temperature, at which the glass is fully converted to the supercooled liquid, and $C_{p2} = C_{p1}$. T_s refers to the temperature at which an enthalpy release shoulder appears, indicating that there is a partial overlap of two enthalpy release peaks. Replotted with permission from ref 162. Copyright 2002 Elsevier B.V.

difference $C_{p1} - C_{p2}$ between the HQ and the standard glasses, $C_{p,exc}$, as a function of temperature T. T_{re} is the onset temperature of the energy release, while T_{eq} is the offset temperature of the glass transition, at which $C_{p1} = C_{p2}$. The asymmetric $C_{p,exc}$ curve with a shoulder at T_s implicitly suggests that the α relaxation (represented by the main peak right below T_g) and the β relaxation (reflected by the $C_{p,exc}$ part below T_s) overlap with each other.[291,292] The direct link of the sub-T_g enthalpy relaxation to α and β relaxations was examined by studying the DSC relaxation patterns of glass fibers with different chemical compositions and thereby different fragilities.[293]

The sub-T_g relaxation is explicitly expressed by the variation of the C_p curves of the HQ glasses subjected to different annealing degrees, i.e., different temperatures (T_a) below T_g for different annealing times (t_a).[14,291−294] The effect of T_a on enthalpy relaxation is similar to that of t_a. Figure 25 shows the effect of T_a on the C_p curves of the basaltic HQ glasses for t_a = 8 days.[294] The methodology for determining the magnitude of

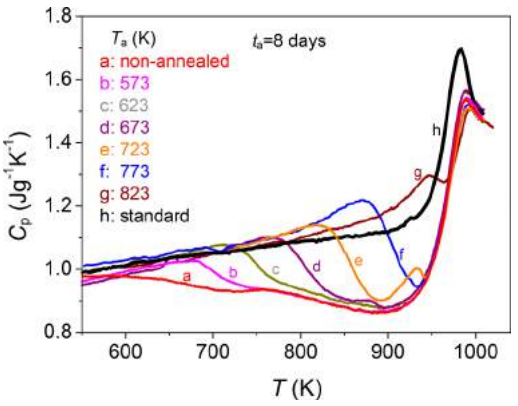

Figure 25. C_p curves of a HQ glass (stone wool fibers quenched at 10^6 K/s) annealed at different temperatures (T_a) for t_a = 8 days obtained from the first DSC upscan at a heating rate of 20 K/min. Adapted from ref 294 with permission. Copyright 2009 Shandong University Publisher.

DOI: 10.1021/acs.chemrev.8b00510
Chem. Rev. XXXX, XXX, XXX−XXX

the excess enthalpy trapped in hyperquenched glasses is to calculate the area enclosed by C_{p2} and C_{p1} curves. The excess enthalpy (ΔH) decreases with increasing T_a in the manner that its onset temperature (T_{re}) shifts from a lower to a higher temperature. In other words, the structural configuration of the glass system approaches a lower energy level in order to attain the energy level corresponding to T_a with annealing, but this takes a long time, even beyond the experimental time window if T_a is well below T_g. Similar findings regarding sub-T_g enthalpy relaxation were also reported in other HQ glasses, e.g., inorganic glass fibers[15,81,162,291−293,295,296] and metallic glasses.[297−299] T_{re} depends on the hyperquenching rate (q_c) and thus on the T_f of the HQ glass.[81]

In addition, another important feature of the relaxation pattern of the annealed HQ glass is the occurrence of the endothermic prepeak followed by an exotherm (curves C−I in Figure 26a), indicating a high degree of structural heterogeneity of the HQ glass;[14,81,293,294,296,300] that is, during annealing, the system accesses a deeper basin in the PEL.

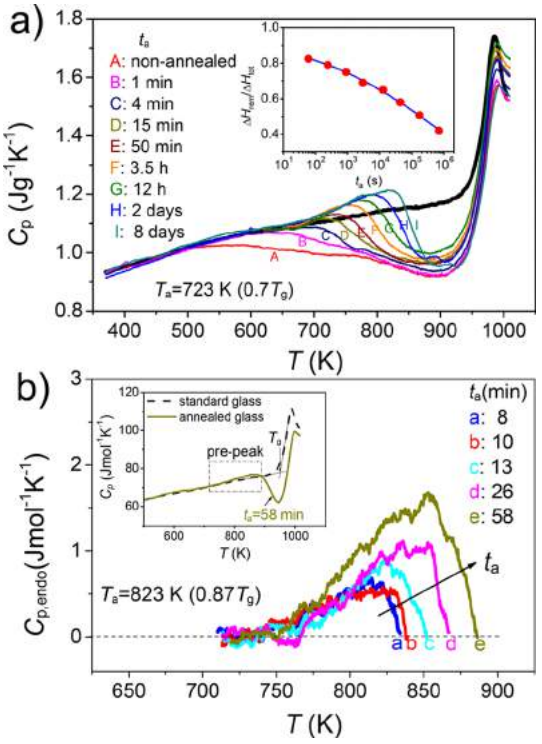

Figure 26. Impact of sub-T_g annealing time (t_a) on the sub-T_g enthalpy relaxation in the stone wool fibers (T_g = 944 K) quenched at 10^6 K/s. (a) C_p curves (obtained from the first DSC upscans at 20 K/min) of the samples annealed at 723 K for various t_a. Black thick curve: the second upscan C_p curve obtained at 20 K/min. The broad C_p peaks above the black curve are termed the prepeak. Inset: The t_a dependence of the remaining excess enthalpy (ΔH_{rem}) after annealing, normalized by the total released enthalpy (ΔH_{tot}), $\Delta H_{rem}/\Delta H_{tot}$. (b) The excess of the heat capacity ($C_{p,endo}$) of the HQ glass annealed at T_a = 823 K for various t_a over that of the "standard glass" within the prepeak region against the upscanning temperature (T). Note: the prepeak ($C_{p,endo}$) is contrary to the exothermic peak ($C_{p,exc}$). All the up and downscans were conducted at 20 K/min. Inset: the C_p curves for both the standard glass (the second upscan curve) and the 58 min-annealed HQ glass (the first upscan curve). The prepeak is indicated by the dashed box, and the sub-T_g exotherm and the glass transition endotherm are illustrated. Reproduced with permission from refs 14 and 301. Copyright 2004, 2005 Nature Publishing Group.

Owing to fluctuations in the glass system, some local domains may reside in energy states lower than that of the standard glass. Thus, in the subsequent DSC upscan, additional energy is needed for these local domains to rejuvenate to the standard state, resulting in the prepeak. The prepeak can be greatly enhanced and shifts to a higher temperature, merging with the glass transition overshoot by further increasing T_a or extending t_a.[81,292,293,296] Remarkably, the prepeak appears even when the HQ glass undergoes a very short t_a, e.g., 8 min annealing at T_a below T_g as shown in Figure 26b. The t_a dependence of the prepeak area of $C_{p,endo}$ is plotted, and the inset demonstrates how $C_{p,endo}$ is obtained.

Yue and Angell studied the glass transition behavior of water by comparison with the sub-T_g relaxation behavior of two HQ oxide glasses.[14,301] They argued that the glass transition around 136 K was likely attributed to the annealing-induced prepeak, which is also termed a "shadow" glass transition in terms of both the jump in C_p at T_g and the activation energy of the apparent glass transition endotherm.[14] However, it should be noted that the assignment T_g of water is still under debate[259,261] since the glass transition of water could not be directly probed due to the intervention of strong crystallization in the temperature region often referred to as "No-Man's Land". Moreover, the correlation between the endothermic prepeak and the structural heterogeneity is reviewed in Section 4.3.1.

The nonexponential decay of the enthalpy relaxation can be described by fitting the enthalpy data (i.e., the remaining enthalpy in the HQ glasses after annealing, normalized by the total released enthalpy) to the stretched exponential function, also known as the Kohlrausch−Williams−Watts (KWW) function,[302−304] from which both the T_a-dependent relaxation time τ and the stretching exponent β can be obtained.[162,295,296] The β value describes the breadth of the relaxation time distribution, reflecting the heterogeneous dynamics of the system. By determining the activation energy for the sub-T_g enthalpy relaxation in the HQ glasses through the relationship between the τ and T_a, Guo et al.[296] inferred that the enthalpy recovery during annealing is mainly due to secondary relaxation.

The abovementioned sub-T_g enthalpy relaxation concerns relatively fragile glass systems. It has been found that the liquid fragility has a profound impact on the enthalpy relaxation behavior in the HQ glasses.[274,305,306] Here we take the HQ GeO_2 glass as an example of a glass derived from a strong liquid, as shown in Figure 27.[274] First, in contrast to the annealed HQ fragile system, the annealed HQ GeO_2 glass exhibits no distinct sub-T_g prepeak in the C_p curve,[274] implying that the strong glass systems involve lower nonexponentiality and less structural heterogeneity.[78] Second, the HQ GeO_2 glass shows a decrease in the sub-T_g exothermic peak area (i.e., the excess enthalpy ΔH) along the y-axis with increasing the annealing degree, i.e., increasing either T_a or t_a (Figure 27), whereas a fragile system displays a decrease of the exothermic peak area along the x-axis (Figures 25 and 26). This indicates the different coupling modes of α and β relaxations upon annealing. Driven by the thermal kinetic energy, GeO_4 tetrahedra collaboratively adjust themselves from their HQ-excited higher energy positions to lower energy and more stable positions. During this process, these structural units are still connected with each other and therefore are influenced by each other, indicating that the cooperative relaxation is a universal feature of strong glass formers.

DOI: 10.1021/acs.chemrev.8b00510
Chem. Rev. XXXX, XXX, XXX−XXX

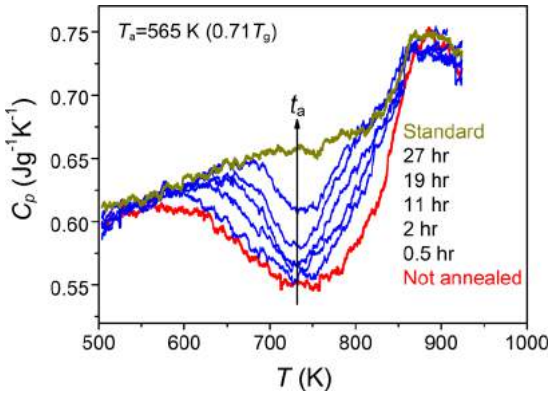

Figure 27. Isobaric heat capacity curves of HQ GeO_2 glasses (fibers) annealed at 565 K (well below T_g = 792 K) for different durations (t_a). Reproduced with permission from ref 274. Copyright 2008 American Chemical Society.

4.1.2.2. Modeling. As reviewed above, DSC is a sensitive method to capture the features of sub-T_g enthalpy relaxation in HQ glasses. However, to gain insights into these effects, it is crucial to establish and apply physical models to simulate or predict the DSC patterns of both HQ glasses and annealed HQ glasses. So far, development of such models has been challenging because of the complexity of the enthalpy relaxation in HQ glasses compared to slowly cooled glasses. As is known, numerous researchers have been making efforts to develop phenomenological or physical models for predicting the C_p curves of the glasses. These efforts have led to remarkable success. For instance, the Tool–Narayanaswamy–Moynihan (TNM) model[70,166,289] and the Adam–Gibbs–Scherer (AGS)[92,177] model have been applied to predict the C_p curves of slowly cooled glasses, which are in good agreement with those determined by DSC. On the one hand, the two models have different expressions for the nonlinear relaxation function; that is, the TNM model adopts Narayanaswamy's nonlinear function,[166] whereas the AGS model includes the Adam–Gibbs function.[92] On the other hand, both models have similarities in two aspects: (1) the response function of the system can be represented by a stretched exponential function; (2) the relaxation time depends not only on real temperature T but also on T_f. However, both models failed to predict or reproduce the C_p curves for both HQ glasses and partially annealed HQ glasses. This was confirmed by the modeling work of Huang and Gupta in 1992 on the sub-T_g enthalpy relaxation in thin glass fibers.[175,307,308] Later on, several research groups attempted to develop phenomenological or physical models for describing the sub-T_g enthalpy relaxation in HQ glasses. In this regard, two modeling studies should be mentioned, which enhanced the understanding of the sub-T_g enthalpy relaxation in HQ glasses, as described below.

The first modeling study of the sub-T_g relaxation in HQ glasses was reported by Giovambattista et al.[309,310] They succeeded in mimicking the difference in enthalpy relaxation between standard and HQ glasses by performing the molecular dynamics (MD) simulations using the extended simple point charge potential. They also obtained the isochoric heat capacity (C_v) curves for the HQ glassy water and the annealed HQ glassy water, which are quite similar to the C_p curves determined by DSC. Even the endothermic prepeak (Section 4.1.2) can be reproduced by the MD simulation for the sub-T_g annealed HQ glasses. The second modeling study was conducted by Hornboell et al. on the HQ glass fibers.[311] To create the DSC C_p curves, they made the following two major modifications to the TNM model.[311]

First, they proposed a composite relaxation function (CRF) to replace the Kohlrausch function. The CRF is written as $M(\xi) = \exp(-\xi^{\beta_c} - \xi)$, where ξ is the reduced time, i.e., the annealing time normalized by the characteristic relaxation time, and β_c is a fitting parameter. This function describes two well-separated distributions of relaxation time. It should be noted that the Kohlrausch parameter β and the CRF β_c parameter have different meanings. β defines the stretching extent of the relaxation time distribution, whereas the CRF β_c does not alone determine the relaxation time distribution, and instead, the sum of ξ^{β_c} and ξ determines it. Moreover, β_c decreases with increasing T_f.

Second, the difference in C_p between glass and liquid was considered to be a temperature dependent variable (ΔC_p) in constructing the relaxation function, and this is in contrast to the Adam–Gibbs' treatment, where ΔC_p is treated as a temperature independent constant. Based on these modifications, Hornboell et al. obtained the C_p curves for both fresh HQ glasses (Figure 28a) and the sub-T_g annealed HQ glasses (Figure 28b), which are in good agreement with those determined by DSC. As shown in Figure 28b, the new approach can also predict the occurrence of the endothermic prepeak. To further increase the modeling accuracy, Zhang et al.[312] considered the difference between the initial annealing and the entire annealing process of HQ glasses. It was shown that the multiexponential relaxation mechanisms for the initial annealing process are crucial for capturing more subtle relaxation processes.

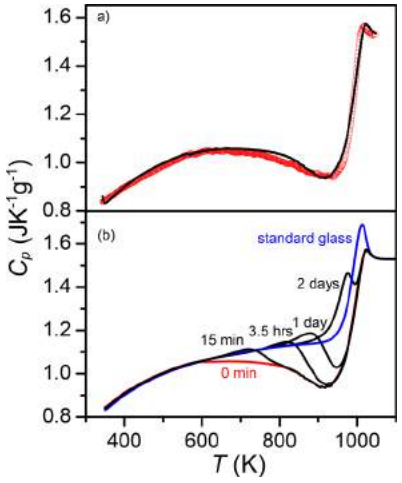

Figure 28. Modeled C_p curves for the HQ E-glass (a) and the HQ glass annealed at 800 K for various durations (b). The DSC upscan rate is 20 K/min. Reproduced with permission from ref 311. Copyright 2010 Elsevier B.V.

As discussed in detail by Mauro et al.,[200] the TNM model is unable to capture the relaxation kinetics of glasses over a wide range of fictive temperatures using a common set of parameters. The limitation is because of the phenomenological functional form assumed by the TNM for the T_f dependence of the relaxation time. This issue was addressed by the new Mauro–Allan–Potuzak (MAP) model for the nonequilibrium dynamics of glasses.[163,200] The MAP model was proposed

DOI: 10.1021/acs.chemrev.8b00510
Chem. Rev. XXXX, XXX, XXX–XXX

based on detailed simulations of the glass kinetics following an enthalpy landscape approach.[200,284] The original MAP model was later extended by Guo et al.,[313] who showed that an improved functional form for the T_f dependence of the glass relaxation time could be derived from the MYEGA equation. This new model showed the deep connection between the equilibrium dynamics of the liquid (as governed by the MYEGA equation) and the nonequilibrium dynamics of the glassy state (governed by the MAP equation). The MAP equation has been further developed to predict the composition dependence of nonequilibrium kinetics.[314] The model has also recently been incorporated into RelaxPy,[315] an open source Python code for calculating the relaxation dynamics of glass systems. The new MAP model could be potentially combined with other modeling approaches including abovementioned ones to predict the C_p curves of both HQ and annealed HQ glasses, which are in better agreement with those determined by DSC.

4.1.2.3. Vibrational Density of States. It is known that the sub-T_g relaxation in HQ glasses has an impact on the atomic vibrational dynamics, which can be described by the vibrational density of states (VDOS) and the boson peak (BP).[15] The BP is a broad peak that represents the excess of VDOS relative to that predicted by Debye theory; it is a fundamental feature of glass found in incoherent inelastic neutron scattering and Raman spectra in low frequencies, e.g., in the 2−10 meV region.[2] The BP may have different sources such as large clusters, nanoparticles, floppy modes, mismatched rings, the rocking of small tetrahedral groups, and connected rings in zeolites.[16] The BP is identified with the intermediate-range order structure in glass, and its intensity depends on temperature, pressure, and the glass type.

Investigation of the vibrational dynamics of HQGs is a good approach for clarifying the origin of the BP since these glasses have much higher potential energy compared to their slowly cooled counterparts.[15] The influence of both hyperquenching and annealing on VDOS can be detected through neutron inelastic scattering measurements, as shown in Figure 29. The $Z(\omega)$ function may be regarded as an approximate representation of the effective VDOS, $G(\omega)$. It is seen that a sharp maximum occurs at ~40 cm^{-1} (5 meV) in the HQ glass. $Z(\omega)/\omega^2$ could be used as a measure of the excess of the VDOS of the HQG relative to that of the standard sample, and hence, the BP is greatly enhanced by hyperquenching. In Figure 29, it is also seen that the BP is lowered by annealing the HQG, i.e., by decreasing T_f. The BP vanishes when the glass crystallizes. There is a distinct configurational excitation, in which low-frequency modes are generated.

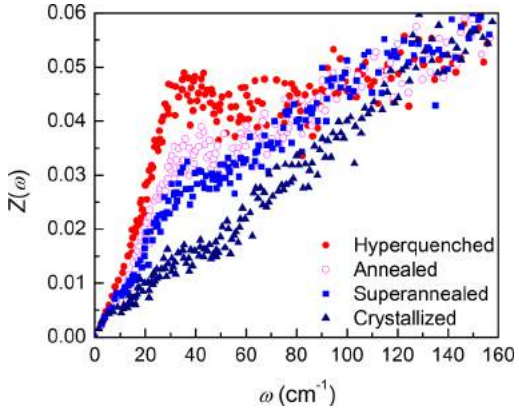

Figure 29. $Z(\omega)$ function (regarded as an approximate representation of the vibrational density of states) versus the frequency of vibration (ω) up to 160 cm^{-1} for a stone wool in hyperquenched, standard-cooled, annealed, and crystalline states, respectively. The annealed glass was obtained by treating a HQ sample for 21 h at 894 K ($0.94T_g$). The crystallized sample was obtained by holding the glass at 1156 K for 150 min. Reproduced with permission from ref 15. Copyright 2003 IOP Publishing.

Different views exist regarding the origin of the enhancement of the VDOS in glasses at low frequencies with increasing T_f. The vibrational properties of both a HQG and a well-annealed glass have been studied using nuclear inelastic scattering.[17,316] As described above, a HQ glass has a higher number of vibrational states in the low-energy region compared to that observed in an annealed glass. However, after rescaling the energy axes in Debye energy units and renormalization of the VDOS peak area, the VDOS values of both glasses become identical. Based on this fact and considering that the decrease in the Debye energy is associated with that in density and sound velocity, the effects of quenching and annealing on the BP could arise from the transformation of the continuous medium. In other words, quenching does not affect the height of the boson peak (i.e., the relative excess of states above the Debye level). According to another study, both the higher heat capacity of a glass compared to its corresponding crystal and the BP itself are not due to structural disorder in glass but instead due to its lower density.[285,317] Thus, the suppression of the BP in a HQ glass by annealing could be ascribed to its increase in density. Moreover, the relationship between BP intensity and density was also studied by performing numerical simulations of several glass-forming systems[318] and by inelastic neutron scattering experiments on zeolites.[319] It was found that the BP intensity is related with lowering of liquid fragility.[319]

4.1.3. Ultrastable Glasses. For traditional melt-quenched glasses, the dynamic slowing-down process upon undergoing the glass transition generally allows the system to be frozen-in at a local minimum with higher energy in the PEL, since the system cannot transition fast enough to find its equilibrium state in the experimental time window. This yields a high degree of instability of the glass. In 2007, Ediger and co-workers invented a kind of ultrastable molecular glass, which exhibits exceptional kinetic and thermodynamic stabilities, through physical vapor deposition routes.[13] Subsequently, additional types of ultrastable glasses emerged.[320−323] These glasses reside in significantly deeper energy minima in the PEL compared to HQ and normally cooled glasses. An ultrastable metallic glass counterpart possessing an enhanced T_g and high elastic modulus was later obtained via a vapor deposition method.[324] The mechanism for ultrastable glass formation is considered to be the fast surface diffusion enabled by the enhanced surface mobility of atoms at free surfaces during deposition.[13] From the relaxation point of view, the surface has faster relaxation kinetics compared to the bulk glass since the ratio of the relaxation time of bulk glass τ_{bulk} to that of the surface $\tau_{surface}$ exceeds 10^5 in the most ultrastable glasses.[325]

Indeed, ultrastable glasses have attracted significant attention and have been extensively studied in recent decades. For instance, Ediger et al. conducted investigations on the variations in structure with deposition process parameters,[323] including the influences of both substrate temperature and the deposition velocity on the stability of glasses.[320,326,327] They

DOI: 10.1021/acs.chemrev.8b00510
Chem. Rev. XXXX, XXX, XXX−XXX

found that the most stable glass can be formed by vapor depositing onto a substrate of about $0.85T_g$, and lower deposition rates enhance the kinetic stability and lower the enthalpy of the glass.[13,326,328]

Using DSC, both the kinetic and thermodynamic stabilities of ultrastable glasses can be evaluated from the onset temperature for molecular mobility and the fictive temperature T_f, respectively. The T_f is determined from the enthalpy of the ultrastable glass, which can indirectly reflect the location depth of the system in the PEL. Figure 30 shows the DSC data for

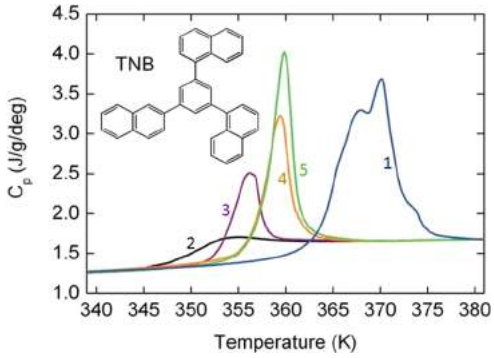

Figure 30. Isobaric heat capacity (C_p) versus temperature for the 1,3-bis-(1-naphthyl)-5-(2-naphthyl)benzene (TNB) glass produced by different methods: vapor deposited at a rate of ~5 nm/s directly into a DSC pan at 296 K (curve 1); the as-produced ordinary glass via cooling the liquid at 40 K/min (curve 2); ordinary glass annealed at 296 K for 174 days (curve 3), 328 K for 9 days (curve 4), and 328 K for 15 days (curve 5), respectively. Inset: structure of TNB. Reproduced with permission from ref 13. Copyright 2008 the American Association for the Advancement of Science.

the TNB glass vapor-deposited onto a substrate at 296 K. Clearly, TNB glass has a substantially higher onset glass transition temperature T_g (363 K), much higher than that of the ordinary melt-quenched glass and even higher than that of the ordinary glass annealed at 328 K for 15 days. The higher T_g of the deposited glass implies its extremely high kinetic stability[13,320,326,327] since more thermal energy is required to overcome the energy barriers to dislodge molecules from their original configurations, i.e., lower minima, in PEL. Furthermore, the deposition process also improves the thermodynamic stability of TNB glass, as confirmed by the enhanced endotherm in the C_p curve compared to those of the ordinary aged samples.[13,320,326,327] This is because the deposited glass resides in the lowest minima in the PEL; as the sample is heated during DSC upscan, more energy is required to overcome different saddle points to transform the glass into supercooled liquids. The energy needed to transform the glass into the supercooled liquid quantifies the thermodynamic stability of the glasses.

As described above, the ultrastable glasses have highly efficient noncrystalline packing and reside in a much lower region of the PEL. It has been estimated that a glass prepared by melt-quenching would require thousands of years of aging to achieve the properties of a glass vapor-deposited onto a substrate at $0.85T_g$.[320] An interesting question arises: if the deposited glass is already ultrastable, does it relax further? Yu et al. performed *in situ* dielectric measurements to compare the relaxation dynamics between the ordinary glass and the as-deposited stable toluene glass.[329] As expected, the β relaxation of the deposited glass is highly suppressed due to the fact that the ultrastable glass with highest kinetic stability is already very close to the long-sought "ideal glass" in terms of potential energy.[329]

In this case, can annealing at a temperature above T_g induce relaxation of the ultrastable glass? If so, in what manner does it relax? Before answering these questions, we first consider one of the intriguing features in the C_p curve of the ultrastable glass, viz., the occurrence of the double-peaked pattern for the transformation from the low-enthalpy glass to higher enthalpy supercooled liquid.[320] This double-peaked pattern suggests the existence of two different noncrystalline packings with different stabilities in this system. That is, during the DSC upscan, the transformation of the glass to liquid results from two different types of molecular packing.

Therefore, studying the relaxation of the ultrastable glasses is an effective route to understand the polyamorphism in a glass-forming system. A typical example of the heat capacities C_p for vapor-deposited indomethacin glasses is shown in Figure 31,[330]

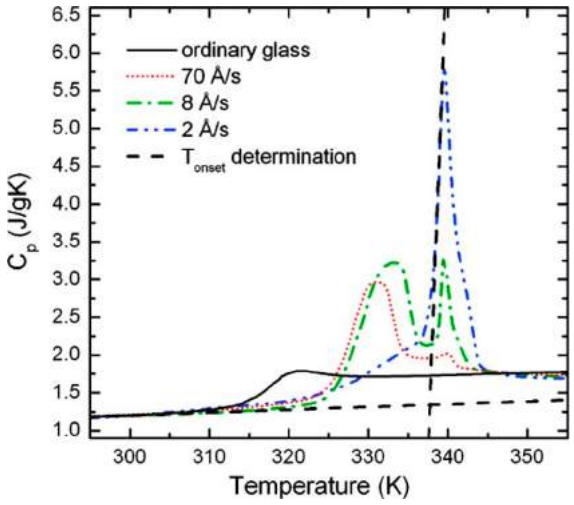

Figure 31. Isobaric heat capacities (C_p) for vapor-deposited indomethacin glasses, which were produced by different deposition rates: 70 Å/s (dotted, red), 8 Å/s (dash-dot, green), and 2 Å/s (dash-dot-dot, blue), measured by conventional DSC. The substrate temperature was 265 K for each deposition. Solid black line: Ordinary indomethacin glass, produced by cooling the liquid at ~40 K/min. The determination of the onset temperature of the glass transition, T_{onset}, is illustrated for the 2 Å/s deposited glass (as an example), and T_{onset} is the temperature of the intercept between the extrapolated glass C_p curve and the tangent line of the rapidly rising C_p (dashed black lines). Reproduced with permission from ref 330. Copyright 2008 American Chemical Society.

which illustrates that the double-peaked pattern (enthalpy overshoots in C_p curve) strongly depends on the deposition rate. The area ratio of the lower temperature peak to the higher temperature peak decreases with decreasing deposition rate, implying an increase in the degree of high-stability packing. For a specific glass system, the critical deposition rates for obtaining glasses with higher or lower stability packing can be determined from the double-peaked structure.[331]

Sepúlveda et al. conducted a systematic study on the sup-T_g relaxation (i.e., relaxation above T_g) of vapor-deposited ultrastable glassy films of toluene.[331] Figure 32 shows the C_p curves of the stable vapor-deposited toluene films annealed at different temperatures above T_g for different times t_a.[331] It should be noted that the original vapor-deposited toluene films

DOI: 10.1021/acs.chemrev.8b00510
Chem. Rev. XXXX, XXX, XXX−XXX

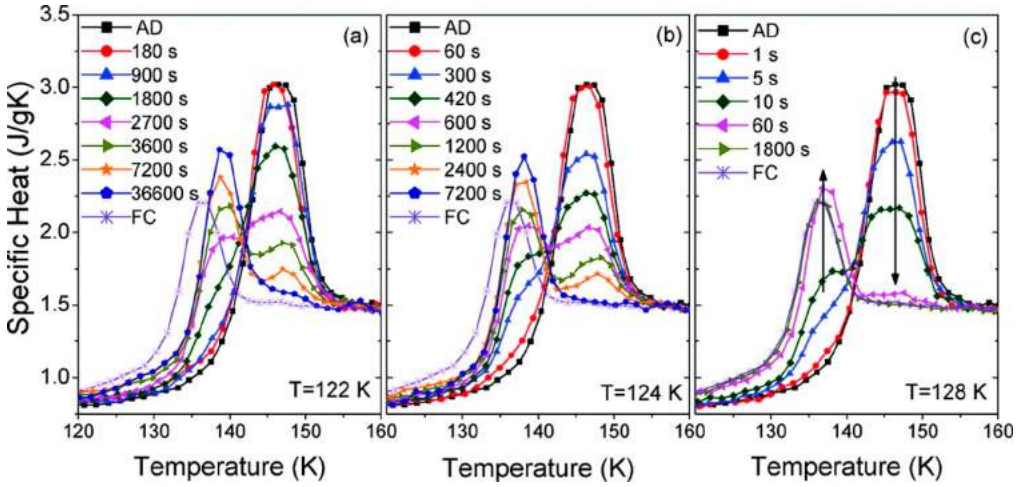

Figure 32. Specific heat for stable vapor-deposited toluene films annealed at T_a = (a) 122, (b) 124, and (c) 128 K for the different durations as a function of temperature. The lines provide guidance to the eye. Vertical arrow in (c): the direction of the increasing annealing time. AD: the as-deposited highly stable glass; FC: the glass obtained after refreezing the supercooled liquid at ~700 K/s. Reproduced with permission from ref 331. Copyright 2008 American Chemical Society.

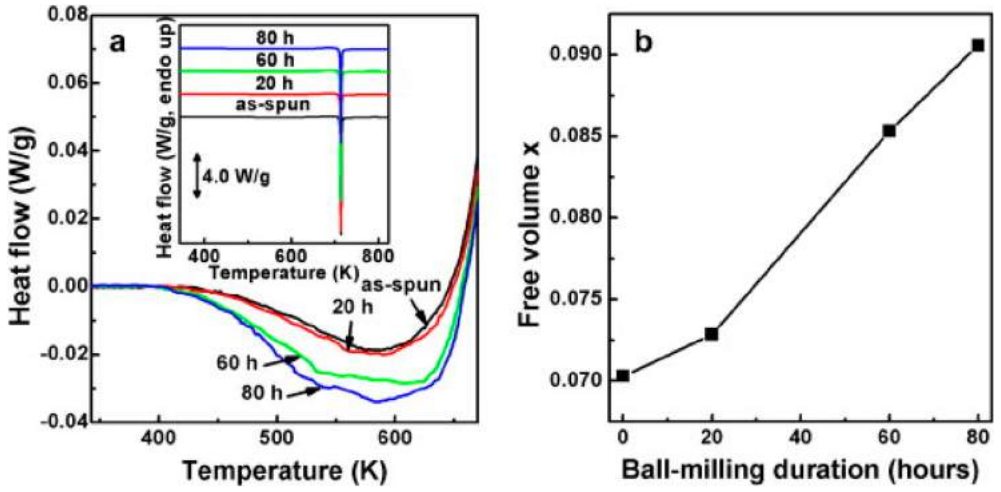

Figure 33. (a) DSC output (heat flow) as a function of temperature, showing the sub-T_g enthalpy relaxation peak and the entire DSC curves including the crystallization peaks (inset) for the samples ball-milled at 120 rpm for different durations. (b) Free volume x in the $Zr_{70}Cu_{20}Ni_{10}$ sample at room temperature as a function of ball milling duration. Reproduced with permission from ref 337. Copyright 2012 Elsevier B.V.

are highly ultrastable and this is confirmed by the appearance of only the higher temperature endothermic peak in the C_p curve. Two significant findings were achieved: (1) with increasing t_a, there is a clear evolution from the initial highly stable glass toward a less stable glass; and (2) with increasing T_a, the stability of the vapor-deposited glass above T_g is more drastically lost.

The sup-T_g annealing provides additional energy to the original ultrastable glass system so that it can be brought from deeper minima of PEL to higher minima. During annealing, the ultrastable glasses gradually evolve from a higher stability packing to a mixture of a partially equilibrated liquid and a remnant vapor-deposited glass. This indicates that a liquid−liquid transition occurs between the highly stable vapor-deposited glass and the low-density supercooled liquid. In addition, with the aid of secondary ion mass spectrometry experiments, Swallen et al.[332] found that the stable glass transformation to supercooled liquid upon sup-T_g annealing started from the surfaces and interfaces, i.e., via a propagating front initiated at the free surface. Despite substantial progress, more studies need to be done for a deeper understanding of both the sup-T_g relaxation of the ultrastable glasses and its structural origin.

4.1.4. Milling Amorphized Materials. The high-energy ball milling approach was first used for producing amorphous metallic alloys about four decades ago.[333−335] It was reported that the physical properties, e.g., the Curie temperature and magnetic moment,[334] changed gradually with the formation of the amorphous structure during ball milling of the starting crystalline powder particles. The ball-milling approach has been widely employed to prepare the amorphous metallic alloys[336,337] and much less so to produce molecular glasses[338,339] and inorganic nonmetallic glasses.[340,341] The mechanisms for the formation of the amorphous state by ball milling have been proposed, e.g., introducing impurities[335] and enhancing the free volume.[337] During the ball milling process, the local strain caused by the mechanical activation progressively lowers both the crystal size and the degree of order, leading to the formation of the amorphous state in which a fraction of the strain energy can be stored.[337,338] As

DOI: 10.1021/acs.chemrev.8b00510
Chem. Rev. XXXX, XXX, XXX−XXX

shown in Figure 33, a pronounced sub-T_g relaxation peak appears during a DSC upscan of the ball-milling derived metallic glass ($Zr_{70}Cu_{20}Ni_{10}$).[337] The exothermic peak becomes larger with the increasing milling time, implying that more and more energy was introduced into the metallic glass by the ball milling process. That is, the ball-milling process brought the metallic glass to a higher energy state in the PEL with a higher T_f.[3,94] The ball milling technique can both induce amorphization of crystals and convert a standard glass state to an excited state with the relaxation features of a HQ glass, i.e., having a higher T_f. A typical example is the indomethacin glass; after 6-day annealing at 25 °C, the enthalpy released during annealing can be rejuvenated by the high energy cryomilling.[339]

As reviewed in Section 4.1.2, the sub-T_g endothermic prepeak in the C_p curve prior to the exothermic peak is one of the typical features of the annealed fragile HQ glasses.[14,81,293,294,296,300] Likewise, the sub-T_g endothermic prepeaks were also observed in the C_p curves of the ball milling amorphized solids after annealing, e.g., the amorphous trehalose[339] and the amorphous Ag_3PS_4.[341] Moreover, the endothermic prepeak gradually shifts to a higher temperature until it merges with the glass transition overshoot, resulting in a significant increase of the glass transition peak, with increasing the degree of annealing.[339] Note that for the molecular glasses, the higher energy amorphous state can be achieved by ball milling either from a crystalline or an amorphous state with lower energy state.[339]

A striking relaxation phenomenon was found by Kim et al.;[338] that is, the sub-T_g endothermic prepeak appeared in the C_p curve of the as-milled glassy starch without any annealing, but it increased with the increasing milling time. This is quite different from the enthalpy relaxation in the HQ glass. The difference is attributed to the fact that the structure of the glassy starch formed by milling is much more heterogeneous than the HQ glass. The real dynamics behind the appearance of the endothermic prepeak during ball milling needs further experimental verification.

Ang et al. reported the sub-T_g enthalpy relaxation in a milling amorphized chalcogenide.[341] The enthalpy relaxation in the milling amorphized Ag_3PS_4 (Figure 34) was found to significantly differ from that of the HQ oxide glasses (Figure 35) in three aspects. First, two decoupled peaks were observed (rather than one) due to the energy released in the C_p curve of the amorphous Ag_3PS_4. The two peaks were linked to the β and α relaxations, respectively, corresponding to different microstructures. Second, the occurrence of the endothermic prepeaks with a high degree of annealing indicates the high nonexponentiality of the sub-T_g enthalpy relaxation and, thus, the high structural heterogeneity of the milling amorphized Ag_3PS_4. Third, the weaker bonds in the amorphous chalcogenides compared to oxide glasses (Figure 34) resulted in the release of its excess energy at a temperature even below the onset temperature of the dynamic heating induced energy release peak.

Despite some progress in understanding the ball-milling induced amorphization, several key questions remain. For instance, how does the ordered structure evolve into the disordered structure during high-energy ball milling? What is the glass formation mechanism when cryomilling an annealed sample? How will the cryomilled sample, i.e., the rejuvenated sample from the annealed one, relax below T_g? Answering these questions will serve as interesting topics for future

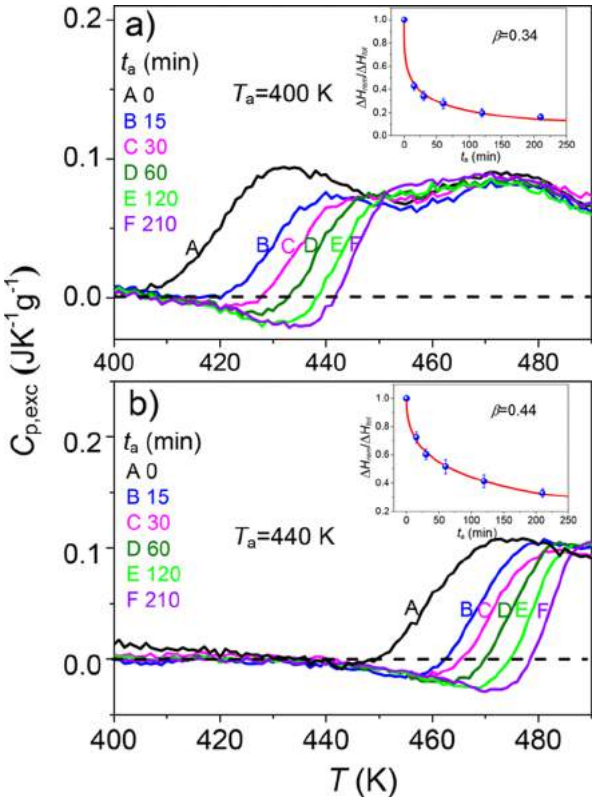

Figure 34. Annealing time (t_a) dependences of the excess heat capacity $\Delta C_{p,exc}$, which is the difference in C_p between the second and the first DSC upscans, for the amorphous Ag_3PS_4 samples annealed at the temperatures (T_a) of 400 K (part a) and 440 K (part b). Insets: The t_a dependence of the remaining excess enthalpy (ΔH_{rem}) after annealing, normalized by the total released enthalpy (ΔH_{tot}), $\Delta H_{rem}/\Delta H_{tot}$, of the samples heated to 400 K (part a) and 440 K (part b), respectively.[341] Red solid curves: fits of the $\Delta H_{rem}/\Delta H_{tot}$ data to the KWW function. Reproduced with permission from ref 341. Copyright 2016 the American Ceramic Society.

research. In fact, it is still an open issue whether these milling derived materials are glassy, or purely amorphous, since they do not show α-relaxation, a glass transition event, and viscous flow. To the best of our knowledge, there is no report showing a clear glass transition peak in a DSC curve of milling-amorphized chalcogenides. It is still a challenge to directly access the viscosities of these materials above the onset temperature of recrystallization.

4.1.5. Stretched Glasses. Anisotropy in glass can be induced by application of external stresses or compression in glass melts that may be frozen-in by cooling under load.[342−345] For instance, a certain degree of preferred structural orientation along the direction of the glass fibers can be generated by the axial stresses during the hyperquenching process.[342] Mechanical quenching (i.e., slowly cooling under uniaxial compression) from a temperature above T_g can lead to a frozen-in anisotropic structure in a glass cylinder.[343] If the pressure is sufficiently high, non-Newtonian flow, i.e., shear thinning, can occur.[345] The anisotropy in the metallic glass is usually caused by the residual stresses developed during a rapid quenching process.[346] The laser light can also give rise to optical anisotropy in glass.[347]

Glass fibers undergo both thermal quenching and mechanical stretching during the fiber draw process. The enthalpy relaxation of glass fibers has been extensively studied by means

DOI: 10.1021/acs.chemrev.8b00510
Chem. Rev. XXXX, XXX, XXX−XXX

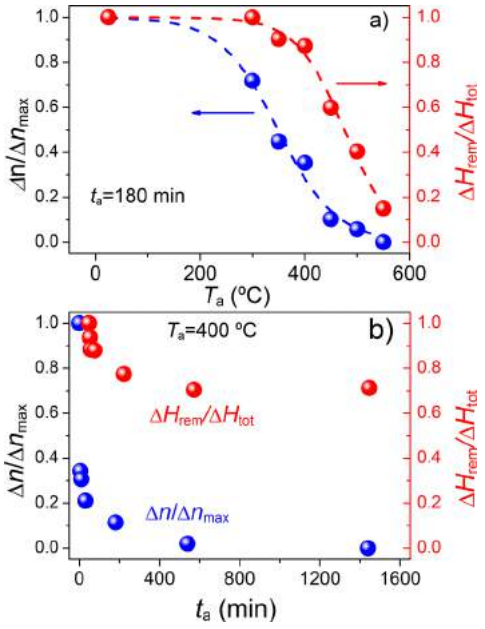

Figure 35. Comparison between the anisotropy relaxation index ($\Delta n/\Delta n_{max}$) and the enthalpy relaxation index ($\Delta H_{rem}/\Delta H_{tot}$) for E-glass fibers with a diameter of 9.3 mm. Δn and Δn_{max} are the optical birefringences of both the annealed fibers and the unannealed fibers, respectively, which are a measure of the glass structural anisotropy. ΔH_{rem} and ΔH_{tot} have the same meaning as that described in the caption of Figure 34. (a) The annealing temperature (T_a) dependence for the duration of t_a = 180 min. (b) The t_a dependence at T_a = 400 °C. Dashed lines: best fits of cumulative distribution functions through the $\Delta n/\Delta n_{max}$ and $\Delta H_{rem}/\Delta H_{tot}$ data. Reproduced with permission from ref 342. Copyright 2007 the American Ceramic Society.

of the HAD method (Section 4.1.1). However, only a few studies have been performed with regard to anisotropy relaxation in glass fibers and its impact on enthalpy relaxation.[342,348−350]

Anisotropy in glass is mainly characterized by optical birefringence. The sub-T_g anisotropic relaxation, also called birefringence relaxation, in oxide glass fibers, was studied by Lu et al.[348] They proposed a phenomenological-modified stretched exponential to describe the time-dependent birefringence relaxation. To quantitatively evaluate the contribution of relaxation in stretching-induced anisotropy to the total enthalpy relaxation of the glass fibers, Martin et al.[349] conducted a DSC study on the enthalpy relaxation in a mechanically stretched calcium metaphosphate glass rod with one-dimensional (chain-like) network structure, i.e., in a glass rod that was stretched using a given stress at a temperature slightly above T_g and then cooled slowly. They found that the mechanically induced excess enthalpy increases with increasing tensile stress.[349] The energy release caused by the anisotropy relaxation of the isothermally stretched silicate glass fibers with a three-dimensional network structure was detected using DSC.[350] This implies that the mechanical strain can excite the system to a higher energy state in the PEL. However, the mechanical stretching-induced energy was much lower than that induced by thermal hyperquenching.[350] Moreover, the increase of the optical birefringence with increasing tensile stress displays a similar trend to that of the excess enthalpy with increasing quenching rate.

Ya et al.[342] investigated the structural origins and mechanisms for both enthalpy and anisotropy relaxations of the glass fibers. For the E-glass fibers, the birefringence relaxation is much faster than the enthalpy relaxation for the same extent of annealing, i.e., for comparable T_a and t_a (Figures 35a and b). This pronounced difference indicates that the structural origins of the anisotropy and enthalpy relaxation are different. The birefringence relaxation was attributed to the relaxation of local anisotropic structure units, whereas the excess enthalpy relaxation was associated with the cooperative rearrangement of the frozen-in isotropic network. Deubener et al.[351] further addressed this issue by studying the optical birefringence and the enthalpy relaxation in E-glass. They observed a sharp decoupling of birefringence relaxation and viscous relaxation, i.e., a large discrepancy between the activation energies for optical recovery and viscous flow at the glass transition by conducting both annealing and viscometric experiments on both fibers and bulk E-glasses, respectively. According to their results, the sub-T_g enthalpy relaxation arose from contributions of α and β relaxations, while the birefringence relaxation had an intimate connection to the γ-relaxation, which is significantly faster than β relaxation. Investigating the anisotropic relaxation in glass is a crucial way to understand the fast relaxation process, i.e., γ-relaxation, and to clarify the significantly higher tensile strength of thin glass fibers compared to bulk glass with the same composition.[178]

4.2. Primary and Secondary Relaxations

4.2.1. Identifying Relaxation Modes. The glass transition results from the ratio of the primary (α) relaxation in supercooled liquids to that of an external observation time scale (i.e., the Deborah number). Significant attention has been focused on the α relaxation process in order to understand the glass transition phenomenon.[271] However, in recent years the search for the secondary (β) relaxation has been a topic of much interest[274,287,293,296,352−356] since it was believed to have an intrinsic correlation with the glass transition and was considered as the basic mechanism for α relaxation.[18,19,357] It is generally considered that the primary (α) and secondary (β) relaxations are the two main relaxation processes in glasses and supercooled liquids.[2,183] Specifically, the α relaxation involves a long or medium range cooperative motion of atoms, which is directly related to viscous flow and, therefore, to the glass transition itself.[358] However, as the α relaxation is frozen well below T_g, the β relaxation process, which initiates at high temperature, still continues. β relaxation corresponds to localized and fast molecular motions in the glassy state, occurring on a shorter time scale compared to the primary (α) relaxation modes. β relaxation is a universal phenomenon of glassy dynamics.[19] However, as mentioned in Section 4.1.5, β relaxation is much slower than γ relaxation and the latter is associated with the even more localized structural relaxation.

Here, it should be mentioned that the secondary relaxation usually includes contributions from both fast and slow β relaxation modes. The fast β relaxation was reported to evolve with only intramolecular motion and plays no important role in affecting the glass transition.[358] Here, we focus on the slow β relaxation, i.e., the Johari−Goldstein (JG) relaxation in glass, which was discovered by Johari and Goldstein in 1970 by performing dielectric measurement on glasses made from rigid molecules.[18] The JG relaxation is believed to be a precursor to α relaxation and, hence, is related to the glass transition. The

DOI: 10.1021/acs.chemrev.8b00510
Chem. Rev. XXXX, XXX, XXX−XXX

JG relaxation is a universal property of glasses and other disordered materials. Fragile glass systems exhibit a distinct JG relaxation peak in dielectric loss curves. However, in strong systems, neither a JG peak nor a JG shoulder is observed; an excess wing is nevertheless exhibited. Using the HAD approach, it was found the strong GeO_2 glass former relaxes in the manner that all the secondary (β) relaxation units contribute to the α relaxation.[274] Some researchers attributed the lack of the JG peak in strong glass systems to the fact that the characteristic JG relaxation time, τ_{JG}, is not much shorter than the α relaxation time, τ_α or that the JG peak is too small. However, some researchers assume that the JG relaxation does not occur in strong glass systems at all. Hu and Yue detected the occurrence of JG relaxation in the typical strong glass former GeO_2 by using the HAD approach.[274] Despite considerable progress in studying the dynamic properties of the JG relaxation, the physical nature of the local JG motion is still far from being understood, especially in inorganic systems.

Here we briefly describe how to identify the JG relaxation in glass by using the HAD approach, choosing a metallic glass former (i.e., the HQ $La_{55}Al_{25}Ni_{20}$ glassy ribbons) as an example.[287] As shown in Figure 36a, the sub-T_g enthalpy relaxation behavior of the glass was characterized by conducting sub-T_g annealing at various temperatures (T_a) prior to the DSC scans. The annealing time (t_a) dependence of the normalized remaining enthalpy ($\Delta H_{rem}/\Delta H_{tot}$) was determined at different T_a below T_g and subsequently was fit to the KWW function for each T_a to find the characteristic time (τ_β) and the stretching exponent (Figure 36b). Afterward, the characteristic time τ_β was plotted against $1/T$ to determine the activation energy for the relaxation by linear fitting as depicted in Figure 36c. This activation energy was found to be 110 kJ/mol, being quite close to the average value of $26.1RT_g$ for the glass formers exhibiting the β relaxation, indicating that β relaxation is involved in the $La_{55}Al_{25}Ni_{20}$ glass. Hence, Hu and Yue used E_β to refer to the activation energy determined above. Combined with a dynamical mechanical analysis, they calculated the E_β/RT_g values for 17 metallic glass systems (Figure 37), the average of which was within the empirical relation ($E_\beta = 24RT_g$) of the JG relaxation found in polymers, small molecules, and ionic liquids.[359,360] The E_β values of GeO_2 glass and As_2S_3 glass are plotted in Figure 37 and are close to $E_\beta = 26.1RT_g$ for JG relaxation of metallic glasses, indicating that they display the nature of JG relaxation. In addition, Wang et al. found experimental evidence for the existence of the JG relaxation in the fragile $Pd_{40}Ni_{10}Cu_{30}P_{20}$ glass[361] and in other La-based bulk metallic glasses[362] through dynamic mechanical measurements.

4.2.2. Oxide Glasses. According to previous studies,[191,274,305,306] the liquid fragility index (m) has a significant effect on the sub-T_g enthalpy relaxation in the glasses. In particular, the correlative degree between the α and β relaxations is closely associated with the liquid fragility. Yue found that strong systems (e.g., SiO_2 and GeO_2) relax in a structurally cooperative manner, whereas the fragile ones (e.g., basaltic and calcium metaphosphate glasses) do in a structurally independent fashion.[305] In addition, the α and β relaxations in HQ glasses of different fragilities have been explored by using the HAD method in the past decade.[274,287,293,296,306,356]

Figure 38 shows the effect of the annealing temperature T_a on the enthalpy relaxation of two fragile (basaltic and calcium metaphosphate systems) and two strong systems (SiO_2 and GeO_2).[305] The enthalpy relaxation patterns can indirectly reflect the different relaxation mechanisms, i.e., the α and β

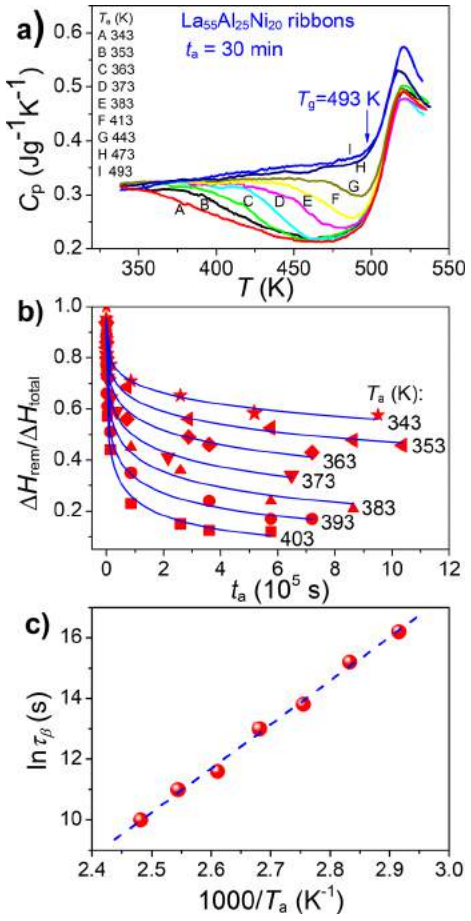

Figure 36. (a) C_p curves of $La_{55}Al_{25}Ni_{20}$ glass ribbons annealed at different temperatures T_a for t_a = 30 min. (b) Annealing duration (t) dependence of the normalized remaining excess enthalpy (H_{rem}/H_{tot}) in glass ribbons annealed at various T_a below T_g = 413 K. The solid lines are the fits of the data to the KWW function. (c) Dependence of the characteristic relaxation time (τ_β) of the secondary relaxation on the reciprocal annealing temperature ($1/T_a$). Dashed line: the fit of the $\tau_\beta \sim 1/T_a$ relation to the KWW function. Reproduced with permission from ref 287. Copyright 2009 American Chemical Society.

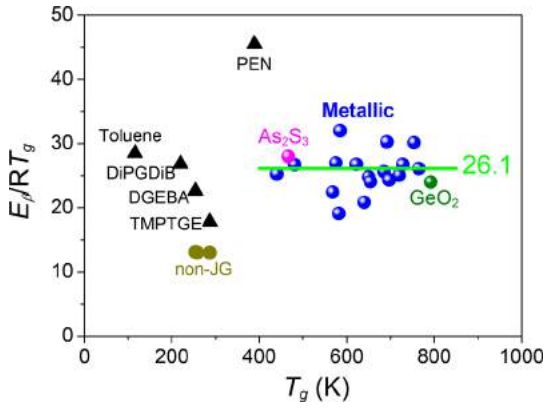

Figure 37. Values of E_β/RT_g versus T_g for different types of glass systems, such as molecular, chalcogenide, oxide, and metallic glasses. The average value of E_β/RT_g is calculated to be 26.1 for 17 metallic glasses (green curve). Reproduced with permission from refs 274, 287, and 363. Copyright 2009 American Chemical Society.

DOI: 10.1021/acs.chemrev.8b00510
Chem. Rev. XXXX, XXX, XXX−XXX

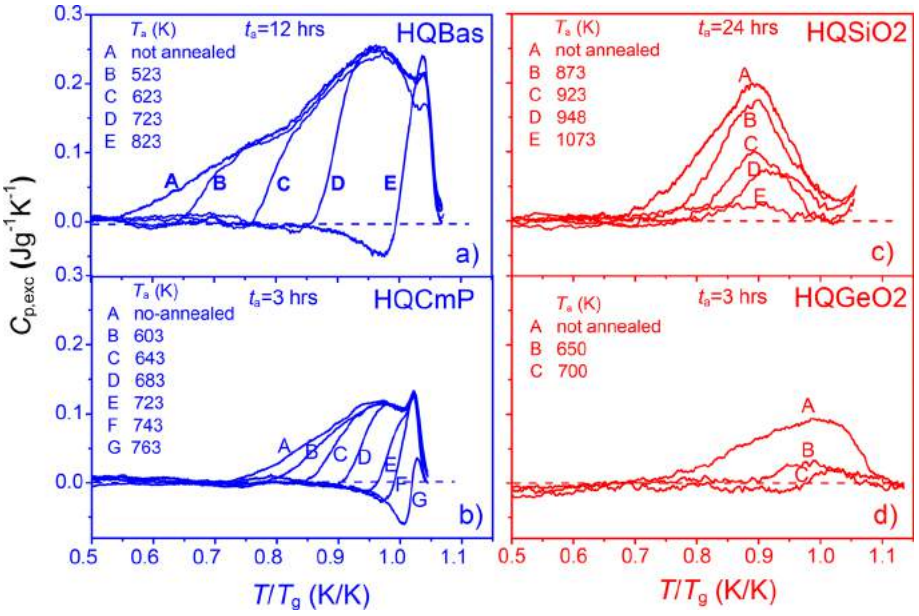

Figure 38. Effect of the annealing temperature T_a on the excess heat capacity $C_{p,exc}$ as a function of T/T_g for a given annealing duration t_a. Left panel (fragile systems): (a) HQ basaltic glass (HQBas); (b) HQ calcium metaphosphate (HQCmP). Right panel (strong systems): (c) HQ silica ($HQSiO_2$); (d) HQ Germania ($HQGeO_2$). The dash lines represent the $C_{p,exc}$ (as reference) of the samples cooled at the standard cooling rate of 20 K/min. Reproduced with permission from ref 305. Copyright 2015 Frontiers in Materials.

relaxations, for the glass systems with different fragilities. Obviously, the β relaxation, which usually appears at the low-temperature side, is superimposed onto the broad sub-T_g exothermic relaxation pattern. In other words, the exothermic peak with the long tail in the excess heat capacity ($C_{p,exc}$) curve is caused by the combined β and α relaxations.[274,287,293,296,306,357] The method for distinguishing between α and β relaxation modes is different between the fragile and strong glass systems. For the fragile systems (see Figure 38a and b), the asymmetrical pattern of enthalpy relaxation indicates an overlap of two domains of relaxation modes. The shoulder at a lower temperature is suggested to correspond to the β relaxation while the main peak at the higher temperature is attributed to the primary α relaxation.[293] With increasing sub-T_g annealing degree, the enthalpy recovery during annealing is mainly due to the β relaxation.[296] When the T_a is close to T_g, in addition to β relaxation, the α relaxation begins to contribute to the enthalpy recovery.[296]

In comparison, for the strong glass systems, as shown in Figure 38c and d, no shoulders are observed in the $C_{p,exc}$ curve. This phenomenon is similar to the lack of a JG relaxation peak or shoulder in the dielectric loss spectrum. With increasing T_a (below T_g), the $C_{p,exc}$ peak decreases vertically in the peak height.[274,305] That is, the shift of the $C_{p,exc}$ peak in the β relaxation region is accompanied by that of the α relaxation region. The relaxation unit involved in the β relaxation process contributes to the α relaxation process.[274] This phenomenon can be explained in terms of the PEL since the shape of the basin in which the glass is trapped depends on the fragility of the glass liquid.[273] For a strong liquid, the secondary relaxation and the primary relaxation generally occur in the same metabasin[1] in the so-called "no β without α" picture.[364] The degree of the overlap between the α and β relaxations is higher for the strong glass formers than that for the fragile glasses.[15]

In addition to the qualitative perspective, β relaxation was also quantitatively determined in both fragile and strong glass systems. By studying the sub-T_g enthalpy relaxation of the basaltic glasses, Guo et al. found the activation energy for the structural relaxation to be 212 kJ/mol (=25.5RT_g),[296] which accords with the empirical relation (E_β = 26 ± 2RT_g) for the JG relaxation.[359,365,366] By using the HAD method, Hu et al. discovered two typical features of the JG relaxation by exploring the sub-T_g enthalpy relaxations in the strong GeO_2 glass.[274] First, the relation between E_β and T_g, E_β = 23.5RT_g, agrees well with the empirical one of the JG relaxation, i.e., E_β = 24RT_g found in polymer and small molecules.[15,365] Second, the characteristic β relaxation time of the GeO_2 glass at T_g is found to be about 10 s, longer than that of relatively fragile systems, but not much shorter than the α relaxation time at T_g (i.e., about 40∼60 s for most oxide systems). This is why the JG peak in strong glass systems is hidden in the α peak of the dielectric loss curves.

4.2.3. Metallic Glasses. The α and β relaxations, particularly the latter, in metallic glasses (MGs) have been studied using various techniques[189,287,367−369] to seek both the universal features of β relaxation and its correlation with many physical properties in the glassy state. Metallic glasses are an important object for studying the universal features since their structure is atomically simple, constituted by dense random packing of hard spheres as their basic building units and free of intramolecular degrees of freedom.[370,371] As discussed above, α relaxation is characterized by the non-Arrhenius temperature dependence and vanishes below T_g, whereas the β relaxation is described by an Arrhenius relationship and can survive in the low-temperature glassy state.[372] The experimental results from both the dynamic-mechanical analysis (DMA)[373] and the DSC methods[189,287,367] have confirmed the inherent competition between the two relaxation modes in the metallic glass-forming liquids.

By combining DSC with other techniques, it was found that the competition between the α and β relaxation modes in metallic glasses was closely correlated both with the dynamic fragile-to-strong (F-S) transition in the supercooled liquid[101,172,189] and with mechanical properties such as the

DOI: 10.1021/acs.chemrev.8b00510
Chem. Rev. XXXX, XXX, XXX−XXX

Poisson's ratio.[319,367] Such competition is generally characterized by a parameter r, i.e., the ratio between the activation energies for the α and the β relaxations (E_α/E_β).[367] The E_α and E_β values for the MGs can be determined by DSC,[189,367] DMA,[373] and dielectric spectra.[359] Sun et al.[189] found an inverse exponential relationship between the extent of the F−S transition extent and the relaxation competition parameter r. This implies that the F−S transition is closely associated with the decoupling of the slow β relaxation from the α relaxation when dropping to a critical temperature. Combining the DSC with the acoustic measurement, it was found that E_α/E_β of metallic glasses was intimately related to the glass ductility reflected by the Poisson's ratio.[367] These findings[189,367] suggested that r could be used as an indicator of glass ductility and a measure of the structural heterogeneity in supercooled liquids.

β relaxation is the most important relaxation process in the metallic glassy state and has aroused much scientific attention since it can assist the self-diffusion of the smallest constituting atoms,[374] trigger the activation of the shear-transformation-zones[366] and spatial heterogeneity,[299] as well as aid in understanding the mechanisms of plastic deformation of MGs.[375] It has recently been shown that a better understanding of the β-relaxation is helpful for explaining numerous unresolved issues in glass science.[357,358,373,376]

The β relaxation in the metallic glasses can be affected by many factors, e.g., physical aging,[377] composition,[378] and hence the liquid fragility,[353,379] as well as T_f.[353] By using mechanical spectroscopy, Qiao et al. investigated the influence of physical aging on the β relaxation in $La_{60}Ni_{15}Al_{25}$ bulk metallic glass.[377] Yu et al.[378] systematically studied the effect of chemical composition on β relaxations in several MG systems and formulated a general rule that the pronounced β relaxations are associated with systems where all the atomic pairs have large similar negative values of enthalpy of mixing while the positive values of enthalpy of mixing suppress β relaxations. Moreover, Yu et al.[379] also found a correlation between fragility m and the degree of separation between α relaxation time τ_α and β relaxation time τ_β in the metallic glass-formers by using dynamical mechanical spectroscopy (DMS). As described in Section 4.2.1, the activation energy of β relaxation (E_β) can be determined by the HAD approach.[274,287] Recently, Hu et al.[353] developed a new hyperquenching-calorimetry (HC) approach to determine the activation energy of β relaxation (E_β) based on the inherent connection between the slow β relaxation and sub-T_g enthalpy relaxation in several metallic glasses. The new HC approach is efficient since it avoids the series of long-time annealing processes required in the HAD method. The core of the new HC method is to determine the critical fictive temperature ($T_{f,c}$), at which E_β is equal to the activation energy of the onset of the sub-T_g enthalpy relaxation of metallic glasses, that is, to find the critical cooling rate for formation of a metallic glass with $T_{f,c}$, at which the structural units hop cooperatively across the subset of basins involved in the JG relaxation. A linear relationship between $T_{f,c}/T_g$ and m manifests the connection between the contribution of the JG relaxation to the entire relaxation process and the liquid fragility of supercooled liquids. The β relaxation was identified to have a connection to the evolution of both the shear transformation zones and the localized flow units,[366,367,380] which is a critical factor influencing the plastic deformation of MGs. Moreover, the β relaxation was also found to have similar activation energy as the self-diffusion of the smallest constituting atoms,[374] the spatial heterogeneity,[299] as well as the irreversible sub-T_g endotherm from TMDSC results.[381] The β relaxations (measured by DMS) and the hopping motions of P atoms (probed by NMR) in the $Pd_{40}Ni_{10}Cu_{30}P_{20}$ glass occur in the same temperature and frequency ranges with the same activation energy, suggesting that the β relaxation relates with the diffusive motions of the smallest constituting atoms in MG.[374] This correlation provided new insights into the structural origin of β relaxation and the mechanism of diffusions in MGs. By combining the DSC measurements with amplitude-modulated AFM measurements, both the characteristic relaxation times and the activation energy of the spatial heterogeneity dynamics were found to be in good accordance with those of the β relaxation, verifying the intrinsic correlation between local structural evolution and the β relaxation.[299]

The microscopic connection between structure and dynamics of MGs provides compelling evidence of the structural origin of β relaxation and has important implications for what governs the mechanical properties and dynamics of MGs. These studies of MGs provide a promising route to understand fundamental issues in glassy physics and materials science.

4.2.4. Molecular Glasses. During the formation of molecular glass systems, the supercooled liquid state involves a high degree of molecular complexity. Moreover, molecular glasses possess a readily controllable structure with a broader range of building blocks compared to strong systems. In the glassy state, the molecular systems relax toward thermodynamic equilibrium during the structural relaxation process, during which two kinds of motions are always detectable: a cooperative motion associated with the α relaxation[183] and a subsegmental relaxation associated with the β relaxation, such as the reorientation of an ester side group.[382] The investigations of the enthalpy relaxation in molecular glasses have led to considerable success because of their structural peculiarities compared to metallic glasses and network glasses. For instance, the existence of the JG process was first confirmed in rigid molecular glasses without the relevant internal molecular (intramolecular) degrees of freedom.[18] Subsequently, it was demonstrated by its ubiquitous presence in different glass formers, such as simple organic molecular liquids,[383] polymers,[384,385] inorganic oxide glasses,[274,296] and metallic glasses.[287]

The relaxation dynamics (in particular, the α and β relaxations) of molecular systems have been widely studied by many techniques including dielectric spectroscopy,[386,387] NMR,[387,388] thermally stimulated depolarization current (a dielectric-related technique),[389] light-scattering spectroscopy,[390] as well as DSC.[354,355] Among these techniques, dielectric spectroscopy and DSC are the most commonly used. For instance, the studies of many different kinds of molecular systems by dielectric spectroscopy focus on detecting the α relaxation, identifying the existence of the β relaxation, and describing features specific to the β relaxation for understanding of the molecular mechanism of the JG process[386,387,391,392] as well as for exploring the origin of the potential connection between the α and the β relaxations in the conceptual basis of the mode-coupling theory.[385] The glass transition and structural relaxations in molecular glasses have been extensively investigated by employing DSC measurements. These investigations have been linked to topographic features of the energy landscape of glass-forming liquids and to liquid fragility.[393−396] Important progress has been made in

DOI: 10.1021/acs.chemrev.8b00510
Chem. Rev. XXXX, XXX, XXX−XXX

determination of the activation energies of both the α and β relaxations, in evaluation of the sizes of cooperatively rearranging regions (CRRs) at the glass transition,[92] and in evaluation of the critical sub-T_g temperature to invoke the β relaxation in molecular systems.[355,356,397]

Upon sub-T_g annealing, the endothermic sub-T_g peak prior to the glass transition peak, i.e., the endothermic prepeak, was also observed in the DSC curves of the annealed molecular glasses,[354,398,399] which are similar to those in the annealed HQ fragile oxide glasses. Vyazovkin et al. conducted a series of DSC studies to evaluate the effective activation energies of the β relaxations (E_β) from the sub-T_g peaks and to determine the sizes of cooperatively rearranging regions at the glass transition in both PS-Clay and some amorphous pharmaceutical systems.[354,356,397] Based on the empirical correlation, $E_\beta = (24 \pm 3)RT_g$,[400] Vyazovkin et al.[397] found the lowest accessible temperature at which the β relaxation can be induced. This low-temperature limit of β relaxation is very important for the application of the amorphous drugs. As T_a rises, the endothermic prepeak shifts toward the glass transition, implying that the longer time relaxation modes associated with α relaxation occur, which correspondingly result in an increase in the effective activation energy.[354,356,397] The increase in activation energy with T_a reflects the coupling of the β- and α-processes, i.e., an increasing contribution of the cooperative α motion to the annealing process.

In addition to the occurrence of the endothermic sub-T_g peak, one of the most striking features of this peak was demonstrated in a biodegradable polymer.[401] When the poly(L-lactide) (PLLA) samples were annealed at a temperature just below T_g, i.e., 0.95T_g, the endothermic peak not only overlapped with the glass transition peak but shifted to higher temperature with the increase of aging time (t_a), as shown in Figure 39. This implies that the sub-T_g annealing can give rise

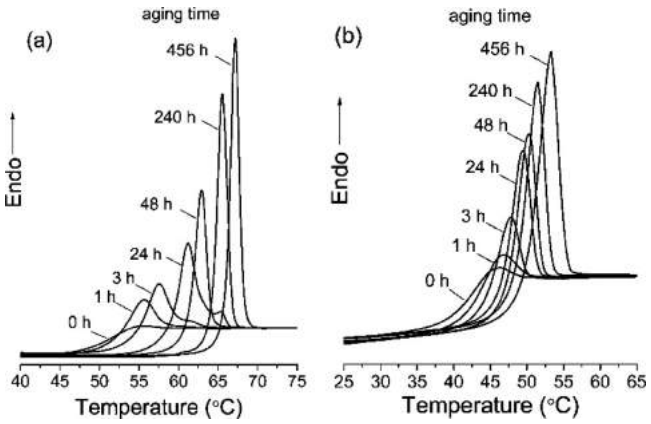

Figure 39. DSC upscan curves in the glass transition region at 10 K/min for molecular glasses: (a) poly(L-lactide) (PLLA) and (b) poly(DL-lactide) (PDLLA) samples annealed at 40 °C for different times (in hours). Adapted with permission from ref 401. Copyright 2007 American Chemical Society.

to α relaxation in this polymer system due to the more easily segmental rearrangement compared to the inorganic oxide glasses.[274,296] In addition, the cooling rates experienced by both the PLLA and the PDLLA during formation can also affect the α relaxation in the system; that is, with decreasing cooling rate, the glass transition peak shifted to a higher temperature, and the peak intensity increases.[401] Similar enthalpy relaxation behavior was also found in a lactose glass[402] and in sucrose.[403] It was found that only when T_a is higher than a certain temperature, e.g., 0.92 T_g, can the α relaxation be initiated.[402]

The nonexponentiality of the structural relaxation of four pharmaceuticals was used to detect their stability against crystallization, i.e., the deleterious tendency for nucleation and crystal growth, in amorphous pharmaceuticals.[355] A higher value of β corresponds to a narrower distribution of dynamics, less susceptible to nucleation. In Figure 39a, it is noticed that a shoulder is present at the high-temperature side of the main endothermic peak when t_a is between 3 and 24 h. It was suggested that the shoulders caused by the existence of small amounts of crystalline phases in the polymer formed during the quenching process. From another perspective, the existence of the shoulder indicates the instability of the PLLA against crystallization during quenching. In addition, the effects of both the temperature and humidity on the annealing process of spray-dried maltodextrin were investigated by DSC.[399] The humidity was found to reduce the T_g values of both the maltodextrin[404] and the SiO_2 glass.[305] Compared to the thermal effect, the humidity plays a less efficient role in affecting the enthalpy relaxation of the maltodextrin.[404]

4.2.5. Chalcogenide Glasses. Chalcogenide glasses are generally composed of covalently bonded rings, chains, layers, and three-dimensional structures, with van der Waals forces acting between structural units. The glass transition temperature T_g of chalcogenide glasses is generally lower compared to that of oxide glasses.[405,406] This means that the enthalpy relaxations in these glasses can occur more easily compared to oxide glasses, particularly at low temperatures. By conducting TMDSC experiments, Lucas et al.[407,408] have studied the photoinduced structural relaxations in both the Ge-Se and As-S-Se glass systems during sub-bandgap irradiation. It was revealed that the mechanisms for the thermal and photoinduced relaxations were quite different. With respect to the relaxation mechanism, Lucas et al.[406] also pointed out the differences in mechanisms between the stress relaxation and the enthalpy relaxation in chalcogenide fibers at room temperature through DSC measurements.

The average coordination number $\langle r \rangle$[409] is a useful quantity for investigating the composition dependence of the structural relaxation behavior.[406−408] The strongest liquid was considered to correspond to a value of 2.4 since the structure reaches the rigidity percolation threshold.[410,411] The $\langle r \rangle$ of chalcogenide glasses tends to decrease with increasing liquid fragility. In terms of the energy landscape formalism, the fragile systems undergo larger structural relaxation because of the availability of a greater number of different structural configurations.[406−408] Moreover, the composition of chalcogenide glasses can also influence their very long-term physical aging.[412,413] A series of binary As_xSe_{1-x} chalcogenide glasses were annealed under the normal ambient conditions for nearly 20 years, and this induced huge increases both in the area of the endothermic peak near the glass transition region and in T_g for the samples with $x < 40$ (i.e., for Se-enriched glasses).[412] This also implies that the α relaxation was invoked during this long-term aging process. In addition, Saiter et al.[413] studied the effects of very long physical aging up to 13 years at low temperature on the enthalpy relaxations of another binary chalcogenide glasses, i.e., the Ge_xSe_{1-x} glasses (x = 4, 8, and 12 at%), by means of DSC. Interestingly, a reversible phase-like separation in the endothermic peak near the glass transition

DOI: 10.1021/acs.chemrev.8b00510
Chem. Rev. XXXX, XXX, XXX−XXX

region was observed in the DSC curves of the glasses with x = 4 and 8 at%, implying that the initial glassy structure gradually evolves into a heterogeneous one during the long-time relaxation process. Moreover, this evolution strongly depends on the composition, since no such phase-like separation in the endothermic peak appears in the glass with x = 12 at%.

A systematic study on the enthalpy relaxation in the Ge_x·Se_{1-x} glasses was carried out by Saiter's group regarding the effect of the degree of annealing and the composition on the enthalpy relaxation.[413−416] Similar to the As_xSe_{1-x} glasses, the Ge_xSe_{1-x} glasses[414] and the $Se_{98}In_{1.5}Sn_{0.5}$ glass[405] exhibit an increase of T_g with increasing T_a and/or t_a. This further confirms that the sub-T_g annealing induced the α relaxation in the Se-based chalcogenide glasses. Since it is known that Se atoms are 2-fold coordinated (forming chains) and Ge atoms are tetrahedrally coordinated, the topological model of Phillips[132] was used to clarify the structural origin of the enthalpy relaxation in the Ge_xSe_{1-x} glasses with different compositions.[414,415]

A study on the volume and enthalpy relaxations of Se glass was conducted by Málek et al.[417] According to their results, the relaxation processes were attributed to the α relaxation since the activation energy of viscous flow in the glass transition region was identical to the activation energy for relaxation. Svoboda et al.[418] also studied the enthalpy relaxation in Ge_2Se_{98} and As_2Se_{98} glasses based on the Tool−Narayanaswamy−Moynihan (TNM) model.[82,166] By studying the enthalpy relaxation in $Ge_2Sb_2Se_5$,[419] Ge-Se glass[420] and $GeTe_4$ glasses[421] by DSC and the TNM and the Adam−Gibbs−Scherer (AGS) models, they found the most convenient and accurate way for determining the parameters of the TNM/AGS models. Structural relaxation of both the isothermally and the isochronally heat treated $Se_{96}In_4$ glasses, respectively, in the glass transition region, has been studied using DSC by Imran and co-workers, from which the activation energy spectra of the enthalpy relaxation were obtained and discussed.[422]

Very recently, Qiao et al. have investigated the sub-T_g relaxation in both the mechanically milled and the quenched As_2S_3 glasses by using DSC and Raman and X-ray photoelectron spectroscopies (XPS).[363] By comparing the activation energy for sub-T_g enthalpy relaxation (E_β) with that for the JG relaxation, they found that the relaxation in the quenched glass exhibits the JG relaxation feature, whereas the relaxation in milled glass has an activation energy of $33RT_g$, which is considerably higher than the average value of $24RT_g$ for the JG relaxation.[274] Upon sufficient sub-T_g annealing, the endothermic prepeak appears in the milled As_2S_3 glass, implying its higher nonexponentiality of the sub-T_g relaxation compared to the quenched glass. The Raman and XPS analyses indicate that both milling and melt-quenching can increase the structural heterogeneity of glass due to the occurrence of the As_4S_4 clusters and -S-S- chains.

4.2.6. Metal−Organic Framework (MOF) Glasses. Zeolitic imidazole frameworks (ZIFs) are a subset of metal−organic frameworks (MOF). The recent discovery of the melt-quenched (MQ) ZIF glasses has captured considerable scientific interest due to their unique structures, dynamics, performances, and potential technical applications.[237,247,248,257] The structure of the ZIF glasses lacks any long-range periodic order but retains the basic building blocks and connectivity of their crystalline counterparts. ZIF consists of metal ions as nodes and their tetrahedrally coordinated organic ligands, and the interconnected tetrahedra constitute an extended three-dimensional (3D) porous framework. As described in Section 3.8.3, upon a DSC upscan the ZIF-4 crystal ($Zn(Im)_2$) experiences a series of thermal responses, owing to the transformation of crystal to low-density amorphous (LDA) phase, high-density amorphous (HDA) phase, and ZIF-zni crystal and owing to melting and finally decomposition.[4,254,255,423]

Using DSC, the coexistence of HDA and LDA in ZIF-4 was demonstrated and explained in terms of the underlying PEL.[4] Study of the enthalpy relaxation in this new family of glasses gives a new perspective for understanding the fundamental glass problems. Recently, Wang and co-workers have conducted a detailed study on the glass relaxation thermodynamics and kinetics in the HDA phase of ZIF-4.[423] It was found that the glass transition and relaxation parameters of HDA ZIF-4 follow all the correlations established for the conventional melt-quenched glasses. Yue and co-workers have studied the enthalpy relaxation in the MQ ZIF-62 ($Zn(Im)_{1.75}(bIm)_{0.25}$) glass by performing sub-T_g annealing and DSC and XRD measurements.[424] From the annealing and the subsequent DSC upscanning experiments, the KWW stretching exponent β is found to be in the wide range of 0.44−0.76, which increases with the annealing temperature. This indicates a substantial degree of structural heterogeneity at medium-range scale in the ZIF-62 glass. The pair distribution function of the annealed glasses demonstrates structural densification during sub-T_g relaxation.

4.3. Structural Heterogeneity

The information about structural heterogeneity is important for understanding structural relaxation and the nature of glass, in particular, for clarifying the structural origin of the dynamic heterogeneity as the temperature approaches T_g in glass-forming liquids.[425−427] From the PEL view, the structural heterogeneity can be simply considered as the spatial correlations of molecular potential energies,[428] and consequently, it has a strong impact on the glass properties, e.g., shear modulus[429] and ductility[367,430] in metallic glasses. Hu et al.[367] found a correlation between the SCL relaxation and the Poisson's ratio (ν) of the glass by comparing the activation energy ratio of the α and the slow β relaxations ($r = E_\alpha/E_\beta$) for the metallic and the nonmetallic glasses. The underlying physics of this correlation lies in the heredity of the structural heterogeneity from liquid to glass. Although the chemical bond types are fundamentally different between the metallic glasses and other glass systems, the heterogeneous structure should be nevertheless their common feature.

In addition, the existence of the structural heterogeneity in the molten state makes it difficult to determine the *liquidus* temperature (T_L)[431,432] above which the structure should be more uniform and homogeneous at medium-range order scale. Over the past decades, much effort has been devoted to clarifying the structural heterogeneity in glasses by means of different experimental techniques, e.g., nanomechanical testing,[430] dynamic force microscopy,[433] solid-state NMR,[434,435] DSC,[431,432] and atomistic modeling,[428] as well as a combination of experiment and modeling.[415] Nonexponential relaxation processes connect the variations in local density or molecular packing with annealing to a distribution of relaxation times,[426] usually quantified by the KWW stretching exponent, β.[296] Assuming that particular regions of the structure correspond to certain relaxation modes, the width of the

DOI: 10.1021/acs.chemrev.8b00510
Chem. Rev. XXXX, XXX, XXX−XXX

structural relaxation time distribution can be used as a measure of the extent of the structural heterogeneity.[295]

The DSC technique has been demonstrated to be very efficient and convenient for detecting structural heterogeneity in both the glassy and supercooled liquid states via the controlled enthalpy relaxation process in different glassy systems, including oxides,[295,296,431,432] metals,[436,437] polymers,[398] and chalcogenides.[413] In the following, we review some recent work about the detection of the structural heterogeneity through the enthalpy relaxation in both the normal and extremely poor glass formers. The extremely poor glass formers here refer to glasses that are highly unstable with respect to crystallization.[295]

4.3.1. Good Glass Formers. The study of enthalpy relaxation in HQGs is a key approach for understanding the structural heterogeneity in glasses.[291,293,296,431,432,437] As described in Section 4.1.2, the HQ and annealed HQ glasses show different and complex features of the enthalpy relaxation compared to slowly cooled glass reflected by a broad temperature range of sub-T_g exothermic response in their C_p curves.[291,293,296,431,432,437] The asymmetrical pattern of the enthalpy relaxation peak in the C_p curve, which manifests itself as an overlap of at least two-domains of relaxation modes during the DSC upscan, is considered as evidence for structural heterogeneity.[291,293] Such a relaxation pattern can be regarded as the first evidence of the structural heterogeneity in the normal glass formers.

The HAD approach is an indirect method to access the structural heterogeneity[291,293,381,431,432,437] in the supercooled liquid state. The HQ strategy is often used to arrest the structure of the supercooled liquid at a temperature T_f well above T_g, and the subsequent annealing lets the arrested structure relax in a controlled manner, and finally, the released enthalpy can be quantified by performing two cycles of DSC up and downscans. The heat capacity C_p of the annealed HQ glasses provides access to the different microstructural regions associated with different relaxation time scales. If the annealing temperature is sufficiently high (but below T_g) or the annealing time is sufficiently long, the occurrence of the endothermic prepeak prior to the sub-T_g energy release peak, which can be eliminated by a second upscaning, is a common phenomenon of the fragile oxide glasses,[291,293,431,432,438] metallic glasses,[381,437] polymer glasses,[398] and chalcogenide glasses.[405,412−414] The endothermic prepeak is attributed to the fast-relaxing regions with high potential energy, implying the existence of the structural heterogeneity of the glass or the supercooled liquid at T_f. In particular, the endothermic prepeak is a reflection of the nonexponential nature of the relaxation in systems far from equilibrium.[431] The structural heterogeneity is described by a series of independent microdomains with different size (≤medium-range order scale), local density, and stability. The diversity of these domains is reflected by the stretching exponent β.[296] The endothermic prepeak is the consequence of the short-time relaxing domains of a broad relaxation time spectrum in the temperature range far below T_g. Moreover, the endothermic prepeak becomes more pronounced with increasing the annealing degree, indicating that more subregions were activated during the annealing process.[291,293,381,413,431,432,437,438]

However, the endothermic prepeak strongly depends on the chemical composition and hence the fragility of glass systems. For example, no distinct endothermic prepeak can be observed in the C_p curves of the annealed strong GeO_2 glass[274] and strong metallic glasses subjected to same annealing degree as that of the fragile glass systems.[287] This indicates a higher degree of structural heterogeneity in fragile glass formers compared to strong glasses.[28] On the other hand, as reviewed in Section 4.2.4, Saiter et al.[413] conducted a very long time of annealing, i.e., 13 years, on chalcogenide Ge_xSe_{1-x} glasses. Such long-time annealing led to two endothermic peaks near T_g in the DSC curves for the glasses with x = 4 and 8 at%. In addition, the two peaks corresponded to two different domains; that is, one is rich in Se-polymeric chains, and the other is rich in Ge, forming a three-dimensional network, indicating a heterogeneous structure of the studied glass. Thus, the endothermic prepeak in the C_p curve of the annealed glass can be considered as the second evidence for the structural heterogeneity.

By studying the enthalpy relaxation behaviors of the HQ Cu-Zr-Al metallic glasses, Hu et al.[436,437] observed an abnormal three-steplike relaxation pattern, i.e., both the onset temperature of the enthalpy recovery during DSC upscan and the released enthalpy of the HQ glasses during annealing varied nonmonotonically with T_a (increase−decrease−increase) in contrast to oxide systems. The origin of this abnormal behavior was revealed by studying the cooling rate dependence, i.e., the T_f dependence, of the remaining enthalpy after annealing and the activation energy for the onset of the energy release in two metallic glasses.[437] These abnormal relaxation phenomena were explained in terms of the competition between the low and the high-temperature clusters during the fragile-to-strong transition,[436,437] indicating the structural heterogeneity in supercooled liquids. The abnormal three-step relaxation pattern could be considered as the third evidence for the structural heterogeneity in supercooled liquids.

The HAD strategy can also be used to detect the structural heterogeneity in liquids. Yue applied the repeated DSC up- and down-scanning approach to detect the structural heterogeneity of a basaltic liquid above T_L.[431,432] He discovered the crystal-memory effect in this liquid over a wide temperature range above T_L and inferred that the structural heterogeneity is also present in the equilibrium liquids. Furthermore, as described in Section 4.1.3, the sup-T_g enthalpy relaxation of the ultrastable glasses is accompanied by the evolution from high energy to the lower energy packing, suggesting the existence of the structural heterogeneity in the supercooled liquid.[331,332] This structural evolution can be considered to be the fourth evidence for the structural heterogeneity in supercooled liquids.

4.3.2. Poor Glass Formers. The binary Al_2O_3−SiO_2 system is a highly unstable system against crystallization, i.e., an extremely poor glass former, since its crystallization peak partially overlaps with the glass transition peak.[14,295,439,440] This glass system is often used for making high-temperature insulation wool fibers. Zhang et al. explored the correlations among the sub-T_g enthalpy relaxation, crystallization, and the structural heterogeneity in the extremely unstable $65SiO_2$-$35Al_2O_3$ glass using the HAD approach.[295] A high degree of structural heterogeneity in the HQ glass, which is inherited from the medium-range ordered domains in the supercooled liquid, can greatly suppress the occurrence of the endothermic prepeak in the C_p curve of the annealed samples. Combined with the sub-T_g annealing effect on the crystallization behavior, the structural heterogeneity in the $65SiO_2$-$35Al_2O_3$ glass was revealed to be closely correlated with two types of structural

DOI: 10.1021/acs.chemrev.8b00510
Chem. Rev. XXXX, XXX, XXX−XXX

domains (silica-rich and alumina-rich domains). By using DSC, NMR spectroscopy, and high-resolution transmission electron microscopy, it was found that structural heterogeneity is the main factor that lowered the glass stability of the alumina−silica glass.[440] It was proposed that the tricoordinated-oxygen clusters in the alumina−silica glass during annealing could act as the nucleation sites for mullite formation.[440]

The hyperquenched ternary $20.8CaO-15.6MgO-62.2SiO_2$ glass is also an extremely poor glass former.[352] There is a tiny exothermic peak right above the glass transition overshoot in the C_p curves of this glass,[352] which was attributed to precipitation of nanocrystals, i.e., diopside crystals. Figure 40

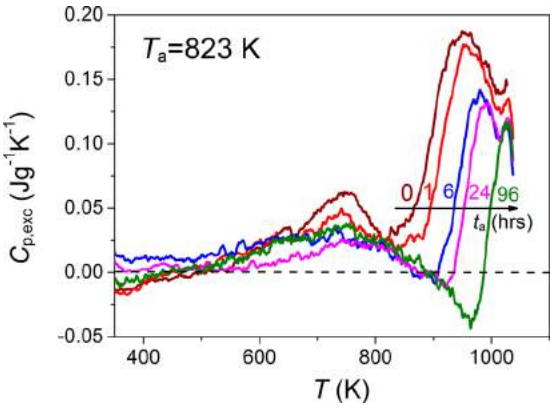

Figure 40. Annealing time (t_a) dependence of the excess heat capacity $C_{p,exc}$ (C_p difference between the standard and the first DSC upscans) for the $20.8CaO-15.6MgO-62.2SiO_2$ (in wt%) fibers annealed at 823 K. Reproduced with permission from ref 352. Copyright 2013 the American Ceramic Society.

shows the plot of the excess heat capacity ($C_{p,exc}$) against temperature, where the enthalpy evolution with t_a can be observed for the HQ $20.8CaO-15.6MgO-62.2SiO_2$ glass at T_a = 823 K. It is seen that two well-separated sub-T_g relaxation peaks appear in the C_p curve, implying that two different structural domains coexist in the supercooled liquid at $T = T_f$. The two peaks behave differently with increasing t_a. In detail, the low-temperature peak vertically diminishes with increasing t_a, similar to the relaxation behavior in strong glass formers, whereas the high-temperature peak horizontally decreases and an endothermic prepeak gradually emerges as a HQ fragile glass former behaves with the proceeding of annealing.[274] This clearly indicates the structural heterogeneity in the glass.

It is known that a glass with higher degree of structural heterogeneity has higher probability for nucleation to occur compared to that with lower degree of structural heterogeneity under the same thermal treatment condition,[295,352,441] and this correlation appears particularly strong for poor glass formers. For instance, the vanadium tellurite glass system is a rather poor glass former with high fragility ($m \approx 80-100$), in which crystallization can easily occur during a DSC upscan.[123,442] Recently, the $60V_2O_5-40TeO_2$ glass was found to be an excellent anode material for lithium-ion batteries owing to its high discharging/charging cycling stability and ionic conductivity.[443,444] The superior performances were attributed to the occurrence of the γ-Li_3VO_4 nanocrystals in the glass, which was induced by Li-ion insertion during the discharging/charging cycles. This kind of nanocrystal formation is in strong contrast to crystallization caused by heat-treatment above T_g. Through detailed DSC characterizations, it was found that $60V_2O_5-40TeO_2$ glass had a high degree of structural heterogeneity.[443] Upon Li insertion, the structural domains with higher potential energy are easy to be transformed into nanocrystals, and simultaneously Li ions join the lattice structure. This suggests that structural heterogeneity plays a critical role in nanocrystal formation in poor glass formers.

In summary, the DSC results of the enthalpy relaxation provide evidence for the existence of structural heterogeneity in both the normal and poor glass formers. With further understanding of the structural heterogeneity in glass, numerous longstanding issues related to dynamic heterogeneities can be clarified.

4.4. Anomalous Relaxation versus Fragile-to-Strong Transition

As mentioned in Section 3.5, glass-forming liquids can be classified as either fragile or strong. However, it has also been found that some glass-forming liquids do not conform to the conventional "strong/fragile" scheme but exhibit a fragile-to-strong (F−S) transition during cooling. As shown in Figure 41a, the temperature dependence of viscosity of these liquids strongly deviates from the Arrhenius relation in the high-temperature region above T_L but is close to the Arrhenius relation in the low-temperature region around T_g.[445] Figure 41a shows a fit of the viscosity versus T_g/T relation to the extended MYEGA equation[20] for the $Cu_{46}Zr_{46}Al_8$ liquid (red solid curve). The blue dashed curve refers to the strong term, whereas the pink dashed curve represents the fragile one. The F−S transition was confirmed to be a general feature of many metallic glass-forming liquids (MGFLs).[20] A question then arises: what is the structural source of the F−S transition in MGFLs and other types of glass-forming liquids? It has been a challenge to answer this question since intense crystallization in the F−S transition region hinders a direct probe of the structural evolution of most of poor glass formers such as water and melt-spun metallic glass systems. For most good glass formers such as some nonmetallic inorganic systems and bulk metallic glass systems, the F−S transition usually lies in a region that viscosity-measuring methods cannot reach. Despite this challenge, some indirect studies have given interesting implications for the structural origin of the F−S transition in MGFLs. Based on HAD experiments, Zhou et al. observed a striking anomalous relaxation phenomenon in the HQ CuZrAl glass ribbons, i.e., the three-stage sub-T_g relaxation with respect to T_a.[445] This behavior corresponds to the dynamic F−S transition, during which a structural evolution occurs as observed by Zhou et al. (Figures 40b and c).[445]

Figure 41b shows the three-stage anomalous relaxation behavior (see curve E and point E in inset) in the HQ $Cu_{46}Zr_{46}Al_8$ glass when T_a increases from 583 to 623 K. Figure 41c demonstrates the changes of the structure factor $S(Q)$ peaks with increasing T_a for the $Cu_{46}Zr_{46}Al_8$ glass ribbons, determined using X-ray scattering. It is clearly seen that there are two low Q minor peaks (P_1 and P_2) and one main peak (P_m) on each curve. The P_m position remains unchanged with T_a, suggesting that the SRO structural units are stable. However, the positions of P_1 and P_2 vary with the annealing degree, particularly evident for P_1. The P_2 position shifts slightly toward a higher Q value with increasing T_a, and this could be associated with the monotonic decrease of intermediate-range ordering units. Below 583 K, P_1 shifts to a lower Q value with increasing T_a. When T_a increases from 593 to 613 K, P_1 shifts to a larger Q value. Above 623 K, P_1

DOI: 10.1021/acs.chemrev.8b00510
Chem. Rev. XXXX, XXX, XXX−XXX

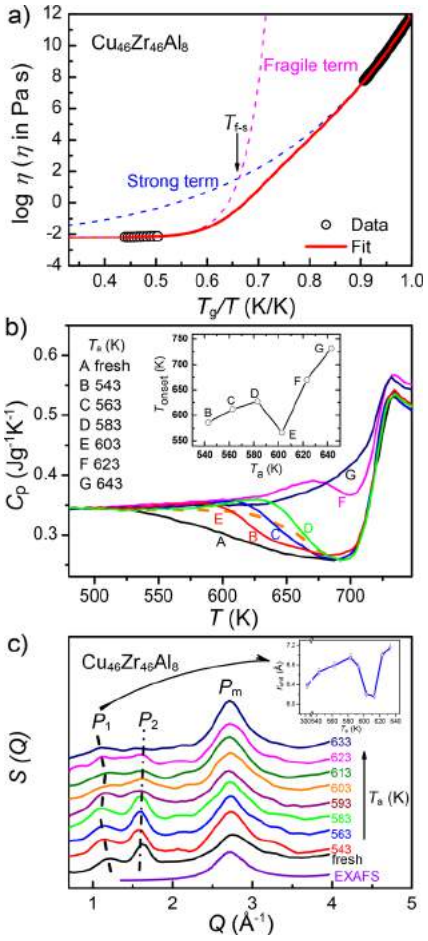

Figure 41. (a) The T_g-scaled temperature dependence of the viscosity of the $Cu_{46}Zr_{46}Al_8$ liquid in both the equilibrium region and the supercooled region (open circles). Solid curve: the fit of the viscosity data to the extended MYEGA equation (eq 7 in ref 20). Dashed pink curve: fragile term. Blue curves: strong term. The intersection point of both dashed lines is the characteristic temperature $T_{f\text{-}s}$ of the fragile-to-strong transition. (b) Isobaric heat capacity (C_p) versus temperature for the $Cu_{46}Zr_{46}Al_8$ glass ribbons cooled at 10^6 K/s and annealed at T_a below T_g for 1 h, exhibiting the T_a effect on the enthalpy relaxation. Inset: the onset temperature of the exothermic peak (T_{onset}) as a function of T_a. (c) Nonmonotonic structural evolution (described by the structure factor $S(Q)$, where Q is the scattering vector) with increasing T_a for 1 h. The bottom curve was extracted from extended X-ray absorption fine structure (EXAFS) analysis. The dashed line and the dot−dashed line illustrate the shift of the first (P_1) and the second prepeak (P_2) with increasing T_a, respectively. Inset: The structural unit size (r_{unit}) was calculated from P_1 with T_a. Reproduced with permission from ref 445. Copyright 2015 AIP Publishing LLC.

shifts to a lower Q with increasing T_a again. The intensity of P_1 decreases when increasing T_a above 583 K. The nonmonotonic evolution of the P_1 position occurs in the same T_a region (Figure 41c) as that of the three-stage enthalpy relaxation (inset of Figure 41b). This implies that a drastic transition of the IRO structure should be responsible for the F−S transition in the CuZrAl liquid. The structural unit size corresponding to the P_1 is calculated using the Ehrenfest's formula $r_{unit} = 1.23 \times 2\pi/Q_{pp}$, where Q_{pp} is the position of P_1. The T_a dependence of r_{unit} is illustrated in the inset of Figure 41c. An anomalous decrease of r_{unit} is observed when T_a increases from 593 to 613 K. Since the increase in T_a generally causes a decrease in T_f, this nonmonotonic change of r_{unit} implies a discontinuity in the MRO structural evolution during the F−S transition of GFLs. The size of the MRO structural units in the supercooled CuZr(Al) GFLs does not increase monotonically upon cooling, and this is in contrast to the trend predicted by Adam−Gibbs theory. Instead, they are dissociated into smaller clusters during the F−S transition. The dramatic decrease in the structural unit size r_{unit} coincides with the anomalous increase in enthalpy of the supercooled CuZr(Al) liquid during cooling around $1.3\sim1.4T_g$. The F−S transition in CuZr(Al) liquid has been attributed to the competition among the MRO clusters composed of different locally ordering configurations. Zhou et al. proposed a phenomenological scenario to explain the structural evolution from the fragile to the strong phase in the CuZr(Al) liquids.[445]

5. INVESTIGATING GLASS TRANSITION AND RELAXATION BY FLASH DSC

5.1. Background

As described above, conventional DSC is a very effective tool for exploring glass transition, enthalpy relaxation, liquid−liquid transition, polyamorphic transition, and phase separation in glasses. A recently developed nanocalorimeter, i.e., Flash DSC 1, has greatly extended the heating and cooling rates in the range of about 6 orders of magnitude, respectively, complementary to the conventional DSC. A brief introduction to Flash DSC is given in Section 2.3. Since Flash DSC was invented,[446,447] its application has already led to much progress in understanding the nature of glass. For instance, some thermodynamic and dynamic properties of some organic glass formers such as the polystyrene (PS) and poly(ethylene terephthalate)-glycol (PETg) were determined by Flash DSC, although they could not be probed by conventional DSC.[448] Flash DSC was also applied to study enthalpy relaxation in some inorganic glasses, e.g., selenium glass, at heating/cooling rates of up to 10^4 K/s.[449] Its rapid response time and ultrahigh heating and cooling rates provide opportunities for researchers to detect those thermal processes that are inaccessible by conventional DSC. The critical cooling and heating rates required to avoid crystallization in Au-based bulk metallic glasses (BMG) were found by Flash DSC to be dependent on sample mass, implying the so-called size-dependent nucleation.[450] This indicates that Flash DSC is advantageous for developing and studying new types of glasses with low glass-forming ability. Although the Flash DSC technology has received increasing attention, only a few studies have been conducted on purely glassy systems. Many studies have been devoted to understanding phase transitions, e.g., crystallization, and the thermal stability, e.g., decomposition of polymers. It is anticipated that Flash DSC will become an important tool for glass science and materials science in general. In this section, we review the Flash DSC studies mainly on both glass transition[451−457] and enthalpy relaxation in glass.[449,457−460] It should be noted that, owing to the relatively low upscanning temperature of Flash DSC 1 (773 K), its application is limited to organic glasses,[448,451−458,461] chalcogenide glasses,[449] and metallic glasses.[459,460] With the arrival of the new generation of Flash DSC 2, whose maximum upscan temperature can reach 1273 K, applying the Flash DSC to oxide glasses becomes possible.

DOI: 10.1021/acs.chemrev.8b00510
Chem. Rev. XXXX, XXX, XXX−XXX

5.2. Glass Transition and Fragility

The effects of thermal history and measurement conditions on the T_f and the nonstandard T_g values can be directly determined by the Flash DSC over a larger range of cooling rates compared to a conventional DSC. The latter can be used to determine the T_f of a hyperquenched glass (Section 4.1.2). The range of cooling rates available in conventional DSC covers only about 2 orders of magnitude, and hence, the dependence of T_f on the cooling rate is usually approximated as an Arrhenius relation, from which the activation energy for structural relaxation in the glass transition region, and thus the liquid fragility index m, can be calculated. However, such a derived fragility is systematically higher than that obtained by fitting the viscosity data to the MYEGA equation because of the abovementioned approximation.[91] Therefore, the DSC-derived m values must be corrected by using an empirical model proposed in ref 91 to obtain the relatively accurate m values. In contrast to the conventionally obtained m, the Flash DSC can be used to directly determine m by taking advantage of a large range of cooling/heating rates covering about 6 orders of magnitude.[448]

A wide range of T_f can be directly accessed using Flash DSC for glassy ultrathin films with different thicknesses since the cooling rates can be varied to a significantly larger extent compared to a conventional DSC.[448,451−454] In these studies, T_f is determined during cooling (downscan) in DSC, during which the supercooled liquid state is vitrified. The T_f can also be determined during heating (DSC upscan) after cooling at a given rate (Section 3.4.3). In some cases, this T_f has also been termed the limiting fictive temperature (T_f'),[462] while it is also referred to as T_g in other cases.[451,452,462] However, for simplicity and convenience, in this article, we use T_f to represent the fictive temperature determined during either cooling or heating and use T_g to express the standard glass transition temperature, i.e., the T_g value measured during a DSC upscan at 10 K/min after a downscan at 10 K/min. The T_g corresponds to the viscosity of 10^{12} Pa s (Figure 8). The exact definitions of T_f and T_g are described in Sections 3.4.1−3. As a typical example, T_f of the polystyrene ultrathin films has been studied as functions of the cooling rate and film thickness by using Flash DSC.[448,451,452,454−456] T_f was found to decrease with the decreasing cooling rate (q_c) independent of heating rate (q_h), along with the increase and shift of the enthalpy overshoot to higher temperatures as shown in Figure 42.[451,452] The dependence of the T_f on q_c can be described by the Williams−Landel−Ferry (WLF) relationship.[452,455] In addition, combining conventional DSC with Flash DSC, the q_c dependence of the T_g of polystyrene was also studied over a range of scan rates covering more than 6 orders of magnitude (3×10^{-3}~4×10^{3} K/s).[454] The influence of the thermal lag during measurement arising from the formation of a temperature gradient in the sample during scanning was taken into account when evaluating T_g, and the corresponding correction methods were established.

It was found by Gao et al. that the nanoconfined polymer films have a substantially lower T_f than the bulk sample.[451,452] As shown in Figure 42, a glass transition depression (i.e., a glass transition overshoot as shown in Section 3.2.1) was detected in the thin film samples that underwent different cooling rates and subsequently the heating rate of 600 K/s. This overshoot decreases with increasing q_c. Only a smaller overshoot occurs at the highest q_c (within the experimental error) while it becomes more intense as q_c decreases. These findings are in line with those reported for polystyrene films[456] and also for the thin polycarbonate films.[453] Moreover, the T_g is dependent on film thickness, leading to a reduction of the liquid fragility m with decreasing film thickness[451,453] since the determination of the fragility is intimately correlated to the value of T_g and thus to the T_g decrease in polymer films. In other words, the liquid fragility, which reflects the structural packing efficiency of the films, is an important factor in governing the T_g-confinement effect.[463]

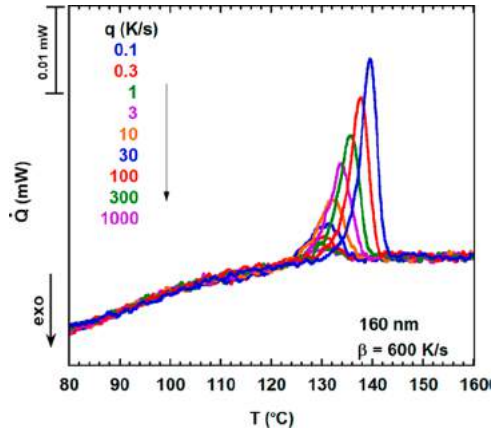

Figure 42. Flash DSC upscans performed at a heating rate (q_h) of 600 K/s for a 160 nm thick polystyrene film on Krytox oil. The endothermic peaks represent the glass transition of the sample subjected to various cooling rates (q_c) from 0.1 to 1000 K/s. The flow rate curves were rotated to be horizontal in the liquid state. Reproduced with permission from ref 451. Copyright 2013 American Chemical Society.

The effect of the film thickness (less than a critical value, e.g., the film thickness of 160 nm for polystyrene) on the glass transition can be compromised by annealing the film at a given temperature (e.g., 160 °C for the polystyrene film) for a period of time.[451] The mechanism of the recovery of the film T_g value to the bulk value, i.e., from confined to bulk behavior, during annealing was elucidated by considering the effects of the morphological change and thickening of the films, and these effects are correlated with the dewetting and microcavity growth of the films.[451]

As described in Section 3.6, the liquid fragility m is associated with the structure and dynamics of glass-forming liquids and can be determined from the dependence of the fictive temperature on the cooling rate q_c in conventional DSC. Due to the rather small range of cooling rates that conventional DSC can reach, the $\log(1/q_c) \sim 1/T_f$ relation follows a near Arrhenius scaling around T_g. However, this relation of the confined films, such as polycarbonate ultrathin films[453] and selenium[449] should be described by a non-Arrhenian model, e.g., by the MYEGA equation[163,218,464] in the extended cooling rate range of Flash DSC. By using a reference temperature $T_{g,ref}$, which is obtained at the reference cooling rate q_{ref} of 0.1 K/s, the T_f dependence of the cooling rate q_c for the ultrathin films can be fitted by the Williams−Landell−Ferry (WLF) equation:[455]

$$\log\left(\frac{q_c}{q_{ref}}\right) = \frac{C_1(T_g - T_{g,ref})}{C_2 + (T_g - T_{g,ref})} \tag{33}$$

where C_1 and C_2 are constants. Thus, the dynamic fragility m can be determined by the following equation:[77]

DOI: 10.1021/acs.chemrev.8b00510
Chem. Rev. XXXX, XXX, XXX−XXX

$$m = -\frac{\mathrm{d}\log q}{\mathrm{d}\left(\frac{T_{g,ref}}{T}\right)} = \frac{T_g C_1}{C_2} \quad (34)$$

Based on the above two equations, both m and the apparent activation energy at T_g were found to decrease as film thickness decreases.[451−453] A similar trend of the $\log(1/q_c) \sim 1/T_f$ relation was also found in two other different polymeric systems (PS and PETg).[448] In their work, Dhote et al.[448] compared the T_f and m values determined by Flash DSC and those by DSC, respectively. They found that the m value determined from DSC is overestimated, while m obtained from Flash DSC is underestimated. The difference between the two m values was directly correlated with the T_f difference. By comparing the Flash DSC derived temperature dependence of the relaxation times with that obtained from Broadband dielectric spectroscopy, the logarithmic shift of the cooling rate dependence of T_f was obtained to determine the calorimetric liquid fragility.

5.3. Enthalpy Relaxation

In Section 4.1, we reviewed recent progress in studying the enthalpy relaxation using conventional DSC for various glass systems. However, conventional DSC has limited response time and sensitivity, which restricts detection of enthalpy responses during annealing, e.g., when the samples are annealed for a very short duration (0.01 s). It is challenging to explore what happens at the very initial stages of annealing processes by conventional DSC.[312] That is because the enthalpy change is too small to be detected, and both the sample's thermal history and the temperature gradient in the sample cause uncertainties in the measurements. In addition, for the conventional DSC studies, the annealing temperatures are limited to the sub-T_g region since the DSC is not sensitive enough to detect the enthalpy response to the short relaxation time above T_g. In contrast, Flash DSC does not have the abovementioned problems owing to its high sensitivity and broad heating and cooling rate ranges. In this section, we review some recent findings in studying the enthalpy relaxation in polymer glasses,[457,458,461] chalcogenide glasses,[449] and metallic glasses[459,460] by means of Flash DSC.

Flash DSC was successfully applied to study the enthalpy relaxation and the glass transition in a single polystyrene thin film annealed at 15 K above T_g and for a duration (t_a) as short as 0.01 s.[465] T_f was used to be an indicator of the enthalpy change during structural relaxation. As shown in the Flash DSC upscan curves in Figure 43, the glass transition behavior strongly depends on t_a at T_a of 102.5 °C after cooling at 1000 K/s.[465] Similar to the effect of decreasing the cooling rate on the glass transition, increasing t_a results in an increase in the glass transition overshoot during the Flash DSC upscans and in a shift of the overshoot to higher temperatures, leading to a reduction of T_f. It is remarkable that the Flash DSC upscan curve of the sample annealed for only 0.01 s is distinguishable from that of the non-annealed sample. The evolution of the T_f with t_a at different T_a (below, above, and close to T_g, respectively) was well described by the modified TNM model.[465]

Koh et al.[466] further investigated the structural recovery of a single polystyrene thin film during sub-T_g relaxation at relatively low T_a, e.g., 50 K below T_g, by using Flash DSC. They found that the departure from equilibrium ($T_f - T_a$) first remains unchanged with increasing $\log_{10}t_a$; that is, an initial plateau appears, and after a critical t_a it linearly decreases. This

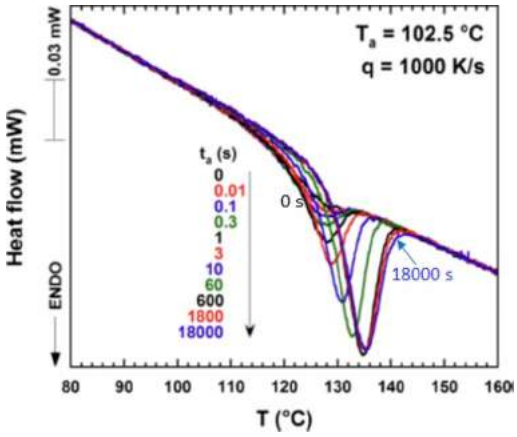

Figure 43. Flash DSC upscanning curves obtained at 600 K/s on the 1 mm thick polystyrene film samples that were subjected to various annealing times (t_a) at T_a = 102.5 °C, and the subsequent cooling at 1000 K/s. The annealing and cooling were conducted in Flash DSC prior to upscanning. Reproduced with permission from ref 465. Copyright 2014 Elsevier B.V.

critical t_a is defined as the induction time, at which the T_f begins to decrease with t_a. Within the induction time length, the aging time is shorter than the relaxation time of the glass state.[466,467] Moreover, the induction time increases with decreasing T_a, and hence, it can be considered as a measure of the relaxation time of the glass state at a certain T_a.

The structural relaxation in a random propylene-co-1-octene copolymer was studied for a sample annealed both below and close to the T_g by using Flash DSC.[457] At a T_a well below T_g, only the structural relaxation was observed. However, when T_a approached T_g for a certain t_a, mesophase ordering occurs in addition to the structural relaxation, suggesting that after completion of the enthalpy relaxation, the homogeneous nucleation and linear growth takes place even below the glass transition.[457] This confirms the poor glass-forming ability of the studied copolymer. Likewise, Androsch et al.[458] reported a similar finding on the enthalpy relaxation in glassy polyamide 6 by using Flash DSC. When the sample was annealed at 20 K below T_g, with t_a from 0 to 10^4 s, only the structural relaxation was induced. When T_a was increased to 10 K below T_g or higher, in addition to enthalpy relaxation, the homogeneous crystal nucleation and crystal growth occurred. The sequence of these processes is strongly dependent on t_a.

As the simplest chalcogenide glass, selenium is often chosen as a model system to study structural relaxation.[468−471] By using Flash DSC, the enthalpy relaxation of the glassy selenium was studied at heating/cooling rates up to 10^4 K/s.[449] To ensure that the enthalpy relaxation can be detected during the heating scan, a sample was first cooled from 150 °C to T_a (37 and 42 °C) at 1000 K/s, subsequently annealed for a selected time t_a, then cooled to −50 °C at 10^4 K/s, and finally upscanned at 1000 K/s. As a result, the relaxation peaks in the Flash DSC upscan start at a lower temperature and end at a higher temperature compared to the conventional DSC measurements, even entering the crystallization region in the DSC curve. Such high rates of Flash DSC do not give the sample sufficient time to crystallize during the first DSC scanning cycle. The reason for the dramatic broadening of the relaxation peak compared to the peak detected by a conventional DSC still needs to be further clarified. However, when the sample undergoes several upscan cycles to a

DOI: 10.1021/acs.chemrev.8b00510
Chem. Rev. XXXX, XXX, XXX−XXX

temperature well above T_g, some crystal growth occurs, leading to a smaller relaxation peak.[449] In summary, both the structural relaxation and nucleation processes induced by sub-T_g or near-T_g annealing can be detected by using Flash DSC.

As described above, the common feature of enthalpy relaxation in glassy polymers is that the glass transition overshoot shifts to higher temperatures with increasing t_a at a certain T_a. This means that T_g increases, and thus the kinetic stability of the glass is enhanced, which is signified by the increase of the temperature range of the glass state. As is known, increasing the kinetic stability of metallic glasses would extend their utility to higher temperatures. By using Flash DSC, Wang et al.[459] succeeded in increasing the kinetic stability, i.e., increasing the temperature range of the glass state by raising the T_g of $Au_{49}Cu_{26.9}Ag_{5.5}Pd_{2.3}Si_{16.3}$ glasses by optimizing the annealing protocol. The optimum annealing protocol was determined by considering both the α and β relaxation processes since the α relaxation is related to the kinetic stability while the thermodynamic stability is linked to both α and β relaxation. The maximum T_g increase of 28 K of the sample annealed at $0.85T_g$ for 10^5 s is illustrated in Figure 44. The enhanced kinetic stability is analogous to that of a vapor-deposited glass. Another striking feature shown in Figure 44 is that the crystallization peak and the onset temperature of crystallization (T_x) remain unchanged with extending t_a, while the glass transition peak shifts to a higher temperature, i.e., T_g increases. This phenomenon implies that the annealing history of all the samples annealed for various t_a has been completely erased upon a Flash DSC upscan, and consequently the supercooled liquids above T_g have the same structure and same level on PEL, and hence, the crystallization behavior (e.g., peak shape, size, and T_x) is the same for all the samples.

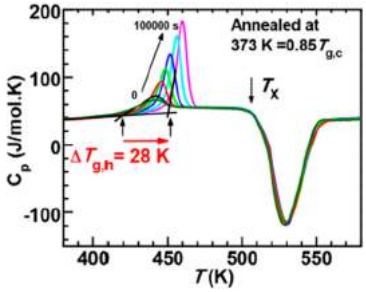

Figure 44. C_p curves for $Au_{49}Cu_{26.9}Ag_{5.5}Pd_{2.3}Si_{16.3}$ glass samples annealed at 373 K (=$0.85T_g$) for various times ($0 \sim 10^5$ s). Vertical black arrows: T_g and the onset temperature of crystallization (T_x). Horizontal red arrow: an increase of T_g of ΔT_g = 28 K from 424 to 452 K by extending t_a from 0 to 10^5 s. Reproduced with permission from ref 459. Copyright 2016 Acta Materialia Inc. Published by Elsevier Ltd.

In regard to a vapor-deposited ultrathin Au-based metallic glass film (i.e., so-called nanoglass), Wang et al.[460] have explored the combined effect of ultrastable character and nanoglobular microstructure on the kinetic behavior by using Flash DSC. The ultrastable nanoglass has much higher T_g and T_c than a normal ribbon sample at low upscan rates, e.g., 300 K/s. The higher kinetic stability of the vapor-deposited glass (e.g., compared to melt-quenched glass) is attributed to both the relaxation during deposition and the nanoglobular microstructure. It was also found that the kinetic stability was reduced, i.e., T_g was lowered, by preheating up to the supercooled liquid region at a certain heating rate.

Recently, Cubeta demonstrated that Flash DSC could provide insights into the slow molecular kinetics of amorphous materials at temperatures far below T_g.[472] Cubeta discovered that the complex devitrification kinetics of glasses reduced to a zero-order, Arrhenius-like rate law in the high limit of heating rates. Both the melt-quenched glasses and the vapor-deposited amorphous phases of methylbenzene underwent heterogeneous, surface-facilitated relaxation when they were heated at a sufficiently high rate. The simplified kinetics is defined primarily by the initial structural state of the sample at low temperatures, which is evidenced by the high activation energies for these relaxation processes. Cubeta proposed a modified Wilson−Frenkel model of front-propagated structural relaxation, which was validated by Flash DSC data. These findings have improved the theoretical understanding of the formation and devitrification of glasses.

6. PROBING GLASS TRANSITION AND RELAXATION BY TMDSC

The microscopic origins of glass formation are more complex than the macroscopic properties measured by DSC. The spatially heterogeneous nature of supercooled liquid dynamics[425] leads to the continuous breaking of the ergodicity[71] in the liquid-to-glass transition. The length scale of the dynamic heterogeneities changes with temperature in liquid,[425] and the heterogeneous liquid structure continuously freezes-in in the glass state.[65,71,110,425] Structural relaxation can be considered as the inverse of the liquid-to-glass transition when the time constraint is removed.[110] Since the distribution of the dynamics of spatial heterogeneities is proportional to the relaxation time distributions, a nonexponential relaxation behavior is observed during the isothermal relaxation.[473] DSC can be used to investigate the nonexponential relaxation processes. However, the heat flow signal obtained from DSC measurements is the convolution of various glass transition range responses.[54,61,474,475] Development of the TMDSC method[54,61] (Section 2.4) opened up a new venue for the detailed calorimetric analysis of dynamic processes in the vicinity of the glass transition. In this section, we describe different approaches for interpreting the TMDSC signals and review recent progress in understanding glass transition and glass relaxation, made by TMDSC.

6.1. Interpretation of TMDSC Signals

6.1.1. Complex Heat Capacity. Birge and Nagel initially introduced the idea of the complex heat capacity in their isothermal specific heat spectroscopy studies.[476,477] The temperature dependence of the resistance of a thin metal heater is used to measure the drop of the product of the heat capacity (C_p) and thermal conductivity in a glass-forming supercooled liquid when a sinusoidal current is passed. The change in the thermal conductivity is negligible in comparison to the rapid drop of C_p. Thus, the total measured product is a function of the heat capacity while the thermal conductivity can be considered as a constant. Then, the same measurements are repeated in a very wide range of frequencies (0.2 Hz−6 kHz) and at various temperatures. A systematic shift in the temperature onset of the C_p drop is observed in the frequency spectrum. The onset temperature of the C_p drop increases with increasing frequency, and the onset of the frequency of the C_p drop increases with increasing temperature.[476] Specific heat spectroscopy experiments proved (i) the frequency dependence of C_p[59,476,478] and (ii) isothermal glass transition when

DOI: 10.1021/acs.chemrev.8b00510
Chem. Rev. XXXX, XXX, XXX−XXX

the external time (t_{ext}) is changed while the internal time (t_{int}) is constant.[65,110,478] The C_p is generally not considered to be a dynamic property,[477] but frequency-dependent heat capacity experiments demonstrated that the heat capacity could be measured as a dynamic susceptibility when a small perturbation is applied to the equilibrium liquid.[476,477] This brilliant experiment helps clarify the distinction between the equilibrium and ergodic systems.[478] Even though the liquid is well above the T_g defined by Angell,[1] which is independent of the thermal history,[313,479] a rapid change in the heat capacity is observed as a function of the frequency.[476] The liquid is in thermodynamic equilibrium, but the breaking of the ergodicity is observed when t_{ext} varied from $t_{ext} \gg t_{int}$ to $t_{ext} \ll t_{int}$, which corresponds to limit $\omega \rightarrow 0$ and limit $\omega \rightarrow \infty$, respectively.[110,478] Although there is no net change in energy between the liquid and the surrounding environment,[476,477,480] the entropy changes.[477] This can be attributed to the lag between the heat flow and temperature oscillations. The phase lag between the input and output functions is proportional to the imaginary part of the complex heat capacity (C_p''). Considering the Kramers–Kronig[481] relations frequency dependent complex heat capacity is shown as

$$C_p^*(\omega) = C_p' - iC_p'' \tag{35}$$

where C_p^* is the frequency dependent complex heat capacity and C_p' and C_p'' are the real and the imaginary parts of the complex heat capacity, respectively.

The complex heat capacity concept provides a basis for Schawe's analysis.[475,482] In TMDSC, a sinusoidal heat ramp is used,[483] unlike the classical specific heat spectroscopy measurements where the glass or liquid is held isothermally.[476,477] Each period of oscillation is considered a steady state, and the amplitude of the temperature is the applied perturbation.[480] In a standard TMDSC measurement in heating mode when heating from a temperature well below the T_g to a temperature well above the T_g in the liquid, the following events are observed:

1. $T \ll T_g$: C_p involves only vibrational contribution, and average relaxation times are much slower than the time scales of each period of oscillation. Hence, the sinusoidal heat flow response is in phase with the sinusoidal heating rate input. The amplitude of the modulated heat flow changes as a function of the change in C_p; however, it is very minimal due to the weak temperature dependence of the heat capacity below the transition.[62]
2. $T \sim T_g$: Near the glass transition, heat capacity continuously increases while it involves both vibrational and configurational contributions. The heat transfer is switching from atomic vibrations to molecular motions as the average relaxation times are in the same range of the external time scale (period of oscillations). Spatially heterogeneous dynamics is the main source for the distribution of relaxation times that could be considered as a system where each dynamic domain has its internal relaxation times and fictive temperatures. Therefore, each dynamic domain's heat flow response starts to lag behind the external time scale at a different temperature. Because of the continuously changing lag between the input and out functions, TMDSC signals yield a phase angle peak.[62]
3. $T \gg T_g$: Relaxation times of all dynamic domains are shorter than the external time scale so that no phase lag is observed. The output signals are very similar to those in the glass, and the phase angle reaches to a zero value.[62]

The phase angle (ϕ) obtained from TMDSC measurements, as introduced in Section 2.4, shows similar characteristics to other dynamic susceptibilities such as those in the dielectric spectroscopy.[474,475,482] In a monolithic and compositionally homogeneous glass, a normal distribution of the phase angle peak can be fitted with a Gaussian function.[484] Accordingly, a complex heat capacity approach requires analysis of the phase angle and input and output functions. The output function, the modulated heat flow rate (Φ_m), can be written as

$$\Phi_m = \omega A' |C_p(\omega)| \cos(\omega t - \phi) \tag{36}$$

where A' is the amplitude of the modulated heating rate, $|C_p(\omega)|$ is the modulus of the complex heat capacity, and ϕ is the phase angle between the input and output functions. $|C_p(\omega)|$ is shown as

$$|C_p(\omega)| = \sqrt{C_p'^2 + C_p''^2} \tag{37}$$

where C_p' is the real and C_p'' is the imaginary part of the complex heat capacity. The modulus of the complex heat capacity can be estimated by calculating the amplitude of the modulated heat flow (Φ_a) and the A' using

$$|C_p(\omega)| = \frac{\Phi_a}{A'\omega} \tag{38}$$

and real and imaginary parts can be calculated from the modulus of complex heat capacity and the phase angle:

$$C_p'(\omega) = |C_p(\omega)| \cos \phi \tag{39}$$

and

$$C_p''(\omega) = |C_p(\omega)| \sin \phi \tag{40}$$

6.1.2. Nonequilibrium Thermodynamics and Linear Response. The linear dynamic susceptibility approach requires the linear response of a system when it is perturbed.[482] In theory, the input function (modulated heating rate) and the output function (modulated heat flow) must be linearly scaled.[485] However, the ideal linear response could occur only if the sample thickness was infinitely small.[62,485,486] To test the linearity of the TMDSC experiments, Lissajous curves are used to examine the relationship between two parametric equations.[62,485] In TMDSC experiments, the linear response can be shown in an elliptical Lissajous curve when the modulated heat flow is plotted against the modulated heating rate. The shape and size of the ellipsoids depend on the thermal conductivity of the material and thickness of the sample. In linearly responding modulation conditions, each period of oscillation is displayed as an ellipse, the slope of which changes with temperature throughout the glass transition. When modulation conditions do not satisfy the linear response, the ellipsoid shape gets distorted or non-geometric and irregular shapes are observed.[485] The change in enthalpy in each period of oscillation must be as small as possible to preserve the linear response of the glass. Since TMDSC is not based on isothermal conditions, rapid changes in C_p might cause a significant heat flow effect in addition to the small sinusoidal heat flow responses. If the underlying heating rate exceeds a maximum limit, C_p changes catastrophically during a period of oscillation. Therefore, the output

DOI: 10.1021/acs.chemrev.8b00510
Chem. Rev. XXXX, XXX, XXX–XXX

function becomes distorted, and the system's response is nonlinear at high heating rates.[485] The amplitude of the oscillations also affects linearity. Perturbations are supposed to be small enough to ensure that the glass is close to its steady state over the period of oscillation.[487]

The nonlinear behavior becomes crucially more problematic in the thermally activated processes where the enthalpy change is relatively significant. Hence, TMDSC is predominantly used in the glass transition range since the enthalpy change in the melting or crystallization is orders of magnitude higher than the enthalpy changes in the glass transition range. Preserving a linear response in the crystallization or melting process is nearly impossible with standard TMDSC conditions due to the rapid change in the enthalpy as a function of time in quasi-isothermal conditions or as a function of temperature during the sinusoidal heating. It was previously reported that even changes in the thermal history (fictive temperature) might lead to a nonlinear behavior in the glass transition range.[62] Since the magnitude of the crystallization peak is often much bigger than the glass transition peak, it can be expected that sustaining the linear response in the crystallization range is much more challenging than in the glass transition range, and in some cases impossible to achieve throughout the crystallization process. One might argue that the use of a very small amplitude of oscillation might help achieve linear behavior; it comes with its own disadvantages, particularly in the signal-to-noise ratio. Concerns about linearity were acknowledged in previous investigations;[62,474,475,482] however, there is no systematic study in the crystallization or melting to prove the possibility of achieving linear behavior neither by providing the Lissajous curves nor by showing the independence of the reversing heat flow from the amplitude of the oscillation. The feasibility of the utilization of TMDSC in glass crystallization studies needs further investigation.

Modulation conditions depend strongly on the physical properties of glasses. The thermal history[62] and fragility[487] of glass-forming systems are the two main parameters that govern the limitations of the linear response. Thermal history might limit the modulation conditions if there were a significant deviation between T_f and T_g. When $T_f \gg T_g$, a strong exothermic peak is observed; and when $T_f \ll T_g$, a large endothermic peak is measured. In both cases, modulation conditions are more limited, and the heating rate must be lower than TMDSC conditions used in glasses when T_f is equal or close to T_g.[62]

Figure 45 displays the Lissajous curves for selenium after long isothermal annealing for over a week at a sub-T_g temperature.[62] When the heating rate (q_h) is slow enough (e.g., 1 °C/min), and the amplitude (A) is relatively small (0.8 °C), linearity could be satisfied even after 249 h of annealing. Figure 45a shows the linear, elliptical Lissajous curves in the glass and liquid regions where it is easier to preserve the linear response. Figure 45b shows the linear response in the glass transition region where strong endothermic contributions could cause nonlinear behavior if proper modulation conditions were not chosen. Figure 45c displays an example of the nonlinear behavior of the selenium sample after 192 h of isothermal annealing at the same sub-T_g temperature when the heating rate is faster (2 °C/min) and the amplitude is slightly larger (1 °C).[62] Even though the annealing time is shorter, making thermal history-related enthalpic contributions smaller, a nonlinear behavior is observed in the glass transition range as the ellipse is distorted. It should also be noted that the liquid

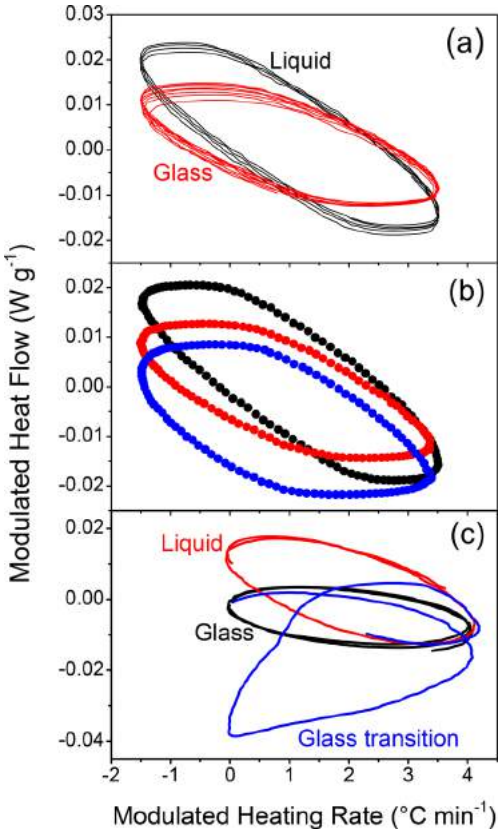

Figure 45. Lissajous curves for glassy selenium after isothermal annealing at 25 °C for 249 h when A = 0.8 °C, q_h = 1 °C/min, and ω = 0.0083 Hz: (a) in the glass and liquid range; (b) in the glass transition range. (c) Nonlinear response in the glass transition region. Reproduced with permission from ref 62. Copyright 2013 the American Institute of Physics.

and glass regions preserve their linearity since the heat flow does not show a rapid change as a function of the underlying mean temperature.[62] This example clearly shows the significance of the thermal history and how small changes in the measurement conditions change the applicability of the dynamic susceptibility approach to TMDSC.

The fragility of glass affects the linearity of the TMDSC conditions, independent of the thermal history.[487] The thermodynamic signature at the glass transition, such as ΔC_p or ΔT_g is directly correlated to the kinetic fragility (m). ΔC_p is proportional to m/T_g (eq 27),[108,214] whereas ΔT_g is inversely correlated with m.[101] Therefore, a more careful selection of TMDSC conditions is needed for fragile glass formers. Arsenic selenides can be used to make a comparison with the previous example of glassy selenium. When selenium is mixed with arsenic, stronger As−Se glass compositions can be obtained.[484] For instance, linearity can be easily satisfied in $As_{30}Se_{70}$ glass composition when modulation conditions of A = 3 °C, q = 3 °C/min, and ω = 0.005 Hz are used.[55] Compared to selenium, $As_{30}Se_{70}$ is a much stronger glass, and the C_p jump is much smaller.[484] Besides, the T_f of $As_{30}Se_{70}$ is very close to T_g as its quenching rate is very close to the underlying mean temperature[55] of the modulation, while the T_f of the isothermally annealed selenium glass is well below the T_g.[62] The significance of the linearity is not limited to chalcogenides or low T_g glasses. In a recent study, the importance of the

DOI: 10.1021/acs.chemrev.8b00510
Chem. Rev. XXXX, XXX, XXX−XXX

fragility under TMDSC conditions was demonstrated in calcium alumina silicate glasses.[487]

6.1.3. Reversing and Nonreversing Heat Flow. Derivation of the nonreversing and reversing heat flow involves much less complicated mathematics since the phase angle ϕ is not included in the data analysis. The reversing heat flow H_{rev} corresponds to the amplitude of the modulated heat flow term as in eq 36.[474] It can also be converted to reversing heat capacity by normalizing the amplitude of the modulated heating rate (A'), and it would then be equivalent to the modulus of the complex heat capacity. In this analysis, the method output function is considered to consist of two parts: the thermodynamic reversing part (eq 12 in Section 2.4) and the kinetic part $f(t,T)$ associated with time-dependent events[54,61,474,483] shown as

$$\Phi_u = C_p[q + T\omega \cos(\omega t)] + f(t, T) \quad (41)$$

where Φ_u is the total underlying heat flow and $f(t,T)$ is associated with the nonreversing part of the heat flow. The nonreversing heat flow ΔH_{nr} is obtained by subtraction of the reversing heat flow H_{rev} from the total underlying heat flow that is equivalent to the heat flow in the conventional DSC measurements:[55,474,483]

$$\Delta H_{nr} = \Phi_u - H_{rev} \quad (42)$$

In this analysis, the phase angle is not included, and the assumption is that the kinetic component corresponds to the subtraction of the amplitude of the modulated heat flow from the total heat flow, which should yield the nonreversing heat flow.[55] The comparison of these two methods is presented in the following section.

6.1.4. Comparison of the Data Analysis Methods. There has been an ongoing debate[480] on the methods used for the analysis of TMDSC signals and the meaning of analyzed data since the introduction of TMDSC. The disagreement is not limited to thermophysics scientists and thermal analysis instrument developers but is also debated by glass scientists[488−491] who have been utilizing TMDSC to elucidate fundamental physics questions about glass relaxation,[62,484] glass formability, and topological constraints.[489,492−497] The complex heat capacity approach relies on the linear response theory and is analogous to the methods used in other dynamic susceptibilities.[498,499] The thermodynamic meaning of the imaginary part of the complex heat capacity is debated since there is no heat dissipation.[477,480,500] However, there is a consensus that the complex notation in the glass transition range can be explained by the C_p drop when the period of oscillation is close to the average relaxation times.[480] However, the nonreversing heat flow concept is still being debated due to the empirical nature of the analysis.[62,474] Reversing heat flow is the modulus of a complex quantity, and it is subtracted from the underlying heat flow that is a real quantity. Schawe claims that the two signals are not comparable[474] while Reading claims that it is the difference between these two properties that represents the kinetic component of the heat flow function.[501] Schawe also points out that the nonzero, nonreversing heat flow signals while cooling from the supercooled liquid to the glass do not agree with the interpretation of such peaks as enthalpy relaxation.[474] Frequency correction[502] can be considered as a solution to the confusing peaks observed when the sample is cooled from liquid instead of heating. The ongoing debate among the experimentalists is presented in Section 6.4.

6.2. C_p'' in the Frequency Spectrum

In standard TMDSC measurements, a constant frequency is applied to an average heating ramp cycle. Therefore, C_p'' peaks obtained from TMDSC signals correspond to the response of the glass for a constant frequency. However, consecutive measurement can be conducted by changing the frequency, while all other measurement conditions remain the same. Conventionally available DSC works in limited modulated conditions to provide a period of oscillations in the range of 40−200 s. The observation time range covered by TMDSC is comparable to the relaxation times around T_g. Each dynamic domain has its internal relaxation times for a corresponding temperature. The C_p'' peak is the sum of those corresponding temperatures when the observation time is equal to the internal relaxation time.[62] Therefore, a C_p'' vs temperature plot can be considered as the temperature probability distribution. The tip of the peak is correlated with the mean relaxation time of the glass when the distribution is Gaussian.[62,484] When the frequency is changed, the peak position shifts while the normalized distribution functions remain the same. The external observation time is proportional to the period of oscillation (P_o) and denoted as $P_o/2\pi$. When the frequency is increased, the internal relaxation time deviates from the observation time at higher temperatures. Therefore, the C_p'' peak shifts to higher temperatures at higher frequencies.[484,503,504] The relationship between frequency and peak tip could be expected to be non-Arrhenius in fragile glasses.[1] However, the frequency range of the TMDSC measurements is relatively short. Thus, a short-range Arrhenius relationship between the frequency and the tip of the C_p'' peak position can be used to determine the activation energy for structural relaxation as known from thermally activated processes. Various studies show the correlation between frequency and the peak position in an Arrhenius fashion for a limited frequency range, and a systematic compositional change in activation energy was calculated for those systems.[484,503,504] Figure 46 shows the frequency dependence of the C_p'' peak and the method used to estimate the activation energies from TMDSC signals.[504]

Even though TMDSC does not cover a wide range of frequencies compared to most other dynamic measurements, it still covers a sufficiently wide range to probe the dynamic processes at around T_g. Non-Gaussian C_p'' peaks might be assigned to the phase separation in the glass.[484] Macroscopic and microscopic inhomogeneities can be investigated by examining the frequency dependence of the C_p'' peak. A phase separated arsenic-rich As-Se glass has been investigated by frequency dependent TMDSC measurements.[484] It is a macroscopically phase-separated glass, and the signature of the phase separation could be observed in other macroscopic measurements such as the standard DSC measurements.[484] However, DSC cannot distinguish the dynamics of glassy regions. The As-Se glass structure consists of $AsSe_3$ pyramids and selenium chains depending on the arsenic content.[505] Although the dimensionality of the network changes as a function of composition, the backbone of the structure remains as $AsSe_3$ pyramids.[484,505] When the arsenic content over-exceeds the stoichiometric composition, molecular cagelike structural units start to appear.[505] The dimensionality of these units is very small or zero since they are weakly connected to the backbone of the structure by van der Waals interactions.[484] Therefore, the dynamic response of the pyramidal units, as a function of frequency, is expected to be much slower than that

DOI: 10.1021/acs.chemrev.8b00510
Chem. Rev. XXXX, XXX, XXX−XXX

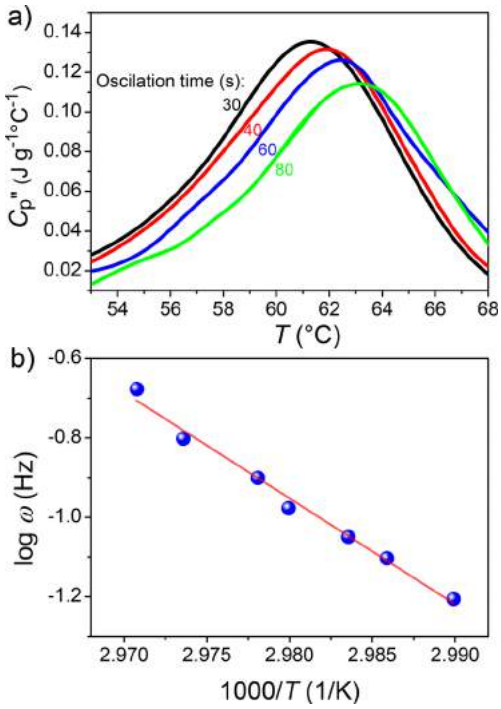

Figure 46. (a) Temperature dependence of C_p'' for various oscillation periods for a side-chain liquid crystalline polymer, i.e., polyM[3-(4@-cyano-4-biphenyloxy)propoxycarbonyl]ethylene. (b) Temperature dependence of the frequency at the C_p'' peak ($\log_{10}\omega$) used to estimate the activation energy. Reproduced with permission from ref 504. Copyright 2000 Royal Society of Chemistry.

of the molecular units. TMDSC measurements are conducted in a period of oscillation range of 100 to 200 s. In each TMDSC scan, two distinct C_p'' peaks are obtained from measurement signals, and the low-temperature peak is observed to be Gaussian, while the high-temperature peak cannot be fitted to a Gaussian function.[484] The high-temperature peak is clearly a convolution of different dynamic responses. The results show more interesting features when the frequency dependence is investigated. As previously explained, the activation energy for structural relaxation can be estimated from the frequency dependence of the tip of the peak positions. The activation energy of the low-temperature Gaussian peak is calculated to be comparable to that of the compositions where there is no significant presence of excess selenium chains or molecular As-Se cage like units.[55,484] In addition to the activation energy, the full width at half-maximum (fwhm) of the low-temperature peak is found to be close to the fwhm value of the $As_{40}Se_{60}$ composition. Thus the low-temperature peak can be assigned to the dynamic response of the backbone of the structure.[55,484] However, there is no significant shift in the high-temperature C_p'', as would be expected from fragile glasses.[55,484] The convoluted non-Gaussian peak shape can be explained by the diversity of the molecular units in the arsenic-rich As-Se compositions.[505] It is known from NMR and Raman studies that various cage-like structures such as As_4Se_4, As_4Se_3, and As_4 form in arsenic-rich glasses.[505] Each of these cage structures has its own independent dynamic response and distribution of structural relaxation.[484] As a result, the backbone of the structure remains in the phase separated glass while the molecular motifs are weakly connected to the glass, and their dynamic responses are significantly different and convoluted in a separate C_p'' peak.[55,505] This study is an excellent example of probing the dynamics and liquid properties of different phases in heterogeneous glasses.

6.3. C_p'' in the Temperature Spectrum

Since the C_p'' peak is correlated to the relaxation time distribution, it can be used to understand the thermal history effects and the liquid dynamic properties of different compositions. To elucidate the dynamical origins of non-exponential relaxation, the thermal history dependent C_p'' peak is analyzed. In a systematic sub-T_g annealing study the nonmonotonic evolution of fwhm is observed while the standard DSC measurements show monotonic evolutions of released enthalpy or T_f. The fwhm scales linearly with the width of the distribution of the relaxation structural times.[62] C_p'' narrows down as a function of annealing time as demonstrated in previous studies in aging polycarbonates.[506] However, the fwhm does not follow the same trend with annealing time due to the nonmonotonic evolution of enthalpy fluctuations.[62] This can be better understood by analyzing the C_p'' peak for each annealing time. Initially, the high-temperature tail of the C_p'' peak shifts with annealing time. The high-temperature tail corresponds to fast relaxing low-density regions. These regions rearrange much quicker than high-density slow regions. Therefore, an asymmetric peak is observed in the initial parts of relaxation.[62] The asymmetric C_p'' peak shape is also reproduced in an aging study in a different glass system,[507] and it can be expected to be a universal feature of the relaxation processes in glasses. After long annealing times, the low-temperature tail of the C_p'' peak, which corresponds to high density and low-mobility regions, starts to move slowly while the high-temperature tail reaches a plateau of shifting rate. Because of this nonmonotonic shifting rate, the C_p'' peak becomes less asymmetric for very long annealing times, and the fwhm broadens again.[62] In standard DSC measurements, these events are represented as a sum of all contributions from all regions. Thus a monotonic stretched exponential behavior is observed. TMDSC allows us to investigate the mechanisms that govern the stretched exponential relaxation. The first-ever experimental demonstration of the nonmonotonic evolution of enthalpy fluctuations is demonstrated by the complex heat capacity approach.[62] The same trend of enthalpy fluctuations is also shown with enthalpy landscape model simulations. These results are also in good agreement with a similar study that shows the nonmonotonic evolution of density fluctuations in both glassy selenium and an oxide glass.[508]

The fwhm of the C_p'' peak can also be correlated with the fragility of different glass compositions.[484] Since the C_p'' peak is correlated to the distribution of relaxation times, it can be used to evaluate the relationship between the fragility and relaxation variation in different compositions. As-Se is a good choice of glass family since arsenic and selenium atoms are very similar in size, it has a broad compositions range for glass formation, and a wide range of fragilities can be studied by simply changing the selenium content.[505] The fwhm of the C_p'' is compared with the m values, which were obtained by equilibrium viscosity measurements near the glass transition range. The results are intriguing because the fwhm of the C_p'' peak is inversely proportional to m up to high arsenic contents where the glass compositions tend to be phase separated. Figure 47 shows the Gaussian fit and fwhm on a C_p'' peak, fwhm as a function of arsenic content, and fragility index values

DOI: 10.1021/acs.chemrev.8b00510
Chem. Rev. XXXX, XXX, XXX−XXX

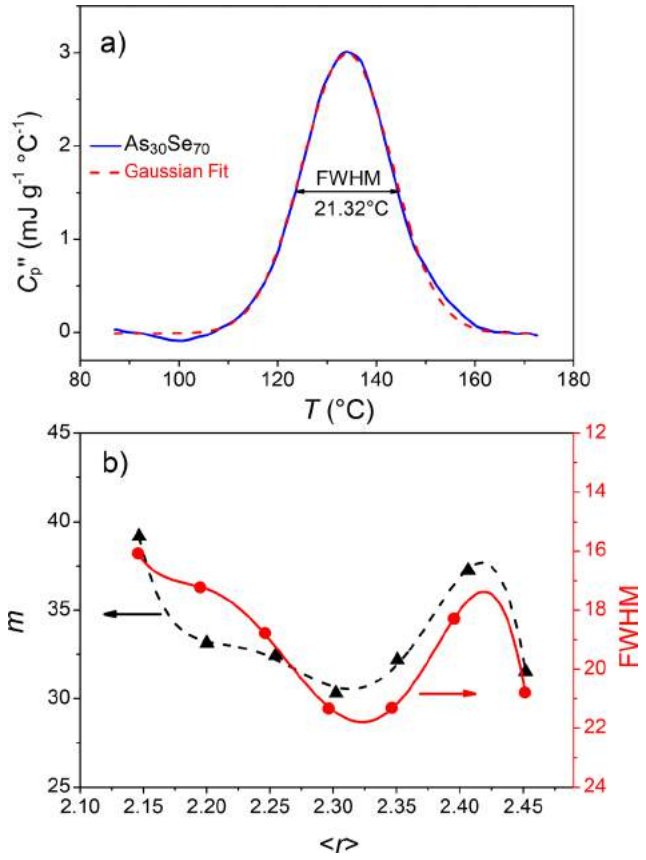

Figure 47. (a) Gaussian fit on C_p'' peak for $As_{30}Se_{70}$; (b) Fragility index m and fwhm as functions of arsenic content (linearly correlated to the average coordination $\langle r \rangle$). Reproduced with permission from ref 484. Copyright 2012 American Physical Society.

as a function of mean coordination number $\langle r \rangle$.[484] It should also be noted that $\langle r \rangle$ has a simple linear correlation with arsenic content in As-Se glasses and it can be shown as $\langle r \rangle = 2 + x$ where x is the arsenic molar fraction content in As_xSe_{1-x} compositions.[505] Another aspect of these results is that higher arsenic content glasses do not follow this trend since the fwhm is artificially broadened due to the diverse dynamics of various macroscopically separated structural units.[484]

The tip point of the C_p'' peak is equal to the temperature where the average relaxation time is $2\pi P$. Since the standard periods used in TMDSC measurements correspond to a range of 40 s < (P) < 200 s, T_g can be estimated by the extrapolation of the arhenius trend of tip points of C_p'' from higher frequencies to lower frequencies in the vicinity of T_g. The frequency dependence of the C_p'' peak temperature can also be used to estimate the temperatures that correspond to the average relaxation time for each oscillation frequency. Then, the peak temperature (T_ω) can be normalized by T_g as in Angell's universal plot to scale viscosity slopes of glass-forming supercooled liquids. The slope of the relaxation time curve when plotted vs T_g/T_ω yielded the m value of the glass.[509] The m values estimated from TMDSC agree well with those reported in the literature, which are estimated using the standard viscosity method.[509] In a recent study, the m values of calcium−alumina−silicate glasses are determined by the TMDSC method,[487] where a systematic offset is observed as a function of silica content.[487,510] A similar systematic deviation is observed in another study when the m values determined by conventional DSC are compared to viscosity data.[91] Empirical models can be used to correct the results if the goals are pragmatic and confined to a single family of glass compositions. However, there is no unambiguous explanation presented to clarify the systematic deviation. To find the origin of such a deviation, it should be considered that both DSC and TMDSC methods for the m determination are based on the thermodynamic properties, e.g., heat flow, enthalpy, and heat capacity, of glass-forming liquids, whereas standard m determination is based on dynamic properties, e.g., shear viscosity and relaxation time. The activation energy for viscous flow and activation energy for enthalpy relaxation are assumed to be equivalent. However, this assumption has not been proven in a wide range of glass compositions. Intuitive assumptions are preferred for preliminary experiments, but more comprehensive studies are needed to judge if the assumption is reasonable. Also, equilibrium viscosity measurements used to estimate the fragility index are challenging and time-consuming and very limited data can be found in the literature based on those measurements.

Another interesting application of TMDSC is the evaluation of the stretched exponential structural relaxation function at T_g, from which the nonexponentiality of the enthalpy relaxation can be quantified. Matsuda et al.[511] analyzed the real and imaginary parts of the complex heat capacity for a series of lithium borate glasses by using an analogy to the dielectric spectroscopy. The Havriliak−Negami (HN) equation was used to fit the Cole−Cole plot,[512] which is displayed

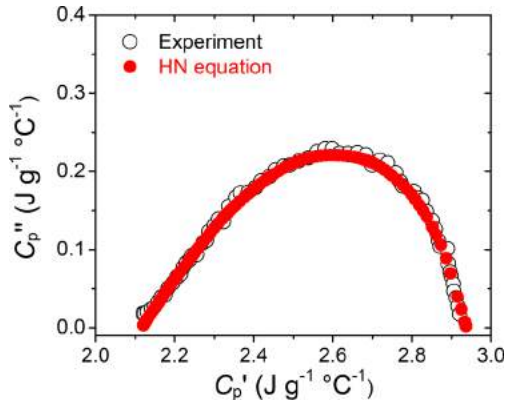

Figure 48. Measured data vs Havriliak−Negami fit used to estimate the stretched exponent for $12Li_2O.88B_2O_3$ glass. Reproduced with permission from ref 510. Copyright 2008 Physical Society of Japan.

in Figure 48 as the imaginary part of the complex heat capacity vs the real part. The HN equation[513] is shown as

$$C_p^*(\omega) = C_p^\infty + \frac{C_p^0 - C_p^\infty}{[1 + (i\omega\tau)^{\alpha_D}]^{\gamma_D}} \quad (43)$$

where C_p^* is the complex isobaric heat capacity, γ_D and α_D are Debye parameters, τ is the relaxation time, and C_p^0 and C_p^∞ are the isobaric heat capacity in the zero and infinite frequency limits. Based on the parameters obtained from the fit and considering their correlation to the KWW stretching exponent β:[514]

$$\gamma_D\alpha_D = \beta^{1.23} \quad (44)$$

DOI: 10.1021/acs.chemrev.8b00510
Chem. Rev. XXXX, XXX, XXX−XXX

nonexponentiality of the relaxation function at T_g can be estimated.

6.4. Probing Glass Relaxation via Nonreversing Heat Flow

Nonreversing heat flow is thought to be correlated with the enthalpy relaxation of glasses.[54,483] The ΔH_{nr} approach is mostly used in relaxation studies and investigations of topological constraints in various glass systems. The concept of intermediate compositions was introduced by Boolchand as an extension to the original topological constraint theory.[493] In their original work, Phillips[133] and Thorpe[409] classified glasses as a function of their mean coordination numbers. In a three-dimensional system such as network glasses, the universal value of $\langle r \rangle = 2.4$ corresponds to the transition from floppy and underconstrained glasses to rigid and overconstrained glasses. $\langle r \rangle = 2.4$ is found to be an ideal composition for achieving the optimum glass forming ability,[133] and it is also found to be a threshold composition point for the trends of various physical properties.[505] Through the intermediate phase the behavior at $\langle r \rangle = 2.4$ is extended to a range of compositions where the glass is believed to be isostatic, i.e., rigid but not stressed. TMDSC is essential to find those intermediate regions since ΔH_{nr} is expected to be zero or near zero for the intermediate phase compositions. The transition from the overconstrained/underconstrained compositions to the intermediate phase can be amplified when the glasses are annealed below the initial fictive temperature for a long time since the intermediate phase compositions are not expected to show significant enthalpy relaxation. Therefore, the value of ΔH_{nr} remains close to the zero, while the value of ΔH_{nr} significantly increases with annealing for compositions outside the intermediate region.[515] Boolchand and co-workers studied intermediate phases for more than two decades in many glass systems including chalcogenides and oxides.[493−496,516] However, there is still debate on the existence of intermediate phases determined by nonreversing heat flow measurements. The following section summarizes some examples of the ongoing debate about the topic.

It is claimed that the ΔH_{nr} is measured for only one frequency and it cannot represent the glass transition behavior.[488] The activation energy for enthalpy relaxation estimated by Moynihan's method shows a different trend than the ΔH_{nr} trend in Ge-Se glass compositions.[488] Figure 49 shows the activation energy vs ΔH_{nr} as a function of average coordination.[488,517]

However, frequency correction simulations proved the frequency dependence of ΔH_{nr} could be overcome by the frequency correction[502] and proper frequency selection. The frequency correction procedure is basically subtraction of the ΔH_{nr} measured during the cooling curve from the ΔH_{nr} measured during the heating scans.[502] Simulations of such corrections in a wide range of frequencies yield a master ΔH_{nr} curve. This study also shows that ΔH_{nr} curves collapse into a master curve both in quenched and in annealed glasses. Based on the results of this study, the frequency correction can be made without interference from the thermal history.[502] This study can be considered as a solution to the problem raised by Schawe, who claims that the ΔH_{nr} should be nonzero in the cooling experiment.[474] However, there is still no clear explanation regarding the difference between the trends of the activation energy for enthalpy relaxation and ΔH_{nr}. The disagreement between the two data sets raises another question about the position of the intermediate phase. As

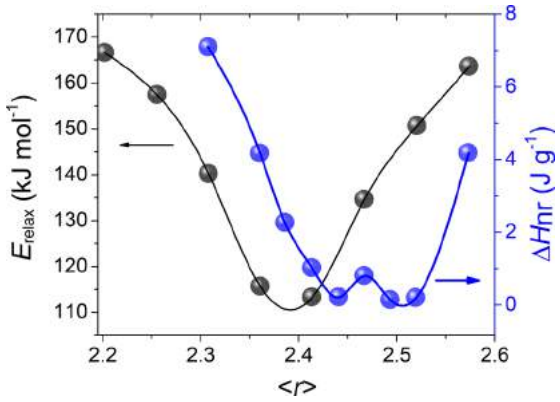

Figure 49. Activation energy for enthalpy relaxation (E_{relax}) and the nonreversing heat flow (ΔH_{nr}) as functions of the mean coordination number $\langle r \rangle$ for Ge-Se glasses. Reproduced with permission from ref 488. Copyright 2009 American Physical Society.

can be seen from Figure 49, the activation energy trend is centered at $\langle r \rangle = 2.4$ as proposed in the original theory and involves a sharp transition from the floppy to the rigid regions. On the other hand, the intermediate region is centered around a higher average coordination number. The structural origins of the existence of the intermediate phase are still being debated and out of the scope of this review.

Reproducibility of the ΔH_{nr} measurements was investigated by Golovchak et al.[489] and by Zeidler et al.,[518] who studied the systems Boolchand and co-workers had studied using TMDSC. Figure 50a shows the comparison of those authors' ΔH_{nr} measurements in the Ge-Se glass system. In the Ge-Se system there is a significant offset between the trends of those two data sets, and Zeidler's data show a narrow range of compositions showing zero ΔH_{nr} values centered around $\langle r \rangle$

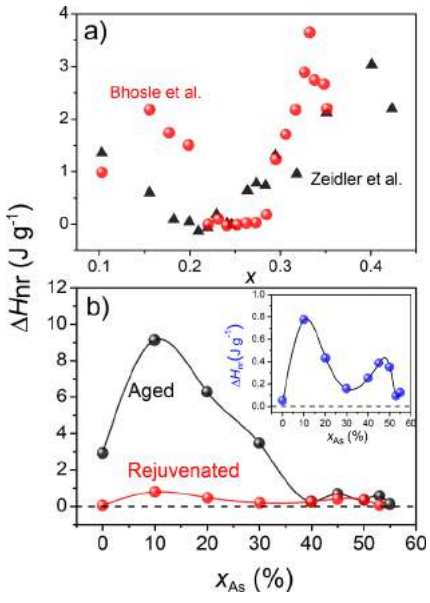

Figure 50. (a) Comparison of ΔH_{nr} measurements in the Ge-Se glass system.[495,518] Reproduced with permission from ref 495 and ref 518. Copyright 2012 John Wiley and Sons. (b) ΔH_{nr} measurements for both aged and rejuvenated conditions in the As-Se system.[489] The inlet shows the rejuvenated trend in a magnified scale. Reproduced with permission from ref 489. Copyright 2008 American Physical Society.

DOI: 10.1021/acs.chemrev.8b00510
Chem. Rev. XXXX, XXX, XXX−XXX

= 2.4 (40 mol% arsenic), while Boolchand's data show a broad range of intermediate compositions with a sharp transition centered well above $\langle r \rangle$ = 2.4.

Golovchak et al.[489] studied the As-Se glass family for both aged and rejuvenated conditions. Figure 50b displays the difference in ΔH_{nr} for two different thermal histories. Golovchak's results show an increase in ΔH_{nr} in aged samples and a zero nonreversing heat flow plateau at and above $\langle r \rangle$ = 2.4. These results are in agreement with Mauro and Varshneya's Monte Carlo simulations,[519] where the rigidity percolation occurs at 40 mol% arsenic composition of As-Se glass, which corresponds to $\langle r \rangle$ = 2.4. As expected, the rejuvenated samples show no such clear distinction, but the difference in ΔH_{nr} values becomes more pronounced in aged glasses. However, Boolchand's data set[494] shows an intermediate phase from approximately $\langle r \rangle$ = 2.28 to $\langle r \rangle$ = 2.38 range. It is claimed that the difference between the ΔH_{nr} values is a result of the inhomogeneity in glasses, and melt homogenization requires longer time than the conventionally used technique to make chalcogenide glasses.[520] It is also claimed that the intermediate phase transition becomes more pronounced when the melt homogenization is fully completed. However, another study showed no measurable difference in the composition or structure when the glass is melted conventionally or longer as recommended by Boolchand.[521] Furthermore, the same study could not find a significant difference in m values of chalcogenide glasses prepared by both conventional and longer melting methods.[521] In addition, the m values of intermediate phases are slightly larger for longer melting methods than for the conventional method,[521] in contrast to what was previously reported.[522]

Lastly, it can also be expected that the measurement of the T_f or released enthalpy as a function of compositions for different thermal histories would give the same results since the ΔH_{nr} measures the macroscopic enthalpy relaxation. T_f measurements are based on the standard DSC method, and the heating rates are 5 to 10 times faster than TMDSC, without requiring exhaustive data collection or analysis. It has been a well-established method[100,173] and is a good representative of the enthalpic state of the glass. Therefore, the ΔH_{nr} approach might not be necessary. However, there is no fully rigorous conclusion about the meaning, use, or interpretation of the ΔH_{nr}. Therefore, more data and involvement of objective observers would be helpful for explaining the meaning and applications of the *nonreversing heat flow* concept.

7. UNDERSTANDING CRYSTALLIZATION IN GLASSES

Glasses are formed when the kinetic demands of thermodynamic equilibrium are not met by manipulating the chemical composition, sample size, or cooling rate of a melt. Following the most common route of glass formation, i.e., quenching from a melt, any SCL can, in principle, be vitrified if crystallization is averted. We stress once more that vitrification occurs at a temperature T_g, where the structural relaxation time of the SCL becomes equal to or longer than the experimental observation time.[65] Understanding the role of critical factors that determine the vitrification and crystallization processes, such as glass composition, the structure of the SCL, thermal history, and diffusion processes, is a vital step for the study and development of new materials that readily form glasses, or for the successful progress of glass-ceramic science and technology.[21]

Nucleation and crystal growth are the two essential stages of crystallization; nucleation is the spontaneous or induced (catalyzed) formation of nuclei at the nanoscale, which is followed by their growth into well-defined crystals. For glass formers, homogeneous nucleation is typically observed in a temperature range well below the temperature of maximum crystal growth rates (T_G), whereas heterogeneous nucleation rate versus temperature curves often are close and even overlap with those of crystal growth.[523]

Crystallization of glasses (or more correctly, crystallization of supercooled liquids) is an exothermic process that can be readily detected by thermal analysis techniques, such as DSC and DTA. In a typical DSC curve of a glass, crystallization is displayed as an exothermic peak after the glass transition, T_g, as depicted in Figure 51. For stoichiometric compositions, the

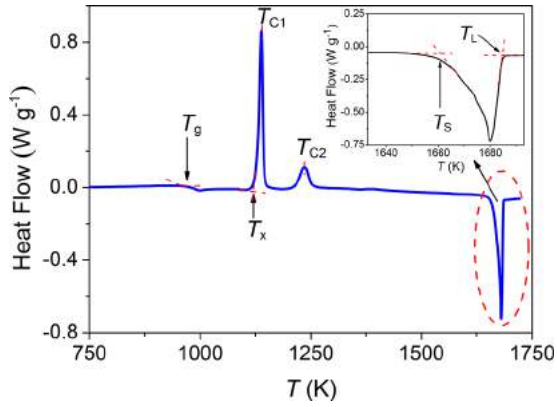

Figure 51. Typical DSC upscan trace for barium disilicate ($BaO \cdot 2SiO_2$) glass showing the glass transition temperature (T_g), the crystallization onset (T_x), the crystallization peaks (T_{c1}, T_{c2}), and the *solidus* (T_S) and the *liquidus* temperatures (T_L). Adapted from ref 525. Copyright 2018 Elsevier Science B.V.

crystallization temperature (T_c), corresponds to the peak temperature in a DSC trace, whereas the onset crystallization temperature is called T_x.[524] Upon continuous heating, in the end, an endothermic peak is a signature of melting (T_L). For off-stoichiometric compositions, two or more crystallization and melting peaks may appear.

Detailed knowledge of the thermodynamics and kinetics of crystal nucleation and growth is crucial, either to avoid devitrification or to control the crystallization of glasses.[22,23,526,527] Glass crystallization-related problems including crystal nucleation rates, induction periods for nucleation, crystal growth rates, glass stability, and glass forming ability are critical parameters in both academic and industrial studies. These phenomena are usually studied by optical and electron microscopy, X-ray diffraction (XRD), nuclear magnetic resonance (NMR), or DSC tests, which will be described here.[528−532]

In addition to the kinetic aspects of crystallization, T_L (Figure 51 inset) is of utmost importance. T_L is the highest temperature of thermodynamic equilibrium between the solid and liquid phases of any material, above which any crystal is unstable and dissolves in the liquid. To accurately manage the temperatures at which glass melting and fining processes can be operated, one must know this *liquidus* temperature, T_L. However, its precise determination is challenging and time-consuming, especially for glass compositions that are difficult to crystallize, i.e., for many commercial glass-forming

DOI: 10.1021/acs.chemrev.8b00510
Chem. Rev. XXXX, XXX, XXX−XXX

compositions, which are designed to resist crystallization. This difficult task is typically conducted by way of a traditional microscopic investigation after treating rod samples in a gradient furnace for a long time and then examining them by microscopy. In this section, we will explain a much faster DSC method that has been successfully tested for determination of T_L.

Here we elaborate on the application of different DSC techniques for the determination of phase transformations in inorganic oxide glasses, including crystal nucleation, crystal growth, overall crystallization kinetics, and the *liquidus* temperature.

7.1. Crystal Nucleation Kinetics

Nucleation is the earliest stage of crystallization and can be categorized into homogeneous and heterogeneous processes. Homogeneous nucleation is stochastic and happens with the same probability in any given volume of a glass sample. On the other hand, nucleation occurring on preferred nucleation sites, such as solid impurities, pre-existing interfaces, previously crystallized phases, and surface defects, is called heterogeneous nucleation. Many inorganic glasses and their corresponding SCLs are fascinating materials for studies of nucleation and crystal growth due to their high viscosities below the *liquidus* temperature, leading to relatively low (measurable) rates of crystallization. These materials then serve as models for detailed studies of nucleation and growth kinetics.[9]

Homogeneous nucleation can indeed be observed in the interior of specific glasses at deep undercoolings ($T/T_L < 0.6$), because inorganic glass-forming melts can readily dissolve most solid impurities (which could act as catalyzes) that exist only as ionic species when the liquid is vitrified. Some of these ionic impurities accelerate or impair nucleation and growth rates by modifying the crystal/liquid surface energy or viscosity, but they do not induce heterogeneous nucleation. Furthermore, the rapid increase in viscosity with decreasing temperature allows for the "freezing" of different states on the crystallization pathway by quenching previously heat-treated specimens to room temperature.[533,534] It was once figuratively mentioned that "glasses did and may serve as the Drosophila of nucleation theory to test different approaches."[535]

Tammann's method[536] is commonly used to determine the number density of supercritical nuclei. This method consists in a double-stage treatment, i.e., the "development" of crystal nuclei at temperatures higher than the typical nucleation temperatures to a size sufficiently large to be visible under an optical or electron microscope. Nucleation rates covering a broad range of values can be determined by this method. For example, measured crystal nucleation rates for various oxide glasses cover a wide range between 10^1 $m^{-3}{\cdot}s^{-1}$ and 10^{17} $m^{-3}{\cdot}s^{-1}$.[512] While Tammann's method can yield correct values of nucleation rates, it is quite laborious and does have limitations.[537]

7.1.1. Estimation of the Temperature of Maximum Nucleation. In the early 1980s, Marotta et al.[538−540] proposed different techniques based on DTA/DSC experiments to study the crystallization kinetics of glass-forming systems. In contrast with Tammann's method, their nonisothermal methods typically consider combined nucleation and growth kinetics. In this method, only the *temperature* of maximum nucleation can be estimated (not the nucleation rates themselves) using the fact that a higher number of nuclei leads to faster overall crystallization kinetics, and hence the DSC crystallization peak moves to lower temperatures. The DSC/DTA crystallization peak temperature, T_c, is proportional to the number density of nuclei.[538] This behavior is illustrated by plotting T_c or $1/T_c$ versus T_N (the temperature of nucleation treatment for a given time), which indicates the temperature dependence of the nucleation rate, or more exactly, the crystal number density (N) nucleated in a definite treatment time. The minimum in the T_c vs T_N curves or maximum in $1/T_c$ vs T_N corresponds to the most efficient nucleation temperature (Figure 52a).

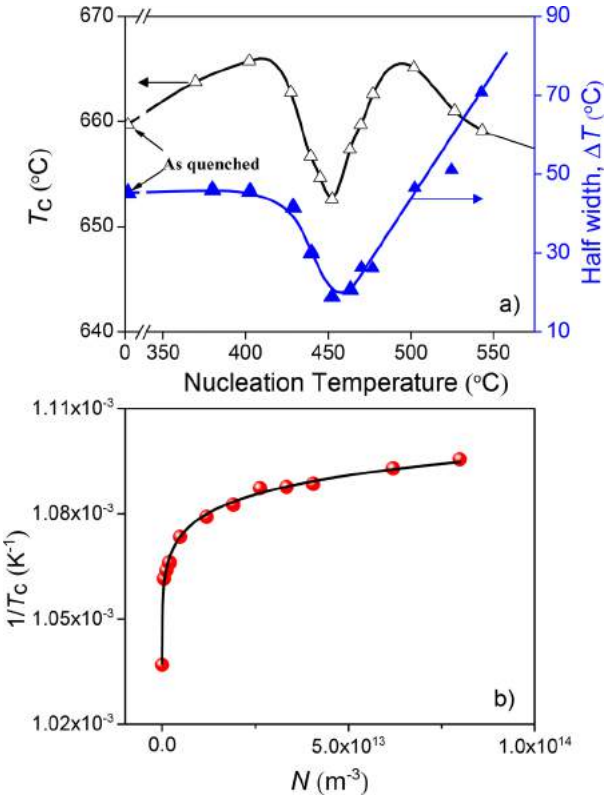

Figure 52. (a) Temperatures of the DTA crystallization peak, T_c, and the half-width at half-maximum, ΔT, as a function of nucleation temperature, T_N (for 3 h) for a $Li_2O{\cdot}2SiO_2$ glass. T_N = 453 °C, from Ray et al. Reproduced with permission from ref 541. Copyright 1990 John Wiley and Sons. (b) $1/T_c$ versus the number of lithium disilicate crystals, N. N increases with the time of nucleation at T_N = 473 °C. Reproduced with permission from ref 546. Copyright 2010 Elsevier Science B.V.

Furthermore, to a first-order approximation, the DSC crystallization peak area is proportional to the remaining amount of residual glass, whereas its width is determined by the time needed for complete crystallization, which depends on both the number of nuclei and the crystal growth rate. For a constant crystal growth rate, the peak width decreases and its height increases with increasing number of nuclei. Therefore, the height or half-width at half-maximum of the crystallization peak can also be used (Figure 52a) to deduce the temperature dependence of the number of nuclei.[541−549]

Weinberg[544] and Kelton[545] independently showed that the peak height method works for lithium disilicate glass (LS2) and is applied by a combination of isothermal preannealing treatments followed by devitrification measurements in nonisothermal DTA experiments. These authors also demonstrated that the use of $1/T_c$ is more accurate than the peak height for predicting the temperature dependence of the

DOI: 10.1021/acs.chemrev.8b00510
Chem. Rev. XXXX, XXX, XXX−XXX

nucleation rates. Specifically, Fokin et al.[546] used a lithium disilicate glass to show both experimentally (Figure 52b) and theoretically that the relationship of $1/T_c$ with N is logarithmic. Furthermore, Xia et al.[547] recently used this method to estimate the crystal nucleation temperature for $BaO{\cdot}2SiO_2$ and $5BaO{\cdot}8SiO_2$ glasses (for the latter, nucleation data were not available). For the $BaO{\cdot}2SiO_2$ glass, the temperature range where considerable nucleation occurs is 660−770 °C, with a maximum rate near 710 °C. Their results were in good agreement with those determined by the traditional two-step annealing, microscopy-based studies (Tammann's method). They found that the temperature range of significant nucleation for the $5BaO{\cdot}8SiO_2$ glass is about 675−790 °C, with a maximum rate near 725 °C, which is slightly higher than for the $BaO{\cdot}2SiO_2$ composition. Xia et al.[547] compared the peak height, peak temperature, and peak area to estimate the temperature where growth starts to overlap considerably with nucleation. The peak height appeared to be a more sensitive indicator for determining this effect. Finally, they concluded that while DTA/DSC methods are not quantitatively predictive, they are useful for providing estimates of the temperature range where significant nucleation occurs.

7.1.2. Estimation of Nucleation Kinetics. *7.1.2.1. Method of Ray et al.* Another type of nonisothermal approach was proposed by Ray et al.[548] and Ranasinghe et al.[549] for quantitative determination of steady-state nucleation rates as a function of temperature. They suggested that the area, A, under the crystallization peak of a DTA/DSC scan of a given stoichiometric glass is proportional to the volume of residual glass, V_g, remaining in a sample that has been *previously treated* to induce partial crystallization. Therefore:

$$A(t) = kV_g(t) = k(V_0 - V_c(t)) = kV_0\left(1 - \frac{V_c}{V_0}\right) = kV_0(1 - \alpha(t)) \tag{45}$$

where V_0 is the volume of the sample before transformation, $V_c(t)$ is the crystallized volume, and $\alpha(t)$ is the fraction of crystallization.

In this method, precrystallized glasses are subjected to a DTA/DSC test according to the schematic illustration in Figure 53, and the crystallized volume fraction is estimated by the decrease of the crystallization peak area, $A(t)$, on a DTA/DSC curve due to the transformation of the residual glass. The fraction of residual glass decreases due to the previous nucleation at T_N for time t_N plus growth at $T_G > T_N$ for time t_G. The crystallized volume fraction, $\alpha(t)$, is then calculated by the Johnson−Mehl−Avrami−Yerofeeyev−Kolmogorov (JMAYK) equation:[550−553]

$$\alpha(t) = \frac{V_c(t)}{V_0} = 1 - \exp[-\alpha'(t)] \tag{46}$$

where $\alpha'(t)$ is the transformed volume of residual glass without taking into consideration the overlap of the growing particles, frequently denoted the "extended volume."

For the particular case of three-dimensional crystals simultaneously nucleating and growing in the interior of a glass sample that is isothermally treated at T, the $I(T)$ and $U(T)$ curves overlap to some extent, and $\alpha'(t)$ is given by

$$\alpha'(t) = g\int_0^t I(T)\left[\int_{t'}^t U(T)\,dt'\right]^3 dt \tag{47}$$

where g is a shape factor, which is equal to $4\pi/3$ for spherical crystals, and t is the time. Assuming that the nucleation and growth rates are time-independent at a given temperature (steady-state homogeneous nucleation and growth), eq 47 becomes

$$\alpha'(t) = \frac{\pi}{3}(I{\cdot}t)(U{\cdot}t)^3 \tag{48}$$

For double-stage heat treatments, i.e., a treatment for nucleation at a temperature T_N followed by another treatment for growth at a higher temperature, T_G, such that no significant nucleation and no significant dissolution of critical nuclei happens during the growth step, one can write eq 47 as follows:

$$\alpha'(t) = \frac{4\pi}{3}\int_0^{t_N} I(T)\,dt\left[\int_0^{t_G} U(T)\,dt'\right]^3 \tag{49}$$

Assuming time-independent rates, after integration, eq 49 becomes

$$\alpha'(t) = \frac{4\pi}{3}(I{\cdot}t_N)(U{\cdot}t_G)^3 \tag{50}$$

Ray et al. combined eqs 46 and 48 to obtain

$$\alpha(t_G) = 1 - \exp\left(-\frac{\pi}{3}(I(T_N)t_N + N_{at})U(T_G)^3 t_G^3\right) \tag{51}$$

where $(I(T_N)t_N + N_{at})$ is the total number of nuclei formed by nucleation at T_N with the rate I plus athermic nuclei (N_{at}), which are the nuclei formed during cooling the melt to form the glass (quenched-in or athermic nuclei, N_{at}), and during the heating up of the glass sample to the temperature T_G. The prior crystallization reduces the DSC crystallization peak area, A. By varying the growth time, t_G, at fixed nucleation conditions (T_N and t_N), the value of α, and therefore A, will change. Ray et al.[548] considered $\alpha(t) = \alpha'(t)$ (an approximation of eq 46 that is valid for small volume fraction crystallized) and combined eq 45 with eq 51. They subsequently proposed the following equation for the ratio of peak areas corresponding to two different values of t_G:

$$\frac{A_1}{A_2} = \frac{V_1\left[1 - \frac{\pi}{3}(It_N + N_{at})(Ut_{G1})^3\right]}{V_2\left[1 - \frac{\pi}{3}(It_N + N_{at})(Ut_{G2})^3\right]} \tag{52}$$

where V_1 and V_2 are the volume of the residual glasses after two cycles of heat treatment. When the density of the residual glass does not vary appreciably, eq 52 reduces to

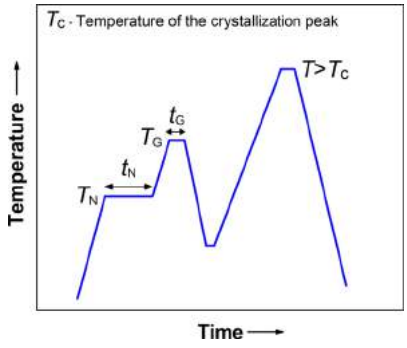

Figure 53. Schematic diagram of the thermal treatment used by Ray et al.[548] to study nucleation kinetics via DSC experiments.

DOI: 10.1021/acs.chemrev.8b00510
Chem. Rev. XXXX, XXX, XXX−XXX

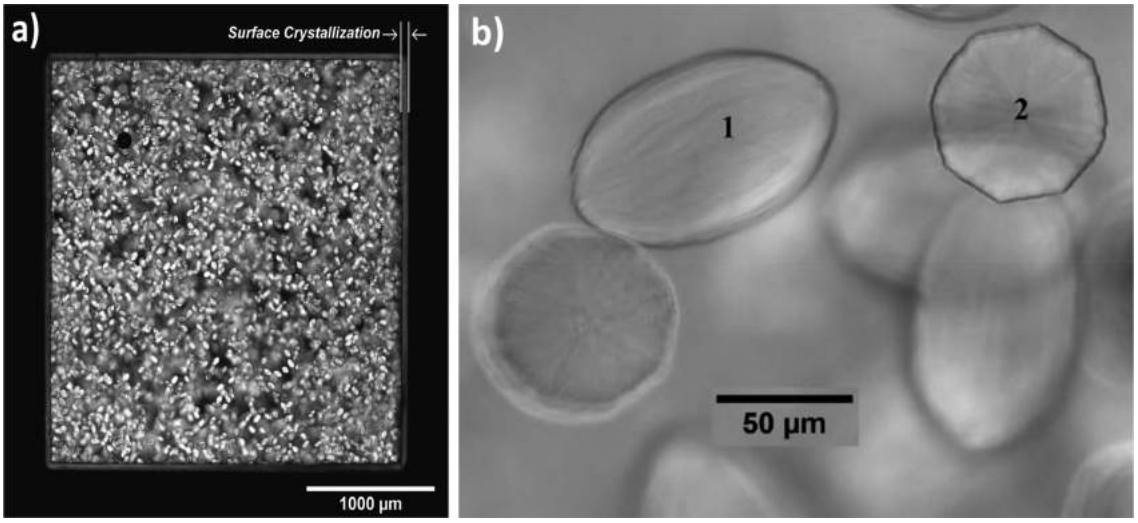

Figure 54. (a) Transmitted light micrograph of a LS2 glass sample after a DSC run (nucleation at 480 °C for 10 min, growth at 620 °C for 10 min, with heating/cooling rates of 20 °C/min). (b) Lithium disilicate crystals in a LS2 glass. Ellipsoids can be observed in the plan (1) and front (2) views. Reproduced with permission from ref 546. Copyright 2010 Elsevier Science B.V.

$$\frac{A_1}{A_2} = \frac{M_1\left[1 - \frac{\pi}{3}(It_N + N_{at})(Ut_{G1})^3\right]}{M_2\left[1 - \frac{\pi}{3}(It_N + N_{at})(Ut_{G2})^3\right]} \quad (53)$$

where M_1 and M_2 are the sample masses for two DSC runs corresponding to times of growth t_{G1} and t_{G2}, respectively. Therefore, the total number (N_{total}) of nuclei ($It_N + N_{at}$) and the number of athermic crystals can be estimated separately by eq 53, which is simplified as follows:

$$N_{total} = It_N + N_{at} = \frac{3(A_1M_2 - A_2M_2)}{\pi U^3(A_1M_2t_{G2}^3 - A_2M_1t_{G1}^3)} \quad (54)$$

The analysis of Ray et al.[548] is based on three assumptions, which can lead to significant errors in some cases: (1) The first assumption is a linear proportionality of A and $\alpha(t)$ in eq 45. (2) The second supposition, i.e., that $\alpha(t) = \alpha'(t)$, is only valid for small crystallized volume fractions. Hence, eq 54 is limited to approximately $\alpha(t) < 0.1$, i.e., before the crystals impinge. (3) Finally, the use of eq 48 instead of eq 50 should not be applied to this type of DSC test because significant nucleation does not normally happen during the growth step. Therefore, eq 50, which assumes a constant number of nuclei in that step, is more appropriate. In other words, if the heating rate in a DSC test is fast enough and crystallization occurs via crystal growth from a fixed number of nuclei, the values calculated from eq 54 must be divided by four, as expressed by eq 50.

By knowing t_{Gi}, A_i, M_i (i = 1 and 2), and U, ($It_N + N_{at}$) can be calculated by eq 54. If the value of $U(T_G)$ is known (e.g., as measured by optical microscopy), the total number of nuclei ($It_N + N_{at}$) per unit volume of the glass and, hence, the steady-state nucleation rate, I, at any temperature can be determined using eq 54. For a comparable sample mass, the area of the second DTA peak (A_2) is smaller than that of the first (A_1) if $t_{G2} > t_{G1}$. For a reasonably high U, A_2 may be too small to measure. In that case, M_2 should be made sufficiently larger than M_1 such that a measurable peak can be obtained for the second DTA run.

In this method, the value of $U(T)$ at any suitable temperature should be known, which, therefore, must be measured first by microscopy (See Section 7.2). Then, the temperature at which U is measured by the conventional method (e.g., T_G) can be used as the crystal-growth temperature in the DTA experiments for all other measurements to determine the quantity ($It_N + N_{at}$), as a function of nucleation time (t_N) at the fixed nucleation temperature (T_N). After the induction time (t_{ind}) for nucleation at the temperature T_N, a plot of ($It_N + N_{at}$) is expected to be a linearly increasing function of t_N. Therefore, the slope of the ($It_N + N_{at}$) vs t_N line is the steady-state nucleation rate, I, at T_N. The value of ($It_N + N_{at}$) for $t_N \ll t_{ind}$ is the number of quenched-in nuclei (N_{at}) in the glass. However, the value of N_{at} also can be determined separately from a pair of DTA runs for glass samples that have not been subjected to any nucleation heat treatment (i.e., $It_N = 0$ in eq 54) but have been subjected to crystal-growth heat treatments at T_G for two different times (t_{G1} and t_{G2}) before the DTA measurements.

The methods of Ray et al. have been successfully tested[541,548] using literature data for the nucleation and growth rates of stoichiometric lithium disilicate, $Li_2O{\cdot}2SiO_2$ (LS2) and sodium calcium silicate, $Na_2O{\cdot}2CaO{\cdot}3SiO_2$ (N1C2S3) glasses, which show internal homogeneous nucleation.[541,548] That method was also justified theoretically by comparing the nucleation rates from model calculations and computer-generated DTA data.[554]

7.1.2.2. Improved Method of Fokin et al. In a detailed study about the changes in the DTA crystallization peak position as a function of pre-DTA heat-treatment times and temperatures, proposed by Marotta, Buri, and Branda,[538−540] Fokin et al.[546] argued that the DSC/DTA crystallization peak position does *not* show a linear dependence with the number of pre-existing nuclei. This fact together with non-steady-state nucleation effects (which is always significant in a temperature range near the glass transition temperature) distorts the real temperature dependence of the nucleation rate when one employs this DSC peak shift method. Fokin et al. made it clear that some other key factors, such as surface crystallization, have also been neglected in previous studies. Surface crystallization has a significant role when the relative volume crystallized is small, e.g., in the case of athermic crystals. Also, the crystal growth rate, $U(T)$, is not constant in nonisothermal heat treatments between the nucleation and growth temperatures.

DOI: 10.1021/acs.chemrev.8b00510
Chem. Rev. XXXX, XXX, XXX−XXX

The formation of nonequilibrium phases can also have a considerable effect on the DTA/DSC crystallization peak. Finally, the calculations in the method of Ray et al.[548] are very sensitive to the crystal growth rate, which appears in cubic form (U^3) and strongly depends on viscosity, which, in turn, is sensitive to the deviation from nominal stoichiometry and also uncontrollable impurities, such as water. Ray et al. tested[541,548] their method using literature data for growth rates of stoichiometric lithium disilicate and $Na_2O{\cdot}2CaO{\cdot}3SiO_2$ glasses, which imposed further errors because the growth rates of glasses prepared in different conditions usually deviate from each other. Additionally, to estimate the value of growth rates correctly, one must know the morphology of the crystals, since, in the case of asymmetric forms, crystal growth cannot be characterized by a single value.[546] All of these factors prevent an accurate analysis of nucleation kinetics by DSC/DTA methods. Additionally, one needs some preliminary data on the nucleation and growth rates of the parent glass to consider all the above effects when employing DTA/DSC methods to determine nucleation kinetics.

Therefore, Fokin et al.[546] have modified Ray's method[541,548] to address all these issues. They measured the growth rate of their glass, considered an average crystal growth rate in different dimensions, and derived the following equation as a substitution for Ray's eq 54:

$$N_{total} = It_N + N_{at} = \frac{3}{4\pi}\left(\frac{1}{U^3(t_{G2}^3 - t_{G1}^3)}\right)\ln\left(\frac{A_1M_2}{A_2M_1}\right) \quad (55)$$

As described earlier, Fokin et al. already knew that the above calculation is very sensitive to the crystal growth rate (U^3), surface crystallization, crystal shape, etc. Therefore, they modified eq 55 in the case of crystallization in lithium disilicate (LS2) glass (Figure 54). Since at T_G the shape of the lithium disilicate crystals is close to an ellipsoid of revolution, with the minimum growth rate U_{min} and the maximum growth rate $U_{max} = kU_{min}$, where k is the proportionality constant, eq 55 should be replaced by eq 56.

$$N_{total} = It_N + N_{at} = \frac{3k^2}{4\pi U_{max}^3}\left(\frac{1}{t_{G2}^3 - t_{G1}^3}\right)\ln\left(\frac{A_1M_2}{A_2M_1}\right) \quad (56)$$

To estimate the role of surface crystallization, a coefficient β was introduced as the ratio between the sample volume reduced by surface crystallization and the initial sample volume. In the case of $M_1 = M_2$, eq 56 was written as

$$N_{total} = It_N + N_{at} = \frac{3k^2}{4\pi U_{max}^3}\left(\frac{1}{t_{G2}^3 - t_{G1}^3}\right)\ln\left(\frac{A_1\beta_2}{A_2\beta_1}\right) \quad (57)$$

where β_1 and β_2 are the ratios between the sample volume reduced by surface crystallization for two different growth times.

It is usually assumed that using relatively high heating and cooling rates (e.g., 20 °C/min or higher) one can neglect crystal growth during the nonisothermal regime before reaching T_G. Hence, growth predominantly happens at T_G. However, this assumption may not always be valid. Also, some overheating may take place during the growth stage. Both effects lead to an underestimate of the growth rate and to an increase in the values of N. Fokin et al. tested this hypothesis by using eq 58, a slightly altered version of eq 57.

$$N_{total} = It_N + N_{at} = \frac{3}{4\pi}K^2\left(\frac{1}{r_2^3 - r_1^3}\right)\ln\left(\frac{A_1\beta_2}{A_2\beta_1}\right) \quad (58)$$

This equation considers the actual crystal sizes r_1 and r_2 after the nucleation and growth steps taking into account nonisothermal growth. The conditions and results of a DSC analysis together with data from optical measurements of samples subjected to DSC runs are shown in Figure 55. In the case of optical microscopy, the last stage of crystallization (Figure 53) was not performed, and the nuclei were developed at a temperature higher than the previous nucleation temperature up to a size large enough to be visible under optical microscopy.

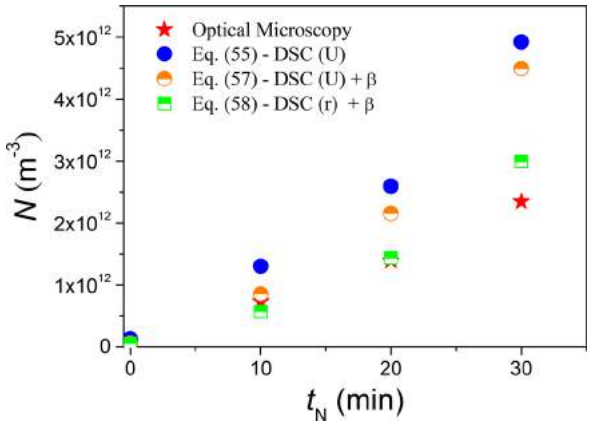

Figure 55. Number of crystals versus time of nucleation at T_N = 480 °C measured by Tammann's method and estimated by the DSC method of Fokin et al. Reproduced with permission from ref 546. Copyright 2010 Elsevier Science B.V.

N_{at} can be calculated from eqs 54 and 56. Cabral et al.[555] compared the results of values measured by Tammann's method in Fokin's study[546] and the values measured and calculated by eqs 54 and 56. They demonstrated that some nuclei might reach the critical size at the temperatures used for crystal growth during the DSC heating runs carried out at 15–20 °C/min. Therefore, the N values provided by both DSC expressions were much higher than the experimental values directly obtained by Tammann's method. It should be noted that, in conventional laboratory experiments (Tammann's method), heating/cooling ramps are usually very short because the samples are pushed quickly into and out of the furnace between the nucleation and growth treatments. In contrast to Cabral et al.,[555] we believe that this difference could also be due to other effects. Recently, experiments by Deubener et al.[556] demonstrated, for the first time, that the heating rate used in typical double-stage heat treatments considerably affects the values of the experimental t_{ind} and N. An increase of t_{ind} and decrease of N with increasing heating rate were observed. These experimental trends were in agreement with earlier results of numerical simulations, which predicted an increase in the size of the surviving critical nuclei with increasing heating rate. When the heating rate is increased, redissolution of clusters smaller than the survival size triggers a "flushing effect" and leads to a longer induction period.[556] More recently, Ranasinghe et al.[557] used eq 55 to estimate N and heterogeneous nucleation rates (I) for lithium disilicate glass doped with different concentrations of platinum particles. However, they did not consider all of the necessary corrections

DOI: 10.1021/acs.chemrev.8b00510
Chem. Rev. XXXX, XXX, XXX−XXX

suggested by Fokin et al. and the effect of heating rate discussed by Deubener et al.[556] Therefore, they attributed the very large measured number of nuclei merely to the effect of heterogeneous nucleation. In the end, it seems that, when properly used, such nonisothermal methods can yield useful kinetic information, which includes the crystal number density and nucleation rate, but they are as arduous as the traditional microscopy methods.

Finally, Gupta et al.[558] argued that most studies of this kind have focused on the kinetics of isochemical crystallization (where the compositions of the crystal and the parent glass are the same). Therefore, they reported on an evaluation of the DTA peak shift in systems where, after a preliminary crystallization treatment, the compositions of the crystal and glass are different. Their results revealed that the exothermic peak temperature decreases in the beginning but increases later on, with an increase in the pre-DTA heat-treatment time at a fixed temperature, finally becoming significantly larger than the initial value. To analyze these results, a model of primary crystallization was developed by Gupta et al.,[558] which included diffusion-controlled growth, the Gibbs−Thomson effect, homogeneous nucleation, and a mean field soft-impingement correction during growth. Based on this model and experimental results, they concluded that an increase in the number of crystal nuclei shifts the crystallization peak to lower temperatures (as found previously by other researchers for the case of polymorphic crystallization) and that diffusion-controlled growth during the pre-DTA heat treatment is responsible for the later shift toward higher temperatures.

7.1.3. Heterogeneous Nucleation. Homogeneous nucleation is a stochastic process in which crystal nuclei randomly and spontaneously appear within any given volume element of a supercooled liquid at different temperatures or times, whereas heterogeneous nucleation takes place at some preferred sites or interfaces. Regarding DSC experiments, Repetitive Scanning Calorimetry (RS-DSC), either with a certain cooling rate or by quenching a SCL to an isothermal hold, has been performed in different materials, such as metals, e.g., aluminum,[559] gold,[560] and tin,[561] water,[562] hydrates[563] and oxides.[564,565] In these experiments, onset temperatures (in isochronal transformations) and onset times (in isothermal transformations) can sometimes be detected, and their probability distributions are combined with the classical nucleation theory to determine delay times and rates of nucleation.

In general, the theory of nucleation is most often verified based on the average behavior of a number of independent nucleation events. The direct observation of these events happening at the nanoscale poses a challenge. Uttormark et al.[559] utilized the RS-DSC technique to show the repeated nucleation of the solid aluminum from the liquid in the same 80 μm droplet. A total of 845 repeats were recorded under nearly identical conditions, and a statistical analysis was performed. Multiple nucleation mechanisms—homogeneous and heterogeneous—were active. Studies of this kind on metallic glass alloys help to understand glass formation and the crystallization reaction that yields a high density (10^{21}−10^{23} m^{-3}) of nanocrystals (7−20 nm). This type of microstructure can also be synthesized by the repeated cold rolling or melt spinning of ribbons.[566,567]

Therefore, nucleation can be homogeneous (intrinsic, in the sample interior) or heterogeneous, e.g., triggered by surface defects, solid impurities, or crucible walls. DSC experiments, especially on cooling melts, usually involve heterogeneous nucleation because the liquid wets the walls of the DSC pan. The major problem with such experiments of heterogeneous nucleation is that the resulting crystallization statistics do not depend solely on the stochasticity of the process; they also depend on the availability of surface nucleation sites, which can vary substantially from one experiment (one DSC run) to another. All in all, it is not trivial to decouple both effects (stochastic from spurious nucleation).

In any case, we describe below an extensive RS-DSC work reported in five consecutive articles on heterogeneous nucleation of LS2 initiated on the Pt pans of a DSC equipment. For supercooled lithium disilicate liquid, the mean undercooling (ΔT) to trigger heterogeneous nucleation was 147 K for cooling at 5 K/min, and the mean delay (half-time = ln $2/I_0$) was 753 s for isothermal dwelling at T_L − 133 K.[564,565,570] In those works,[564,565,568−570] Krüger and Deubener carried out DSC analyses of several hundred repetitive crystallization events. For instance, in ref 570 the isothermal liquid-to-crystal transformation kinetics of (non-Gaussian) Poisson-distributed exothermic DSC signals were calculated individually. They found that random and regular dispersions of crystals fail to accurately predict the growth exponent (Avrami exponent) if only a small number of crystals were growing. Nonstationary effects were evident at low and large crystallized fractions.[570] The overall conclusion of the combined articles is that RS-DSC can be a useful technique to probe heterogeneous nucleation kinetics. It could be very interesting to repeat this same type of experiment with vitreous carbon pans, which do not trigger heterogeneous nucleation in LS2 glass, to check whether it could be used to probe homogeneous nucleation.

7.2. Crystal Growth Kinetics

Microscopy techniques are commonly used to determine crystal growth rates in supercooled liquids, $U(T)$. The simplest and most used method is to perform heat treatments for different periods at a given temperature. Samples are then polished for microscopic analysis, where the sizes of the crystals on the sample surface or in their volume are measured, along with the thickness of the crystallized surface layer. Then, the growth rates are calculated from the slopes of the crystal size versus time curves at different temperatures. Hot stage microscopes can also be employed, in which case the growing crystals on the sample surface are directly observed *in situ*.

Ray et al.[548,549] proposed methods to estimate the crystal growth by DTA/DSC. Later, Fokin et al.[546] modified Ray's procedure and introduced eq 55, which can be used to estimate the growth rate at any temperature using eq 59:

$$U(T) = \left[\frac{3}{4\pi N_{at}}\left(\frac{1}{(t_{G2}^3 - t_{G1}^3)}\right)\ln\left(\frac{A_1 M_2}{A_2 M_1}\right)\right]^{1/3} \quad (59)$$

where, t_{G1} and t_{G2} are the heat-treatment times at a temperature T for samples of mass M_1 and M_2, respectively. A_1 and A_2 are the respective areas of the resulting DTA peaks. N_{at} is the number of athermal or quenched-in nuclei.

In Fokin's method, two DSC runs are performed to determine the number of athermal crystals (N_{at}) within the volume of a glass sample. These runs include an isothermal step for crystal growth at a temperature at which the growth rate is already known. After obtaining the number of crystals (N_{at}) for a given glass sample, the growth rate can be

DOI: 10.1021/acs.chemrev.8b00510
Chem. Rev. XXXX, XXX, XXX−XXX

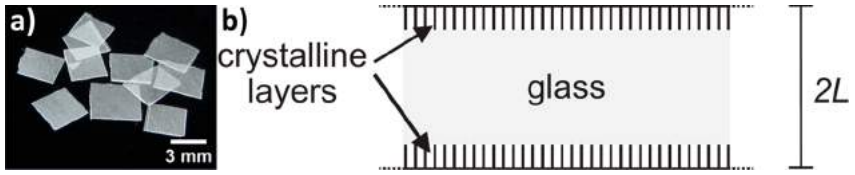

Figure 56. (a) Initial glass pieces used to measure growth rates via DSC. (b) Scheme for the surface nucleated crystallization of a glass sheet of thickness 2*L*. Reproduced with permission from ref 571. Copyright 2016 John Wiley and Sons.

determined with two extra DSC runs using eq 59.[549] Therefore, for each temperature where U is desired, two DSC runs are needed, plus two additional DSC runs for determination of the number of crystals (N_{at}), and then further experiments for the initial evaluation of U at an appropriate temperature using conventional optical microscopy. However, Fokin et al.[546] demonstrated that this approach (to approximate N_{at}) is sensitive to the crystal growth taking place during the heating and cooling steps, surface crystallization, and the shape of the crystal, which are difficult to be taken into account. The same caution should apply to the determination of the growth rate.

Recently, Reis et al.[571] proposed and successfully tested an innovative new method for the calculation of crystal growth rates using a *single DSC run* over a given temperature range. Their method is based on determining crystal growth rates from the DSC crystallization peak of a thin glass sheet. The $U(T)$ curve in the temperature range where the crystallization peak is detected results from this method. They assumed the following criteria to derive an expression for the growth rate: (i) The sample is a thin glass sheet; (ii) Only surface nucleation from a very large number of sites takes place; (iii) The crystallization rate is interface controlled and does not depend on long-range diffusion.

The crystallization of such a sample is represented schematically in Figure 56. The crystals grow in one direction from the sample surface toward the interior, with two crystallization fronts. Because the area of the crystallization front is constant, the liberated heat of crystallization at any given time is proportional to the rate of interfacial advance, that is, the crystal growth rate. At any time, the crystallized fraction can be estimated by the ratio of the crystallized layer thickness and half the sample thickness. In the case of nonisothermal heat treatment with a constant heating rate (q_h), the dependence of crystallized volume fraction to the temperature, $\alpha(T)$, is given by eq 60:

$$\alpha(T) = \frac{1}{L}\int_{T_0}^{T} \frac{U(T)}{q_h}\,dT \tag{60}$$

where T_0 is a temperature where the growth rate, U, is negligible. The following equation shows that the rate of the enthalpy release of a gram of glass due to crystallization, $dH_c(T)/dt$ (J g^{-1} s^{-1}), is proportional to the rate of crystallization, $d\alpha(T)/dT$ (vol% K^{-1}), when the temperature rises from the onset to the offset of the crystallization peak:

$$\frac{dH_c(T)}{dt} = \frac{d\alpha(T)}{dT}\cdot q_h \cdot H_c \tag{61}$$

where q_h and H_c are the heating rate (K/s) and the total crystallization enthalpy (J g^{-1}) (i.e., the enthalpy released during the entire crystallization process), respectively. As shown in Figure 57, $dH_c(T)/dt$ is actually the difference between the as-measured DSC output $\Phi(T)$ (J g^{-1} s^{-1}) and the background signal $\Phi_0(T)$ in the temperature range of the crystallization peak, which is expressed as

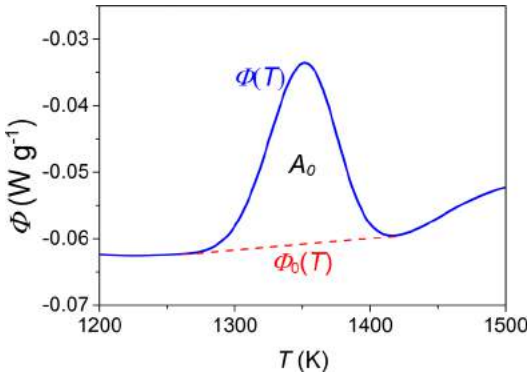

Figure 57. Typical DSC downscan signal showing the difference between the as-measured DSC output $\Phi(T)$ (J g^{-1} s^{-1}) and the background signal $\Phi_0(T)$ in the temperature range of the crystallization peak. This difference is equal to the rate of the enthalpy released during upscanning ($dH_c(T)/dt$). Reproduced with permission from ref 572. Copyright 2007 Elsevier Science B.V.

$$dH_c(T)/dt = \Phi(T) - \Phi_0(T) = \Delta\Phi(T) \tag{62}$$

The area of the exothermal peak (A_{peak}) is obtained by integrating dH_c/dt over T, yielding $q_h \cdot H_c$. Substituting eq 62 into eq 61 leads to the equation

$$\frac{d\alpha(T)}{dT} = \frac{\Delta\Phi(T)}{A_{peak}} \tag{63}$$

From eqs 60 and 63, the growth rate, $U(T)$, can then be calculated from the DSC crystallization peak area using eq 64:

$$U(T) = \frac{\Delta\Phi(T)}{A_{peak}}\cdot L \cdot q_h \tag{64}$$

Equation 64 predicts that the crystallization enthalpy releasing rate, $\Delta\Phi$, has the same temperature dependence as $U(T)$. Hence, when the two crystalline layers collide in the center of the sample, a sharp drop is expected in the DSC curve. This method allows for the determination of $U(T)$, which depends on the values of q and L, over the temperature range of the crystallization peak. An increase in L increases the crystallization peak width because of an increase in the time needed for full crystallization and, therefore, the offset of the crystallization process. An increase in the heating rate shifts the crystallization peak to higher temperatures. Both effects can be used to broaden the temperature range of crystal growth determination by changing sample thickness and heating rates. It is worth mentioning that using units of μV/mg for the DSC signal does not modify the form of eq 64 since any conversion factor is canceled out in the $\Delta\Phi/A_0$ fraction.

The linear relation between the crystal volume fraction and the released crystallization enthalpy for glass wool fibers with a

DOI: 10.1021/acs.chemrev.8b00510
Chem. Rev. XXXX, XXX, XXX−XXX

diameter of 5∼15 μm was also reported by Moesgaard et al.[572] They derived an equation to calculate the crystallinity in glass directly from the heat treatment temperature and time.

In the study of Reis et al.,[571] the crystal growth rate, U vs T curves (in the temperature range of the DSC crystallization peak) for lithium disilicate, diopside, and lithium calcium metasilicate glasses were determined. The experimental growth rates obtained from their DSC method agreed very well with literature data obtained by the microscopy method. Figure 58 summarizes the results obtained for lithium disilicate glass.

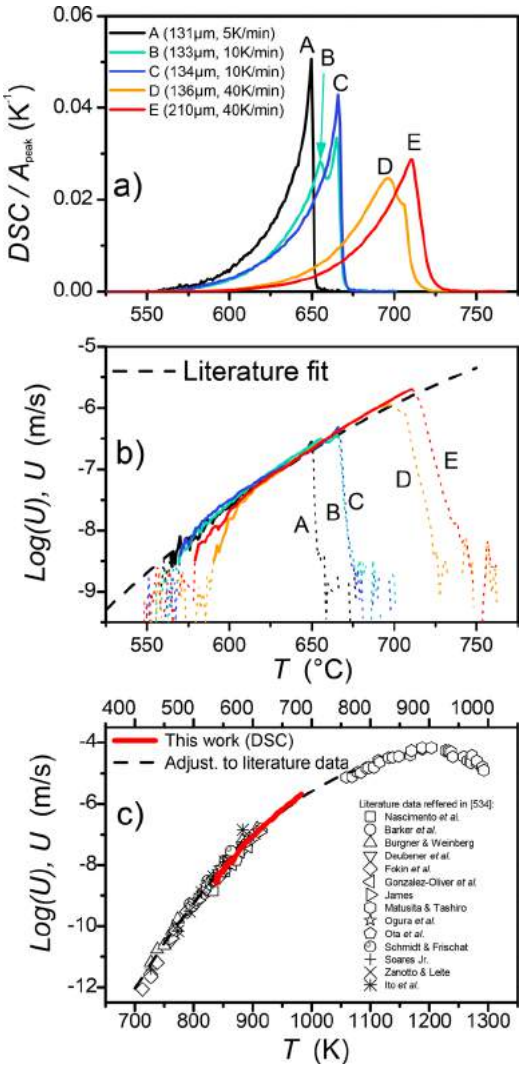

Figure 58. (a) Normalized DSC crystallization peaks for lithium disilicate glass. The numbers in parentheses are the sample thickness ($2L$) and heating rate (q_h), respectively. (b) Growth rates calculated from the DSC peaks using eq 64. (c) Results of Reis et al., other experimental data, and a fitted dashed line. Reproduced with permission from ref 571. Copyright 2016 John Wiley and Sons.

For nonstoichiometric crystallization of lithium metasilicate from a lithium calcium metasilicate glass, the DSC results underestimated the actual crystal growth rate. However, the use of the peak area up to the temperature of the maximum of the crystallization peak (T_c) improved the results because in DSC runs the signal (energy release) reaches the maximum when crystallization is completed, and then it drops, bringing the signal back to the background. This method is indeed quite useful to estimate the growth rates of any glass that undergoes predominantly surface nucleation (as most glasses do).

7.3. Overall Crystallization Kinetics

Crystal nucleation occurring simultaneously with or followed by subsequent growth results in overall crystallization. This process can be described by determining the evolution of the volume fraction crystallized, $\alpha(t)$, as a function of time and temperature. The theory of crystallization kinetics under isothermal conditions was developed in the late 1930s independently by Johnson, Mehl, Avrami, Yerofeeyev, and Kolmogorov and is known as JMAYK theory. According to their model, the volume fraction of the new phase (in this case a crystal) is given by eq 65, which is the combination of eqs 46 and 47.[8,66,573]

$$\alpha(t) = 1 - \exp\left\{-g\int_0^t I(T)\left[\int_{t'}^t U(T)\,dt'\right]^3 dt\right\} \quad (65)$$

where g is a shape factor that depends on the shape of crystals. If the nucleation (I) and growth (U) rates are constant throughout the transformation, eq 65 can be rewritten as

$$\alpha(t) = 1 - \exp\left[-\frac{gIU^3t^4}{4}\right] \quad (66)$$

when the number of growing crystals, N_0, does not change with time (as it is typical for fast heterogeneous nucleation on a finite number of active sites or from quenched-in, athermal nuclei), eq 65 transforms to

$$\alpha(t) = 1 - \exp[-gN_0U^3t^3] \quad (67)$$

Avrami proposed that, in the general case, the following relation should be used:

$$\alpha(t) = 1 - \exp[-Kt^n] \quad (68)$$

where K represents the overall rate constant, and n is the Avrami coefficient. In typical applications, eq 68 is used in the form

$$\ln(-\ln(1-\alpha)) = \ln K + n \ln t \quad (69)$$

The values of K and n can be estimated by fitting the experimental data of $\acute{a}(t)$ to eq 69. Thus the coefficient K includes I and U, or N_0 and U.

For nucleation starting from a fixed number of nuclei at temperatures below the so-called "decoupling temperature", the growth rates become approximately Arrhenian. Below this decoupling temperature, the temperature dependence of K can be described by

$$K = \nu_0 \exp\left(-\frac{E_c}{RT}\right) \quad (70)$$

where both the pre-exponential term, ν_0, and the activation energy for crystal growth, E_C, are temperature independent, and R is the gas constant.[8,66,573]

In eq 69, n is called the Avrami coefficient and depends on both nucleation and growth mechanisms, as shown in Table 1. The knowledge of that coefficient is very helpful to understand the mechanism of phase transformation at any given temperature.[574]

7.3.1. Isothermal Method. If the phase transformation mechanism is unchanged during the experiment, a plot of $\ln(-\ln(1-\alpha))$ versus $\ln(t)$ at a number of temperatures

DOI: 10.1021/acs.chemrev.8b00510
Chem. Rev. XXXX, XXX, XXX−XXX

Table 1. Values of the Avrami Exponent (n) for Several Mechanisms of Crystallization[574]

Polymorphic change, interface-controlled growth[a]	n	Diffusion-controlled growth[a]	n
Increasing nucleation rate, 3D	>4	Increasing nucleation rate, 3D	>2.5
Constant nucleation rate, 3D	4	Constant nucleation rate, 3D	2.5
Decreasing nucleation rate, 3D	3–4	Decreasing nucleation rate, 3D	1.5–2.5
Zero nucleation rate (nucleation site saturation) 3D	3	Constant nucleation rate, 2D	2
Constant nucleation rate, 2-D (plate)	3	Zero nucleation rate, 3D	1.5
Zero nucleation rate, 2-D (plate)	2	Constant nucleation rate, 1D	1.5
Constant nucleation rate (nucleation site saturation), 1D	2	Zero nucleation rate, 2D	1
Zero nucleation rate, 1D (needle)	1	Zero nucleation rate, 1D	0.5

[a]D: Dimensional growth

should yield a series of parallel lines with slope n and intercept $\ln(K)$ at each temperature. The value of α is approximately equal to the fractional area under the isothermal crystallization peak as a function of time at that temperature, which is usually determined using the software from commercial DSC equipment (Figure 59). For example, if A is the DTA peak

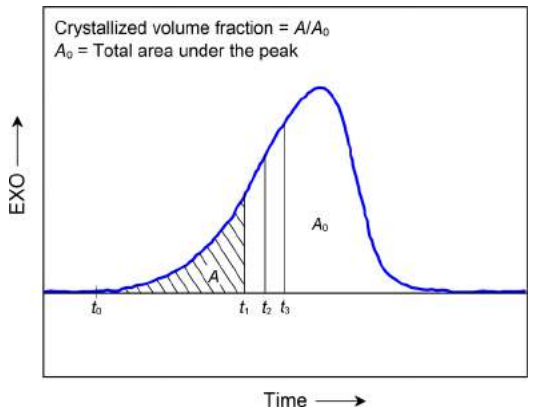

Figure 59. Typical crystallization exotherm. A method for calculating the volume fraction crystallized, α, for any time, t, is illustrated.

area per unit volume of a glass that has already been given an isothermal heat treatment at a temperature T for a time t, and α is the volume fraction crystallized during the DSC run, then

$$A = A_0(1 - \alpha) \tag{71}$$

where A_0 is the area of the exothermic peak for an as-quenched (uncrystallized) glass sample. For a partially crystallized specimen, the crystallinity, α, in the glass is given by $\left[1 - \frac{A}{A_0}\right]$. Combining eq 71 with eq 69, we obtain

$$\ln\left(\frac{A_0}{A}\right) = \ln K + n \ln t \tag{72}$$

thus, plots of $\ln\left(\frac{A_0}{A}\right)$ vs $\ln t$ can be used to determine n and K, the kinetic parameters for crystallization.[8,66,573]

In their study in 1991, Ray et al.[575] investigated the crystallization kinetics of a nonstoichiometric $40Li_2O{\cdot}60SiO_2$ (mol%) glass via DSC to reveal the effects of (1) particle size of the glass powder, (2) crucible, e.g., alumina or platinum, (3) DSC atmosphere, e.g., nitrogen, oxygen, or argon, and (4) surface treatment of the glass powder with deionized water, HCl, or HF. According to eq 70, both the pre-exponential factor and the activation energy for crystal growth varied, as the particle size of the glass powder changed, but neither the atmosphere nor the crucible had a significant effect on the crystallization kinetics. Washing the glass with deionized water, HCl, or HF before the measurements decreased the crystallization temperature by 25 to 30 °C. E_C and ν_0 remained unchanged by this treatment. This particular glass crystallizes predominantly in the interior; that is why the surface condition did not affect the results.

In 2007, Ray et al.[576] subsequently simplified their isothermal DSC method originally published in 1991. They argued that the determination of crystallization parameters by the conventional isothermal heating techniques is a tedious and time-consuming operation because it is often difficult to obtain an idealized crystallization exotherm experimentally, as shown in Figure 59. Obtaining such an exotherm depends upon two factors: (1) the choice of a suitable isothermal hold temperature, which is generally unknown for an unknown system, and that depends upon the characteristic temperature-time-transformation (TTT) diagram of the supercooled liquid, and (2) the efficiency and capability to attain a proper hold temperature quickly and precisely that, in most cases, lies within a very narrow range. As a result, often one cannot find a proper treatment temperature that falls within the temperature range for observable crystallization, or the temperature shows oscillations before stabilizing at the desired treatment temperature, making it difficult to identify the crystallization event and, hence, to accurately determine the time taken for a particular volume fraction to crystallize. Therefore, they proposed a simplified method. Their new experimental protocol includes first an isothermal heat treatment of glass as a function of time in a separate furnace to achieve a time-dependent partial crystallization at a particular temperature. The isothermal heat treatment is then followed by a DSC scan of the partially crystallized glass sample at a fixed heating rate, which generates a crystallization peak for a fraction of glass that did not crystallize during the previous isothermal heat-treatment step. From the area of this DSC peak, the portion of the sample that crystallized during the isothermal heat treatment can be readily determined and analyzed using eqs 70 and 72 to calculate the crystallization parameters. This method was tested by Ray et al.[576] using a lithium disilicate glass, which is frequently taken as a model glass for studies of nucleation and crystallization, and hence numerous experimental data are available for comparison. The results are illustrated in Figure 60.

7.3.2. Nonisothermal Methods. The isothermal method described above is time-consuming and difficult to carry out over a wide temperature range. A much easier method, based on determining the temperature of the crystallization peak maximum, T_c, for samples heated at different rates was developed by Kissinger in the mid-1950s.[196,577] The derivation of the Kissinger method will be described later when we critically analyze this approach.[577] His final expression relates the heating rate and the temperature of the exothermic peak maximum by

DOI: 10.1021/acs.chemrev.8b00510
Chem. Rev. XXXX, XXX, XXX–XXX

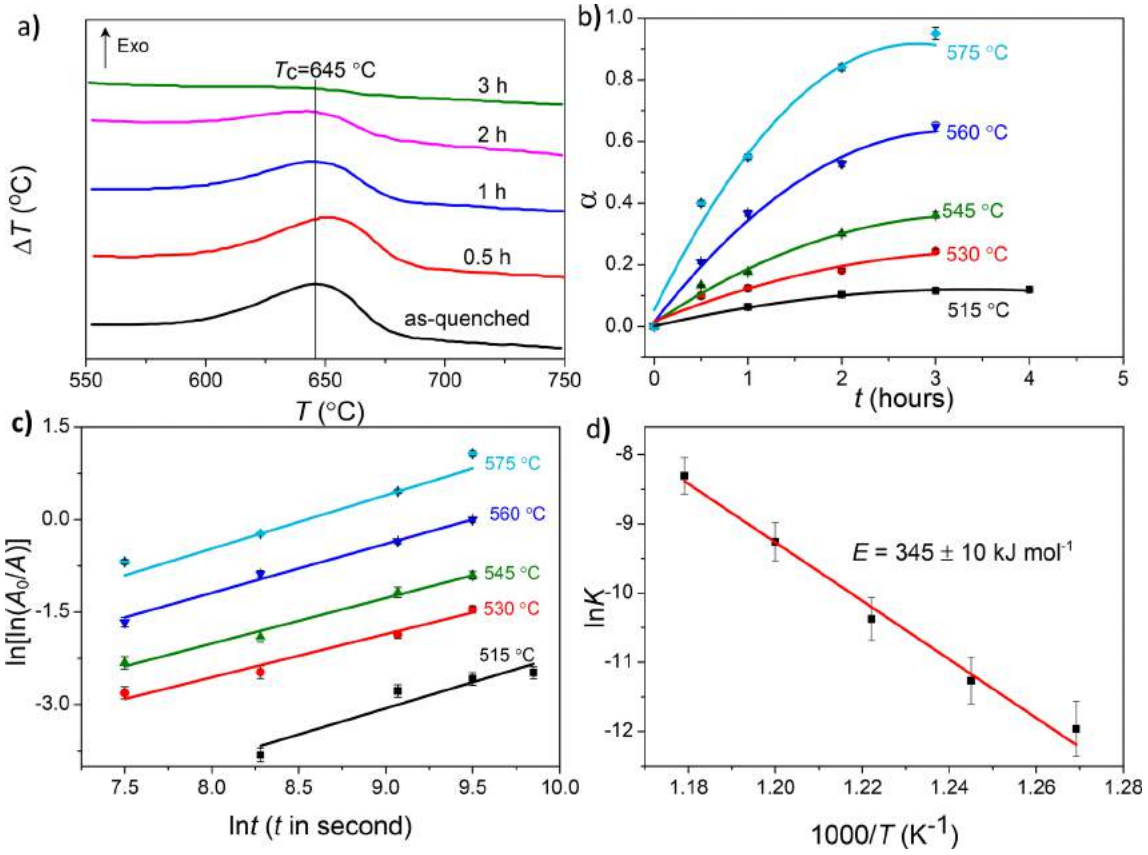

Figure 60. (a) DTA curves at 10 °C/min for an as-quenched LS2 glass with particle sizes between 425 and 500 μm, and after an isothermal holding at 575 °C for 0.5, 1, 2 and 3 h. The peak area decreases with increasing heat treatment time, but the peak temperature (T_c) remains virtually unchanged at 645 °C. (b) Crystallized volume fraction, α, as a function of time for an LS2 glass heated at the indicated temperatures. Lines are polynomial fits through the data points. (c) Avrami plots (Eq. 72) for the same glass using crystallized volume fraction data obtained at the indicated temperatures. (d) Arrhenius plot (eq 70) using ln$K$-values obtained from the Avrami analysis of the data in (b). Reproduced with permission from ref 576. Copyright 2007 John Wiley and Sons.

$$\ln\left(\frac{q_h}{T_c^2}\right) = \ln\left(\frac{ZR}{E}\right) - \frac{E}{RT_c} \tag{73}$$

where q_h is the heating rate, E is the activation energy for the overall crystallization, Z is a constant, and T_c is the temperature at the peak maximum. If this equation is valid for the system under study, a plot of $\ln\left(\frac{q_h}{T_c^2}\right)$ versus $\frac{1}{T_c}$ should yield a straight line with a slope of $\frac{E}{R}$ and an intercept $\ln\left(\frac{ZR}{E}\right)$.

Due to its simplicity, this method has been widely used to determine the activation energy for the overall crystallization process of many glasses. An example is shown in Figure 61 for LS2.

We emphasize here that, in principle, this method can only be applied to the case of crystal growth from a *fixed* number of nucleation sites in a temperature range where the $U(T)$ is Arrhenian, i.e., below the temperature of breakdown of the Stokes−Einstein equation (SEE).

Another widely used nonisothermal method for calculation of E and n was proposed by Ozawa in 1971.[579] For a constant heating rate (q_h), given by $q_h = \left(\frac{T - T_0}{t}\right)$, eq 68 can be rewritten as

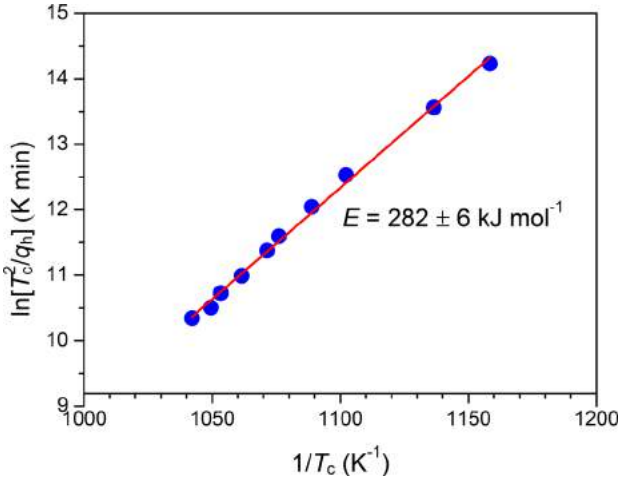

Figure 61. Kissinger plot—$\ln\left(\frac{q_h}{T_c^2}\right)$ vs $\frac{1}{T_c}$ (eq 73)—of the DTA experiments for a lithium disilicate glass with a particle size of 425−600 μm. Reproduced with permission from ref 578. Copyright 2015 John Wiley and Sons.

$$\alpha(t) = 1 - \exp\left[-K\left(\frac{T - T_0}{q_h}\right)^n\right] \tag{74}$$

DOI: 10.1021/acs.chemrev.8b00510
Chem. Rev. XXXX, XXX, XXX−XXX

By applying logarithms to both sides in eq 74, the following equation is obtained:

$$\ln(-\ln(1-\alpha)) = \ln[K(T-T_0)] - n\ln q_h \quad (75)$$

Therefore, n can be estimated from the slope of the straight line of a plot of $\ln(-\ln(1-\alpha))$ versus $\ln q_h$. The crystallized *volume* fraction, α, at any time, t, is estimated according to the method explained in Figure 59. We should keep in mind that the heat liberation during crystallization in a DSC run is proportional to the *mass* of the glass. Therefore, if the density of the residual glass does not significantly change during crystallization, we can consider that the crystallized mass fraction is proportional to the volume fraction.

The parameter n can also be evaluated using the Augis–Bennett method, derived in 1978:[580]

$$n = \frac{2.5}{\text{fwhm}}\frac{RT_c^2}{E} \quad (76)$$

where E is the activation energy for overall crystallization, which includes crystal nucleation and growth, R is the gas constant, and fwhm and T_c are the "full width at half maximum" and the temperature of the DTA crystallization peak, respectively. This model can only be used if the activation energy is known.

The three methods mentioned above are frequently used by the glass research community to estimate the Avrami constant and the activation energy for crystallization. Several others, which are different variations of the Avrami, Ozawa, and Kissinger models, have been proposed by Piloyan-Borchardt[581,582] and Coats-Redfern.[583] Approaches by Šesták[584,585] and Ligero et al.[586] are sometimes used in the community.

While most of the DSC/DTA treatments are based on the formal theory of transformation kinetics, they differ significantly in their assumptions and in many cases lead to contradictory results. Therefore, controversy exists with respect to each of these models, and great care should be taken when using them. In many cases, they extend the Avrami equation to transformation cases under linearly increasing (nonisothermal) treatments, which imposes further complications on the theoretical interpretation of the kinetic results. Therefore, we highly encourage researchers to refer to review papers written by members of the Committee of the International Confederation for Thermal Analysis and Calorimetry (ICTAC) before starting kinetic studies by DSC/DTA.[587,588] Their recommendations offer useful guidance for preparing proper samples, collecting data, and reliably evaluating the kinetic parameters (the activation energy, the pre-exponential factor, and the reaction model) in the thermal analysis using thermogravimetry (TG), DSC, and DTA. The recommendations cover the most common kinetic methods, including model-free (iso-conversional) as well as model-fitting. Their focus is on the problems faced by various kinetic methods and on the ways how these problems can be resolved. Recommendations for making reliable kinetic predictions are also provided. The objective of those recommendations is to help researchers with efficient (rather complicated, but indispensable) analysis.[587] Additionally, Henderson,[589,590] Matusita and Sakka,[591] Yinnon and Ulhmann,[592] Málek,[7,593] and Šesták[594] have published critical analyses of the non-isothermal methods and show under which conditions these methods are justified as we shortly discuss below.

Aside from surface crystallization, which still has several issues before full understanding,[7,590−597] the practical applicability of the JMAYK transformation kinetics for the bulk crystallization process under nonisothermal conditions depends on the knowledge of the nucleation and growth kinetics. It is well accepted that the JMAYK model successfully describes the case of crystal growth from pre-existing nuclei even under nonisothermal conditions. However, in some cases, the application of the JMAYK kinetics under nonisothermal conditions leads to incorrect results when the number of pre-existing nuclei changes, depending on the sample thermal history, within the temperature range of nucleation. For example, Everton and Cabral[598] determined the crystallized fraction, $\alpha(t)$ directly by optical microscopy (OM) and indirectly by DSC under isothermal conditions. In their work, the kinetic crystallization parameters E (activation energy) and n (Avrami index) of a lithium disilicate glass ($Li_2O{\cdot}2SiO_2$) were studied. First, bulk samples were fast heated in a vertical tube furnace to temperatures between 500 and 530 °C for different periods. The same samples were heated in a calorimeter from room temperature to 850 °C at 10 °C/min. The following E and n values were obtained: (i) OM: 462 ± 1 kJ/mol and 4, respectively; and (ii) DSC: 188 ± 1 kJ/mol and 2.4, respectively. The results indicated that in the nonisothermal (DSC) case, the activation energy for crystal growth was reduced due to the formation of new crystals and growing of "pre-existing" crystals during the nonisothermal DSC experiments and that the predominant crystallization mechanism in the samples changed according to the thermal history.[598]

There are several limitations regarding the application of the Kissinger method. The first important concern refers to the mathematical derivation of his equation; the reaction (e.g., glass → crystal) is assumed to be a first-order function defining the reaction rate as $\frac{d\alpha}{dt} = k(T)(1-\alpha)$, where α is the fraction of reactant remaining after a time t and $k(T)$ is the rate constant at a temperature T. The particular form of $f(\alpha)$ used is called the "kinetic model function".[577] In the above expression used by Kissinger $f(\alpha) = (1-\alpha)$. The assumption of a first-order reaction is *not* valid for many cases of crystallization in glasses.

Therefore, some authors have extended the Kissinger method to other kinetic models. For example, Elder[599] extended the Kissinger equation to n^{th} order reactions. Another extension is that of Augis and Bennett[580] and the follow-up article by Boswell,[600] which modified the original Kissinger method for the Avrami model to be applicable to autocatalytic reactions, such as thermoset cure. This problem has also been studied by Matsushita and Sakka,[601] who introduced two parameters on the nucleation behavior and growth dimension for modifying the conventional Kissinger method to evaluate the activation energy for glass crystallization, E. The form of the reaction rate has been discussed further by Matsushita et al.,[602] Ozawa,[603] and Kemeny and Šesták,[604] who modified the conventional iso-conversional methods in integral and differential forms. The iso-conversional methods yield values of the activation energy as a function of the degree of conversion (crystallization). Koga and Šesták generalized the reaction rate as a modification of the generalized kinetic equation with an accommodation function[605,606] by studying the whole course of the kinetic analysis for the crystallization of a $Li_2O{\cdot}2B_2O_3$ glass.[607] Koga and Šesták[596] have explained a generalized

DOI: 10.1021/acs.chemrev.8b00510
Chem. Rev. XXXX, XXX, XXX−XXX

approach for the case of crystal growth from pre-existing nuclei, exemplified by the crystallization kinetics of a $Na_2O·CaO·2SiO_2$ glass.[596] Another concern is that the Kissinger method is associated with the fact that the determination of an accurate E value requires the degree of crystallization at the peak maximum to be independent of the heating rate. Otherwise, the dependence given by eq 73 deviates from a straight line, producing a systematic error in E.[608] Another limitation is that the Kissinger method is applicable only to linear heating conditions. Another commonly encountered incorrect application of the Kissinger method is regarding the kinetic analysis of data obtained under linear cooling conditions, such as in the case of the melt crystallization. In the Kissinger method, q_h cannot be replaced with a positive value for the cooling rate, because such a practice results in incorrect values of the kinetic parameters.[609] In this case, dropping the negative sign for q_h in order to make the Kissinger equation applicable to cooling processes is an invalid procedure, because the derivative of the rate equation, which is used to obtain Kissinger's equation, would require the process rate to pass through a minimum to yield a downward rate peak. This requirement contradicts experimental observations for crystallization, where the rate passes through a maximum and gives rise to an upward peak. Vyazovkin[609] has identified this conclusion and reported on the correct calculation of the activation energy of crystallization of polymer melts by applying the differential iso-conversional method and/or by the integral iso-conversional method.[609] All of these modifications to the original approach are time-consuming but indispensable, and they should be tested for each glass. However, most researchers avoid considering these complex issues and simply employ the original equations of Kissinger or Ozawa, which yield meaningless values of the activation energy. Interested readers can refer to review papers dedicated to Kissinger,[577] Ozawa,[610] and recommendations of the ICTAC Kinetics Committee[587,588] to find (rather complex) modifications that should be applied to these original methods.

7.4. Modeling of DSC Signals

In his pioneering work in 1989, Müller[611] proposed a kinetic model to reproduce the exothermic DSC or DTA signal for surface-induced crystallization and tested it with a cordierite glass. Uniform glass particle size, a constant density of heterogeneous surface sites, and a steadily increasing temperature throughout the reaction were assumed. Using the (previously known) crystal growth rates, the density of surface sites for powders of widely different size was estimated from the DTA peaks.[611] In a following publication, Sandu and Singh provided mathematical solutions for the heat of transformation in both single and multiple physical chemical transformations.[612]

Recently, Reis and Zanotto[613] proposed a new model for the kinetics of phase transformation of glass particles of well-defined geometries starting from the surface and/or internal nucleation sites. Their analytical equation is simple but accurate, allowing for easy usage and interpretation. The model's ability to describe the overall crystallization kinetics of glass particles was tested by DSC experiments using spherical diopside ($CaO·MgO·2SiO_2$) glass particles having different number densities of surface nucleation sites. This glass only undergoes surface crystallization. Experiments were also performed with cubic particles of lithium disilicate ($Li_2O·2SiO_2$) glass, which shows simultaneous surface and internal crystallizations, having different number densities of internal nuclei. The model simulations of the DSC crystallization peaks agreed very well with the experiments and provided accurate predictions of the particle transformation kinetics for both materials.[613]

Additionally, Fernandes and Ferreira calculated DSC-like crystallization peaks for glass particles having regular-geometry.[614] The results of their calculations were in close agreement with the experimental DSC peaks of a diopside glass. This study provides an approximate method to calculate the crystallization kinetics of glass particles of regular geometries and constant size, considering heterogeneous surface nucleation starting from a high number of nucleation sites. Based on a geometric-contraction transformation model, they derived equations for cubic, spherical, parallelepipedal and ellipsoidal particles enabling the calculation of the transformation rate due to the evolution of a crystalline layer growing into the particle under nonisothermal conditions.[614] Figure 62 shows the calculated crystallization curves for different particle morphologies of a diopside glass powder. This figure summarizes the calculated crystallization curves for cubic, spherical, prismatic, and ellipsoidal particles, comparing them with the experimental DSC crystallization peak of a jagged diopside glass powder with 30 μm average particle size (22−38 μm sieve meshes). The experimental DSC crystallization peak was normalized by dividing the corresponding DSC experimental data points, whose unit is (μV mg^{-1}), by the total area under the peak, whose unit results from the product of heat flow sign and temperature (μV K mg^{-1}), to make possible the comparison with the calculated peaks. Thus, the unit of the normalized heat flow is the ratio between the first and second mentioned units, i.e., K^{-1}. The values of Ω and γ expressed in the figure caption were chosen to establish the effect of different shapes. At the considered levels of Ω and γ in Figure 62a, the onset of the crystallization peaks occurs approximately at the same temperature, 1140 K. However, the peak shapes change from low-intensity and broad to more intense and sharp, whereas their end point shifts to lower temperatures as Ω and γ deviate from 1. Such behavior is due to the increase of the surface-to-volume ratio for geometries deviating from cube and sphere; hence, the overall transformation rate is faster in plates or prolate ellipsoids than in needle-shaped particles, which in turn is faster than in cubic and spherical particles. This is best observed by comparing the full width at half-maximum (fwhm) of the calculated crystallization peaks for the different shapes (Figure 62b).[614] Additionally, the shape, intensity, and end point of the crystallization peaks are affected by the direction of the crystal growth fronts. For example, the crystallization peak of a platelike particle is more intense, due to an initially larger crystalizing surface, and drops more abruptly, when the crystal growth fronts perpendicular to its larger faces meet in the particle center than spherical and cubic particles. In summary, the Fernandes−Ferreira research shows an agreement, yet not perfect, between the calculated curves and the experimental DSC peaks. Most importantly, the glass particle shape significantly influences the crystallization kinetics and thus must be taken into account in the analysis of glass crystallization kinetics by DSC. To the best of our knowledge, this is one scarce example of studies that estimated the effect of glass particle shape on the DSC crystallization peaks, particularly for the case of heterogeneous surface crystallization.[614] Several other more complicated variables, such as

DOI: 10.1021/acs.chemrev.8b00510
Chem. Rev. XXXX, XXX, XXX−XXX

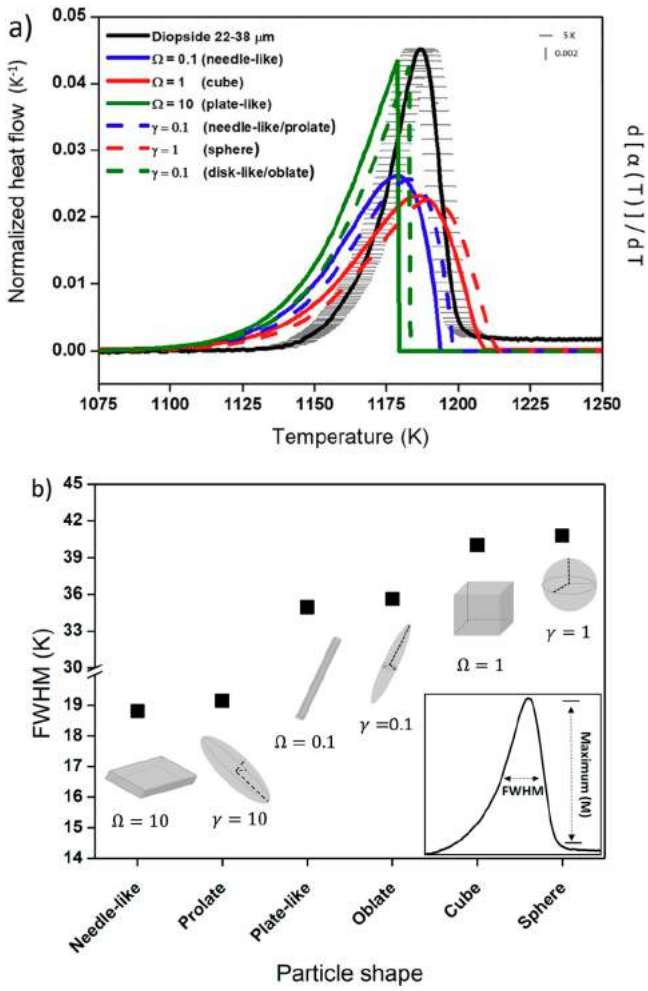

Figure 62. (a) Calculated and experimental DSC curves for diopside glass particles with an edge cube equivalent to 30 μm. The calculated crystallization peak is based on different morphologies: cube, platelike, and needle-like (Ω = the side length to the height of right square prisms) and sphere, disklike (oblate ellipsoid), and needle-like (prolate ellipsoid) ($\gamma = R_1/R_2$ for ellipsoids of revolution or spheroids, where R_1 is the radius of their central circular plane perpendicular to the axis of revolution and R_2 is their radius parallel to the same axis). (b) Full width at half-maximum (fwhm) of the calculated crystallization peaks for different particle shapes. Adapted from ref 614. Copyright 2018 Elsevier B.V.

simultaneous homogeneous nucleation in the glass interior, and testing conditions still need to be taken into account for the modeling of DSC signals and warrant further study.

7.5. Glass-Forming Ability

Glass-forming ability (GFA) is the aptitude of a melt to vitrify upon cooling. Quantifying glass-forming ability is very important for the design of new glass compositions, but it is a laborious process. Several methods are available to estimate GFA.[66] The ease of glass formation can be defined by the critical cooling rate, R_c, required to prevent crystallization of a certain sample. The critical cooling rate is a quantitative measure of the ability of a liquid to vitrify and is defined as the slowest rate at which a liquid can be cooled from its *liquidus* temperature (T_L) to below the glass transition temperature (T_g) without "detectable" crystallization, i.e., a crystallized volume fraction normally assumed to be in the range of 10^{-6}–10^{-2}. The smaller the R_c, the greater the glass-forming ability of a liquid. Thus, R_c is a very important characteristic parameter of liquids that should be known to predict the ease or difficulty of glass formation and, hence, to determine the processing conditions of any glass.[615] For instance, the R_c of metallic glasses falls between 1 and 10^6 K/s, whereas commercial oxide glasses, such as window glass, often have a R_c of $<10^{-2}$ K/s! However, even more important than measuring or estimating the GFA of different substances is the ability to *predict* the GFA as a function of composition. While this is not yet possible for complex, multicomponent systems, research efforts should and are moving in this direction.

While the concept of the critical cooling rate is easy to understand, its measurement is tedious and complicated. A melt must be heated to a predetermined temperature above its *liquidus*, held for a sufficiently long time to dissolve any residual crystals, and then cooled at a rate until it becomes a rigid body, which is then examined to determine if it is a glass or a crystal. If it is still a glass, the sample is reheated, and the experiment is repeated using a slower cooling rate. This procedure is repeated until the sample fails to vitrify. The slowest cooling rate which produces a glass is then defined as the critical cooling rate. Although only two cooling experiments are required to bracket the critical cooling rate, the determination of the actual R_c needs several tests for each composition.[66,615−617] Determination of the critical cooling rate can, in principle, be much faster if carried out using DSC/DTA. In this case, the process can be automated, with a computer-guided system repeatedly experimenting with a series of decreasing cooling rates. Cooling rates below the critical value will often be characterized by an exothermic peak in the thermal spectrum, due to the release of the heat of crystallization. The absence of such a peak in a DSC/DTA trace is often taken as evidence of a lack of crystallization (Figure 63a).[618] This technique is best suited for low melting temperature batches, which readily crystallize with a large exothermic effect if cooled at any rate slower than R_c.[66,615] But extreme caution should be taken because more often, the DTA/DSC pan induces surface (heterogeneous) crystallization of the sample.

Additionally, it is possible to estimate R_c by drawing a continuous cooling transformation curve (CCT curve) based on the time to detect (a certain small degree of) crystallization at different temperatures during cooling a melt at various constant rates (see inset in Figure 63a). On the other hand, in the case of isothermal experiments, the temperature of an equilibrated melt is quickly decreased from above the melting (or *liquidus*) temperature, T_m, to a predetermined temperature, where the supercooled liquid is held until crystallization occurs, as indicated by an exothermic peak in the DSC trace. The result is a curve of the temperature versus time required to crystallize (for a certain small fraction) of the supercooled liquid, a nose-shaped temperature−time−transformation (TTT) diagram, shown schematically in Figure 63b. The nose in this figure, and also in the case of continuous cooling, CCT (Figure 63a) curve, corresponds to the temperature T_n where the melt, when held isothermally or cooled continuously, crystallizes in the shortest possible time (nose time, t_n). The slope of the straight line from T_m to the nose of the TTT/CCT curves is a measure of $R_c = \frac{T_m - T_n}{t_n}$ for that substance (of a given sample size). A melt of that material cooled at a rate $q_c > R_c$ forms a glass.[615−617] Constructing a TTT-curve from isothermal cooling experiments is very time-consuming. In

DOI: 10.1021/acs.chemrev.8b00510
Chem. Rev. XXXX, XXX, XXX−XXX

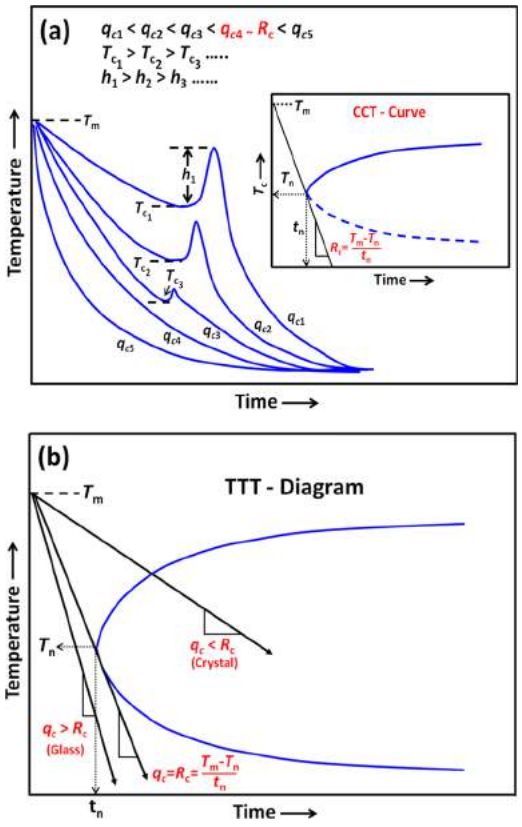

Figure 63. (a) Schematic diagrams of temperature−time cooling curves for a hypothetical melt cooled at different speeds, q_c. The melt crystallizes, as exhibited by exothermic peaks, when cooled at rates less than the R_c. The onset temperature of crystallization, T_c, and the peak height, h, decrease with increasing q_c, and the cooling rate for which the crystallization peak disappears is the R_c. The inset shows a continuous-cooling-transformation diagram based on the temperature−time cooling curves. (b) Schematics of a typical nose-shaped isothermal temperature−time−transformation (TTT) diagram. T_m: melting point, T_n: nose temperature where the supercooled liquid crystallizes in the shortest possible time, t_n (nose time), R: cooling rate, R_c: critical cooling rate for glass formation. Reproduced with permission from ref 617. Copyright 2005 Elsevier Science B.V.

addition, the isothermal cooling approach does not replicate common glass manufacturing processes and overestimates the real R_c by about 5−10 times.[618,619] A more realistic approach, and which is less time-consuming, is to analyze the nonisothermal crystallization event for a melt cooled from above T_m at different rates.

Another method to estimate R_c by DTA/DSC was proposed by Barandiarán and Colmenero in 1981[620] based on an empirical equation for evaluation of cooling curves. This method has been utilized by several authors, e.g., Whichard et al.[621] and Huang et al.[622] The crystallization temperature, T_c, of a given supercooled liquid (Figure 63a) is related to the corresponding cooling rate, q_c, as[575,620,621]

$$\ln q_c = \ln R_c - \frac{\omega_c}{(T_m - T_c)^2} \quad (77)$$

where ω_c is a constant. A plot of ln q_c versus $\frac{1}{(T_m - T_c)^2}$ yields a straight line, and the critical cooling rate, R_c, for that liquid is determined from the intercept of the straight line with the ln q_c axis.

Each of the methods discussed above requires a detectable crystallization DSC/DTA peak during a cooling experiment to determine R_c. However, certain melts, particularly silica-rich melts, exhibit very broad crystallization peaks during cooling that are unclear, either due to slow crystallization kinetics or because of small heats of crystallization.[623] Therefore, the determination of R_c for such melts using the methods described above poses an additional experimental challenge.

Beyond DSC, several key experimental tools are available, such as optical microscopy, scanning/transmission electron microscopy (SEM/TEM), small angle X-ray scattering (SAXS), extended X-ray absorption fine structure (EXAFS), small-angle neutron scattering (SANS), X-ray absorption spectroscopy (XAS), Raman spectroscopy (RS), nuclear magnetic resonance (NMR), X-ray diffraction (XRD), and atomic force microscopy (AFM), which, together with molecular dynamics (MD) simulations, can reveal specific hidden details of glass formation, nucleation, and crystallization in glasses. The combined use of these techniques has provided valuable insights into the complicated and rapidly changing structural environments in which crystallization happens, challenging several hypotheses and assumptions, which lead to the development of more rigorous approaches. Several good reviews and papers dealing with these techniques have been published. A few examples are provided elsewhere.[239,534,573,624−630]

Another issue is that, in general, for any glass-forming liquid the thermodynamic barrier is larger for homogeneous nucleation than for heterogeneous nucleation. As a result, the homogeneous nucleation, $I(T)$ curve, is always located at a lower temperature range than that of heterogeneous nucleation, and this last mechanism predominates on cooling, which leads to complications in the determination of R_c. Another DTA method has been proposed by Ray et al.[617] in 2005 for determining R_c for glass-forming melts, which is based on analyzing the relatively larger exothermic crystallization peaks that result when glasses with a known precrystallization degree after slow cooling are reheated at a constant rate in a DSC or DTA as described below.

The area of a DTA/DSC peak on reheating is directly proportional to the amount of heat evolved during crystallization, and, hence, to the amount of residual glass present after cooling an equilibrated melt, which, in turn, depends upon the initial cooling rate of the melt. If a glass is partially crystallized (for a sufficiently slow q_c, for example), the subsequent DTA peak area on reheating will be smaller than those for a crystal-free glass cooled at a faster rate, since the partially crystallized sample will contain less residual glass. A solid sample produced at $q_c \geq R_c$ should be crystal-free, and the area of the subsequent reheated DTA peak should be a maximum. This means that no further increase in the area of the DTA peak would be observed for samples prepared by cooling the melt at rates higher than R_c. The primary task of determining R_c by this method, therefore, is to identify a cooling rate which produces a sample whose subsequent rate-heated DTA yields a crystallization peak with maximum area.

Ray et al.[617] tested three different glasses: a $38Na_2O{\cdot}62SiO_2$ (mol%) glass with a previously known R_c (~20 K/min) and two complex, multicomponent $Li_2O{\cdot}2SiO_2$ based dental glass-ceramics. Three DTA heating curves, collected at 15 °C/min, for the $38Na_2O{\cdot}62SiO_2$ (mol%) melts are shown in Figure 64. These curves were obtained after cooling each melt at different rates (q_c) indicated in the figures. Similar DTA results were

DOI: 10.1021/acs.chemrev.8b00510
Chem. Rev. XXXX, XXX, XXX−XXX

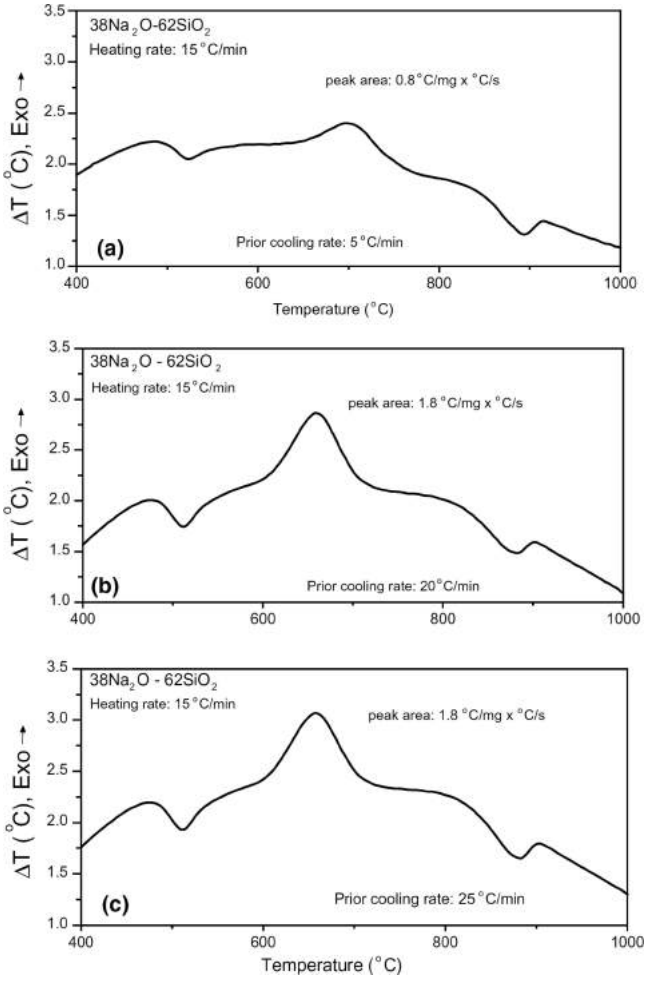

Figure 64. DTA heating curves (15 °C/min) for the solidified melts of a $38Na_2O{\cdot}62SiO_2$ (mol%) composition after cooling the melts at (a) 5 °C/min, (b) 20 °C/min, and (c) 25 °C/min. The area and height of the crystallization peak increased as the prior cooling rate increased from (a) 5 °C/min to (b) 20 °C/min, but no such increase in their values is observed when the prior cooling rate exceeded the critical cooling rate, R_c, for this melt; compare (b) and (c). Reproduced with permission from ref 617. Copyright 2005 Elsevier Science B.V.

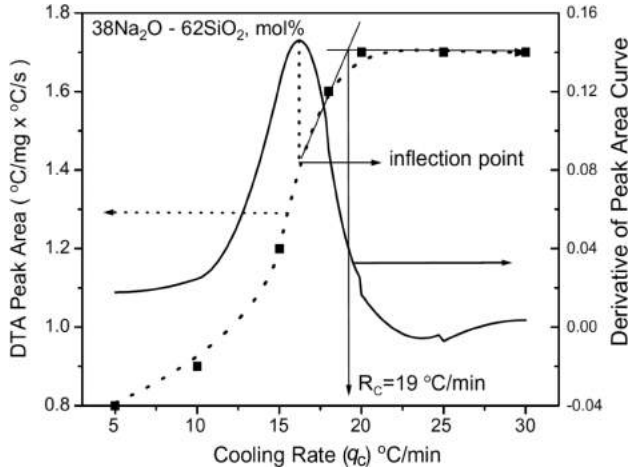

Figure 65. Calculation of R_c by Ray's method using a tangent intersection procedure. Results for a $38Na_2O{-}62SiO_2$ (mol%) glass from Figure 64 were used to calculate peak area for each cooling rate (q_c). With permission from ref 617. Copyright 2005 Elsevier Science B.V.

obtained for all three melts cooled at different rates, and the DTA peak areas are drawn as a function of q_c in Figure 65 for glass $38Na_2O{\cdot}62SiO_2$ (mol%). Figure 65 shows that the DTA peak areas for all the samples initially increased with increasing R, indicating the existence of a higher fraction of residual glass in the cooled samples. The DTA peak area was maximum at a particular q_c and remained constant with further increase of q_c. The critical cooling rate for glass formation, R_c, was taken as the value of q_c where the crystallization peak area on the subsequent reheating cycle is maximized, i.e., when the melt completely vitrifies. As shown in Figure 65, the value of R_c was determined from the intersection of the tangent drawn at the inflection point of the ascending curve, and the straight line produced by backward extrapolation of the plateau region. For the $38Na_2O{\cdot}62SiO_2$ (mol%) melt, this method predicted R_c of 19 ± 1 °C/min, which was close to the value of ~ 20 °C/min determined for this composition by standard techniques. For the two *multicomponent* Li_2O-SiO_2 based glasses, the R_c was also determined by the conventional methods described above and compared with the new method. The results showed that the values of R_c determined by the different methods were in excellent agreement, except using eq 77. The value of R_c determined by this equation (41 ± 3 and 53 ± 3 °C/min for the two different *multicomponent* lithium silicate glasses) was 10 °C/min higher than those determined by CCT curve technique. However, the values of R_c (33 ± 1 and 41 ± 2 °C/min) obtained by the method of Ray et al.[617] agreed very well with those obtained by the more conventional cooling rate analyses (32 ± 2 and 43 ± 2 °C/min, respectively).

However, traditional DSC methods have some limitations in determining R_c of either extremely poor glass formers (e.g., metals) or exceptionally good glass formers (e.g., some certain soda lime silicates and some atactic polymers). Normal DSC equipment cannot provide a sufficiently high cooling rate for vitrifying metallic liquids or a sufficiently low cooling rate to devitrify some polymers. On the other hand, new DSC techniques are being rapidly developed such as Flash DSC (see Section 5), which are able to heat a sample at heating and cooling rates of about 0.1−40,000 K/s enabling investigation of various properties of polymers, such as the determination of the R_c of very poor glass formers. Some older and updated reviews[42,631,632] have focused on the application of conventional and Flash DSC in studying polymers. For instance, the heat capacity can be studied under two extreme limits, that is, under quasi-isothermal conditions (limit of zero heating rate) and under fast heating/cooling rates. Flash DSC studies of semicrystalline polymers, which are far from equilibrium, also reveal recrystallization and reorganization during rapid heating. For example, the last endotherm detected under standard DSC scanning of some polymers, e.g., poly(ethylene terephthalate), is caused by molecular reorganization and vanishes under rapid heating conditions.[631]

In Flash DSC, the choice of scan rate depends on the polymer being tested. The scan rates for semicrystalline polymers are a particular case because the phase transitions are time-dependent.[632] Another interesting advantage of the Flash DSC method is the fact that it allows not only for the analysis of crystallization but also for reorganization processes that could not be measured previously. With currently available equipment, such tests can be carried out in the temperature

DOI: 10.1021/acs.chemrev.8b00510
Chem. Rev. XXXX, XXX, XXX−XXX

range −95 to 1000 °C. Some representative examples are provided here.[42]

Treviño-Quintanilla and co-workers reported results regarding the nonisothermal crystallization of high-density polyethylene (HDPE) resins.[633] The melting enthalpy was determined by Flash DSC. Different cooling rates in a wide range, 50 to 4000 K/s, were used for studying the thermal activity of HDPE. The crystallization temperature decreases with higher cooling rate,[633] as expected. In isothermal studies, in which the sample is fast cooled from the melt to the crystallization temperature, and the isothermal heat flow is measured, the same dependence between the crystallization temperature and the cooling rate of HDPE was also observed.[633]

In a recent work, Li and co-workers used Flash DSC to study the nucleation kinetics of poly(L-lactic acid)/poly(D-lactic acid) blends. The proposed method is useful in analyzing the nucleation kinetics, irrespective of the crystallization rates.[634] In this study, which was complementary to the nucleation kinetics determination by Tammann's method[536] reported by Schick's group,[635] nucleated samples were heated at a relatively slow rate (0.5 K/s) to the growth temperature (T_G) range, instead of fast heating the nucleated samples (Tammann's method), or by isothermally crystallizing a nucleated sample at higher temperature. Also, Flash DSC was instrumental to make the glass, quench the nucleated sample, and reheat it to T_m at a sufficiently fast rate (2000−3000 K/s) (Figure 66).[634]

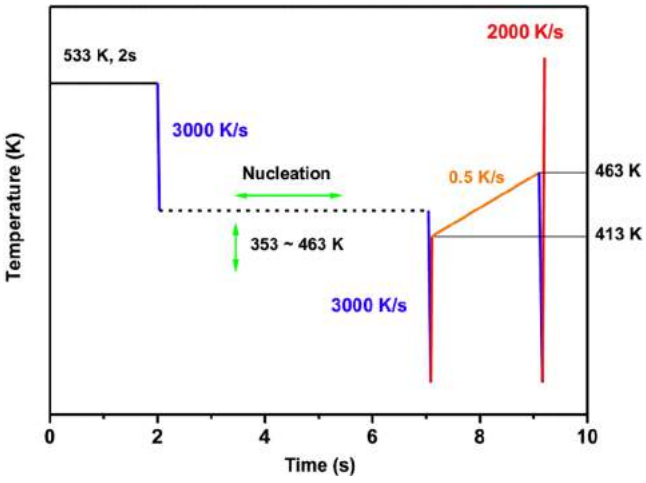

Figure 66. Temperature−time profile of the experimental protocol designed by Li et al. for determination of nucleation kinetics for PLLA/PDLA blends, where PDLA refers to poly(D-lactic acid). Reproduced from ref 634. Copyright 2018 Elsevier B.V.

After heating a nucleated sample of 20 kg/mol PLLA/PDLA blends from 413 K (T_N) to 463 K (T_G) at 0.5 K/s, the sample is crystallized and then fast-quenched to room temperature. The melting enthalpy (ΔH_m) of the crystallized sample was measured by heating the sample at 2000 K/s to above the melting point in a Flash DSC. The ΔH_m resulting from the melting of the crystals reflected the nucleation density in the primary sample.

Thermally induced crystallization of polymers can be carried out by crystallizing them either from the molten state or from the glassy state. The former is called melt crystallization, and the latter is called cold-crystallization.[636] The nucleation kinetics of polymers can be measured by using optical microscopy and evaluating the spherulite number density and size increasing with time.[637] Additionally, in calorimetry, nucleation of polymer crystals can also be determined by monitoring the evolution of enthalpy of cold-crystallization during subsequent heating, since this property depends on the number of previously formed nuclei.[638,639] Figure 67(a) shows the final Flash DSC heating curves of the samples corresponding to different nucleation times at 433 K. The melting enthalpy on the final heating curves as a function of nucleation time is plotted in Figure 67(b). Figure 67(a) shows the final heating curves with significant changes depending on the nucleation time. For nucleation times less than 50 s, the area of the melting peaks is almost equal. Therefore, homogeneous nucleation has not happened yet; the melting enthalpy on the final heating curves, namely the enthalpy of cold-crystallization during slow heating from 413 to 463 K, must be initiated by heterogeneous nucleation in the sample, e.g., solid impurities or at the interfaces between the sample and the chip sensor. Predictably, when the nucleation time is longer than 50 s, the area of the melting peaks continuously increases with time, which means that homogeneous nucleation has taken place. Thus, it is worth emphasizing that by using a commercially available fast-scan chip-calorimeter, slow heating of the PLLA/PDLA blends in an assigned temperature range makes it possible to initiate their cold-crystallization by different amounts of the nucleus, and the protocol presented in Figure 66 is valid for the PLA nucleation kinetics determination. Subsequently, after nucleation at different temperatures for different times and following cold-crystallization during heating at 0.5 K/s from 413 K to 463 K, the melting enthalpies of the PLLA/PDLA blends sample were recorded in Figure 67(c). Inspection of this figure reveals that the melting enthalpies corresponding to the early nucleation period are still indistinguishable at different temperatures, although the induction time of the melting depends on the nucleation temperature. This result further confirms the assumption that heterogeneous nuclei initiated the cold-crystallization process with shorter nucleation time. Following the approaches originally proposed by Schick's group[635] and by Wang et al.[640] by drawing a horizontal line (dash line in Figure 67c) at a constant ΔH_m, i.e., half of the saturated crystallization enthalpy (1.0 μJ for this sample), one can use the intersections, denoted as half-nucleation time, to extract the data points for nucleation time vs nucleation temperatures. The resulting curve based on these data is shown in Figure 68, which shows the best nucleation temperature referring to the minimum required time for nucleation. By using this experimental protocol and commercially available Flash DSC, for the 20 kg/mol PLLA/PDLA blends, the final temperature versus nucleation time curve was determined and showed a minimum value around 493 K, which is 20 K higher than the published results by using Tammann's two-stage nuclei development method.[634]

By applying the classical nucleation theory, Liu et al.[641] established a new approach for determining the R_c of glass-forming liquids based on DSC and viscosity data. Their method involves either the Turnbull equation[642] or the Thompson−Spaepen equation[643] for ΔG. For three different types of glass-forming systems (oxide, metallic, and molecular systems), they found that the R_c values obtained through the Thompson−Spaepen equation are more reliable than those from the Turnbull equation. To further verify the applicability of the new approach in quantifying GFA, a broad range of

DOI: 10.1021/acs.chemrev.8b00510
Chem. Rev. XXXX, XXX, XXX−XXX

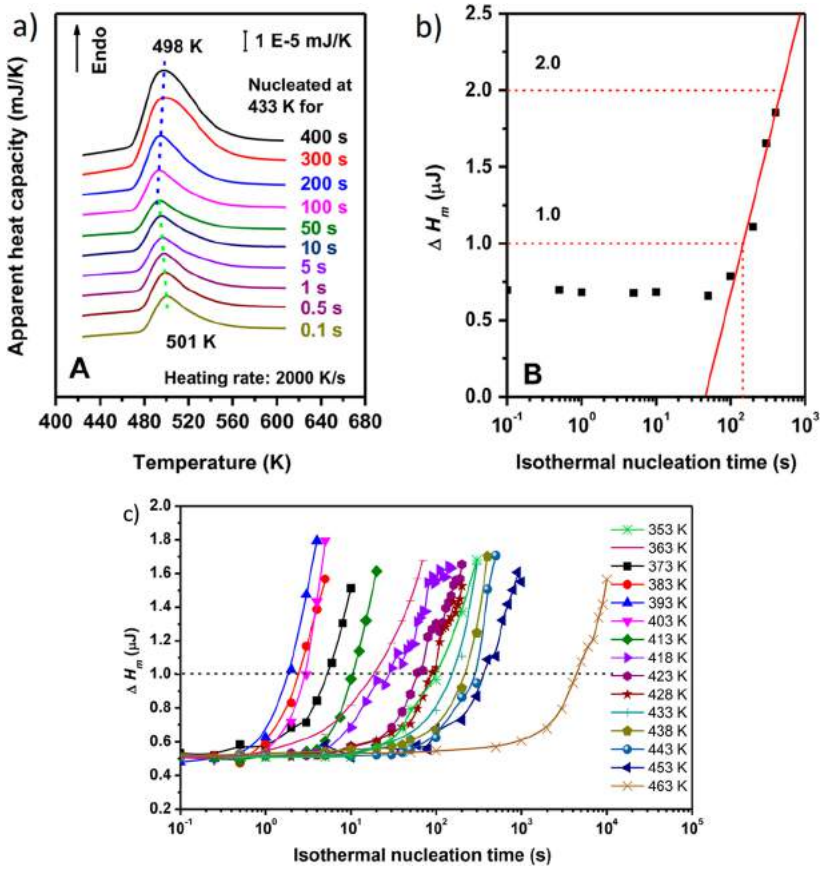

Figure 67. Melting behaviors of PLLA/PDLA blends after being cold-crystallized over a temperature range between 413 and 463 K at 0.5 K/s, following a previous isothermal nucleation at 433 K for different times using the protocol of Figure 66. (a) Flash DSC curves. (b) Melting enthalpy as a function of the nucleation time at 433 K. (c) Melting enthalpy of samples nucleated at different temperatures for different times and following cold-crystallization during heating at 0.5 K/s from 413 K to 463 K. Reproduced from ref 634. Copyright 2018 Elsevier B.V.

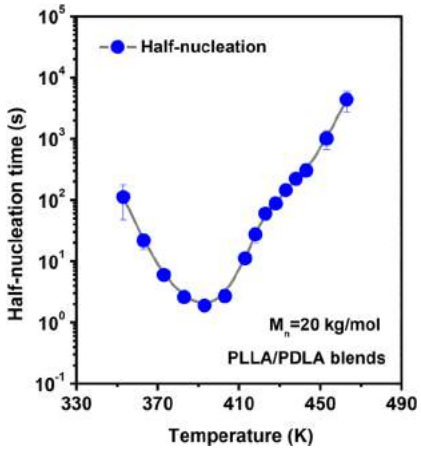

Figure 68. Half-nucleation time as a function of temperature, measured after applying the experimental protocol presented in Figures 66 and 67c. Adapted from ref 634. Copyright 2018 Elsevier B.V.

cooling rates (5 to 12,455 K/s), which was realized by three quenching methods—casting, pressing, and water-quenching—was used to determine the R_c of a phosphosilicate melt. This R_c value was estimated to be 3,700 K/s, which is consistent with 4,000 K/s reported elsewhere.[617]

7.6. Glass Stability

While glass-forming ability (GFA) is defined as the resistance to crystallization of a supercooled liquid during cooling, glass stability (GS) is defined as the resistance to devitrification of glass or supercoooled liquid during heating. GFA is most important during processes requiring vitrification, while GS is very important during operations involving thermal treatment of existing glass, such as annealing, tempering, or treatment for ceramization. Although these two properties are not identical, they are frequently confused in the literature and technological practice. It is often (reasonably) assumed that poor glass-forming ability automatically leads to poor glass stability, and vice versa.[66]

Glass stability is frequently characterized by the difference between the onset temperature of the glass transition (T_g) and the DSC/DTA crystallization peak temperature (T_c) for a sample heated at a given rate. The exact definitions of T_g and T_c are subjected to the preference of the experimenter, as discussed in Figure 51. A drawback of this method is that these two temperatures depend not only on the chemical composition but also on glass particle size and heating rate; hence these two experimental parameters should be kept constant for a proper evaluation of glass stability. Some authors argued that the quantity ($T_c - T_g$), should be normalized by T_g, T_c, or T_m of the crystalline phase, to compare the behavior of glasses which crystallize in very different temperature ranges. As a result, there is no unanimously accepted criterion for glass stability. In general, however, as long as samples of different

DOI: 10.1021/acs.chemrev.8b00510
Chem. Rev. XXXX, XXX, XXX−XXX

compositions are compared using identical characteristics (particle size and heating rate), several of the proposed parameters, especially those containing all three characteristic temperatures, yield similar results.[66]

We first summarize the GS criteria following the study of Kozmidis-Petrovic and Šesták.[644] They have compared the famous Hrubý parameter with other measures of the glass stability and vitrification ability. Some of these criteria are listed in Table 2.

Table 2. Examples of Glass Stability Parameters Based on the Characteristic Temperatures (in Kelvin) Determined by DSC/DTA[a]

Glass stability parameters	Proposed by
$K_H = (T_x - T_g)/(T_m - T_x)$	Hrubý[645]
$K_{SP} = (T_c - T_x)(T_x - T_g)/T_g$	Saad and Poulain[646]
$K_W = (T_c - T_g)/T_m$	Weinberg[647]
$K_{LL} = T_c/(T_g + T_m)$	Lu and Liu[648,649]
$K_{ZW} = T_g/(2T_x - T_g) - T_g/T_m$	Zhang et al.[650]
$K_{DH} = (2T_x - T_g)/T_m$	Du et al.[651]
$K_{FC} = T_{rg}(\Delta T_{xg}/T_g)$	Fan et al.[652]
$K_{LX} = T_g/T_c - 2T_g/(T_g + T_m)$	Long et al.[653]
$K_{YB} = T_xT_g/(T_m - T_x)^2$	Yuan et al.[654]

[a] T_x: onset crystallization peak temperature, T_c: crystallization peak temperature, T_g: glass transition temperature, T_m: melting temperature, $T_{rg} = T_g/T_m$: reduced glass transition temperature, T_x-T_g: supercooled region (adapted from ref 644).

DSC traces (see Figure 51) may contain one or more exothermic peaks due to the crystallization of different phases, but only the lowest crystallization peak is considered when calculating glass stability because once significant crystallization occurred, subsequent events at higher temperatures no longer affect the GS.

There has been a long debate whether glass stability parameters can infer glass-forming ability.[655−661] For instance, Cabral et al.[656] used experimental nucleation, $I(T)$, and growth rates, $U(T)$, for some glasses ($Li_2O·2SiO_2$, $BaO·2SiO_2$, $Na_2O·2CaO·3SiO_2$, and $2Na_2O·CaO·3SiO_2$ glasses) that nucleate (supposedly homogeneously) in the sample interior to calculate critical cooling rates for glass formation (R_c) by the TTT method. The R_c for small 20 mg pieces of lithium disilicate glass ($R_c \sim 0.2-0.3$ K/s, estimated from a TTT curve which was calculated from the JMAK model) agreed with quenching practice in laboratories and also with literature data.[660] A strong correlation between the Hrubý parameter of glass stability and the glass-forming ability, evaluated by R_c, was found. Therefore, they suggested that the Hrubý parameter can be used to estimate the glass-forming ability at least for glasses that exhibit *volume* nucleation.

In a complementary study, Nascimento et al.[659] assessed and compared the GFA and several GS parameters for different glasses. GFA and GS were estimated for six stoichiometric oxide glass-forming liquids that show predominant *surface* (heterogeneous) crystallization in laboratory time scales. These glasses were GeO_2, $Na_2O·2SiO_2$, $PbO·SiO_2$, $CaO·Al_2O_3·2SiO_2$, $CaO·MgO·2SiO_2$, and $2MgO·2Al_2O_3·5SiO_2$. They also investigated $Li_2O·2SiO_2$ and $Li_2O·2B_2O_3$ glasses that, besides surface nucleation, also undergo homogeneous (internal) crystallization. They gauged GFA by the critical cooling rate, R_c, which was calculated from experimental crystal growth rates, $U(T)$, and an estimated number of heterogeneous nucleation sites per unit surface, N_s, assuming a detectable surface crystallized fraction $X_c = 0.001$. They calculated GS parameters using 14 different combinations of the characteristic DTA or DSC temperatures: the glass transition temperature (T_g), the onset crystallization temperature of heating (T_x), the peak crystallization temperature on heating (T_c), and the melting point (T_m). To obtain the experimental GS criteria for each glass, they ran DSC using coarse and fine glass powders and completed the necessary calculations using literature values for T_m. Similar results were obtained for fine and coarse particles. Most of the GS parameters that involve the *three* characteristic DSC temperatures showed an excellent correlation with GFA. On the other hand, rather poor correlations were revealed for criteria that use only two characteristic temperatures. This study thus showed that certain, but not all, GS parameters could be used to infer GFA[659] of the tested glasses, for samples that show predominantly heterogeneous crystallization.

Then, Ferreira et al.[661] re-evaluated nine parameters of glass stability (GS) on heating using DSC experiments to predict the GFA of oxide liquids. $Li_2O·B_2O_3$ glasses with 20.0−66.7 mol% Li_2O were tested. The samples were prepared using both commercial chemicals and powders obtained via a solution method. The GS parameters were calculated using the characteristic T_g, T_x, and T_m of DSC thermograms (Table 2). They found that seven stability parameters give similar trends for compositions up to 33.3 mol% Li_2O, and as expected, the GS significantly decreased with lithia content. Beyond that, up to 66.7 mol% Li_2O, GS showed a broad, shallow maximum but was approximately constant, indicating that, surprisingly, the composition did not significantly affect the GFA in this compositional range. This result qualitatively agreed with their successful experience of preparing glasses with compositions up to 74 mol% Li_2O and corroborated the adequacy of simple DSC tests to comparatively gauge the GS and GFA of glass-forming liquids.[661]

Furthermore, the review of Kozmidis-Petrovic and Šesták[644] revealed that some generalized correlations between glass-forming ability and glass stability do exist. The relative change of the Hrubý parameter is the highest in almost all cases. Compared to other parameters (Table 2), this parameter is more sensitive to the change of both the supercooled region ($T_x - T_g$) and the reduced glass-transition temperature (T_{rg}). The relationship between the Hrubý parameter and GFA is satisfying for oxide glasses and thus can be employed as a reliable proxy for GFA. Associated problems are the experimental determination of the proper temperatures.[644]

In another endeavor to test GS parameters for oxide glasses, Marques and Cabral[662] determined the GS parameters proposed by Hrubý (K_H),[645] Weinberg (K_W),[647] Lu and Liu (K_{LL}),[648] Long et al. (K_{LX}),[653] and Zhang et al. (K_{ZW})[650] (Table 2) for $Li_2O·2SiO_2$, $BaO·2SiO_2$, $Na_2O·2CaO·3SiO_2$, and $2BaO·TiO_2·2SiO_2$ glasses, which show predominant internal crystallization. DSC experiments were performed in air, using Pt-Rh crucibles, at heating rates (q_h) of 2, 5, 10, 15, 20, 25, and 30 °C/min on monolithic specimens from room temperature up to their melting temperatures. The results revealed that all the criteria under investigation change significantly as a function of the heating rate. The K_H, K_W, and K_{LL} increased

DOI: 10.1021/acs.chemrev.8b00510
Chem. Rev. XXXX, XXX, XXX−XXX

with HR while K_{ZW} and K_{LX} decreased. To evaluate the consistency of these criteria in envisaging GFA, they were correlated to the critical cooling rates estimated by the continuous cooling (R_{CC}) and "nose" (R_{CN}) methods using experimental data of steady-state nucleation and crystal growth rates, the viscosity of each vitreous material, and free energy per unit of volume. They found that the correlation between the GFA (R_{CC} or R_{CN}) and all the GS parameters investigated persists if changes of the GS parameters with heating rate are considered.[662]

However, some relatively stable glasses crystallize so slowly that they do not exhibit a crystallization exotherm during heating at 5∼20 K/min. When used in normal DSC/DTA studies, they cannot be characterized by GS parameters. In these cases, it is usually necessary to carry out a series of isothermal heat treatments, to determine the conditions under which such glasses crystallize to a detectable extent. Creation of a TTT diagram, as described in Section 7.5, often proves to be a good method for defining their stability and GFA.

Finally, the T_g/T_m ratio can be regarded as a (rough) measure of GS. The larger this ratio, the higher the GS and inferentially the GFA. For most of the glass formers, this ratio is close to or below T_g/T_m = 2/3. Recently it has been discovered that the metal−organic framework, ZIF-62 (Zn-($Im_{2-x}bIm_x$)) exhibits ultrahigh GFA, and this is corroborated by the fact that its T_g/T_m ratio is 0.84, higher than any other known glass former.[663] For instance, B_2O_3 and Albite, the best oxide glass formers, have T_g/T_m of approximately 0.76−0.78.[664]

7.7. *Liquidus* Temperature

It is critical in laboratory and industrial practice to define the temperatures for the glass melting, homogenization, and fining processes, so that the manufacturing can be conducted without the risk of incipient devitrification. However, the accurate determination of T_L is not trivial and takes a long time for compositions that are reluctant to crystallization, i.e., for most commercial products.[66]

The *liquidus* temperature of systems that crystallize readily can be determined with DSC/DTA, a method which is remarkably simpler than the conventional "uniform temperature method". The latter is performed according to the American Society for Testing and Materials (ASTM)-C829 and is accelerated using a gradient temperature furnace and subsequent microscopic analysis for tracking of the liquid−crystal equilibrium.[665] The reliability of the ASTM method depends heavily on the experience and eyes of the operator and his/her interpretation. Another difficulty is the fact that, in most cases, slowly crystallizing glasses are desired for most commercial products. Hence, the determination of the liquid−crystal equilibrium temperature can be effortful, inexact, and time-consuming.

The statistical error in the T_L determination by the gradient furnace method in 20 tests of the same glass in the same laboratory was about ±7 K. Then, in a round-robin study, Beerkens and Conradt[666] reported that investigation of samples from the same glass batch in 6 different laboratories yielded variations of 50−60 K. Although thermodynamic models, computer modeling, and empirical methods based on the chemical composition are available to predict the *liquidus* of glass-forming systems,[666−669] they have serious limitations; for example, thermodynamic data are often unavailable or difficult to determine, and it is often not practical to extrapolate to compositions out of the range of previous experiments.[666−669] In this regard, the use of deep learning or artificial intelligence (such as artificial neural networks) warrants more study and should be further developed for the reliable prediction of the *liquidus* temperatures (and other properties) of multicomponent glass-forming systems.[147]

As described in Section 7.1, any characteristic DSC trace for a stoichiometric, and easily crystallized glass shows at least three distinct signatures during heating: T_g, T_c, and T_L (Figure 51). However, DSC curves of complex multicomponent glasses that resist crystallization (such as most commercial glasses) frequently show no crystallization and melting peaks, whereas others show multiple T_g (phase separated systems) and T_c and melting peaks. The correct interpretation of T_L even for compositions that show clear melting peaks also presents some difficulties. Some of the problems discussed in the literature regarding the use of DSC techniques for the determination of the *liquidus* temperature are reviewed henceforth.

First, thermocouples are not always calibrated as they should be. The geometry and thermal properties of the sample holder should be introduced to the DSC/DTA software. However, when simultaneous melting processes occur,[670] as in multicomponent glasses, it is particularly difficult to interpret the results. Any DSC peak can be identified by its onset, maximum, and offset temperatures (Figure 51). It is simple to acquire the temperature of a DSC melting peak, although its physical meaning is not so clear. The determination of the other characteristic temperatures, such as the onset and offset temperatures, is not so easy. Conventionally, these last two temperatures are typically determined by the meeting point of tangents to the curve, traced on the baseline and the peak side, on the low- and high-temperature peak side, respectively. However, this so-called "tangent method" is not a standard practice, and its uncertainty is difficult to estimate. Furthermore, it is also hard to draw tangents on a nonstraight DSC peak side, on broad, or low-intensity, or overlapped peaks. All these parameters increase the uncertainty of this method. Garidel et al.[671] compared the tangent method with another method for marking the onset and offset temperatures of the DSC melting peak. Their method simulates the variation of heat capacity as a function of temperature, assuming that the onset and offset points of the DSC melting peak are the *solidus* and the *liquidus*, respectively. They established binary-phase diagrams for organic compounds using the proposed technique and compared the results with those built by the tangent method. The resulting diagrams revealed that the *liquidus* values determined from both methods were in good agreement, while the *solidus* values deviated considerably.

Pedersen et al.[672] applied another DSC method to figure out the *solidus* and *liquidus* of a Sn-Pb eutectic phase diagram. They used the tangent method to determine the onset and offset of DSC melting peaks at various heating rates by changing the heating rates from 0.1 to 30 °C/min. These authors also supposed that a fit to the data points plotted as a function of the heating rate and extrapolated to zero heating rate represented the *solidus* for the onset and the *liquidus* for the offset. They found, for their system, that the onset of the melting peak (the eutectic temperature in this case) was independent of composition and heating rate, whereas the end point temperature changed linearly with the heating rate, with approximately the same slope for all compositions. The *solidus* and *liquidus* were in agreement with a published phase diagram within a few percent errors. Pedersen et al.[672] used several

DOI: 10.1021/acs.chemrev.8b00510
Chem. Rev. XXXX, XXX, XXX−XXX

heating rates, high-purity elements (Pb-99.9999% and Sn-99.999%), and small sample masses, corroborating their method. In a conventional DSC curve, when melting is observed as an endothermic peak, the first shift from the baseline rather than the typical onset temperature, (see detail in Figure 51) can be considered the best estimate of the *solidus*. This definition agrees with the description of the *solidus*, the temperature below which no liquid exists in equilibrium. Thus, the first sign of melting shows that this temperature has been reached. In the case studied by Pedersen et al.,[672] this point was near to the onset obtained by the tangent method. However, when the DSC melting peak is excessively broad, the onset temperature determined by the tangent method differs considerably from the first divergence from the baseline.

DSC methods have been used in the construction of binary-phase diagrams of organic compounds in other works. In one of them, Young et al.[673] determined the *liquidus* and compared the results with the calculated *liquidus* as a function of composition, assuming an ideal solid solution, knowing the T_m, the latent heat of fusion of the pure components, and their molar fraction in the mixture. Low heating rates were applied to reach conditions near equilibrium. However, the use of very low heating rates is sometimes not practical for commercial multicomponent glasses, as they often do not crystallize, even after long heat-treatments, thus precluding the detection of the melting peak during a DSC run.

A different method of DSC analysis, called the stepwise method, can also be utilized to reach near equilibrium conditions. Charsley et al.[674] introduced this approach, also known as isothermal calibration, whereby the temperature of the sample is increased stepwise with isothermal intervals between the steps until melting is completed. The occurrence of melting is observed as an endothermic shift from the baseline of the DSC curve determined by this method. A comparison between the T_L determined by the stepwise method (taken as reference) and by extrapolation of the onset temperature (T_x) determined at different rates to zero heating rate revealed that the extrapolated T_x provided the *liquidus* at equilibrium. T_x values determined by the tangent method and at heating rates of 0.5−10 °C/min were utilized in the second case. The use of the T_x was justified by the fact that pure (stoichiometric) reference compounds were utilized. However, similar difficulties are expected when applying either the stepwise or the dynamic extrapolation methods to complex glass-forming compositions, i.e., because of the peak shape and overlap. According to Höhne et al.,[675] wide melting peaks appear in DSC analyses of nonstoichiometric and noneutectic compositions. In these cases, the onset temperature is associated with melting in the eutectic reaction, and the "subsequent broad endothermic effect is caused by the dissolution of the remaining solid component into the equilibrium melt." Therefore, the offset temperature could be attributed to the *liquidus*. On the other hand, pure or eutectic compositions melt during a DSC run at a well-defined "temperature" and this temperature usually corresponds to the onset estimated by the tangent method. This brief review shows that (i) there is no standard procedure to determine T_L by DSC/DTA and (ii) there is no agreement about the most satisfactory method to determine the T_L using DSC/DTA, even though most evidence favors the extrapolated offset temperature for noncongruent melting and nonstoichiometric compositions.

Because the traditional procedures to measure the *liquidus* of difficult-to-crystallize glasses are problematic and time-consuming, alternative methods are welcome. Ferreira et al.[676] established a new DSC method for reliable and faster estimation of the *liquidus* of multicomponent glasses that are reluctant to crystallize. They chose three multicomponent commercial glasses for which the *liquidus* was previously carefully determined by the traditional gradient furnace method. The characteristic temperatures of DSC melting peaks (end points) were obtained at different heating rates and extrapolated to 0 °C/min; the resulting values compared quite well with the known *liquidus* of the three glasses. DSC tests were conducted on 22−38 μm powders placed in covered Pt pans.[676] Before the DSC analysis, the glasses were also heat treated well below the known *liquidus* (920 °C) for a sufficient time (24 h) to promote crystallization, enabling the detection of a melting signal by DSC. Ferreira et al.[676] thus demonstrated that, for multicomponent glasses that do not crystallize during a DSC run, a primary heat treatment is necessary to reach near-equilibrium conditions. Then, the offset of the DSC melting peaks measured at different heating rates and (linearly) extrapolated to null heating rate is the best estimate of the *liquidus* of such glasses (Figure 69). In this way,

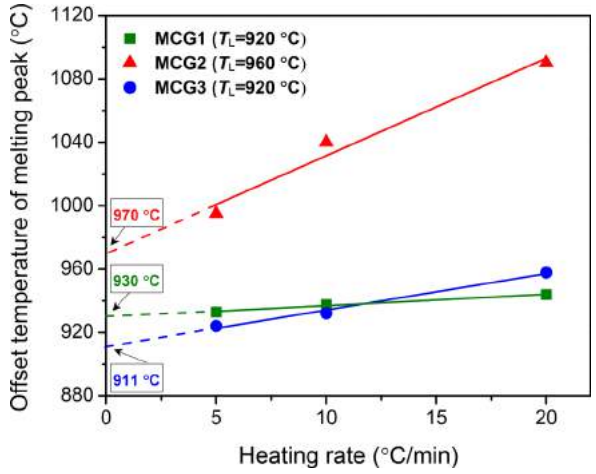

Figure 69. DSC end points, i.e., the offset temperatures of the melt peaks for three multicomponent commercial glasses extrapolated to null heating rate (in the boxes), which reasonably agree with the *Liquidus* determined by the standard gradient furnace technique: T_L indicated in the legend. Reproduced with permission from ref 676. Copyright 2010 John Wiley and Sons.

they found a good agreement (most results differed by less than 10 °C) with the known values of the *liquidus* of those compositions. Ferreira et al. also checked their method for several compositions of a well-known binary system, $Li_2O-B_2O_3$ analyzed by DSC; and the results were compared with the published equilibrium phase diagram. Hence, they successfully demonstrated this DSC method to estimate the *liquidus* of difficult-to-crystallize, good glass-forming systems. As a consequence of the small amount of glass needed, the flexibility of computer-aided detection, the immediate crystallization pretreatment of many different compositions at the same time, and the speed of the DSC analysis developed in this method, this technique is an advantaged alternative for determining the *liquidus* of simple or multicomponent glasses. This proposed nonisothermal technique is beneficial for screening glass compositions. In addition to the study of

DOI: 10.1021/acs.chemrev.8b00510
Chem. Rev. XXXX, XXX, XXX−XXX

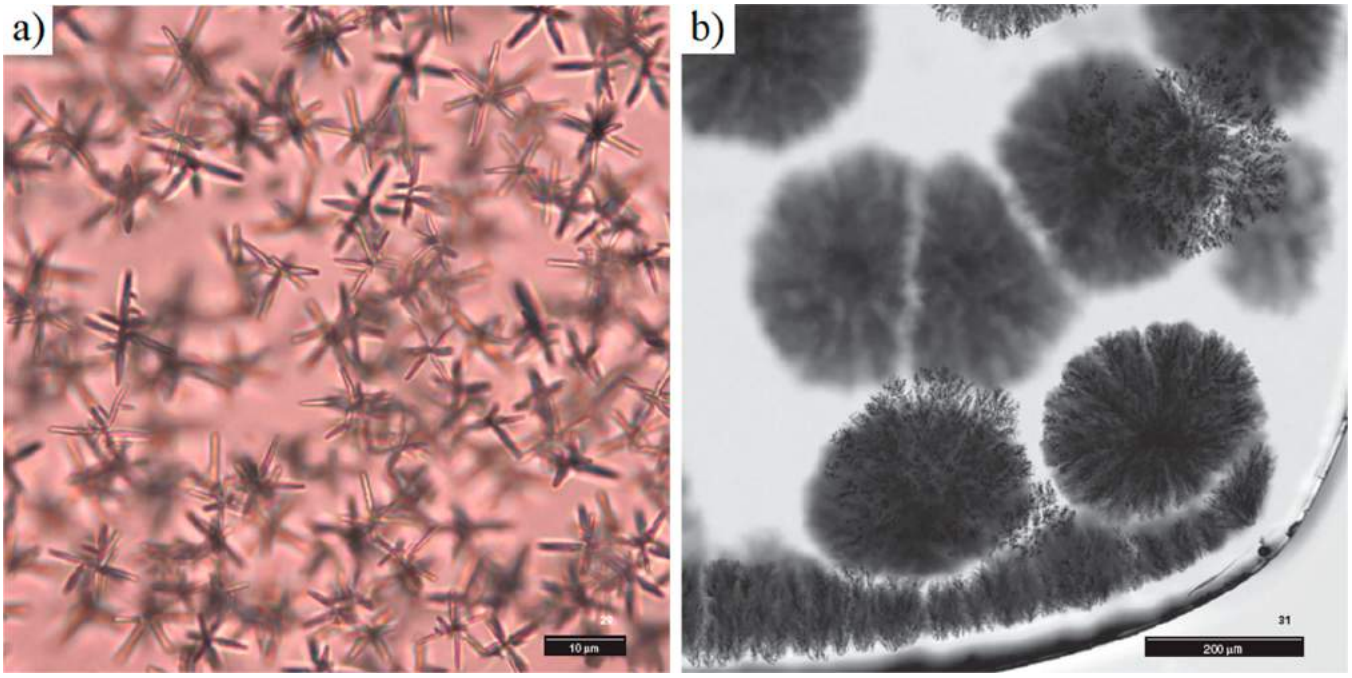

Figure 70. (a) NaF crystals in the interior of a PTR glass-ceramic. Treatment at a high temperature near the solubility limit. UV-unexposed, heat-treated at 700 °C for 30 min. (b) At more advanced stages, after precipitation of the desired NaF crystals, spherulitic cristobalite crystals appear in PTR glass. In this case, the glass was not exposed to UV and was hyperdeveloped by extensive thermal treatment. Optical microscopy, transmitted light. Reproduced with permission from ref 682. Copyright by John Wiley and Sons, Inc. and the American Ceramic Society.

Ferreira et al.,[676] it has been reported in several papers that the *offset* of the melting reaction for binary systems should be used as a proxy for T_L.[672,673,677] The linear extrapolation approach of determining T_L was confirmed by a recent study of basaltic glass compositions.[217]

More recently, the *liquidus* temperatures (T_L) of good glass-forming systems within the $CaO\text{-}SiO_2\text{-}MgO\text{-}Al_2O_3$ system (CMAS) were evaluated by Veit et al.[678] The reproducibility of T_L via DTA was studied and compared with results from the gradient furnace method. Since these glasses were reluctant to crystallize, a previous heat treatment was performed to induce crystallization. The onset and the offset temperatures of the melting peaks of precrystallized glasses were determined at a heating rate of 2 K/min and compared with the *liquidus* temperatures obtained by the gradient furnace method.[666] The offset temperatures of the melting peaks were closest to the results determined using the ASTM procedure. The majority of offset results via DTA differed by not more than 10 K compared to the isothermal (gradient) *liquidus* temperatures. This method is indeed a very helpful option to estimate the *liquidus* temperature of complex multicomponent glasses.[678]

7.8. Applications in Developing Glass-Ceramics

DTA/DSC are valuable tools for developing an important group of materials, i.e., glass-ceramics (GCs). Numerous novel glass-ceramics have been developed so far for domestic, electronic, optical, dental, and biomedical applications.[22,530−532] As discussed by Davis and Zanotto,[23] no other class of materials possesses such valuable and unusual *combination* of properties in an advantageous and feasible manner.[23] "*Glass-ceramics are inorganic, non-metallic materials prepared by controlled crystallization of glasses via different processing methods. They contain at least one type of functional crystalline phase and a residual glass. The volume fraction crystallized may vary from ppm to almost 100%*".[679] Heat treatment is usually (but not always) performed in two stages: first, at relatively low temperatures, not far from the glass transition, T_g, to induce internal nucleation, followed by a second stage at a higher temperature to promote the growth of different phases. Therefore, accurate determinations of nucleation and growth temperatures and their kinetics are crucial for establishing precise heat treatments.[528] In this context, quick estimation of optimum nucleation/growth temperature (e.g., by DSC), kinetic parameters such as crystal nucleation rate, nucleation time-lag (or induction period), and growth rate are of great importance, because they can be used to define the crystal number density, N (nuclei/m^3), which in turn limits the average size and the shape of the crystals in the resulting microstructure. These quantities determine, to a great extent, the properties and applications of GCs. For example, new classes of advanced nanoglass-ceramics can be developed if the average size is kept at less than 200 nm.[680,681] The same composition that is transparent with nanosized crystallites will become opaque with larger crystals. Crystallite morphologies range from blocky "coast and island" microstructures to long and narrow dendritic structures. A wide and most beautiful variety of crystallite morphologies have been shown by Zanotto in ref 682, including starlike NaF and spherulitic cristobalite crystals in the volume of PTR (photothermo-refractive) glass as in Figure 70. For a thorough insight into the application and prospects of glass-ceramics, we refer the interested readers to some recent reviews.[22,23,529−532,309] Finally, we can safely state that a DSC/DTA analysis is the first, and perhaps the most important, test in scrutinizing candidate glass compositions for subsequent glass-ceramic development.

More than 3,300 studies indexed in the Scopus database report on the use of DSC/DTA analysis for investigations of inorganic glasses, and many other studies deal with metallic

DOI: 10.1021/acs.chemrev.8b00510
Chem. Rev. XXXX, XXX, XXX−XXX

and organic glasses. Most of them consider the laboratory use of DSC/DTA as a useful and fast method of analysis. However, in most cases, DTA/DSC is merely utilized to estimate the maximum nucleation temperature (Section 7.1.1), the activation energy for overall crystallization (E), or the Avrami constant (n) (Section 7.3.2). There are only a few studies, reported herein, that deal with the application of DTA/DSC to investigate nucleation or growth rates, GFA, GS, and T_L. Therefore, in this section, we elaborated on the versatility and usefulness of DTA/DSC methods to examine a variety of glass characteristics. We also wanted to bring the reader's attention to some advantages and problems of DTA/DSC methods and to caution them against its "automatic" application. For example, in the case of calculating the activation energy for crystallization or crystallization mechanism via the Kissinger/Ozawa-based equations, ultimate care should be devoted. DSC/DTA analysis well describes the nucleation/growth kinetics in a condition where it is isothermal, and the number of nuclei (N) and growth rate (U) are constant. In other situations, e.g., nonisothermal condition, unsteady nucleation before induction period, growing N, unsettled U, or multiple phase formations, this study may lead us to superficial results which demand precise (usually complicated) explanations or modifications. Therefore, it would be highly advisable to consider numerous recommendations by the ICTAC Kinetics Committee[587,588,594] and many other modifications/criteria[7,589−593] to recalculate the values of E and n reported in many papers that apply the Kissinger/Ozawa equation to the process of crystallization. Because of the uncertainty regarding the reported values of E and n, we did not refer to many of these articles herein. However, there is still an exciting line of research for expanding/simplifying the application of DSC/DTA for more complex conditions, because these techniques are less tedious, require a smaller amount of sample, and are faster than most conventional methods.

8. CONCLUDING REMARKS AND PERSPECTIVES

8.1. Calorimetric Glass Transition

Following this comprehensive review, we can indeed state that DSC has played a critical role in clarifying fundamental scientific questions related to the glass transition and the glassy state. The glass transition is still considered to be one of the most challenging and interesting problems in condensed matter science. The abrupt jump of the configurational heat capacity during the glass-to-liquid transition is a calorimetric signature of the glass transition and one of its most striking features. The magnitude of this heat capacity jump strongly depends on the composition, which is found to be intimately associated with the change of the medium-range structure (Section 3.2.2.).

The calorimetric glass transition characteristics of oxide glasses are found to be connected to the topology of the glass network since the compositional dependence of the T_g and m values can be predicted using temperature-dependent constraint theory. However, for a multicomponent (>4 components) glass series, the prediction becomes more difficult to derive analytically.[146] Topological models can be extended by considering the modifying ion subnetwork constraints and the relative strengths of the modifier constraints.[144] As such, a comprehensive understanding of the calorimetric glass transition must combine DSC measurements with knowledge of the underlying glass structure and topology.

Another important feature of the calorimetric glass transition is the significant impact of pressure, viz., the pressure-induced enhancement of the endothermic overshoot. For a borosilicate glass series, it is evident that increasing pressure causes an increase in the glass density and a commensurate drop in the topological degrees of freedom due to the conversion of BO_3 to BO_4 units, which entails an increase of network connectivity and rigidity. Interestingly, upon annealing near T_g, the pressure-induced boron speciation remains unchanged while the macroscopic properties (e.g., density, refractive index, and hardness) recover, implying that the change in macroscopic properties is not a consequence of a change in short-range order but rather of the increase in both medium- and long-range ordering.

A recent discovery made by DSC is that melt-quenched metallic glasses can be energetically excited, i.e., rejuvenated, by thermal cycling in the temperature range well below room temperature, in contrast to the typical structural relaxation toward higher density and lower enthalpy states. Thermal cycling enhances the structural heterogeneity (i.e., nonaffine strains) and hence causes the excitation of potential energy. This phenomenon is found to increase the plasticity of metallic glasses, which is a crucial property for engineering applications. This result also gives insight into energy fluctuations in glassy materials.

DSC is more than just a simple characterization instrument: it is truly a tool to enable many aspects of advanced glass research. This article introduced some of the new DSC approaches developed for glass research, e.g., the universal method for determination of the fictive temperature, cooling rate, liquid fragility, and viscosity of any MQ glass systems and the HAD approach for probing the enthalpy relaxation and the energetic and structural heterogeneity in glass.

DSC is a sensitive technique for detecting polyamorphic transitions, which occur in some materials. The pressure/temperature-induced polyamorphic transitions in zeolites can be identified using DSC with the help of XRD, SAXS, and thermal expansion measurements. Zeolite amorphization is time-dependent, and the dynamics of order−disorder transitions under temperature and pressure are equivalent. Zeolites behave as strong liquids during amorphization. In addition, DSC was used to detect the coexistence of both high-density and low-density amorphous phases in ZIF-4, a metal−organic framework material (see Section 3.7). From the DSC data, a semiquantitative PEL was deduced.[4]

8.2. Sub- and Sup-T_g Enthalpy Relaxation

We documented several advances in DSC studies of enthalpy relaxation for different glassy systems. DSC is a powerful tool for exploring various thermodynamic relaxation events, including sub- and sup-T_g enthalpy relaxations, and for clarifying features of α and β relaxations, from which structural heterogeneity and fragile-to-strong transition can be evaluated. Within the PEL framework, hyperquenching and physical vapor deposition are two opposite synthesis routes, by which the formed glass systems were brought to comparatively higher and lower energy states, respectively. Ball milling and stretching are another two mechanical methods for forming glasses at different energy levels. The glasses formed via different synthesis routes exhibit their own relaxation characteristics in terms of the evolution of C_p curves, providing detailed information about the thermodynamic evolution, e.g., during annealing. Exploring the microstructural changes at the

DOI: 10.1021/acs.chemrev.8b00510
Chem. Rev. XXXX, XXX, XXX−XXX

medium range order level during the enthalpy relaxation process of the glass systems produced by different routes, particularly for ultrastable glasses, could be of great importance for future research. In case of the ball-milling derived amorphous materials, whose enthalpy relaxation has not yet been extensively studied, understanding their glass formation mechanism and relaxation behavior, along with those of the cryomilled glass (rejuvenated glass from annealing a ball-milled sample), is crucial for establishing a universal relaxation theory for describing the relaxation dynamics.

In Section 4, we introduced the hyperquenching-annealing-DSC (HAD) approach for glass relaxation studies. Using the HAD strategy, substantial progress has been made in understanding the two important dynamical relaxation processes, i.e., α and β relaxations. In particular, significant research work has been done on the slow β or JG relaxation and confirmed its universality in different glass formers and its connection to the glass transition. Despite extensive studies of this issue, there is lack of a definite correlation between the relaxation modes, atomic structures, and macroscopic properties/behaviors of glassy systems. Combination of DSC with other techniques, e.g., dynamical mechanical spectrum (DMS) measurements,[366,367,380] has demonstrated the relationship between β relaxation and the plastic deformation of metallic glasses, which is of significant importance for the practical application of BMGs. Hence, the effect of relaxation modes on the functional properties of other glass systems should be given special attention, especially for widely used oxide glasses. Of course, it will be helpful to establish the relationship between relaxation modes and the physical properties of the glasses when determining which local structures dominate the various relaxation processes.

Analyzing C_p curve patterns for glasses subjected to different degrees of annealing is a powerful way to elucidate the structural heterogeneity in both normal and poor glass formers. An especially striking anomalous relaxation phenomenon, i.e., the three-stage sub-T_g relaxation patterns in a typical metallic glass was revealed to correspond to the dynamic fragile-to-strong transition. The underlying physics of this phenomenon lies in the competition of low and the high-temperature clusters, i.e., the structural heterogeneity of the glass-forming liquids. To understand structural heterogeneities more fully, further investigations regarding both the driving force for such heterogeneity and the underlying atomic configurations are desired.

Flash DSC (Section 5) has also been employed to study both the glass transition and the enthalpy relaxation in organic, chalcogenide, and metallic glasses. The extremely high heating/cooling rates of Flash DSC significantly open the instrument parameter space compared to traditional DSC. Using the unique capabilities of Flash DSC, both the liquid fragility of several polymers and the apparent activation energies of relaxation were found to vary with the film size and cooling rate. Both the underlying physics of m determined by Flash DSC and the detection of different relaxation modes in various glasses by means of Flash DSC should be considered as interesting issues for further investigation.

In Section 6, we reviewed the TMDSC technique, in which a modulated heat flow signal can be decomposed into both thermodynamic and kinetic components. Two methods exist for interpretation of the TMDSC signal, viz., complex signal analysis and decomposition into reversing and nonreversing heat flows. The latter approach has been used to report the discovery of intermediate phase glasses where the nonreversing heat flow is observed to be at a minimum over a range of compositions. This minimum is claimed to correspond to a minimum in aging; however, a rigorous analysis of the physical meaning of the nonreversing heat flow is still lacking. Further research is needed to reconcile these interpretations of the TMDSC signal and to understand the full meaning of the reported intermediate phases in various glass families.

8.3. Crystallization

The present article also elaborated on the versatility and utility of several DSC techniques for examining the dynamics related to nucleation, growth, glass-forming ability (GFA) and stability (GS). We draw attention to the advantages and problems related to the use of DSC and caution the reader against its "automatic" application. For example, DSC is very useful for providing estimates of the temperature range where significant nucleation occurs (Section 7.1.1). When properly used, *isothermal* DSC runs yield useful information regarding crystallization processes, including the crystal number density, the nucleation and growth kinetics, the activation energy for overall crystallization (E_c), and the Avrami constant (n) (Sections 7.2 and 7.3). In the case of GFA (Section 7.5), traditional DSC methods have limitations in determining the critical cooling rate (R_c) for vitrification of either extremely poor glass formers (e.g., metallic alloys) or good glass formers (e.g., some soda lime silicates and some polymers). Traditional DSC equipment cannot provide sufficiently high cooling rates for vitrifying metallic liquids and cannot provide a sufficiently low cooling rate to devitrify some polymers. On the other hand, new DSC techniques are being rapidly developed. For instance, Flash DSC can heat small samples at a rate up to 10^6 K/s (Section 4.1.2), enabling determination of the R_c of more reluctant glass formers. In Section 7.6, we summarized the GS criteria and compared them with the well-known Hrubý parameter to measure the glass stability and glass-forming ability. We also discussed how GS equations could be employed as a reliable proxy for GFA. Additionally, we regarded the T_g/T_m ratio only as a (rough) measure of GS. The higher this ratio, the greater the GS and therefore the GFA. Our critical review also revealed that (i) there is no standard procedure to determine the T_L by DSC; and (ii) there is no agreement regarding the most satisfactory method for determining the T_L by DSC, even though most evidence favors extrapolating the offset temperature of the endothermic melting peak to zero heating rate for noncongruent melting and nonstoichiometric compositions (Section 7.7). For multicomponent glasses that do not crystallize during a typical DSC run, a preliminary heat treatment is necessary to crystallize the material to reach near-equilibrium conditions. Then, the offset of the DSC melting peaks measured at different heating rates and (linearly) extrapolated to null heating rate provides a good estimate of the *liquidus* (Section 7.7). As a consequence of the small amount of glass needed, the flexibility, and the speed of DSC analysis, this method is recommended for determining the *liquidus* of simple or multicomponent glasses. Finally, in Section 7.8, we emphasized that DSC analyses have been used to develop an important class of materials, glass-ceramics. Numerous glass-ceramics have already been commercialized for domestic, electronic, optical, dental, and biomedical applications. These materials allow for an unusual and valuable combination of properties. They are usually developed (but not always) via two-stage heat

DOI: 10.1021/acs.chemrev.8b00510
Chem. Rev. XXXX, XXX, XXX−XXX

treatments: first, at relatively low temperatures, to induce internal nucleation, followed by a second stage at a higher temperature to promote the growth of different crystals. Therefore, accurate determinations of nucleation and growth temperatures and their kinetics are crucial for establishing precise heat treatments. In this context, quick estimation of the optimum nucleation/growth temperature by DSC, kinetic parameters—such as crystal nucleation rate, nucleation time-lag (or induction period), and growth rate—are of great importance, since they can be used to define the crystal number density, N (nuclei/m^3), which in turn limits the average size of the crystals in the resulting microstructure. These quantities determine, to a great extent, their properties and applications and can boost the development of new types of advanced glass-ceramics.

8.4. Perspectives

DSC is a highly sensitive and versatile technique for detecting thermodynamic changes in glass-forming systems upon heating or cooling. To build a comprehensive understanding of the glass transition, DSC should be used in combination with other characterization techniques such as dielectric spectroscopy, microscopy, vibrational spectroscopy, and structural analysis. This experimental understanding should then be understood in terms of underlying physical theories such as energy landscape and topological constraint theories. Deeper insights into the sub-T_g enthalpy relaxation can still be obtained through computer simulation techniques, such as molecular dynamics simulation and phenomenological modeling, although some initial progress has been made in modeling the enthalpy relaxation patterns of the annealed HQ glasses.[309,312] One of the main challenges regarding the origin of the calorimetric glass transition is the detection of the structural evolution during glass transition and relaxation. To overcome this challenge, *in situ* NMR and Raman measurements during heating or cooling can be designed in such a manner that the enthalpy signal can be detected simultaneously. To date, Flash DSC has only been used for studying the glass transition and relaxation in organic or metallic glasses. It is still challenging to apply this technique to oxide glasses due to the difficulty of obtaining full contact between the oxide sample and the sensor of the Flash DSC. Significant progress can be achieved in future studies of glass transition, relaxation, and crystallization phenomena in nonmetallic inorganic glass systems.

The *quantitative* estimation of crystallization kinetics using a *nonisothermal* DSC run, which is much faster than isothermal, is still difficult and complex. For example, great care should be taken when calculating the activation energy for crystallization or the crystallization mechanism via the popular Kissinger/Ozawa-based equations. DSC analysis can accurately describe the nucleation/growth mechanism under *isothermal* conditions. In other situations, such as nonisothermal conditions, non-steady-state nucleation, time-dependent growth rates, or multiple phase formation, DSC experiments may lead to superficial results that demand especially complicated interpretation. Therefore, it is highly advisable to consider the numerous recommendations of the ICTAC Kinetics Committee and other modifications and criteria to recalculate the values of E_c and n reported in many papers that apply the Kissinger/Ozawa equation to crystallization processes. There is still scope for expanding/simplifying the application of DSC methods for more complicated conditions, since the DSC technique is less tedious, is faster, and requires smaller sample sizes, compared to most conventional methods.

The inorganic, organic, and metallic glass communities have been extensively utilizing DSC to explore the various aspects of glass science reported herein. However, to date, there has often been a lack of interaction among these communities to define some adequate DSC methods for all materials types. We hope that this comprehensive review article can promote and advance calorimetry-driven glass research across all of these communities.

AUTHOR INFORMATION

Corresponding Author

*E-mail: yy@bio.aau.dk.

ORCID

Maziar Montazerian: 0000-0002-1409-9182
Ozgur Gulbiten: 0000-0001-9156-7659
John C. Mauro: 0000-0002-4319-3530
Yuanzheng Yue: 0000-0002-6048-5236

Author Contributions

○Q.Z., Y.Z., and M.M. contributed equally to the paper.

Notes

The authors declare no competing financial interest.

Biographies

Qiuju Zheng is Associate Professor at the Qilu University of Technology. In 2012, she received her Ph.D. in Materials Chemistry from Aalborg University in Denmark. During her Ph.D. study, she did a summer internship in Corning Incorporated, USA, in 2010. From 2012 to 2015, she was a postdoctoral fellow at Aalborg University, sponsored by Rockwool International (Denmark). Her research focuses on structure, properties, relaxation, and crystallization of glass and glass fibers. She has published more than 20 peer-reviewed papers and has been granted two patents. She has given over 15 international conference presentations, including several invited talks.

Yanfei Zhang is Associate Professor at the Qilu University of Technology, Jinan, China. She received her Ph.D. degree in Physics at Shandong University, China, in 2009. She was a postdoctoral fellow in the Department of Chemistry and Bioscience, Aalborg University, Denmark (2011~2012). She joined the School of Materials Science and Engineering at Qilu University of Technology in 2009. Her research interests are in glass relaxation, glass transition, structure and properties of oxide glasses and glass fibers, and glassy electrode materials for lithium/sodium-ion batteries. She has published more than 20 peer-reviewed papers.

Maziar Montazerian received his Ph.D. degree in Materials Science and Engineering from the Iran University of Science and Technology in 2015. He is currently a postdoctoral fellow at CeRTEV, UFSCar, Brazil. He intends to develop novel bioactive glasses/glass-ceramics for biomedical applications. His research interests also include nucleation and crystallization theories, dental materials, and mechanical properties. He has published 6 review papers, 14 scientific articles, and 3 book chapters and gave over 10 international conference presentations. He was a recipient of a Ph.D. scholarship from The World Academy of Science (TWAS) and Iran National Science Foundation (INFS) and a postdoctoral fellowship from São Paulo Research Foundation (FAPESP).

Ozgur Gulbiten is a senior research scientist at the science and technology division of Corning Incorporated in Corning, New York. Ozgur joined Corning in 2014 after completing his Ph.D. in materials

DOI: 10.1021/acs.chemrev.8b00510
Chem. Rev. XXXX, XXX, XXX−XXX

science and engineering at the University of Arizona. He is currently focused on solving product-related questions about the thermophysical properties of glass and glass-ceramic materials. His academic research interests include relaxation processes, the dynamics of the glass transition, and structure and physical property relationships in supercooled liquids. Ozgur is the author of 17 peer-reviewed scientific papers.

John C. Mauro is Professor of Materials Science and Engineering at The Pennsylvania State University. John earned a B.S. in Glass Engineering Science (2001), B.A. in Computer Science (2001), and Ph.D. in Glass Science (2006), all from Alfred University. He joined Corning Incorporated in 1999 and served in multiple roles there, including Senior Research Manager of the Glass Research department. John is the inventor or coinventor of several new glass compositions for Corning, including Corning Gorilla Glass products. John joined the faculty at Penn State in 2017 and is currently a world-recognized expert in fundamental and applied glass science, statistical mechanics, computational and condensed matter physics, thermodynamics, and the topology of disordered networks. John is the author of over 220 peer-reviewed publications and is Editor of the *Journal of the American Ceramic Society*.

Edgar Dutra Zanotto is a Professor of Materials Science and Engineering and Director of the Center for Research, Technology and Education in Vitreous Materials, both at the Federal University of São Carlos (UFSCar), Brazil, and an editor of the *Journal of Non-Crystalline Solids*. His main research interests include dynamic processes in inorganic glass-forming liquids (diffusion, viscous flow, relaxation, crystal nucleation and growth, crystallization and glass-forming ability) and properties of glasses and glass-ceramics. He has been working for forty-two years in this field and has published over 260 scientific articles, 3 books, 27 patents, and 5 book prefaces, and delivered approximately 150 invited and plenary conference talks. He has supervised approximately 80 research students and postdocs. He is a member of both Brazilian and São Paulo State Academy of Sciences, National Academy of Engineering, The World Academy of Sciences, and World Academy of Ceramics, and Fellow of the Society of Glass Technology, UK, the American Ceramic Society, and the Brazilian Ceramic Society.

Yuanzheng Yue is Professor of Chemistry at Aalborg University, Denmark. He is the founder of the inorganic glass research laboratory in Denmark and the head of Center for Amorphous Materials. He is a distinguished visiting professor at Wuhan University of Technology and Qilu University of Technology, China. He received his Ph.D. degree at Berlin University of Technology, Germany, in 1995. His research interests are in glass science, glass fiber technology, amorphous materials for thermal insulation, energy storage and membrane, and metal−organic framework glasses. He is the author/coauthor of over 290 papers in peer-refereed journals and has given more than 100 invited and plenary talks at international conferences. He has supervised about 30 Ph.D. students and 16 postdocs. He is an editor of *European Journal of Glass Science and Technology*. He is the founding chair of the Technical Committee for Glass Fibers under ICG. He is an honorary member of Glass Division of Chinese Ceramic Society. He is a member of the EU Academy of Sciences.

ACKNOWLEDGMENTS

Q.J.Z. wishes to acknowledge support from National Natural Science Foundation of China (51802165) and Shandong Provincial Natural Science Foundation (ZR2017LEM007). Y.F.Z. would like to acknowledge support by National Natural Science Foundation of China (grant no. 51402156) and Shandong Provincial Natural Science Foundation (grant no. ZR2014EMQ003). Q.J.Z and Y.F.Z. acknowledge Shandong Provincial Key Project Funding (2018YFJH0402). M.M. and E.D.Z. are grateful to the São Paulo Research Foundation (FAPESP, # 2013/07793-6) - CEPID/CeRTEV - for financial support of this work, and the postdoctoral fellowship granted to Maziar Montazerian (# 2015/13314-9). J.C.M. acknowledges support from the National Science Foundation (CMMI 1762275). Y.Z.Y. acknowledges support from the Danish Research Council (grant no. 26-03-0096 and no. 09-064216) and the Shandong Taishan Scholar Program.

SYMBOLS AND ABBREVIATIONS

A'	Amplitude of the modulated heating rate
A_0	Total area of crystallization peak
A	Area of crystallization peak
A_t	Amplitude of the sinusoidal oscillation
$A(x_R)$	Proportionality constant for the reference composition x_R
CF	Correction factor
$C(\lvert CF\rvert)$	Proportionality as a function of CF
C_v	Isochoric heat capacity
C_p	Isobaric heat capacity
$C_{p,vib}$	Vibrational heat capacity
C_{pg}	Glass C_p
C_{pl}	Liquid C_p
ΔC_p	$C_{pl} - C_{pg}$ as a function of T
$\Delta C_p(T_g)$	$C_{pl} - C_{pg}$ at T_g
$C_{p,conf}$	Configurational heat capacity as a function of T
$C_{p,conf}(T_g)$	$C_{p,conf}$ at T_g
$C_{p,exc}$	Excess of C_p of the standard glass over its HQ state
$C_{p,endo}$	Difference in C_p between the annealed HQ glass and the standard glass within the endothermic prepeak below T_g
C_p^0	C_p at zero frequency
C_p^∞	C_p at the high frequency limit
C_p^*	Complex C_p
C_p'	Real part of C_p^*
C_p''	Imaginary part of C_p^*
$\lvert C_p(\omega)\rvert$	Modulus of C_p^*
D	The Deborah number
E	Activation energy for overall crystallization
E_g	Activation energy for equilibrium viscous flow
E_α	Activation energy for α relaxation
E_β	Activation energy for β relaxation
E_{relax}	Activation energy for enthalpy relaxation
E_c	Activation energy for crystal growth
F	Atomic degree of freedom
G_∞	Shear modulus at the high limit of frequency
$G(\omega)$	Effective vibrational density of states
H_c	Total crystallization enthalpy
ΔH_m	Melting enthalpy
ΔH_{nr}	Nonreversing heat flow
ΔH_{rel}	Enthalpy of relaxation
ΔH_{rem}	Remaining excess enthalpy in HQ or ball-milled glasses after annealing
H_{rev}	Reversing heat flow
ΔH_{tot}	Total excess enthalpy in as-prepared HQ or ball-milled glasses
I	Nucleation rate
K_A	Avrami fitting parameter
K_c	Shift factor for determination of cooling rate

DOI: 10.1021/acs.chemrev.8b00510
Chem. Rev. XXXX, XXX, XXX−XXX

K_Φ	Proportionality between the measured and the true heat flow rate
K_Q	Proportionality between the measured and the true exchanged heat
K_w	Glass stability parameter proposed by Weinberg
$M(\xi)$	Relaxation function in terms of the reduced time
N	Crystal number density
N_0	Number of growing crystals,
N'	Number of thermocouples
N_{at}	Number of quenched-in or athermic nuclei
$N_i(x)$	Molar fraction of network-forming species i for composition x
N_{total}	Total number of nuclei
P_0	Period of oscillation
ΔP	Compensating heating power
Q	Scattering vector
Q_{exch}	Exchanged heat
Q_{SAXS}	Small-angle X-ray scattering invariant
Q_{true}	True exchanged heat
R	Gas constant
R_c	Critical cooling rate
R_{CC}	Critical rate for continuous cooling method
R_{CN}	Critical rate for "nose" method
R_{th}	Thermal resistance of the sensor
S	Sensitivity of a thermocouple
S_{conf}	Configurational entropy
S_{ex}	Excess entropy
S_{DT}	Device transfer
$S(Q)$	Structural factor as a function of scattering vector
T	Temperature
ΔT	Differential temperature signal
T_0	Starting temperature
T_a	Annealing temperature
T_A	Collapsing temperature of zeolite
T_c	Peak temperature of crystallization
T_d	Starting temperature of the departure of C_p curve from C_{pg} curve
T_{eq}	Starting temperature of equilibrium liquid
T_f	Fictive temperature
$T_{f,c}$	Critical fictive temperature
$T_{f,s}$	Characteristic temperature of the fragile-to-strong transition
T_g	Glass transition temperature
$T_{g,DSC}$	Glass transition temperature measured by DSC
$T_{g,infl}$	Temperature at the inflection point of the C_p drop curve during liquid−glass transition
$T_{g,end}$	Ending temperature of glass−liquid transition
$T_{g,onset}$	Onset temperature of the glass transition
$T_{g,ref}$	Glass transition temperature at reference cooling rate (0.1 K/s)
$T_{g,vis}$	T_g determined by viscosity
T_K	The Kauzmann temperature
T_L	*Liquidus* temperature
T_m	Melting point
T_N	Temperature for the first isothermal treatment (Figure 53)
T_n	"Nose" temperature
T_{onset}	Onset temperature of glass transition
T_G	Temperature for the second stage isothermal treatment (Figure 53)
T_R	Temperature to the reference crucible
$T_{rg}T_g/T_m$	Reduced glass transition temperature T_g/T_m
T_S	Temperature to the sample crucible
T_{sh}	Temperature of sub-T_g relaxation peak shoulder
T_x	Onset temperature of crystallization peak
T_z	Onset temperature of the energy release of a HQ glass
T_ω	Peak temperature at the average relaxation time of $2\pi P$
T^*	A temperature above the glass transition region
U	Crystal growth rate
U_{min}	Minimum crystal growth rate
U_{max}	Maximum crystal growth rate
V	Sensor signal in voltage
V_0	Volume of the sample before transformation
V_c	Volume of crystal
V_g	Volume of residual glass
Z	Constant in eq 73
$Z(\omega)$	Approximate representation of the vibrational density of states
g	Shape factor
k	Proportionality constant in eq 56
$k(T)$	Rate constant at T
$f(t,T)$	Kinetic part of the heat flow related to part of nonreversing
m	Liquid fragility index of glass-forming liquids
m_0	Liquid fragility index of a perfectly strong glass-forming liquid
m_{DSC}	Liquid fragility index determined by DSC
m_{vis}	Liquid fragility index determined by viscosity
m_S	Sample mass
$n(T, x)$	Average number of constraints per atom at T and x
n	Avrami coefficient
Δn	Optical birefringence of annealed fibers
Δn_{max}	Optical birefringence of not-annealed fibers
p	Isostatic pressure
q	DSC scan rate
$q_{c,s}$	Standard downscan rate, typically 10 K/min
q_h	Heating rate or DSC upscan rate
q_c	Cooling rate or DSC downscan rate
q_α	Rigidity of α-constraint
q_r	Molar ratio: $B_2O_3/(B_2O_3 + SiO_2)$
q_{ref}	Reference cooling rate (0.1 K/s)
r	E_α/E_β
$\langle r \rangle$	Mean coordination number
r_{unit}	Structural unit size
t	Time
t_a	Annealing time
t_{ext}	External time
t_G	first stage isothermal treatment time
t_{ind}	Induction time for nucleation
t_{int}	Internal time
t_N	first stage isothermal treatment time
t_n	Nose time on the TTT curve
t_{obs}	External observation time
ν	Poisson's ratio
ν_0	Pre-exponential term in eq 70
$w_{i,\alpha}$	Number of α-type constraints associated with species i
x	Composition variable
x_R	Reference composition
x_{zeo}	Volume fraction of zeolite
α type	Constraint type
α	Volume fraction of crystals
$\alpha(t)$	Volume fraction of crystals as a function of t

DOI: 10.1021/acs.chemrev.8b00510
Chem. Rev. XXXX, XXX, XXX−XXX

$\acute{a}'(t)$	Transformed volume of residual glass as a function of t
α_{Expan}	Linear thermal expansion coefficient
α_D	Debye parameter in eqs 43 and 44
α_s	Seebeck coefficient
β	Stretching exponent
β_c	Fitting parameter of composite relaxation funaction (CRF)
γ	R_1/R_2 for ellipsoids of revolution or spheroids, where R_1 is the radius of their central circular plane perpendicular to the axis of revolution and R_2 is their radius parallel to the same axis
γ_D	Debye parameter in eqs 43 and 44
τ	Relaxation time
τ_α	α relaxation time
τ_β	β relaxation time
τ_{ext}	External time scale
τ_{int}	Internal time scale
τ_{JG}	Characteristic JG relaxation time
τ_{system}	Internal relaxation time of a glass-forming system
ξ	Reduced relaxation time
ϕ	The phase angle between the input and output functions
ω	Angular frequency of the sinusoidal oscillation
ω_c	Fitting parameter in eq 77
Φ	DSC output, i.e., heat flow
Φ_0	Background line of DSC output curve
Φ_a	Amplitude of modulated heat flow
Φ_u	Total underlying heat flow
Φ_{bl}	Baseline heat flow signal
Φ_m	Modulated heat flow rate
Φ_R	Heat flow to the reference crucible
Φ_S	Heat flow to the sample crucible
Φ_{true}	True heat flow rate
$\Delta\Phi$	Difference between Φ and Φ_0
η	Viscosity
η_∞	Viscosity at high temperature limit
Ω	Side length to the height of right square prisms
AFM	Atomic Force Microscopy
AG	Adam−Gibbs
AGS	Adam−Gibbs−Scherer
ASTM	American Society for Testing and Materials
BMGs	Bulk metallic glasses
BP	Boson peak
CCT	Continuous cooling transformation
CRF	Composite relaxation function
CRRs	Cooperatively rearranging regions
DMA	Dynamic-mechanical analysis
DMS	Dynamical mechanical spectroscopy
DSC	Differential scanning calorimetry
EXAFS	X-ray absorption fine structure
FEM	Finite element simulation
F-S	Fragile-to-strong
FSC	Fast scanning calorimeter
fwhm	Full width at half-maximum
GCs	Glass-ceramics
GFA	Glass-forming ability
GIC	Glass ionomer cement
GS	Glass stability
HAD	Hyperquenching-annealing-DSC
HC	Hyperquenching-calorimetry
HDA	High-density amorphous
HDL	High-density liquid
HDPE	High-density polyethylene
HN	Havriliak−Negami
HQ_	Hyperquenched
HQG	Hyperquenched glass
ICTAC	International Confederation for Thermal Analysis and Calorimetry
IRO	Intermedium range order
JG	Johari−Goldstein
JMAYK	Johnson−Mehl−Avrami−Yerofeeyev−Kolmogorov
KWW	Kohlrausch−Williams−Watts
LDA	Low-density amorphous
LDL	Low-density liquid
HDPE	High-density polyethylene
LRO	Long-range order
LS2	Lithium disilicate glass
MG	Metallic glass
MAP	Mauro−Allan−Potuzak
MD	Molecular dynamics
MEMS	Micro-Electro-Mechanical Systems
MGFLs	Metallic glass-forming liquids
MGs	Metallic glasses
MOF	Metal−organic Frameworks
MQ_	Melt-quenched
MYEGA	Mauro−Yue−Ellison−Gupta−Allan
NMR	Nuclear magnetic resonance
OM	Optical microscopy
PEL	Potential energy landscape
PETg	Poly(ethylene terephthalate)-glycol
PDLA	Poly(D-lactic acid)
PDLLA	Poly(DL-lactide)
PLLA	Poly(L-lactide)
PTR	Photothermo-refractive
RS	Raman spectroscopy
RS-DSC	Repetitive scanning DSC
RT	Room temperature
SANS	Small-angle neutron scattering
SAXS	Small angle X-ray scattering
SCL	Supercooled liquid
SEE	Stokes−Einstein equation
SEM	Scanning electron microscopy
SRO	Short-range order
STG	Standard glass
TEM	Transmission electron microscopy
TMDSC	Temperature-modulated DSC
TNB	1,3-bis-(1-naphthyl)-5-(2-naphthyl)benzene
TNM	Tool−Narayanaswamy−Moynihan
TTT	Temperature−time transformation
VDOS	Vibrational density of states
WLF	Williams−Landel−Ferry
XAS	X-ray absorption spectroscopy
XPS	X-ray photoelectron spectroscopies
XRD	X-ray diffraction
ZIFs	Zeolitic imidazolate frameworks

REFERENCES

(1) Angell, C. A. Formation of Glasses from Liquids and Biopolymers. *Science* **1995**, *267*, 1924−1935.
(2) Greaves, G. N.; Sen, S. Inorganic Glasses, Glass-forming Liquids and Amorphizing Solids. *Adv. Phys.* **2007**, *56*, 1−166.
(3) Debenedetti, P. G.; Stillinger, F. H. Supercooled Liquids and the Glass Transition. *Nature* **2001**, *410*, 259−267.

DOI: 10.1021/acs.chemrev.8b00510
Chem. Rev. XXXX, XXX, XXX−XXX

(4) Bennett, T. D.; Tan, J. C.; Yue, Y. Z.; Baxter, E.; Ducati, C.; Terrill, N. J.; Yeung, H. H. M.; Zhou, Z.; Chen, W.; Henke, S.; et al. Hybrid Glasses from Strong and Fragile Metal-Organic Framework Liquids. *Nat. Commun.* **2015**, *6*, 8079.
(5) Richet, P.; Bottinga, Y. Thermochemical Properties of Silicate Glasses and Liquids: A Review. *Rev. Geophys.* **1986**, *24*, 1−25.
(6) Moynihan, C. T. Structural Relaxation and the Glass Transition. *Rev. Mineral.* **1995**, *32*, 1−19.
(7) Málek, J. Kinetic Analysis of Crystallization Processes in Amorphous Materials. *Thermochim. Acta* **2000**, *355*, 239−253.
(8) Šesták, J., Šimon, P., Eds. *Thermal Analysis of Micro, Nano- and Non-Crystalline Materials: Transformation, Crystallization, Kinetics and Thermodynamics*; Springer: Netherlands, 2013.
(9) Orava, J.; Greer, A. L. *Handbook of Thermal Analysis and Calorimetry*; Elsevier: Netherlands, 2018.
(10) Zheng, Q. J.; Potuzak, M.; Mauro, J. C.; Smedskjaer, M. M.; Youngman, R. E.; Yue, Y. Z. Composition-Structure-Property Relationships in Boroaluminosilicate Glasses. *J. Non-Cryst. Solids* **2012**, *358*, 993−1002.
(11) Liu, H.; Smedskjaer, M. M.; Tao, H. Z.; Jensen, L. R.; Zhao, X. J.; Yue, Y. Z. A Medium Range Order Structural Connection to the Configurational Heat Capacity of Borate-silicate Mixed Glasses. *Phys. Chem. Chem. Phys.* **2016**, *18*, 10887−10895.
(12) Wales, D. J. *Energy Landscapes: With Applications to Clusters, Biomolecules and Glasses*; Cambridge Molecular Science; Cambridge University Press: Cambridge, U.K., 2002.
(13) Swallen, S. F.; Kearns, K. L.; Mapes, M. K.; Kim, Y. S.; McMahon, R. J.; Ediger, M. D.; Wu, T.; Yu, L.; Satija, S. Organic Glasses with Exceptional Thermodynamic and Kinetic Stability. *Science* **2007**, *315*, 353−356.
(14) Yue, Y. Z.; Angell, C. A. Clarifying the Glass-transition Behaviour of Water by Comparison with Hyperquenched Inorganic Glasses. *Nature* **2004**, *427*, 717−720.
(15) Angell, C. A.; Yue, Y. Z.; Wang, L. M.; Copley, J. R. D.; Borick, S.; Moss, S. Potential Energy, Relaxation, Vibrational Dynamics and the Boson Peak of Hyperquenched Glasses. *J. Phys.: Condens. Matter* **2003**, *15*, S1051−S1068.
(16) Greaves, G. N.; Meneau, F.; Majerus, O.; Jones, D. G.; Taylor, J. Identifying Vibrations that Destabilize Crystals and Characterize the Glassy State. *Science* **2005**, *308*, 1299−1302.
(17) Monaco, A.; Chumakov, A. I.; Yue, Y. Z.; Monaco, G.; Comez, L.; Fioretto, D.; Crichton, W. A.; Rüffer, R. Density of Vibrational States of a Hyperquenched Glass. *Phys. Rev. Lett.* **2006**, *96*, 205502.
(18) Johari, G. P.; Goldstein, M. Viscous Liquids and the Glass Transition II. Secondary Relaxations in Glasses of Rigid Molecules. *J. Chem. Phys.* **1970**, *53*, 2372−2388.
(19) Johari, G. P.; Goldstein, M. Viscous Liquids and the Glass Transition III. Secondary Relaxations in Aliphatic Alcohols and Other Nonrigid Molecules. *J. Chem. Phys.* **1971**, *55*, 4245−4252.
(20) Zhang, C. Z.; Hu, L. N.; Yue, Y. Z.; Mauro, J. C. Fragile-to-Strong Transition in Metallic Glass-Forming Liquids. *J. Chem. Phys.* **2010**, *133*, 014508.
(21) Mauro, J. C.; Zanotto, E. D. Two Centuries of Glass Research: Historical Trends, Current Status, and Grand Challenges for the Future. *Int. J. Appl. Glass Sci.* **2014**, *5*, 313−327.
(22) Montazerian, M.; Singh, S. P.; Zanotto, E. D. An Analysis of Glass-Ceramic Research and Commercialization. *Am. Ceram. Soc. Bull.* **2015**, *94*, 30−35.
(23) Davis, M. J.; Zanotto, E. D. Glass-Ceramics and Realization of the Unobtainable: Property Combinations that Push the Envelope. *MRS Bull.* **2017**, *42*, 195−199.
(24) Hill, J. O. *For Better Thermal Analysis and Calorimetry*, 3rd ed.; International Confederation for Thermal Analysis and Calorimetry, 1991.
(25) Pignatello, R. *Drug-Biomembrane Interaction Studies*; Woodhead Publishing Limited: Cambridge, 2013.
(26) Höhne, G. W. H.; Hemminger, W. F.; Flammersheim, H. J. *Differential Scanning Calorimetry*, 2nd ed.; Springer: Berlin, 2003.
(27) Mackenzie, R. C. A. History of Thermal Analysis. *Thermochim. Acta* **1984**, *73*, 251−306.
(28) Spink, C. H. Differential Scanning Calorimetry. *Methods Cell Biol.* **2008**, *84*, 115−41.
(29) Haines, P. J. *Principles of Thermal Analysis and Calorimetry*; Royal Society of Chemistry: Cambridge, 2002.
(30) Boersma, S. L. Theory of DTA and New Methods of Measurement and Interpretation. *J. Am. Ceram. Soc.* **1955**, *38*, 281−284.
(31) Mathot, V. B. F.; Benoist, L. *Calorimetry and Thermal Analysis of Polymers*; Hanser/Gardner Publications: Munich, 1994.
(32) *ASTM E 968-99: Standard Practice for Heat Flow Calibration of Differential Scanning Calorimeters*, 1999.
(33) *ASTM E 793-01: Standard Test Method for Enthalpies of Fusion and Crystallization by Differential Scanning Calorimeters*, 2001.
(34) Tanaka, S. Theory of Power-compensated DSC. *Thermochim. Acta* **1992**, *210*, 67−76.
(35) Watson, E. S.; O'Neill, M. J.; Justin, J.; Brenner, N. A DSC for Quantitative Differential Thermal Analysis. *Anal. Chem.* **1964**, *36*, 1233−1238.
(36) Höhne, G. W. H.; Glöggler, E. Some Peculiarities of the DSC-2/-7 (Perkin-Elmer) and Their Influence on Accuracy and Precision of the Measurements. *Thermochim. Acta* **1989**, *151*, 295−304.
(37) Pijpers, M. F. J.; Mathot, V. B. F.; Goderis, B.; Scherrenberg, R. L.; van der Vegte, E. W. High-Speed Calorimetry for the Study of the Kinetics of (De)vitrification, Crystallization, and Melting of Macromolecules. *Macromolecules* **2002**, *35*, 3601−3613.
(38) Efremov, M. Y.; Warren, J. T.; Olson, E. A.; Zhang, M.; Kwan, A. T.; Allen, L. H. Thin-Film Differential Scanning Calorimetry: A New Probe for Assignment of the Glass Transition of Ultrathin Polymer Films. *Macromolecules* **2002**, *35*, 1481−1483.
(39) Minakov, A. A.; Adamovsky, S. A.; Schick, C. Non-adiabatic Thin-film (chip) Nanocalorimetry. *Thermochim. Acta* **2005**, *432*, 177−185.
(40) Mileva, D.; Androsch, R.; Zhuravlev, E.; Schick, C. Critical Rate of Cooling for Suppression of Crystallization in Random Copolymers of Propylene with Ethylene and 1-butene. *Thermochim. Acta* **2009**, *492*, 67−72.
(41) Tol, R. T.; Minakov, A. A.; Adamovsky, S. A.; Mathot, V. B. F.; Schick, C. Metastability of Polymer Crystallites Formed at Low Temperature Studied by Ultra Fast Calorimetry: Polyamide 6 Confined in Sub-micrometer Droplets vs. Bulk PA6. *Polymer* **2006**, *47*, 2172−2178.
(42) Schick, C. Differential Scanning Calorimetry (DSC) of Semicrystalline Polymers. *Anal. Bioanal. Chem.* **2009**, *395*, 1589−1611.
(43) Mathot, V.; Pyda, M.; Pijpers, T.; Vanden Poel, G.; van de Kerkhof, E.; van Herwaarden, S.; van Herwaarden, F.; Leenaers, A. The Flash DSC 1, A Power Compensation Twin-type, Chip-based Fast Scanning Calorimeter (FSC): First Findings on Polymers. *Thermochim. Acta* **2011**, *522*, 36−45.
(44) van Herwaarden, S.; Iervolino, E.; van Herwaarden, F.; Wijffels, T.; Leenaers, A.; Mathot, V. Design, Performance and Analysis of Thermal Lag of the UFS1 Twin-calorimeter Chip for Fast Scanning Calorimetry Using the Mettler-Toledo Flash DSC 1. *Thermochim. Acta* **2011**, *522*, 46−52.
(45) Iervolino, E.; van Herwaarden, A. W.; van Herwaarden, F. G.; van de Kerkhof, E.; van Grinsven, P. P. W.; Leenaers, A. C. H. I.; Mathot, V. B. F.; Sarro, P. M. Temperature Calibration and Electrical Characterization of the Differential Scanning Calorimeter Chip UFS1 for the Mettler-Toledo Flash DSC 1. *Thermochim. Acta* **2011**, *522*, 53−59.
(46) Greaves, G. N.; Fontaine, A.; Lagarde, P.; Raoux, D.; Gurman, S. J. Local Structure of Silicate Glasses. *Nature* **1981**, *293*, 611−616.
(47) Poel, G. V.; Mathot, V. B. F. High Performance Differential Scanning Calorimetry (HPer DSC): A Powerful Analytical Tool for the Study of the Metastability of Polymers. *Thermochim. Acta* **2007**, *461*, 107−121.

DOI: 10.1021/acs.chemrev.8b00510
Chem. Rev. XXXX, XXX, XXX−XXX

(48) van Herwaarden, A. W. Overview of Calorimeter Chips for Various Applications. *Thermochim. Acta* **2005**, *432*, 192−201.
(49) Vanden Poel, G.; Mathot, V. B. F. High-speed/high Performance Differential Scanning Calorimetry (HPer DSC): Temperature Calibration in the Heating and Cooling Mode and Minimization of Thermal Lag. *Thermochim. Acta* **2006**, *446*, 41−54.
(50) Neuenfeld, S.; Schick, C. Verifying the Symmetry of Differential Scanning Calorimeters Concerning Heating and Cooling Using Liquid Crystal Secondary Temperature Standard. *Thermochim. Acta* **2006**, *446*, 55−65.
(51) Zhuravlev, E.; Schick, C. Fast Scanning Power Compensated Differential Scanning Nano-calorimeter: 1. The Device. *Thermochim. Acta* **2010**, *505*, 1−13.
(52) van de Kerkhof, E.; van Grinsven, P. P. W. U.S. Patent 14,466,068, 2009.
(53) *DIN Specification 91127: Recommendation for Temperature Calibration of Fast Scanning Calorimeters (FSCs) for Sample Mass and Scan Rate*, 2011.
(54) Gill, P. S.; Sauerbrunn, S. R.; Reading, M. Modulated Differential Scanning Calorimetry. *J. Therm. Anal.* **1993**, *40*, 931−939.
(55) Gulbiten, O. *An Investigation of Dynamic Processes in Selenium Based Chalcogenide Glasses*. Ph.D. Thesis, University of Arizona: Tucson, 2014.
(56) Gobrecht, H.; Hamann, K.; Willers, G. Complex Plane Analysis of Heat Capacity of Polymers in Glass Transition Region. *J. Phys. E: Sci. Instrum.* **1971**, *4*, 21−23.
(57) Birge, N. O.; Nagel, S. R. Specific-Heat Spectroscopy of the Glass-Transition. *Phys. Rev. Lett.* **1985**, *54*, 2674−2677.
(58) Palmer, R. G. Broken Ergodicity. *Adv. Phys.* **1982**, *31*, 669−735.
(59) Mauro, J. C.; Loucks, R. J.; Sen, S. Heat Capacity, Enthalpy Fluctuations, and Configurational Entropy in Broken Ergodic Systems. *J. Chem. Phys.* **2010**, *133* (16), 164503.
(60) Reiner, M. The Deborah Number. *Phys. Today* **1964**, *17*, 62−62.
(61) Reading, M.; Luget, A.; Wilson, R. Modulated Differential Scanning Calorimetry. *Thermochim. Acta* **1994**, *238*, 295−307.
(62) Gulbiten, O.; Mauro, J. C.; Lucas, P. Relaxation of Enthalpy Fluctuations during Sub-T_g Annealing of Glassy Selenium. *J. Chem. Phys.* **2013**, *138*, 244504.
(63) Yang, G.; Gulbiten, O.; Gueguen, Y.; Bureau, B.; Sangleboeuf, J. C.; Roiland, C.; King, E. A.; Lucas, P. Fragile-strong Behavior in the As_xSe_{1-x} Glass Forming System in Relation to Structural Ddimensionality. *Phys. Rev. B: Condens. Matter Mater. Phys.* **2012**, *85*, 144107.
(64) Schawe, J. E. K.; Hutter, T.; Heitz, C.; Alig, I.; Lellinger, D. Stochastic Temperature Modulation: A New Technique in Temperature-modulated DSC. *Thermochim. Acta* **2006**, *446*, 147−155.
(65) Zanotto, E. D.; Mauro, J. C. The Glassy State of Matter: Its Definition and Ultimate Fate. *J. Non-Cryst. Solids* **2017**, *471*, 490−495.
(66) Shelby, J. E. *Introduction to Glass Science and Technology*; The Royal Society of Chemistry: Cambridge, 2005.
(67) Varshneya, A. K.; Mauro, J. C. *Fundamentals of Inorganic Glasses*, 3rd ed.; Elsevier: Amsterdam, Netherlands, 2019.
(68) Varshneya, A. K.; Mauro, J. C. Comment on Misconceived ASTM Definition of "Glass" by A. C. Wright. *Glass Technol.: Eur. J. Glass Sci. Technol. A* **2010**, *51*, 28−30.
(69) Anderson, P. W. Through the Glass Lightly. *Science* **1995**, *267*, 1615−1616.
(70) Moynihan, C. T.; Macedo, P. B.; Montrose, C. J.; Gupta, P. K.; DeBolt, M. A.; Dill, J. F.; Dom, B. E.; Drake, P. W.; Easteal, A. J.; Elterman, P. B.; et al. Stuctural Relaxation in Vitreous Materials. *Ann. N. Y. Acad. Sci.* **1976**, *279*, 15−35.
(71) Mauro, J. C.; Gupta, P. K.; Loucks, R. J. Continuously Broken Ergodicity. *J. Chem. Phys.* **2007**, *126*, 184511.
(72) Bantilan, F. T., Jr.; Palmer, R. G. Magnetic Properties of a Model Spin Glass and the Failure of Linear Response Theory. *J. Phys. F: Met. Phys.* **1981**, *11*, 261.
(73) Monthus, C.; Bouchaud, J.-P. Models of Traps and Glass Phenomenology. *J. Phys. A: Math. Gen.* **1996**, *29*, 3847−3869.
(74) Bel, G.; Barkai, E. Weak Ergodicity Breaking in the Continuous-Time Random Walk. *Phys. Rev. Lett.* **2005**, *94*, 240602.
(75) Mauro, J. C.; Loucks, R. J.; Varshneya, A. K.; Gupta, P. K. Enthalpy Landscapes and the Glass Transition. *Sci. Model. Simul.* **2008**, *15*, 241−281.
(76) Alba, C.; Busse, L. E.; Angell, C. A. Thermodynamic Aspects of the Vitrification of Toluene, and Xylene Isomers, and the Fragility of Liquid Hydrocarbons. *J. Chem. Phys.* **1990**, *92*, 617−624.
(77) Angell, C. A. Relaxation in Liquids, Polymers and Plastic Crystals - Strong/fragile Patterns and Problems. *J. Non-Cryst. Solids* **1991**, *131*−*133*, 13−31.
(78) Böhmer, R.; Ngai, K. L.; Angell, C. A.; Plazek, D. J. Nonexponential Relaxations in Strong and Fragile Glass Formers. *J. Chem. Phys.* **1993**, *99*, 4201−4209.
(79) Stickel, F.; Fischer, E. W.; Richert, R. Dynamics of Glass-forming Liquids. I. Temperature-Derivative Analysis of Dielectric Relaxation Data. *J. Chem. Phys.* **1995**, *102*, 6251−6257.
(80) Stickel, F.; Fischer, E. W.; Richert, R. Dynamics of Glass-forming Liquids. II. Detailed Comparison of Dielectric Relaxation, Dc-conductivity, and Viscosity Data. *J. Chem. Phys.* **1996**, *104*, 2043−2055.
(81) Yue, Y. Z. Characteristic Temperatures of Enthalpy Relaxation in Glass. *J. Non-Cryst. Solids* **2008**, *354*, 1112−1118.
(82) Moynihan, C. T.; Easteal, A. J.; DeBolt, M. A.; Tucker, J. Dependence of the Fictive Temperature of Glass on Cooling Rate. *J. Am. Ceram. Soc.* **1976**, *59*, 12−16.
(83) Angell, C. A. Liquid Fragility and the Glass Transition in Water and Aqueous Solutions. *Chem. Rev.* **2002**, *102*, 2627−2650.
(84) Hallbrucker, A.; Mayer, E.; Johari, G. P. Glass-liquid Transition and the Enthalpy of Devitrification of Annealed Vapor-deposited Amorphous Solid Water. A Comparison with Hyperquenched Glassy Water. *J. Phys. Chem.* **1989**, *93*, 4986−4990.
(85) Angell, C. A. Water II is A "Strong" Liquid. *J. Phys. Chem.* **1993**, *97*, 6339−6341.
(86) Chen, H. S.; Coleman, E. Structural Relaxation in Metallic Glasses. *Appl. Phys. Lett.* **1976**, *28*, 245−247.
(87) Barrat, J. L.; Badro, J.; Gillet, P. A. Strong to Fragile Transition in a Model of Liquid Silica. *Mol. Simul.* **1997**, *20*, 17−25.
(88) Hemmati, M.; Moynihan, C. T.; Angell, C. A. Interpretation of the Molten BeF_2 Viscosity Anomaly in terms of a High Temperature Density Maximum, and Other Waterlike Features. *J. Chem. Phys.* **2001**, *115*, 6663−6671.
(89) Way, C.; Wadhwa, P.; Busch, R. The Influence of Shear Rate and Temperature on the Viscosity and Fragility of the $Zr_{41.2}Ti_{13.8}Cu_{12.5}Ni_{10.0}Be_{22.5}$ Metallic-Glass-Forming Liquid. *Acta Mater.* **2007**, *55*, 2977−2983.
(90) Maxwell, J. C. On the Dynamical Theory of Gases. *Phil. Trans. Roy. Soc. Lon.* **1867**, *157*, 49−88.
(91) Zheng, Q. J.; Mauro, J. C.; Yue, Y. Z. Reconciling Calorimetric and Kinetic Fragilities of Glass-forming Liquids. *J. Non-Cryst. Solids* **2017**, *456*, 95−100.
(92) Adam, G.; Gibbs, J. H. On the Temperature Dependence of Cooperative Relaxation Properties in Glass-forming Liquids. *J. Chem. Phys.* **1965**, *43*, 139−146.
(93) Goldstein, M. Some Thermodynamic Aspects of the Glass Transition: Free Volume, Entropy, and Enthalpy Theories. *J. Chem. Phys.* **1963**, *39*, 3369−3374.
(94) Stillinger, F. H.; Weber, T. A. Hidden Structure in Liquids. *Phys. Rev. A: At., Mol., Opt. Phys.* **1982**, *25*, 978−989.
(95) Götze, W. The Essentials of the Mode-coupling Theory for Glassy Dynamics. *Condens. Matter Phys.* **1998**, *1*, 873−904.
(96) Tarjus, G.; Kivelson, S. A.; Nussinov, Z.; Viot, P. The Frustration-based Approach of Supercooled Liquids and the Glass Transition: A Review and Critical Assessment. *J. Phys.: Condens. Matter* **2005**, *17*, R1143.
(97) Dyre, J. C.; Olsen, N. B.; Christensen, T. Local Elastic Expansion Model for Viscous-flow Activation Energies of Glass-forming Molecular Liquids. *Phys. Rev. B: Condens. Matter Mater. Phys.* **1996**, *53*, 2171−2174.

DOI: 10.1021/acs.chemrev.8b00510
Chem. Rev. XXXX, XXX, XXX−XXX

(98) Jaccani, S. P.; Gulbiten, O.; Allan, D. C.; Mauro, J. C.; Huang, L. P. Modified Elastic Model for Viscosity in Glass-forming Systems. *Phys. Rev. B: Condens. Matter Mater. Phys.* **2017**, *96*, 224201.
(99) Mauro, J. C.; Yue, Y. Z.; Ellison, A. J.; Gupta, P. K.; Allan, D. C. Viscosity of Glass-forming Liquids. *Proc. Natl. Acad. Sci. U. S. A.* **2009**, *106*, 19780−19784.
(100) Guo, X. J.; Potuzak, M.; Mauro, J. C.; Allan, D. C.; Kiczenski, T. J.; Yue, Y. Z. Unified Approach for Determining the Enthalpic Fictive Temperature of Glasses with Arbitrary Thermal History. *J. Non-Cryst. Solids* **2011**, *357*, 3230−3236.
(101) Ito, K.; Moynihan, C. T.; Angell, C. A. Thermodynamic Determination of Fragility in Liquids and a Fragile-to-strong Liquid Transition in Water. *Nature* **1999**, *398*, 492−295.
(102) Hodge, I. M. Enthalpy Recovery in Amorphous Materials. *J. Non-Cryst. Solids* **1994**, *169*, 211−266.
(103) Hodge, I. M.; Berens, A. R. Effects of Annealing and Prior History on Enthalpy Relaxation in Glassy Polymers. 2. Mathematical Modelling. *Macromolecules* **1982**, *15*, 762−770.
(104) Boehm, L.; Ingram, M. D.; Angell, C. A. Test of a Year-annealed Glass for the Cohen-grest Percolation Transition. *J. Non-Cryst. Solids* **1981**, *44*, 305−313.
(105) Yue, Y. Z. The Iso-structural Viscosity, Configurational Entropy and Fragility of Oxide Liquids. *J. Non-Cryst. Solids* **2009**, *355*, 737−744.
(106) Martinez, L. M.; Angell, C. A. A Thermodynamic Connection to the Fragility of Glass-forming Liquids. *Nature* **2001**, *410*, 663−667.
(107) Mauro, N. A.; Blodgett, M.; Johnson, M. L.; Vogt, A. J.; Kelton, K. F. A Structural Signature of Liquid Fragility. *Nat. Commun.* **2014**, *5*, 4616.
(108) Smedskjaer, M. M.; Mauro, J. C.; Youngman, R. E.; Hogue, C. L.; Potuzak, M.; Yue, Y. Z. Topological Principles of Borosilicate Glass Chemistry. *J. Phys. Chem. B* **2011**, *115*, 12930−12946.
(109) Mauro, J. C.; Loucks, R. J.; Gupta, P. K. Metabasin Approach for Computing the Master Equation Dynamics of Systems with Broken Ergodicity. *J. Phys. Chem. A* **2007**, *111*, 7957−7965.
(110) Gupta, P. K.; Mauro, J. C. The Laboratory Glass Transition. *J. Chem. Phys.* **2007**, *126*, 224504.
(111) Hubert, M.; Faber, A. J. On the Structural Role of Boron in Borosilicate Glasses. *Phys. Chem. Glasses: Eur. J. Glass Sci. Technol., Part B* **2014**, *55*, 136−158.
(112) Johari, G. P. Examining the Entropy Theory's Application to Viscosity Data and the Inference for a Thermodynamic Transition in an Equilibrium Liquid. *J. Non-Cryst. Solids* **2001**, *288*, 148−158.
(113) Johari, G. P. Decrease in the Configurational and Vibrational Entropies on Supercooling a Liquid and Their Relations with the Excess Entropy. *J. Non-Cryst. Solids* **2002**, *307−310*, 387−392.
(114) Bruning, R.; Levelut, C.; Faivre, A.; Leparc, R.; Simon, J.; Bley, F.; Hazemann, J. Characterization of the Glass Transition in Vitreous Silica by Temperature Scanning Small-angle X-ray Scattering. *Europhys. Lett.* **2005**, *70*, 211−217.
(115) Sen, S. Temperature Induced Structural Changes and Transport Mechanisms in Borate, Borosilicate and Boroaluminate Liquids: High-resolution and High-temperature NMR Results. *J. Non-Cryst. Solids* **1999**, *253*, 84−94.
(116) Majerus, O.; Cormier, L.; Calas, G.; Beuneu, B. Temperature-induced Boron Coordination Change in Alkali Borate Glasses and Melts. *Phys. Rev. B: Condens. Matter Mater. Phys.* **2003**, *67*, 024210.
(117) Stebbins, J. F.; Ellsworth, S. E. Temperature Effects on Structure and Dynamics in Borate and Borosilicate Liquids: High-resolution and High-temperature NMR Results. *J. Am. Ceram. Soc.* **1996**, *79*, 2247−2256.
(118) Angeli, F.; Villain, O.; Schuller, S.; Charpentier, T.; De Ligny, D.; Bressel, L.; Wondraczek, L. Effect of Temperature and Thermal History on Borosilicate Glass Structure. *Phys. Rev. B: Condens. Matter Mater. Phys.* **2012**, *85*, 054110.
(119) Wu, J.; Stebbins, J. F. Quench Rate and Temperature Effects on Boron Coordination in Aluminoborosilicate Melts. *J. Non-Cryst. Solids* **2010**, *356*, 2097−2108.
(120) Smedskjaer, M. M.; Mauro, J. C.; Sen, S.; Yue, Y. Z. Quantitative Design of Glassy Materials Using Temperature-dependent Constraint Theory. *Chem. Mater.* **2010**, *22*, 5358−5365.
(121) Zheng, Q. J.; Mauro, J. C.; Smedskjaer, M. M.; Youngman, R. E.; Potuzak, M.; Yue, Y. Z. Glass-Forming Ability of Soda Lime Borate Liquids. *J. Non-Cryst. Solids* **2012**, *358*, 658−665.
(122) Kjeldsen, J.; Smedskjaer, M. M.; Youngmann, R.; Mauro, J. C.; Yue, Y. Z. Mixed Alkaline Earth Effect in Sodium Aluminosilicate Glasses. *J. Non-Cryst. Solids* **2013**, *369C*, 61−68.
(123) Kjeldsen, J.; Rodrigues, A. C. M.; Mossin, S.; Yue, Y. Z. Critical V_2O_5/TeO_2 Ratio Inducing Abrupt Property Changes in Vanadium Tellurite Glasses. *J. Phys. Chem. B* **2014**, *118*, 14942−14948.
(124) Paraschiv, G. L.; Muñoz, F.; Jensen, L. R.; Yue, Y. Z.; Smedskjaer, M. M. Impact of Nitridation of Metaphosphate Glasses on Liquid Fragility. *J. Non-Cryst. Solids* **2016**, *441*, 22−28.
(125) Bechgaard, T. K.; Mauro, J. C.; Bauchy, M.; Yue, Y. Z.; Lamberson, L. A.; Jensen, L. R.; Smedskjaer, M. M. Fragility and Configurational Heat Capacity of Calcium Aluminosilicate Glass-forming Liquids. *J. Non-Cryst. Solids* **2017**, *461*, 24−34.
(126) Kushima, A.; Lin, X.; Li, J.; Qian, X. F.; Eapen, J.; Mauro, J. C.; Diep, P.; Yip, S. Computing the Viscosity of Supercooled Liquids. II. Silica and Strong-fragile Crossover Behavior. *J. Chem. Phys.* **2009**, *131*, 164505.
(127) Li, J.; Kushima, A.; Eapen, J.; Lin, X.; Qian, X.; Mauro, J. C.; Diep, P.; Yip, S. Computing the Viscosity of Supercooled Liquids: Markov Network Model. *PLoS One* **2011**, *6*, 17909.
(128) Gupta, P. K.; Mauro, J. C. Composition Dependence of Glass Transition Temperature and Fragility. I. A Topological Model Incorporating Temperature-dependent Constraints. *J. Chem. Phys.* **2009**, *130*, 094503.
(129) Mauro, J. C.; Gupta, P. K.; Loucks, R. J. Composition Dependence of Glass Transition Temperature and Fragility. II. A Topological Model of Alkali Borate Liquids. *J. Chem. Phys.* **2009**, *130*, 234503.
(130) Mauro, J. C. Topological Constraint Theory of Glass. *Am. Ceram. Soc. Bull.* **2011**, *90*, 31−37.
(131) Bauchy, M.; Micoulaut, M. Atomic Scale Foundation of Temperature-dependent Bonding Constraints in Network Glasses and Liquids. *J. Non-Cryst. Solids* **2011**, *357*, 2530−2537.
(132) Phillips, J. C. Topology of Covalent Non-Crystalline Solids I: Short-Range Order in Chalcogenide Alloys. *J. Non-Cryst. Solids* **1979**, *34*, 153−181.
(133) Phillips, J. C.; Thorpe, M. F. Constraint Theory, Vector Percolation and Glass Formation. *Solid State Commun.* **1985**, *53*, 699−702.
(134) Naumis, G. G. Glass Transition Phenomenology and Flexibility: An Approach using the Energy Landscape Formalism. *J. Non-Cryst. Solids* **2006**, *352*, 4865−4870.
(135) Hermansen, C.; Rodrigues, B. P.; Wondraczek, L.; Yue, Y. Z. An Extended Topological Model for Binary Phosphate Glasses. *J. Chem. Phys.* **2014**, *141*, 244502.
(136) Hermansen, C.; Youngman, R. E.; Wang, J.; Yue, Y. Z. Structural and Topological Aspects of Borophosphate Glasses and Their Relation to Physical Properties. *J. Chem. Phys.* **2015**, *142*, 184503.
(137) Ellison, A.; Cornejo, I. A. Glass Substrates for Liquid Crystal Displays. *Int. J. Appl. Glass Sci.* **2010**, *1*, 87−103.
(138) Jantzen, C. M.; Brown, K. G.; Pickett, J. B. Durable Glass for Thousands of Years. *Int. J. Appl. Glass Sci.* **2010**, *1*, 38−62.
(139) Zielniok, D.; Cramer, C.; Eckert, H. Structure/Property Correlations in Ion-Conducting Mixed-Network Former Glasses: Solid-State NMR Studies of the System $Na_2O−B_2O_3−P_2O_5$. *Chem. Mater.* **2007**, *19*, 3162−3170.
(140) Sen, S.; Youngman, R. E. High-Resolution Multinuclear NMR Structural Study of Binary Aluminosilicate and Other Related Glasses. *J. Phys. Chem. B* **2004**, *108*, 7557−7564.
(141) Martin, S. W. Ionic Conduction in Phosphate Glasses. *J. Am. Ceram. Soc.* **1991**, *74*, 1767−1784.

DOI: 10.1021/acs.chemrev.8b00510
Chem. Rev. XXXX, XXX, XXX−XXX

(142) Schuch, M.; Müller, C. R.; Maass, P.; Martin, S. W. Mixed Barrier Model for the Mixed Glass Former Effect in Ion Conducting Glasses. *Phys. Rev. Lett.* **2009**, *102*, 145902.
(143) Zheng, Q. J.; Youngman, R. E.; Hogue, C. L.; Mauro, J. C.; Potuzak, M.; Smedskjaer, M. M.; Yue, Y. Z. Structure of Boroaluminosilicate Glasses: Impact of $[Al_2O_3]/[SiO_2]$ Ratio on the Structural Role of Sodium. *Phys. Rev. B: Condens. Matter Mater. Phys.* **2012**, *86*, 054203.
(144) Hermansen, C.; Mauro, J. C.; Yue, Y. Z. A Model for Phosphate Glass Topology Considering the Modifying Ion Subnetwork. *J. Chem. Phys.* **2014**, *140*, 154501.
(145) Rodrigues, B. P.; Wondraczek, L. Cationic Constraint Effects in Metaphosphate Glasses. *J. Chem. Phys.* **2014**, *140*, 214501.
(146) Mauro, J. C.; Ellison, A. J.; Allan, D. C.; Smedskjaer, M. M. Topological Model for the Viscosity of Multicomponent Glass-Forming Liquids. *Int. J. Appl. Glass Sci.* **2013**, *4*, 408−413.
(147) Mauro, J. C.; Tandia, A.; Vargheese, K. D.; Mauro, Y.; Smedskjaer, M. M. Accelerating the Design of Functional Glasses through Modeling. *Chem. Mater.* **2016**, *28*, 4267−4277.
(148) Micoulaut, M.; Yue, Y. Z. Material Functionalities from Molecular Rigidity: Maxwell's Modern Legacy. *MRS Bull.* **2017**, *42*, 18−22.
(149) Smedskjaer, M. M.; Hermansen, C.; Youngman, R. E. Topological Engineering of Glasses Using Temperature-dependent Constraints. *MRS Bull.* **2017**, *42*, 29−33.
(150) Mishima, O.; Calvert, L. D.; Whalley, E. An Apparently First-order Transition between Two Amorphous Phases of Ice Induced by Pressure. *Nature* **1985**, *314*, 76−78.
(151) Yue, Y. Z.; Wondraczek, L.; Behrens, H.; Deubener, J. Glass Transition in an Iso-statically Compressed Calcium Metaphosphate Glass. *J. Chem. Phys.* **2007**, *126*, 144902.
(152) Yarger, J. L.; Smith, K. H.; Nieman, R. A.; Diefenbacher, J.; Wolf, G.; Poe, B. T.; Mcmillan, P. F. Al Coordination Changes in High-pressure Aluminosilicate Liquids. *Science* **1995**, *270*, 1964−1967.
(153) Guthrie, M.; Tulk, C. A.; Benmore, C. J.; Xu, J.; Yarger, J. L.; Klug, D. D.; Tse, J. S.; Mao, H. -K.; Hemley, R. J. The Formation and Structure of a Dense Octahedral Glass. *Phys. Rev. Lett.* **2004**, *93*, 115502.
(154) Monaco, A.; Chumakov, A. I.; Monaco, G.; Crichton, W. A.; Meyer, A.; Comez, L.; Fioretto, D.; Korecki, J.; Ruffer, R. Effect of Densification on the Density of Vibrational States of Glasses. *Phys. Rev. Lett.* **2006**, *97*, 135501.
(155) Smedskjaer, M. M.; Youngman, R. E.; Striepe, S.; Potuzak, M.; Bauer, U.; Deubener, J.; Behrens, H.; Mauro, J. C.; Yue, Y. Z. Irreversibility of Pressure Induced Boron Speciation Change in Glass. *Sci. Rep.* **2015**, *4*, 3770.
(156) Wondraczek, L.; Behrens, H.; Yue, Y.; Deubener, J.; Scherer, G. W. Relaxation and Glass Transition in an Isostatically Compressed Diopside Glasses. *J. Am. Ceram. Soc.* **2007**, *90*, 1556−1561.
(157) Wolf, G.; McMillan, P. F. Pressure Effects on Silicate Melt − Structure and Properties. *Rev. Mineral.* **1995**, *32*, 505−561.
(158) Ketov, S. V.; Sun, Y. H.; Nachum, S.; Lu, Z.; Checchi, A.; Beraldin, A. R.; Bai, H. Y.; Wang, W. H.; Louzguineluzgin, D. V.; Carpenter, M. A.; Greer, A. L. Rejuvenation of Metallic Glasses by Non-affine Thermal Strain. *Nature* **2015**, *524*, 200−203.
(159) Sun, Y.; Concustell, A.; Greer, A. L. Thermomechanical Processing of Metallic Glasses: Extending the Range of the Glassy State. *Nat. Rev. Mater.* **2016**, *1*, 16039.
(160) Tian, K. V.; Yang, B.; Yue, Y.; Bowron, D. T.; Mayers, J.; Donnan, R. S.; Dobó-Nagy, C.; Nicholson, J. W.; Fang, D. C.; Greer, A. L.; et al. Atomic and Vibrational Origins of Mechanical Toughness in Bioactive Cement during Setting. *Nat. Commun.* **2015**, *6*, 8631.
(161) Pedersen, M. T.; Tian, K. V.; Dobó-Nagy, C.; Chass, G. A.; Greaves, G. N.; Yue, Y. Z. Phase Separation in an Ionomer Glass: Insight from Calorimetry and Phase Transitions. *J. Non-Cryst. Solids* **2015**, *415*, 24−29.
(162) Yue, Y. Z.; Christiansen, J. D.; Jensen, S. L. Determination of the Fictive Temperature for a Hyperquenched Glass. *Chem. Phys. Lett.* **2002**, *357*, 20−24.
(163) Zheng, Q. J.; Mauro, J. C. Viscosity of Glass-Forming Systems. *J. Am. Ceram. Soc.* **2017**, *100*, 6−25.
(164) Tool, A. Q.; Eichlin, C. G. Variations Caused in the Heating Curves of Glass by Heat Treatment. *J. Am. Ceram. Soc.* **1931**, *14*, 276−308.
(165) Ritland, H. N. Limitations of the Fictive Temperature Concept. *J. Am. Ceram. Soc.* **1956**, *39*, 403−406.
(166) Narayanaswamy, O. S. A Model of Structural Relaxation in Glass. *J. Am. Ceram. Soc.* **1971**, *54*, 491−498.
(167) Mauro, J. C.; Loucks, R. J.; Gupta, P. K. Fictive Temperature and the Glassy State. *J. Am. Ceram. Soc.* **2009**, *92*, 75−86.
(168) DeBolt, M. A.; Easteal, A. J.; Macedo, P. B.; Moynihan, C. T. Analysis of Structural Relaxation in Glass Using Rate Heating Data. *J. Am. Ceram. Soc.* **1976**, *59*, 16−21.
(169) Moynihan, C. T. Correlation between the Width of the Glass Transition Region and the Temperature Dependence of the Viscosity of High-T_g Glasses. *J. Am. Ceram. Soc.* **1993**, *76*, 1081−1087.
(170) Yue, Y. Z. *Hyperquenched Glasses: Relaxation and Properties. An Encyclopedia of Glass Science, Technology, History, Culture (in press).*
(171) Stillinger, F. H.; Weber, T. A. Packing Structures and Transitions in Liquids and Solids. *Science* **1984**, *225*, 983−989.
(172) Saika-Voivod, I.; Poole, P. H.; Sciortino, F. Fragile-to-strong Transition and Polyamorphism in the Energy Landscape of Liquid Silica. *Nature* **2001**, *412*, 514−517.
(173) Yue, Y. Z.; von der Ohe, R.; Jensen, S. L. Fictive Temperature, Cooling Rate, and Viscosity of Glasses. *J. Chem. Phys.* **2004**, *120*, 8053. (a) Yue, Y. Z.; von der Ohe, R.; Jensen, S. L. Erratum: Fictive Temperature, Cooling Rate, and Viscosity of Glasses. *J. Chem. Phys.* **2004**, *121*, 11508.
(174) Priven, A. I. Calculation of Temperature Dependences of the Viscosity and Volume Relaxation Time for Oxide Glass-Forming Melts from Chemical Composition and Dilatometric Glass Transition Temperature. *Glass Phys. Chem.* **2001**, *27*, 527−542.
(175) Huang, J.; Gupta, P. K. Enthalpy Relaxation in Thin Glass Fibers. *J. Non-Cryst. Solids* **1992**, *151*, 175−181.
(176) Velikov, V.; Borick, S.; Angell, C. A. The Glass Transition of Water, Based on Hyperquenching Experiments. *Science* **2001**, *294*, 2335−2338.
(177) Scherer, G. W. Use of the Adam-Gibbs Equation in the Analysis of Structural Relaxation. *J. Am. Ceram. Soc.* **1984**, *67*, 504−511.
(178) Lund, M. D.; Yue, Y. Z. Impact of Drawing Stress on the Tensile Strength of Oxide Glass Fibers. *J. Am. Ceram. Soc.* **2010**, *93*, 3236−3243.
(179) Von der Ohe, R. *Simulation of Glass Fiber Forming Processes*. Ph.D. thesis, Aalborg University, Aalborg, Denmark, 2003.
(180) Moynihan, C. T.; Lee, S. K.; Tatsumisago, M.; Minami, T. Estimation of Activation Energies for Structural Relaxation and Viscous Flow from DTA and DSC Experiments. *Thermochim. Acta* **1996**, *280*, 153−162.
(181) Avramov, I.; Milchev, A. Effect of Disorder on Diffusion and Viscosity in Condensed Systems. *J. Non-Cryst. Solids* **1988**, *104*, 253−260.
(182) Angell, C. A. Spectroscopy, Simulation, and the Medium Range Order Problem in Glass. *J. Non-Cryst. Solids* **1985**, *73*, 1−17.
(183) Angell, C. A.; Ngai, K. L.; McKenna, G. B.; McMillan, P. F.; Martin, S. W. Relaxation in Glassforming Liquids and Amorphous Solids. *J. Appl. Phys.* **2000**, *88*, 3113−3157.
(184) Angell, C. A. Glass Formation and Glass Transition in Supercooled Liquids, with Insights from Study of Related Phenomena in Crystals. *J. Non-Cryst. Solids* **2008**, *354*, 4703−4712.
(185) McKenna, G. B. A Brief Discussion: Thermodynamic and Dynamic Fragilities, Non-divergent Dynamics and the Prigogine−Defay Ratio. *J. Non-Cryst. Solids* **2009**, *355*, 663−671.

DOI: 10.1021/acs.chemrev.8b00510
Chem. Rev. XXXX, XXX, XXX−XXX

(186) Ma, H.; Fecht, H. J. Thermodynamic and Kinetic Fragilities of Mg-based Bulk Metallic Glass-forming Liquids. *J. Mater. Res.* **2008**, *23*, 2816−2820.
(187) Yang, X. N.; Zhou, C.; Sun, Q. J.; Hu, L. N.; Mauro, J. C.; Wang, C. Z.; Yue, Y. Z. Anomalous Crystallization as a Signature of the Fragile-to-Strong Transition in Metallic Glass-Forming Liquids. *J. Phys. Chem. B* **2014**, *118*, 10258−10265.
(188) Evenson, Z.; Schmitt, T.; Nicola, M.; Gallino, I.; Busch, R. High Temperature Melt Viscosity and Fragile to Strong Transition in Zr−Cu−Ni−Al−Nb(Ti) and $Cu_{47}Ti_{34}Zr_{11}Ni_8$ Bulk Metallic Glasses. *Acta Mater.* **2012**, *60*, 4712−4719.
(189) Sun, Q. J.; Zhou, C.; Yue, Y. Z.; Hu, L. N. A Direct Link between the Fragile-to-Strong Transition and Relaxation in Supercooled Liquids. *J. Phys. Chem. Lett.* **2014**, *5*, 1170−1174.
(190) Zheng, Q. J.; Mauro, J. C.; Ellison, A. J.; Potuzak, M.; Yue, Y. Z. Universality of the High-temperature Viscosity Limit of Silicate Liquids. *Phys. Rev. B: Condens. Matter Mater. Phys.* **2011**, *83*, 212202.
(191) Mauro, J. C.; Loucks, R. J. Impact of Fragility on Enthalpy Relaxation in Glass. *Phys. Rev. E* **2008**, *78*, 021502.
(192) Zheng, Q. J.; Mauro, J. C. Variability in the Relaxation Behavior of Glass: Impact of Thermal History Fluctuations and Fragility. *J. Chem. Phys.* **2017**, *146*, 074504.
(193) Urbain, G.; Bottinga, Y.; Richet, P. Viscosity of Liquid Silica, Silicates and Alumino-silicates. *Geochim. Cosmochim. Acta* **1982**, *46*, 1061−1072.
(194) Langstaff, D.; Gunn, M.; Greaves, G. N.; Marsing, A.; Kargl, F. Aerodynamic Levitator Furnace for Measuring Thermophysical Properties of Refractory Liquids. *Rev. Sci. Instrum.* **2013**, *84*, 124901.
(195) Chen, Z. M.; Li, Z. J.; Zhang, Y. Q.; Liu, R. P.; Tian, Y. J.; Wang, L. M. Calorimetric Determination of Fragility in Glass Forming Liquids: T_f vs. $T_{g\text{-onset}}$ Methods. *Eur. Phys. J. E* **2014**, *37*, 1−7.
(196) Kissinger, H. E. Reaction Kinetics in Differential Thermal Analysis. *Anal. Chem.* **1957**, *29*, 1702−1706.
(197) Wang, L. M.; Velikov, V.; Angell, C. A. Direct Determination of Kinetic Fragility Indices of Glassforming Liquids by Differential Scanning Calorimetry: Kinetic versus Thermodynamic Fragilities. *J. Chem. Phys.* **2002**, *117*, 10184.
(198) Huang, D.; McKenna, G. B. New Insights into the Fragility Dilemma in Liquids. *J. Chem. Phys.* **2001**, *114*, 5621−5630.
(199) Potuzak, M.; Mauro, J. C.; Kiczenski, T. J.; Ellison, A. J.; Allan, D. C. Communication: Resolving the Vibrational and Configurational Contributions to Thermal Expansion in Isobaric Glass-forming Systems. *J. Chem. Phys.* **2010**, *133*, 091102.
(200) Mauro, J. C.; Allan, D. C.; Potuzak, M. Nonequilibrium Viscosity of Glass. *Phys. Rev. B: Condens. Matter Mater. Phys.* **2009**, *80*, 754−758.
(201) Angell, C. A.; Richards, B. E.; Velikov, V. Simple Glass-forming Liquids: their Definition, Fragilities, and Landscape Excitation Profiles. *J. Phys.: Condens. Matter* **1999**, *11*, A75−A94.
(202) Angell, C. A. In *Structure and Properties of Glassy Polymers*; Tant, M. R., Hill, A. J., Eds.; American Chemical Society: Washington, DC, 1998; Chapter 3, pp 37−52.
(203) Ferry, J. D. *Viscoelastic Properties of Polymers*, 3rd ed.; Wiley: New York, 1980.
(204) *40 Years of Entropy and the Glass Transition, Special Issue*; edited by McKenna, G. B., Glotzer Mauro, S. L., Loucks, J. C. *J. Res. Natl. Inst. Stand. Technol.* 1997, *102*, 2.
(205) Angell, C. A. Strong and Fragile Liquids. In *Relaxations in Complex Systems*; Ngai, K. L., Wright, G. B., Eds.; Naval Research Laboratory: Washington, DC, 1985; p 3−11.
(206) Matyushov, D. V.; Angell, C. A. Two-Gaussian Excitations Model for the Glass Transition. *J. Chem. Phys.* **2005**, *123*, 34506.
(207) Ruocco, G.; Sciortino, F.; Zamponi, F.; De Michele, C.; Scopigno, T. Landscapes and Fragilities. *J. Chem. Phys.* **2004**, *120*, 10666−10680.
(208) Stillinger, F. H.; Debenedetti, P. G. Energy Landscape Diversity and Supercooled Liquid Properties. *J. Chem. Phys.* **2002**, *116*, 3353−3361.
(209) Velikov, V.; Borick, S.; Angell, C. A. Molecular Glasses with High Fictive Temperatures for Energy Landscape Evaluations. *J. Phys. Chem. B* **2002**, *106*, 1069−1080.
(210) Angell, C. A. Ten Questions on Glassformers, and A Real Space "Excitations" Model with Some Answers on Fragility and Phase Transitions. *J. Phys.: Condens. Matter* **2000**, *12*, 6463−6475.
(211) Stevenson, J. D.; Wolynes, P. G. Thermodynamic-kinetic Correlations in Supercooled Liquids: A Critical Survey of Experimental Data and Predictions of the Random First Order Transition Theory of Glasses. *J. Phys. Chem. B* **2005**, *109*, 1−15.
(212) Cangialosi, D.; Alegría, A.; Colmenero, J. A Thermodynamic Approach to the Fragility of Glass-forming Polymers. *J. Chem. Phys.* **2006**, *124*, 024906.
(213) Prevosto, D.; Lucchesi, M.; Capaccioli, S.; Casalini, R.; Rolla, P. A. Correlation between Configurational Entropy and Structural Relaxation Time in Glass-forming Liquids. *Phys. Rev. B: Condens. Matter Mater. Phys.* **2003**, *67*, 174202.
(214) Wang, L. M.; Angell, C. A.; Richert, R. Fragility and Thermodynamics in Nonpolymeric Glass-forming Liquids. *J. Chem. Phys.* **2006**, *125*, 074505.
(215) Xia, X.; Wolynes, P. G. Fragilities of Liquids Predicted from the Random First Order Transition Theory of Glasses. *Proc. Natl. Acad. Sci. U. S. A.* **2000**, *97*, 2990−2994.
(216) Stevenson, J. D.; Wolynes, P. G. Thermodynamic-kinetic Correlations in Supercooled Liquids: A Critical Survey of Experimental Data and Predictions of the Random First-order Transition Theory of Glasses. *J. Phys. Chem. B* **2005**, *109*, 15093−15097.
(217) Yue, Y. Z.; Zheng, Q. J. Fiber Spinnability of Glass Melts. *Int. J. Appl. Glass Sci.* **2017**, *8*, 37−47.
(218) Fulcher, G. S. Analysis of Recent Measurements of the Viscosity of Glasses. *J. Am. Ceram. Soc.* **1925**, *8*, 339−355.
(219) McMillan, P. F.; Wilson, M.; Wilding, M. C.; Daisenberger, D.; Mezouar, M.; Greaves, G. N. Polyamorphism and Liquid−liquid Phase Transitions: Challenges for Experiment and Theory. *J. Phys.: Condens. Matter* **2007**, *19*, 415101.
(220) Mishima, O.; Calvert, L. D.; Whalley, E. An Apparently 1st-order Transition between Two Amorphous Phases of Ice Induced by Ressure. *Nature* **1985**, *314*, 76−78.
(221) Gallo, P.; Amann-Winkel, K.; Angell, C. A.; Anisimov, M. A.; Caupin, F.; Chakravarty, C.; Lascaris, E.; Loerting, T.; Panagiotopoulos, A. Z.; Russo, J.; et al. Water: A Tale of Two Liquids. *Chem. Rev.* **2016**, *116*, 7463−7500.
(222) Woutersen, S.; Ensing, B.; Hilbers, M.; Zhao, Z.; Angell, C. A. A Liquid-liquid Transition in Supercooled Aqueous Solution Related to the HDA-LDA Transition. *Science* **2018**, *359*, 1127−1131.
(223) Chatterjee, S.; Debenedetti, P. G. Fluid-phase Behavior of Binary Mixtures in Which One Component Can Have Two Critical Points. *J. Chem. Phys.* **2006**, *124*, 154503.
(224) Anisimov, M. A. Cold and Supercooled Water: A Novel Supercritical-fluid Solvent. *Russ. J. Phys. Chem. B* **2012**, *6*, 861−867.
(225) Biddle, J. W.; Holten, V.; Anisimov, M. A. Behavior of Supercooled Aqueous Solutions Stemming from Hidden Liquid−liquid Transition in Water. *J. Chem. Phys.* **2014**, *141*, 074504.
(226) Greaves, G. N.; Meneau, F.; Kargl, F.; Ward, D.; Holliman, P.; Albergamo, F. Zeolite Collapse and Polyamorphism. *J. Phys.: Condens. Matter* **2007**, *19*, 415102.
(227) Loerting, T.; Giovambattista, N. Amorphous Ices: Experiments and Numerical Simulations. *J. Phys.: Condens. Matter* **2006**, *18*, R919−R977.
(228) Mishima, O.; Calvert, L. D.; Whalley, E. 'Melting ice' I at 77 K and 10 kbar: A New Method of Making Amorphous Materials. *Nature* **1984**, *310*, 393−395.
(229) Poole, P. H.; Grande, T.; Angell, C. A.; McMillan, P. F. Polymorphic Phase Transitions in Liquids and Glasses. *Science* **1997**, *275*, 322−323.
(230) Aasland, S.; McMillan, P. F. Density-driven Liquid−liquid Phase Separation in the System Al_2O_3−Y_2O_3. *Nature* **1994**, *369*, 633−636.

DOI: 10.1021/acs.chemrev.8b00510
Chem. Rev. XXXX, XXX, XXX−XXX

(231) Greaves, G. N.; Wilding, M. C.; Fearn, S.; Langstaff, D.; Kargl, F.; Cox, S.; Van, Q.; Majerus, O.; Benmore, C. J.; Weber, R.; et al. Detection of First-Order Liquid/Liquid Phase Transitions in Yttrium Oxide-Aluminum Oxide Melts. *Science* **2008**, *322*, 566−570.
(232) Greaves, G. N.; Wilding, M. C.; Langstaff, D.; Kargl, F.; Hennet, L.; Benmore, C. J.; Weber, J. K. R.; Van, Q. V.; Majérus, O.; McMillan, P. F. Composition and Polyamorphism in Supercooled Yttria−alumina Melts. *J. Non-Cryst. Solids* **2011**, *357*, 435−441.
(233) Barnes, A. C.; Skinner, L. B.; Salmon, P. S.; Bytchkov, A.; Pozdnyakova, I.; Farmer, T. O.; Fischer, H. E. Liquid-liquid Phase Transition in Supercooled Yttria-alumina. *Phys. Rev. Lett.* **2009**, *103*, 225702.
(234) Inamura, Y.; Katayama, Y.; Utsumi, W.; Funakoshi, K. I. Transformations in the Intermediate-range Structure of SiO2 Glass under High Pressure and Temperature. *Phys. Rev. Lett.* **2004**, *93*, 015501.
(235) Richet, P.; Gillet, P. Pressure-induced Amorphisation of Minerals: A Review. *Eur. J. Mineral.* **1997**, *9*, 907−934.
(236) Haines, J.; Levelut, C.; Isambert, A.; Hébert, P.; Kohara, S.; Keen, D. A.; Hammouda, T.; Andrault, D. Topologically Ordered Amorphous Silica Obtained from the Collapsed Siliceous Zeolite, Silicalite-1-F: A Step toward "Perfect" Glasses. *J. Am. Chem. Soc.* **2009**, *131*, 12333−12338.
(237) Bennett, T. D.; Goodwin, A. L.; Dove, M. T.; Keen, D. A.; Tucker, M. G.; Barney, E. R.; Soper, A. K.; Bithell, E. G.; Tan, J. C.; Cheetham, A. K. Structure and Properties of an Amorphous Metal-organic Framework. *Phys. Rev. Lett.* **2010**, *104*, 115503.
(238) Sharma, S. M.; Sikka, S. K. Pressure-induced Amorphisation of Materials. *Prog. Mater. Sci.* **1996**, *40*, 1−77.
(239) Colyer, L. M.; Greaves, G. N.; Carr, S. W.; Fox, K. K. Collapse and Recrystallization Processes in Zinc-Exchanged Zeolite-A: A Combined X-ray Diffraction, XAFS, and NMR Study. *J. Phys. Chem. B* **1997**, *101*, 10105−10114.
(240) Wondraczek, L.; Pan, Z.; Palenta, T.; Erlebach, A.; Misture, S. T.; Sierka, M.; Micoulaut, M.; Hoppe, U.; Deubener, J.; Greaves, G. N. Kinetics of Decelerated Melting. *Adv. Sci.* **2018**, *5*, 1700850.
(241) Dove, M. T.; Hammonds, K. D.; Trachenko, K. In *Rigidity Theory and Applications*; Thorpe, M. F., Duxbury, P. M., Eds.; Springer, 1999; pp 217−238.
(242) Hammonds, K. D.; Deng, H.; Heine, V.; Dove, M. T. How Floppy Modes Give Rise to Adsorption Sites in Zeolites. *Phys. Rev. Lett.* **1997**, *78*, 3701−3704.
(243) Villaescusa, L. A.; Lightfoot, P.; Teat, S. J.; Morris, R. E. Variable-temperature Microcrystal X-ray Diffraction Studies of Negative Thermal Expansion in the Pure Silica Zeolite IFR. *J. Am. Chem. Soc.* **2001**, *123*, 5453−5459.
(244) Sciortino, F.; Essmann, U.; Stanley, H. E.; Hemmati, M.; Shao, J.; Wolf, G. H.; Angell, C. A. Crystal Stability Limits at Positive and Negative Pressures, and Crystal-to-glass Transitions. *Phys. Rev. E: Stat. Phys., Plasmas, Fluids, Relat. Interdiscip. Top.* **1995**, *52*, 6484−6491.
(245) Greaves, G. N.; Meneau, F.; Sapelkin, A.; Colyer, L. M.; Ap Gwynn, I.; Wade, S.; Sankar, G. The Rheology of Collapsing Zeolites Amorphized by Temperature and Pressure. *Nat. Mater.* **2003**, *2*, 622−629.
(246) Wharmby, M. T.; Henke, S.; Bennett, T. D.; Bajpe, S. R.; Schwedler, I.; Thompson, S. P.; Gozzo, F.; Simoncic, P.; Mellot-Draznieks, C.; Tao, H. Z.; et al. Extreme Flexibility in a Zeolitic Imidazolate Framework: Porous to Dense Phase Transition in Desolvated ZIF 4. *Angew. Chem., Int. Ed.* **2015**, *54*, 6447−6451.
(247) Tao, H. Z.; Bennett, T. D.; Yue, Y. Z. Melt-Quenched Hybrid Glasses from Metal-organic Frameworks. *Adv. Mater.* **2017**, *29*, 1601705.
(248) Bennett, T. D.; Cheetham, A. K. Amorphous Metal-organic Frameworks. *Acc. Chem. Res.* **2014**, *47*, 1555−1562.
(249) van de Voorde, B.; Stassen, I.; Bueken, B.; Vermoortele, F.; de Vos, D.; Ameloot, R.; Tan, J. C.; Bennett, T. D. Improving the Mechanical Stability of Zirconium-based Metal-organic Frameworks by Incorporation of Acidic Modulators. *J. Mater. Chem. A* **2015**, *3*, 1737−1742.
(250) Park, K. S.; Ni, Z.; Cote, A. P.; Choi, J. Y.; Huang, R. D.; Uribe- Romo, F. J.; Chae, H. K.; O'Keeffe, M.; Yaghi, O. M. Exceptional Chemical and Thermal Stability of Zeolitic Imidazolate Frameworks. *Proc. Natl. Acad. Sci. U. S. A.* **2006**, *103*, 10186−10191.
(251) Tian, Y. Q.; Zhao, Y. M.; Chen, Z. X.; Zhang, G. N.; Weng, L. H.; Zhao, D. Y. Design and Generation of Extended Zeolitic Metal-organic Frameworks (ZMOFs): Synthesis and Crystal Structures of Zinc(II) Imidazolate Polymers with Zeolitic Topologies. *Chem. - Eur. J.* **2007**, *13*, 4146−4154.
(252) Chapman, K. W.; Sava, D. F.; Halder, G. J.; Chupas, P. J.; Nenoff, T. M. Trapping Guests within A Nanoporous Metal-organic Framework through Pressure-induced Amorphization. *J. Am. Chem. Soc.* **2011**, *133*, 18583.
(253) Horcajada, P.; Serre, C.; Vallet-Regi, M.; Sebban, M.; Taulelle, F.; Férey, G. Metal-organic Frameworks as Efficient Materials for Drug Delivery. *Angew. Chem., Int. Ed.* **2006**, *45*, 5974−5978.
(254) Bennett, T. D.; Yue, Y. Z.; Li, P.; Qiao, A.; Tao, H. Z.; Greaves, G. N.; Richards, T.; Lampronti, G. I.; Redfern, S. A. T.; Blanc, F.; et al. Melt-quenched Glasses of Metal-organic Frameworks. *J. Am. Chem. Soc.* **2016**, *138*, 3484−3492.
(255) Qiao, A.; Bennett, T. D.; Tao, H. Z.; Krajnc, A.; Mali, G.; Doherty, C. M.; Thornton, A. W.; Mauro, J. C.; Greaves, G. N.; Yue, Y. Z. A Metal-organic Framework with Ultrahigh Glass-forming Ability. *Sci. Adv.* **2018**, *4*, No. eaao6827.
(256) MacMillan, J. A.; Los, S. C. Kinetics of Glass Transformation by Thermal Analysis. I. Glycerol. *J. Chem. Phys.* **1965**, *42*, 3497−3501.
(257) Greaves, G. N. *Hybrid Glasses: from Metal Organic Frameworks and Co-ordination Polymers to Hybrid Perovskites*; Musgraves, J. D., Hu, J., Calvez, L., Eds.; Springer Handbook of Glass; Springer: Cham, 2019.
(258) Hofer, K.; Mayer, E.; Johari, G. P. Glass-liquid Transition of Water and Ethylene Glycol Solution in Poly(2-hydroxyethyl methacrylate) Hydrogel. *J. Phys. Chem.* **1990**, *94*, 2689−2696.
(259) Johari, G. P.; Hallbrucker, A.; Mayer, E. The Glass Transition of Hyperquenched Glassy Water. *Nature* **1987**, *330*, 552−553.
(260) Hofer, K.; Hallbrucker, A.; Mayer, E.; Johari, G. P. Vitrified Dilute Aqueous-solutions. 3. Plasticization of Waters H-bonded Network and the Glass-transition Temperatures Minimum. *J. Phys. Chem.* **1989**, *93*, 4674−4677.
(261) Angell, C. A. Insights into Phases of Liquid Water from Study of Its Unusual Glass-Forming Properties. *Science* **2008**, *319*, 582−587.
(262) Longley, L.; Collins, S. M.; Zhou, C.; Smales, G. J.; Norman, S. E.; Brownbill, N. J.; Ashling, C. W.; Chater, P. A.; Tovey, R.; Schönlieb, C.; et al. Liquid Phase Blending of Metal-organic Frameworks. *Nat. Commun.* **2018**, *9*, 2135.
(263) Singh, S.; Ediger, M. D.; de Pablo, J. J. Ultrastable Glasses from in Silico Vapour Deposition. *Nat. Mater.* **2013**, *12*, 139−144.
(264) Perez-Castaneda, T.; Rodriguez-Tinoco, C.; Rodriguez-Viejo, J.; Ramos, M. A. Suppression of Tunneling Two-level Systems in Ultrastable Glasses of Indomethacin. *Proc. Natl. Acad. Sci. U. S. A.* **2014**, *111*, 11275−11280.
(265) Navrotsky, A.; Tian, Z. R. Systematics in the Enthalpies of Formation of Anhydrous Aluminosilicate Zeolites, Glasses, and Dense Phases. *Chem. - Eur. J.* **2001**, *7*, 769−774.
(266) Peral, I.; Iniguez, J. Amorphization Induced by Pressure: Results for Zeolites and General Implications. *Phys. Rev. Lett.* **2006**, *97*, 225502.
(267) Rogez, G.; Viart, N.; Drillon, M. Multiferroic Materials: The Attractive Approach of Metal-organic Frameworks (MOFs). *Angew. Chem., Int. Ed.* **2010**, *49*, 1921−1923.
(268) Stillinger, F. H.; Weber, T. A. Dynamics of Structural Transitions in Liquids. *Phys. Rev. A: At., Mol., Opt. Phys.* **1983**, *28*, 2408.
(269) Wales, D. J. *Energy Landscapes with Applications to Clusters, Biomolecules and Glasses*; Cambridge University Press: Cambridge, 2003.
(270) Goldstein, M. Viscous Liquids and the Glass Transition: A Potential Energy Barrier Picture. *J. Chem. Phys.* **1969**, *51*, 3728−3739.

DOI: 10.1021/acs.chemrev.8b00510
Chem. Rev. XXXX, XXX, XXX−XXX

(271) Stillinger, F. H. A Topographic View of Supercooled Liquids and Glass Formation. *Science* **1995**, *267*, 1935−1939.
(272) Angelani, L.; Leonardo, R. D.; Ruocco, G.; Scala, A.; Sciortino, F. Saddles in the Energy Landscape Probed by Supercooled Liquids. *Phys. Rev. Lett.* **2000**, *85*, 5356−5359.
(273) Angell, C. A. Calorimetric Studies of the Energy Landscapes of Glass Formers by Hyperquenching Methods. *J. Therm. Anal. Calorim.* **2002**, *69*, 785−794.
(274) Hu, L. N.; Yue, Y. Z. Secondary Relaxation Behavior in a Strong Glass. *J. Phys. Chem. B* **2008**, *112*, 9053−9057.
(275) Stillinger, F. H. Supercooled Liquids, Glass Transitions, and The Kauzmann Paradox. *J. Chem. Phys.* **1988**, *88*, 7818−7825.
(276) Diezemann, G. A Free-energy Landscape Model for Primary Relaxation in Glass-forming Liquids: Rotations and Dynamic Heterogeneities. *J. Chem. Phys.* **1997**, *107*, 10112−10120.
(277) Diezemann, G.; Sillescu, H.; Hinze, G.; Bohmer, R. Rotational Correlation Functions and Apparently Enhanced Translational Diffusion in a Free-energy Landscape Model for the α Relaxation in Glass-forming Liquids. *Phys. Rev. E: Stat. Phys., Plasmas, Fluids, Relat. Interdiscip. Top.* **1998**, *57*, 4398−4410.
(278) Diezemann, G. Aging in a Free-energy Landscape Model for Glassy Relaxation. *J. Chem. Phys.* **2005**, *123*, 204510.
(279) Diezemann, G.; Mohanty, U.; Oppenheim, I. Slow Secondary Relaxation in a Free-energy Landscape Model for Relaxation in Glass-forming Liquids. *Phys. Rev. E: Stat. Phys., Plasmas, Fluids, Relat. Interdiscip. Top.* **1999**, *59*, 2067−2083.
(280) Johari, G. P. Disorder, Configurational Relaxations and Heat Capacity of Glasses. *Phase Transitions* **1985**, *5*, 277−300.
(281) Ngai, K. L.; Paluch, M. Classification of Secondary Relaxation in Glass-formers Based on Dynamic Properties. *J. Chem. Phys.* **2004**, *120*, 857−870.
(282) Ngai, K. L.; Tsang, K. Y. Similarity of Relaxation in Supercooled Liquids and Interacting Arrays of Oscillators. *Phys. Rev. E: Stat. Phys., Plasmas, Fluids, Relat. Interdiscip. Top.* **1999**, *60*, 4511−4517.
(283) Mauro, J. C.; Smedskjaer, M. M. Minimalist Landscape Model of Glass Relaxation. *Phys. A* **2012**, *391*, 3446−3459.
(284) Mauro, J. C.; Loucks, R. J. Selenium Glass Transition: A Model Based on the Enthalpy Landscape Approach and Non-equilibrium Statistical Mechanics. *Phys. Rev. B: Condens. Matter Mater. Phys.* **2007**, *76*, 174202.
(285) Mauro, J. C.; Varshneya, A. K. Model Interaction Potentials for Selenium from ab initio Molecular Simulations. *Phys. Rev. B: Condens. Matter Mater. Phys.* **2005**, *71*, 214105.
(286) Mauro, J. C.; Loucks, R. J.; Balakrishnan, J. Split-Step Eigenvector-Following Technique for Exploring Enthalpy Landscapes at Absolute Zero. *J. Phys. Chem. B* **2006**, *110*, 5005.
(287) Hu, L. N.; Yue, Y. Z. Secondary Relaxation in Metallic Glass Formers: Its Correlation with the Genuine Johari-Goldstein Relaxation. *J. Phys. Chem. C* **2009**, *113*, 15001−15006.
(288) Wang, L. M.; Borick, S.; Angell, C. A. An Electrospray Technique for Hyperquenched Glass Calorimetry Studies: Propylene Glycol and di-n-butyl Phthalate. *J. Non-Cryst. Solids* **2007**, *353*, 3829−3837.
(289) Tool, A. Q. Relation between Inelastic Deformability and Thermal Expansion of Glass in Its Annealing Range. *J. Am. Ceram. Soc.* **1946**, *29*, 240−253.
(290) Inoue, A.; Masumoto, T.; Chen, H. S. Enthalpy Relaxation Behaviour of Metal-metal (Zr-Cu) Amorphous Alloys upon Annealing. *J. Mater. Sci.* **1985**, *20*, 4057−4068.
(291) Yue, Y. Z.; Jensen, S. L.; Christiansen, J. deC Physical Aging in a Hyperquenched Glass. *Appl. Phys. Lett.* **2002**, *81*, 2983−2985.
(292) Yue, Y. Z. Influence of Physical Ageing on the Excessive Heat Capacity of Hyperquenched Silicate Glass Fibers. *J. Non-Cryst. Solids* **2004**, *348*, 72−77.
(293) Hornbøll, L.; Yue, Y. Z. Enthalpy Relaxation of Hyperquenched Glasses and Its Possible Link to α and β -relaxations. *J. Non-Cryst. Solids* **2008**, *354*, 350−354.
(294) Yue, Y. Z. Relaxation in Glasses Far from Equilibrium State. *J. Shandong University − Eng. Ed.* **2009**, *39*, 1−26.
(295) Zhang, Y. F.; Hu, L. N.; Liu, S. J.; Zhu, C. F.; Yue, Y. Z. Sub-T_g Enthalpy Relaxation in an Extremely Unstable Oxide Glass and Its Implication for Structural Heterogeneity. *J. Non-Cryst. Solids* **2013**, *381*, 23−28.
(296) Guo, X. J.; Mauro, J. C.; Potuzak, M.; Yue, Y. Z. Structural Relaxation in Annealed Hyperquenched Basaltic Glasses: Insights from Calorimetry. *J. Non-Cryst. Solids* **2012**, *358*, 1356−1361.
(297) Wang, X. H.; Inoue, A.; Kong, F. L.; Zhu, S. L.; Wang, H.; Shalaan, E.; Al-Marzouki, F. Annealing-induced Enthalpy Relaxation Behavior of Ni-Pd-P-B Bulk Glassy Type Alloys. *Mater. Sci. Eng., A* **2016**, *674*, 250−255.
(298) Slipenyuk, A.; Eckert, J. Correlation between Enthalpy Change and Free Volume Reduction during Structural Relaxation of $Zr_{55}Cu_{30}Al_{10}Ni_5$ Metallic Glass. *Scr. Mater.* **2004**, *50*, 39−44.
(299) Zhu, F.; Nguyen, H. K.; Song, S. X.; Aji, D. P. B.; Hirata, A.; Wang, H.; Nakajima, K.; Chen, M. W. Intrinsic Correlation between β-relaxation and Spatial Heterogeneity in a Metallic Glass. *Nat. Commun.* **2016**, *7*, 11516.
(300) Senapati, H.; Angell, C. A. Glass Formation and Anomalous Annealing Effects in the Mixed Oxyanion System AgI Ag_2SO_4 Ag_2WO_4. *J. Non-Cryst. Solids* **1991**, *130*, 58−66.
(301) Yue, Y. Z.; Angell, C. A. Glass Transition in Hyperquenched Water? Reply. *Nature* **2005**, *435*, E1−E2.
(302) Kohlrausch, R. Nachtrag uber die elastiche Nachwirkung beim Cocon und Glasladen. *Prog. Ann. Phys.* **1847**, *12*, 393.
(303) Kohlrausch, R. Theorie des elektrischen Rückstandes in der Leidener Flasche. *Ann. Phys.* **1854**, *167*, 179.
(304) Williams, G.; Watts, D. C. Non-symmetrical Dielectric Relaxation Behaviour Arising from a Simple Empirical Decay Function. *Trans. Faraday Soc.* **1970**, *66*, 80−85.
(305) Yue, Y. Z. Anomalous Enthalpy Relaxation in Vitreous Silica. *Front. Mater.* **2015**, *2*, 54.
(306) Hornbøll, L.; Yue, Y. Z. Enthalpy Relaxation in Hyperquenched Glasses of Different Fragility. *J. Non-Cryst. Solids* **2008**, *354*, 1862−1870.
(307) Huang, J.; Gupta, P. K. Temperature Dependence of the Isostructural Heat Capacity of a Soda Lime Silicate Glass. *J. Non-Cryst. Solids* **1992**, *139*, 239−247.
(308) Ducroux, J. P.; Rekhson, S. M.; Merat, F. L. Structural Relaxation in Thermorheologically Complex Materials. *J. Non-Cryst. Solids* **1994**, *172−174*, 541−553.
(309) Giovambattista, N.; Angell, C. A.; Sciortino, F.; Stanley, H. E. Glass-Transition Temperature of Water: A Simulation Study. *Phys. Rev. Lett.* **2004**, *93*, 047801.
(310) Giovambattista, N.; Angell, C. A.; Sciortino, F.; Stanley, H. E. Structural Relaxation in the Glass Transition Region of Water. *Phys. Rev. E* **2005**, *72*, 011203.
(311) Hornbøll, L.; Knusen, T.; Yue, Y. Z.; Guo, X. J. Heterogeneous Enthalpy Relaxation in Glasses far from Equilibrium. *Chem. Phys. Lett.* **2010**, *494*, 37−40.
(312) Zhang, Y. F.; Guo, X. J.; Yue, Y. Z. Effect of the Initial Stage of Annealing on Modeling of Enthalpy Relaxation in a Hyperquenched Glass. *J. Non-Cryst. Solids* **2013**, *378*, 121−125.
(313) Guo, X.; Smedskjaer, M. M.; Mauro, J. C. Linking Equilibrium and Nonequilibrium Dynamics in Glass-Forming Systems. *J. Phys. Chem. B* **2016**, *120*, 3226−3231.
(314) Guo, X.; Mauro, J. C.; Allan, D. C.; Smedskjaer, M. M. Predictive Model for the Composition Dependence of Glassy Dynamics. *J. Am. Ceram. Soc.* **2018**, *101*, 1169−1179.
(315) Wilkinson, C. J.; Mauro, Y. Z.; Mauro, J. C. RelaxPy: Python Code for Modeling of Glass Relaxation Behavior. *SoftwareX* **2018**, *7*, 255−258.
(316) Chumakov, A. I.; Monaco, G.; Fontana, A.; Bosak, A.; Hermann, R. P.; Bessas, D.; Wehinger, B.; Crichton, W. A.; Krisch, M.; Rüffer, R.; Baldi, G.; Carini, G.; D'Angelo, G.; Gillioli, E.; Tripodo, G.; Zanatta, M.; Winkler, B.; Milman, V.; Refson, K.; Tucker, M.; Dubrovinsky, L.; Keding, R.; Yue, Y. Z. Role of Disorder

DOI: 10.1021/acs.chemrev.8b00510
Chem. Rev. XXXX, XXX, XXX−XXX

in the Thermodynamics and Atomic Dynamics of Glasses. *Phys. Rev. Lett.* **2014**, *112*, 025502.
(317) Chumakov, A. I.; Monaco, G.; Monaco, A.; Crichton, W. A.; Bosak, A.; Rüffer, R.; Meyer, A.; Kargl, F.; Comez, L.; Fioretto, D.; Giefers, H.; Roitsch, S.; Wortmann, G.; Manghnani, M. H.; Hushur, A.; Williams, Q.; Balogh, J.; Parlinski, K.; Jochym, P.; Piekarz, P. Equivalence of the Boson Peak in Glasses to the Transverse Acoustic van Hove Singularity in Crystals. *Phys. Rev. Lett.* **2011**, *106*, 225501.
(318) Shintani, H.; Tanaka, H. Universal Link between Transverse Phonons in Glass. *Nat. Mater.* **2008**, *7*, 870−877.
(319) Greaves, G. N.; Greer, A. L.; Lakes, R. S.; Rouxel, T. Poisson's Ratio and Modern Materials. *Nat. Mater.* **2011**, *10*, 823−837.
(320) Kearns, K. L.; Swallen, S. F.; Ediger, M. D.; Wu, T.; Sun, Y.; Yu, L. Hiking down the Energy Landscape: Progress toward the Kauzmann Temperature via Vapor Deposition. *J. Phys. Chem. B* **2008**, *112*, 4934−4942.
(321) Dawson, K. J.; Kearns, K. L.; Yu, L.; Steffen, W.; Ediger, M. D. Physical Vapor Deposition as a Route to Hidden Amorphous States. *Proc. Natl. Acad. Sci. U. S. A.* **2009**, *106*, 15165−15170.
(322) Kearns, K. L.; Still, T.; Fytas, G.; Ediger, M. D. High-Modulus Organic Glasses Prepared by Physical Vapor Deposition. *Adv. Mater.* **2010**, *22*, 39−42.
(323) Fakhraai, Z.; Still, T.; Fytas, G.; Ediger, M. D. Structural Variations of an Organic Glassformer Vapor-deposited onto a Temperature Gradient Stage. *J. Phys. Chem. Lett.* **2011**, *2*, 423−427.
(324) Yu, H. B.; Luo, Y. S.; Samwer, K. Ultrastable Metallic Glass. *Adv. Mater.* **2013**, *25*, 5904−5908.
(325) Léonard, S.; Harrowell, P. Macroscopic Facilitation of Glassy Relaxation Kinetics: Ultrastable Glass Films with Frontlike Thermal Response. *J. Chem. Phys.* **2010**, *133*, 244502.
(326) Kearns, K. L.; Swallen, S. F.; Ediger, M. D.; Wu, T.; Yu, L. Influence of Substrate Temperature on the Stability of Glasses Prepared by Vapor Deposition. *J. Chem. Phys.* **2007**, *127*, 154702.
(327) Kearns, K. L.; Krzyskowski, P.; Devereaux, Z. Using Deposition Rate to Increase the Thermal and Kinetic Stability of Vapor-deposited Hole Transport Layer Glasses via a Simple Sublimation Apparatus. *J. Chem. Phys.* **2017**, *146*, 203328.
(328) Whitaker, K. R.; Tylinski, M.; Ahrenberg, M.; Schick, C.; Ediger, M. D. Kinetic Stability and Heat Capacity of Vapor-deposited Glasses of o-terphenyl. *J. Chem. Phys.* **2015**, *143*, 084511.
(329) Yu, H. B.; Tylinski, M.; Guiseppi-Elie, A.; Ediger, M. D.; Richert, R. Suppression of β Relaxation in Vapor-deposited Ultrastable Glasses. *Phys. Rev. Lett.* **2015**, *115*, 185501.
(330) Kearns, K. L.; Swallen, S. F.; Ediger, M. D.; Sun, Y.; Yu, L. Calorimetric Evidence for Two Distinct Molecular Packing Arrangements in Stable Glasses of Indomethacin. *J. Phys. Chem. B* **2009**, *113*, 1579−1586.
(331) Sepúlveda, A.; Leon-Gutierrez, E.; Gonzalez-Silveira, M.; Clavaguera-Mora, M. T.; Rodríguez-Viejo, J. Anomalous Transformation of Vapor-Deposited Highly Stable Glasses of Toluene into Mixed Glassy States by Annealing Above T_g. *J. Phys. Chem. Lett.* **2012**, *3*, 919−923.
(332) Swallen, S. F.; Traynor, K.; McMahon, R. J.; Ediger, M. D. Stable Glass Transformation to Supercooled Liquid via Surface-Initiated Growth Front. *Phys. Rev. Lett.* **2009**, *102*, 065503.
(333) Ermakov, A. E.; Yurchikov, E. E.; Barinov, V. A. The Magnetic Properties of Amorphous Yttrium−Cobalt Alloy Powders Obtained by Mechanical Comminution. *Fiz. Metal. Metalloved.* **1981**, *52*, 1184−1193.
(334) Ermakov, A. E.; Barinov, V. A.; Yurchikov, E. E. Changes in the Magnetic Properties of Powders of Alloys in the Gd-Co System as a Result of Their Amorphization by Milling. *Fiz. Metal. Metalloved.* **1982**, *54*, 935−941.
(335) Koch, C. C.; Cavin, O. B.; McKamey, C. G.; Scarbrough, J. O. Preparation of "Amorphous" $Ni_{60}Nb_{40}$ by Mechanical Alloying. *Appl. Phys. Lett.* **1983**, *43*, 1017.
(336) Kim, K. J.; El-Eskandarany, M. S.; Sumiyama, K.; Suzuki, K. Structural and Calorimetric Studies of Amorphous $Cu_{71}Ni_{11}P_{18}$ Alloy Produced by Ball-milling. *J. Non-Cryst. Solids* **1993**, *155*, 165−170.
(337) Shao, H.; Xu, Y.; Shi, B.; Yu, C.; Hahn, H.; Gleiter, H.; Li, J. High Density of Shear Bands and Enhanced Free Volume Induced in $Zr_{70}Cu_{20}Ni_{10}$ Metallic Glass by High-energy Ball Milling. *J. Alloys Compd.* **2013**, *548*, 77−81.
(338) Kim, Y. J.; Suzuki, T.; Hagiwara, T.; Yamaji, I.; Takai, R. Enthalpy Relaxation and Glass to Rubber Transition of Amorphous Potato Starch Formed by Ball-milling. *Carbohydr. Polym.* **2001**, *46*, 1−6.
(339) Descamps, M.; Aumelas, A.; Desprez, S.; Willart, J. F. The Amorphous State of Pharmaceuticals Obtained or Transformed by Milling: Sub-T_g Features and Rejuvenation. *J. Non-Cryst. Solids* **2015**, *407*, 72−80.
(340) Noi, K.; Hayashi, A.; Tatsumisago, M. Structure and Properties of the Na_2S-P_2S_5 Glasses and Glass-ceramics Prepared by Mechanical Milling. *J. Power Sources* **2014**, *269*, 260−265.
(341) Qiao, A.; Tao, H. Z.; Yue, Y. Z. Sub-T_g Enthalpy Relaxation in a Milling-derived Chalcogenide Glass. *J. Am. Ceram. Soc.* **2017**, *100*, 968−974.
(342) Ya, M.; Deubener, J.; Yue, Y. Z. Enthalpy and Anisotropy Relaxation of Glass Fibers. *J. Am. Ceram. Soc.* **2008**, *91*, 745−752.
(343) Wu, J. S.; Deubener, J.; Stebbins, J. F.; Grygarova, L.; Behrens, H.; Wondraczek, L.; Yue, Y. Z. Structural Response of a Highly Viscous Aluminoborosilicate Melt to Isotropic and Anisotropic Compressions. *J. Chem. Phys.* **2009**, *131*, 104504.
(344) Braun, M.; Yue, Y. Z.; Rüssel, C.; Jäger, C. Two-dimensional Nuclear Magnetic Resonance Evidence for Structural Orientation in Extruded Phosphate Glass. *J. Non-Cryst. Solids* **1998**, *241*, 204−207.
(345) Yue, Y. Z.; Brückner, R. A New Description and Interpretation of the Flow Behaviour of Glass Forming Melts. *J. Non-Cryst. Solids* **1994**, *180*, 66−79.
(346) Szewczyk, R. Extension of the Model of the Magnetic Characteristics of Anisotropic Metallic Glasses. *J. Phys. D: Appl. Phys.* **2007**, *40*, 4109−4113.
(347) Tanaka, K.; Ishida, K. Photoinduced Anisotropic Structures in Chalcogenide Glasses. *J. Non-Cryst. Solids* **1998**, *227*, 673−676.
(348) Lu, X.; Arruda, E. M.; Schultz, W. W. The Effect of Processing Parameters on Glass Fiber Birefringence Development and Relaxation. *J. Non-Newtonian Fluid Mech.* **1999**, *86*, 89−104.
(349) Martin, B.; Wondraczek, L.; Deubener, J.; Yue, Y. Z. Mechanically Induced Excess Enthalpy in Inorganic Glasses. *Appl. Phys. Lett.* **2005**, *86*, 121917.
(350) Hornbøll, L.; Lonnroth, N.; Yue, Y. Z. Energy Release in Isothermally Stretched Silicate Glass fibers. *J. Am. Ceram. Soc.* **2006**, *89*, 70−74.
(351) Deubener, J.; Yue, Y. Z.; Bornhöft, H.; Ya, M. Decoupling between Birefringence Decay, Enthalpy Relaxation and Viscous Flow in Calcium Boroalumosilicate Glasses. *Chem. Geol.* **2008**, *256*, 298−304.
(352) Zhang, Y. F.; Yang, G.; Yue, Y. Z. Calorimetric Signature of Structural Heterogeneity in a Ternary Silicate Glass. *J. Am. Ceram. Soc.* **2013**, *96*, 3035−3037.
(353) Zhou, C.; Yue, Y. Z.; Hu, L. N. Revealing the Connection between the Slow β Relaxation and Sub-T_g Enthalpy Relaxation in Metallic Glasses. *J. Appl. Phys.* **2016**, *120*, 225110.
(354) Vyazovkin, S.; Dranca, I. A DSC Study of α- and β-Relaxations in a PS-Clay System. *J. Phys. Chem. B* **2004**, *108*, 11981−11987.
(355) Tombari, E.; Ferrari, C.; Johari, G. P.; Shanker, R. M. Calorimetric Relaxation in Pharmaceutical Molecular Glasses and Its Utility in Understanding Their Stability against Crystallization. *J. Phys. Chem. B* **2008**, *112*, 10806−10814.
(356) Vyazovkin, S.; Dranca, I. Comparative Relaxation Dynamics of Glucose and Maltitol. *Pharm. Res.* **2006**, *23*, 2158−2164.
(357) Capaccioli, S.; Paluch, M.; Prevosto, D.; Wang, L. M.; Ngai, K. L. Many-Body Nature of Relaxation Processes in Glass-Forming Systems. *J. Phys. Chem. Lett.* **2012**, *3*, 735−743.
(358) Hu, L. N.; Zhang, C. Z.; Yue, Y. Z.; Bian, X. F. A New Threshold of Uncovering the Nature of Glass Transition: The slow β Relaxation in Glassy States. *Chin. Sci. Bull.* **2010**, *55*, 457−472.

DOI: 10.1021/acs.chemrev.8b00510
Chem. Rev. XXXX, XXX, XXX−XXX

(359) Ngai, K. L.; Capaccioli, S. Relation between the Activation Energy of the Johari-Goldstein β Relaxation and T_g of Glass Formers. *Phys. Rev. E* **2004**, *69*, 031501.
(360) Rivera, A.; Rossler, E. A. Evidence of Secondary Relaxations in the Dielectric Spectra of Ionic Liquids. *Phys. Rev. B: Condens. Matter Mater. Phys.* **2006**, *73*, 212201.
(361) Zhao, Z. F.; Wen, P.; Wang, W. H.; Shek, C. H. Observation of Secondary Relaxation in a Fragile $Pd_{40}Ni_{10}Cu_{30}P_{20}$ Bulk Metallic Glass. *Appl. Phys. Lett.* **2006**, *89*, 071920.
(362) Wang, Z.; Yu, H. B.; Wen, P.; Bai, H. Y.; Wang, W. H. Pronounced Slow β-relaxation in La-based Bulk Metallic Glasses. *J. Phys.: Condens. Matter* **2011**, *23*, 142202.
(363) Qiao, A.; Wang, P. P.; Tao, H. Z.; Yue, Y. Z. Sub-T_g Enthalpy Relaxation in Milled and Quenched As_2S_3 Glasses. *J. Non-Cryst. Solids* **2018**, *500*, 225−230.
(364) Donth, E. *The Glass Transition: Relaxation Dynamics in Liquids and Disordered Materials*; Springer: Berlin, 2001.
(365) Kudlik, A.; Tschirwitz, C.; Blochowicz, T.; Benkhof, S.; Rossler, E. Slow Secondary Relaxation in Simple Glass Formers. *J. Non-Cryst. Solids* **1998**, *235*−*237*, 406−411.
(366) Yu, H. B.; Wang, W. H.; Bai, H. Y.; Wu, Y.; Chen, M. W. Relating Activation of Shear Transformation Zones to β Relaxations in Metallic Glasses. *Phys. Rev. B: Condens. Matter Mater. Phys.* **2010**, *81*, 220201.
(367) Sun, Q. J.; Hu, L. N.; Zhou, C.; Zheng, H. J.; Yue, Y. Z. Correlation between Supercooled Liquid Relaxation and Glass Poisson'S Ratio. *J. Chem. Phys.* **2015**, *143*, 164504.
(368) Ngai, K. L.; Wang, Z.; Gao, X. Q.; Yu, H. B.; Wang, W. H. A Connection between the Structural α-relaxation and the β-relaxation Found in Bulk Metallic Glass-formers. *J. Chem. Phys.* **2013**, *139*, 014502.
(369) Hachenberg, J.; Bedorf, D.; Samwer, K.; Richert, R.; Kahl, A.; Demetriou, M. D.; Johnson, W. L. Merging of the α and β Relaxations and Aging via the Johari-Goldstein Modes in Rapidly Quenched Metallic Glasses. *Appl. Phys. Lett.* **2008**, *92*, 131911.
(370) Miracle, D. B. A Structural Model for Metallic Glasses. *Nat. Mater.* **2004**, *3*, 697−702.
(371) Sheng, H. W.; Luo, W. K.; Alamgir, F. M.; Bai, J. M.; Ma, E. Atomic Packing and Short-to-medium-range Order in Metallic Glasses. *Nature* **2006**, *439*, 419−425.
(372) Fan, G. J.; Fecht, H. J. A Cluster Model for the Viscous Flow of Glass-Forming Liquids. *J. Chem. Phys.* **2002**, *116*, 5002−5006.
(373) Yu, H. B.; Wang, W. H.; Samwer, K. The β Relaxation in Metallic Glasses: An Overview. *Mater. Mater. Today* **2013**, *16*, 183−191.
(374) Yu, H. B.; Samwer, K.; Wu, Y.; Wang, W. H. Correlation between β Relaxation and Self-Diffusion of the Smallest Constituting Atoms in Metallic Glasses. *Phys. Rev. Lett.* **2012**, *109*, 095508.
(375) Chen, M. W. Mechanical Behavior of Metallic Glasses: Microscopic Understanding of Strength and Ductility. *Annu. Rev. Mater. Res.* **2008**, *38*, 445−469.
(376) Ngai, K. L. *Relaxation and Diffusion in Complex Systems*; Springer: New York, NY, 2011.
(377) Qiao, J. C.; Casalini, R.; Pelletier, J. M. Effect of Physical Aging on Johari-Goldstein Relaxation in La-based Bulk Metallic Glass. *J. Chem. Phys.* **2014**, *141*, 104510.
(378) Yu, H. B.; Samwer, K.; Wang, W. H.; Bai, H. Y. Chemical Influence on β-relaxations and the Formation of Molecule-like Metallic Glasses. *Nat. Commun.* **2013**, *4*, 2204.
(379) Yu, H. B.; Wang, Z.; Wang, W. H.; Bai, H. Y. Relation between β Relaxation and Fragility in LaCe-based Metallic Glasses. *J. Non-Cryst. Solids* **2012**, *358*, 869−971.
(380) Wang, Z.; Sun, B. A.; Bai, H. Y.; Wang, W. H. Evolution of Hidden Localized Flow during Glass-to-liquid Transition in Metallic Glass. *Nat. Commun.* **2014**, *5*, 5823.
(381) Evenson, Z.; Naleway, S. E.; Wei, S.; Gross, O.; Kruzic, J. J.; Gallino, I.; Possart, W.; Stommel, M.; Busch, R. β Relaxation and Low-temperature Aging in a Au-based Bulk Metallic Glass: From Elastic Properties to Atomic-scale Structure. *Phys. Rev. B: Condens. Matter Mater. Phys.* **2014**, *89*, 174204.
(382) Struik, L. C. E. *Physical Aging in Amorphous Polymers and Other Materials*; Elsevier: Netherlands, 1978.
(383) Ngai, K. L. Do Theories of Glass Transition That Address Only the α-relaxation Need a New Paradigm? *J. Non-Cryst. Solids* **2005**, *351*, 2635−2642.
(384) Ngai, K. L. Correlation between the Secondary β-relaxation Time at T_g and the Kohlrausch Exponent of the Primary α-relaxation. *Phys. A* **1998**, *261*, 36−50.
(385) Ngai, K. L. Correlation between the Secondary β-relaxation Time at T_g with the Kohlrausch Exponent of the Primary α Relaxation or the Fragility of Glass-forming Materials. *Phys. Rev. E: Stat. Phys., Plasmas, Fluids, Relat. Interdiscip. Top.* **1998**, *57*, 7346−7349.
(386) Vij, J. K.; Power, G. Physical Ageing and the Johari-Goldstein Relaxation in Molecular Glasses. *J. Non-Cryst. Solids* **2011**, *357*, 783−792.
(387) Döß, A.; Paluch, M.; Sillescu, H.; Hinze, G. Dynamics in Supercooled Polyalcohols: Primary and Secondary Relaxation. *J. Chem. Phys.* **2002**, *117*, 6582−6589.
(388) Vogel, M.; Medick, P.; Rossler, E. A. Secondary Relaxation Processes in Molecular Glasses Studied by Nuclear Magnetic Resonance Spectroscopy. *Annu. Rep. NMR Spectrosc.* **2005**, *56*, 231−299.
(389) Correia, N. T.; Alvarez, C.; Ramos, J. J. M.; Descamps, M. Molecular Motions in Molecular Glasses as Studied by Thermally Stimulated Depolarisation Currents (TSDC). *Chem. Phys.* **2000**, *252*, 151−163.
(390) Li, G.; Du, W. M.; Sakai, A.; Cummins, H. Z. Light-scattering Investigation of α and β Relaxation near the Liquid-glass Transition of the Molecular Glass Salol. *Phys. Rev. A: At., Mol., Opt. Phys.* **1992**, *46*, 3343−3356.
(391) Ngai, K. L. Johari-Goldstein Secondary Relaxation in Methylated Alkanes. *Phys. Rev. B: Condens. Matter Mater. Phys.* **2005**, *71*, 214201.
(392) Capaccioli, S.; Prevosto, D.; Lucchesi, M.; Rolla, P. A.; Casalini, R.; Ngai, K. L. Identifying the Genuine Johari−Goldstein β-relaxation by Cooling, Compressing, and Aging Small Molecular Glass-formers. *J. Non-Cryst. Solids* **2005**, *351*, 2643−2651.
(393) Liu, Y. T.; Bhandari, B.; Zhou, W. Study of Glass Transition and Enthalpy Relaxation of Mixtures of Amorphous Sucrose and Amorphous Tapioca Starch Syrup Solid by Differential Scanning Calorimetry (DSC). *J. Food Eng.* **2007**, *81*, 599−610.
(394) Sakatsuji, W.; Konishi, T.; Miyamoto, Y. Effects of Thermal History on Enthalpy Relaxation. *J. Therm. Anal. Calorim.* **2013**, *113*, 1129−1134.
(395) Hodge, I. M.; Heslin, R. Effects of Thermal History on Enthalpy Relaxation in Glasses 7. Thermal Time Constants. *J. Non-Cryst. Solids* **2010**, *356*, 1479−1487.
(396) Wang, L. M. Enthalpy Relaxation upon Glass Transition and Kinetic Fragility of Molecular Liquids. *J. Phys. Chem. B* **2009**, *113*, 5168−5171.
(397) Vyazovkin, S.; Dranca, I. Probing Beta Relaxation in Pharmaceutically Relevant Glasses by Using DSC. *Pharm. Res.* **2006**, *23*, 422−428.
(398) Berens, A. R.; Hodge, I. M. Effects of Annealing and Prior History on Enthalpy Relaxation in Glassy Polymers. 1. Experimental Study on Poly(viny1 chloride). *Macromolecules* **1982**, *15*, 756−761.
(399) Descamps, N.; Palzer, S.; Zuercher, U. The Amorphous State of Spray-dried Maltodextrin: Sub−sub-T_g Enthalpy Relaxation and Impact of Temperature and Water Annealing. *Carbohydr. Res.* **2009**, *344*, 85−90.
(400) Kudlik, A.; Benkhof, S.; Blochowicz, T.; Tschirwitz, C.; Rossler, E. The Dielectric Response of Simple Organic Glass Formers. *J. Mol. Struct.* **1999**, *479*, 201−218.
(401) Pan, P. J.; Zhu, B.; Inoue, Y. Enthalpy Relaxation and Embrittlement of Poly(L-lactide) during Physical Aging. *Macromolecules* **2007**, *40*, 9664−9671.

DOI: 10.1021/acs.chemrev.8b00510
Chem. Rev. XXXX, XXX, XXX−XXX

(402) Haque, M. K.; Kawai, K.; Suzuki, T. Glass Transition and Enthalpy Relaxation of Amorphous Lactose Glass. *Carbohydr. Res.* **2006**, *341*, 1884−1889.
(403) Urbani, R.; Sussich, F.; Prejac, S.; Cesàro, A. Enthalpy Relaxation and Glass Transition Behavior of Sucrose by Static and Dynamic DSC. *Thermochim. Acta* **1997**, *304*−*305*, 359−367.
(404) Kilburn, D.; Claude, J.; Schweizer, T.; Mezzenga, R.; Dlubek, G.; Alam, A.; Ubbink, J. Water in Glassy Carbohydrates: Opening It up at the Nanolevel. *J. Phys. Chem. B* **2004**, *108*, 12436−12441.
(405) Imran, M. M. A.; Al-Shawabkeh, A. F. Structural Relaxation due to Sub-T_g Annealing of $Se_{98}In_{1.5}Sn_{0.5}$ Chalcogenide Glass. *J. Alloys Compd.* **2010**, *500*, 237−240.
(406) Lucas, P.; King, E. A.; Gueguen, Y.; Sangleboeuf, J.; Keryvin, V.; Erdmann, R. G.; Delaizir, G.; Boussard-Pledel, C.; Bureau, B.; Zhang, X. H.; et al. Correlation Between Thermal and Mechanical Relaxation in Chalcogenide Glass Fibers. *J. Am. Ceram. Soc.* **2009**, *92*, 1986−1992.
(407) Lucas, P.; Doraiswamy, A.; King, E. A. Photoinduced Structural Relaxation in Chalcogenide Glasses. *J. Non-Cryst. Solids* **2003**, *332*, 35−42.
(408) Lucas, P.; King, E. A.; Horner, A. D.; Johnson, B. R.; Sundaram, S. K. Photostructural Relaxation in As-Se-S Glasses: Effect of Network Fragility. *J. Non-Cryst. Solids* **2006**, *352*, 2067−2072.
(409) Thorpe, M. F. Continuous Deformations in Random Networks. *J. Non-Cryst. Solids* **1983**, *57*, 355−370.
(410) Tatsumisago, M.; Halfpap, B. L.; Green, J. L.; Lindsay, S. M.; Angell, C. A. Fragility of Ge-As-Se Glass-forming Liquids in Relation to Rigidity Percolation, and the Kauzmann Paradox. *Phys. Rev. Lett.* **1990**, *64*, 1549.
(411) Stolen, S.; Grande, T.; Johnsen, H. B. Fragility Transition in $GeSe_2$-Se Liquids. *Phys. Chem. Chem. Phys.* **2002**, *4*, 3396−3399.
(412) Golovchak, R. Y.; Gorecki, C.; Kozdras, A.; Shpotyuk, O. I. Physical Ageing Effects in Vitreous Arsenic Selenides. *Solid State Commun.* **2006**, *137*, 67−69.
(413) Saiter, J. M.; Arnoult, M.; Grenet, J. Very Long Physical Ageing in Inorganic Polymers Exemplified by the Ge_xSe_{1-x} Vitreous System. *Phys. B* **2005**, *355*, 370−376.
(414) Saiter, J. M.; Assou, A.; Grenet, J.; Vautier, C. Relaxation Processes and Structural Models in Glassy Chalcogenide Materials: Application to the $Se_{1-x}Ge_x$ Alloys. *Philos. Mag. B* **1991**, *64*, 33−47.
(415) Cortes, P.; Montserrat, S.; Ledru, J.; Saiter, J. M. Enthalpy Relaxation in Ge_xSe_{1-x} Chalcogenide Glasses. *J. Non-Cryst. Solids* **1998**, *235*−*237*, 522−526.
(416) Saiter, J. M. Physical Ageing in Chalcogenide Glasses. *J. Optoelectron. Adv. M.* **2001**, *3*, 685−694.
(417) Málek, J.; Svoboda, R.; Pustková, P.; Cicmanec, P. Volume and Enthalpy Relaxation of a-Se in the Glass Transition Region. *J. Non-Cryst. Solids* **2009**, *355*, 264−272.
(418) Svoboda, R.; Pustková, P.; Málek, J. Relaxation in Ge_2Se_{98} and As_2Se_{98} Glasses. *J. Non-Cryst. Solids* **2010**, *356*, 447−455.
(419) Svoboda, R.; Honcova, P.; Málek, J. Enthalpic Relaxation in $Ge_2Sb_2Se_5$ Glass. *J. Non-Cryst. Solids* **2012**, *358*, 804−809.
(420) Svoboda, R.; Málek, J. Enthalpy Relaxation in Ge-Se Glassy System. *J. Therm. Anal. Calorim.* **2013**, *113*, 831−842.
(421) Svoboda, R.; Málek, J. Enthalpy Relaxation Kinetics of $GeTe_4$ Glass. *J. Non-Cryst. Solids* **2015**, *422*, 51−56.
(422) Imran, M. M. A.; Bhandari, D.; Saxena, N. S. Enthalpy Recovery during Structural Relaxation of $Se_{96}In_4$ Chalcogenide Glass. *Phys. B* **2001**, *293*, 394−401.
(423) Xu, D.; Liu, Y.; Tian, Y. J.; Wang, L. M. Communication: Enthalpy Relaxation in a Metal-organic Zeolite Imidazole Framework (ZIF-4) Glass-former. *J. Chem. Phys.* **2017**, *146*, 121101.
(424) Zhou, C.; Stepniewska, M.; Longley, L.; Chater, P. A.; Keen, D. A.; Bennett, T. D.; Yue, Y. Z. Thermodynamic Features and Enthalpy Relaxation in a Metal-organic Framework Glass. *Phys. Chem. Chem. Phys.* **2018**, *20*, 18291−18296.
(425) Ediger, M. D. Spatially Heterogeneous Dynamics in Supercooled Liquids. *Annu. Rev. Phys. Chem.* **2000**, *51*, 99−128.
(426) Sillescu, H. Heterogeneity at the Glass Transition: A Review. *J. Non-Cryst. Solids* **1999**, *243*, 81−108.
(427) Glotzer, S. C. Spatially Heterogeneous Dynamics in Liquids: Insights from Simulation. *J. Non-Cryst. Solids* **2000**, *274*, 342−355.
(428) Matharoo, G. S.; Razul, M. S. G.; Poole, P. H. Structural and Dynamical Heterogeneity in a Glass-forming Liquid. *Phys. Rev. E* **2006**, *74*, No. 050502(R).
(429) Huo, L. S.; Zeng, J. F.; Wang, W. H.; Liu, C. T.; Yang, Y. The Dependence of Shear Modulus on Dynamic Relaxation and Evolution of Local Structural Heterogeneity in a Metallic Glass. *Acta Mater.* **2013**, *61*, 4329−4338.
(430) Li, W. D.; Bei, H.; Tong, Y.; Dmowski, W.; Gao, Y. F. Structural Heterogeneity Induced Plasticity in Bulk Metallic Glasses: From Well-relaxed Fragile Glass to Metal-like Behavior. *Appl. Phys. Lett.* **2013**, *103*, 171910.
(431) Yue, Y. Z. Experimental Evidence for the Existence of an Ordered Structure in a Silicate Liquid above Its *Liquidus* Temperature. *J. Non-Cryst. Solids* **2004**, *345*−*346*, 523−527.
(432) Yue, Y. Z. Calorimetric Studies of the Structural Heterogeneity of Silicate Liquids. *Ceram. Trans.* **2004**, *170*, 31−45.
(433) Liu, Y. H.; Wang, D.; Nakajima, K.; Zhang, W.; Hirata, A.; Nishi, T.; Inoue, A.; Chen, M. W. Characterization of Nanoscale Mechanical Heterogeneity in a Metallic Glass by Dynamic Force Microscopy. *Phys. Rev. Lett.* **2011**, *106*, 125504.
(434) Schmidt-Rohr, K.; Spiess, H. W. Nature of Nonexponential Loss of Correlation above the Glass Transition Investigated by Multidimensional NMR. *Phys. Rev. Lett.* **1991**, *66*, 3020.
(435) Li, M. Z.; Wang, C. Z.; Hao, S. G.; Kramer, M. J.; Ho, K. M. Structural Heterogeneity and Medium-range Order in Zr_xCu_{100-x} Metallic Glasses. *Phys. Rev. B: Condens. Matter Mater. Phys.* **2009**, *80*, 184201.
(436) Hu, L. N.; Yue, Y. Z.; Zhang, C. Z. Abnormal Sub-T_g Enthalpy Relaxation in the CuZrAl Metallic Glasses Far from Equilibrium. *Appl. Phys. Lett.* **2011**, *98*, 081904.
(437) Hu, L. N.; Zhou, C.; Zhang, C. Z.; Yue, Y. Z. Thermodynamic Anomaly of the Sub-T_g Relaxation in Hyperquenched Metallic Glasses. *J. Chem. Phys.* **2013**, *138*, 174508.
(438) Yue, Y. Z. Features of the Relaxation in Hyperquenched Inorganic Glasses during Annealing. *Phys. Chem. Glasses* **2005**, *46*, 354−358.
(439) Zhang, Y. F.; Zhao, D. H.; Yue, Y. Z. Phase Transitions and Glass Transition in a Hyperquenched Silica-alumina Glass. *J. Am. Ceram. Soc.* **2017**, *100*, 3434−3439.
(440) Zhang, Y. F.; Liu, S. J.; Tao, H. Z.; Zhao, D. H.; Yue, Y. Z. Structural Response to Sub-T_g Annealing in a hyperquenched SiO_2-Al_2O_3 Glass. *J. Alloys Compd.* **2018**, *741*, 331−336.
(441) Takahashi, Y.; Osada, M.; Masai, H.; Fujiwara, T. Structural Heterogeneity and Homogeneous Nucleation of $1BaO\text{-}2SiO_2$ glass. *Appl. Phys. Lett.* **2009**, *94*, 211907.
(442) Kjeldsen, J.; Yue, Y. Z.; Bragatto, C. B.; Rodrigues, A. C. M. Electronic Conductivity of Vanadium-Tellurite Glass-Ceramics. *J. Non-Cryst. Solids* **2013**, *378*, 196−200.
(443) Zhang, Y. F.; Wang, P. X.; Li, G. D.; Fan, J. H.; Gao, C. W.; Wang, Z. Y.; Yue, Y. Z. Clarifying the Charging Induced Nucleation in Glass Anode of Li-ion Batteries and Its Enhanced Performances. *Nano Energy* **2019**, *57*, 592−599.
(444) Zhang, Y. F.; Wang, P. X.; Zheng, T.; Li, D. M.; Li, G. D.; Yue, Y. Z. Enhancing Li-ion Battery Anode Performances via Disorder/order Engineering. *Nano Energy* **2018**, *49*, 596−602.
(445) Zhou, C.; Hu, L. N.; Sun, Q. J.; Zheng, H. J.; Zhang, C. Z.; Yue, Y. Z. Structural Evolution during Fragile-to-strong Transition in CuZr(Al) Glass-forming Liquids. *J. Chem. Phys.* **2015**, *142*, 064508.
(446) Huth, H.; Minakov, A. A.; Serghei, A.; Kremer, F.; Schick, C. Differential AC-chip Calorimeter for Glass Transition Measurements in Ultra Thin Polymeric Films. *Eur. Phys. J.: Spec. Top.* **2007**, *141*, 153−160.
(447) Zhou, D.; Huth, H.; Gao, Y.; Xue, G.; Schick, C. Calorimetric Glass Transition of Poly(2,6-dimethyl-1,5-phenylene oxide) Thin Films. *Macromolecules* **2008**, *41*, 7662−7666.

DOI: 10.1021/acs.chemrev.8b00510
Chem. Rev. XXXX, XXX, XXX−XXX

(448) Dhotel, A.; Rijal, B.; Delbreilh, L.; Dargent, E.; Saiter, A. Combining Flash DSC, DSC and Broadband Dielectric Spectroscopy to Determine Fragility. *J. Therm. Anal. Calorim.* **2015**, *121*, 453−461.
(449) Pilar, R.; Honcová, P.; Schulz, G.; Schick, C.; Málek, J. Enthalpy Relaxation of Selenium Observed by Fast Scanning Calorimetry. *Thermochim. Acta* **2015**, *603*, 142−148.
(450) Pogatscher, S.; Leutenegger, D.; Hagmann, A.; Uggowitzer, P. J.; Löffler, J. F. Characterization of Bulk Metallic Glasses via Fast Differential Scanning Calorimetry. *Thermochim. Acta* **2014**, *590*, 84−90.
(451) Gao, S.; Koh, Y. P.; Simon, S. L. Calorimetric Glass Transition of Single Polystyrene Ultrathin Films. *Macromolecules* **2013**, *46*, 562−570.
(452) Gao, S.; Simon, S. L. Measurement of the Limiting Fictive Temperature over Five Decades of Cooling and Heating Rates. *Thermochim. Acta* **2015**, *603*, 123−127.
(453) Shamim, N.; Koh, Y. P.; Simon, S. L.; McKenna, G. B. Glass Transition Temperature of Thin Polycarbonate Films Measured by Flash Differential Scanning Calorimetry. *J. Polym. Sci., Part B: Polym. Phys.* **2014**, *52*, 1462−1468.
(454) Schawe, J. E. K. Measurement of the Thermal Glass Transition of Polystyrene in A Cooling Rate Range of More than Six Decades. *Thermochim. Acta* **2015**, *603*, 128−134.
(455) Williams, M. L.; Landel, R. F.; Ferry, J. D. The Temperature Dependence of Relaxation Mechanisms in Amorphous Polymers and Other Glass-forming Liquids. *J. Am. Chem. Soc.* **1955**, *77*, 3701−3707.
(456) Fakhraai, Z.; Forrest, J. A. Probing Slow Dynamics in Supported Thin Polymer Films. *Phys. Rev. Lett.* **2005**, *95*, 025701.
(457) Arranz-Andrés, J.; Cerrada, M. L.; Pérez, E. Fast Scanning Calorimetry Study of the Structural Relaxation in A Random Propylene-co-1-octene Copolymer. *Thermochim. Acta* **2015**, *603*, 116−122.
(458) Androsch, R.; Schick, C.; Schmelzer, J. W. P. Sequence of Enthalpy Relaxation, Homogeneous Crystal Nucleation and Crystal Growth in Glassy Polyamide 6. *Eur. Polym. J.* **2014**, *53*, 100−108.
(459) Wang, J. Q.; Shen, Y.; Perepezko, J. H.; Ediger, M. D. Increasing the Kinetic Stability of Bulk Metallic Glasses. *Acta Mater.* **2016**, *104*, 25−32.
(460) Wang, J. Q.; Chen, N.; Liu, P.; Wang, Z.; Louzguine-Luzgin, D. V.; Chen, M. W.; Perepezko, J. H. The Ultrastable Kinetic Behavior of An Au-based Nanoglass. *Acta Mater.* **2014**, *79*, 30−36.
(461) Monnier, X.; Saiter, A.; Dargent, E. Physical Aging in PLA through Standard DSC and Fast Scanning Calorimetry Investigations. *Thermochim. Acta* **2017**, *648*, 13−22.
(462) Badrinarayanan, P.; Zheng, W.; Li, Q.; Simon, S. L. The Glass Transition Temperature versus the Fictive Temperature. *J. Non-Cryst. Solids* **2007**, *353*, 2603−2612.
(463) Evans, C. M.; Deng, H.; Jager, W. F.; Torkelson, J. M. Fragility is a Key Parameter in Determining the Magnitude of T_g-Confinement Effects in Polymer Films. *Macromolecules* **2013**, *46*, 6091−6103.
(464) Vogel, H. The Law of the Relation between the Viscosity of Liquids and the Temperature. *Phys. Z.* **1921**, *22*, 645−646.
(465) Koh, Y. P.; Grassia, L.; Simon, S. L. Structural Recovery of A Single Polystyrene Thin Film using Nanocalorimetry to Extend the Aging Time and Temperature Range. *Thermochim. Acta* **2015**, *603*, 135−141.
(466) Koh, Y. P.; Gao, S.; Simon, S. L. Structural Recovery of A Single Polystyrene Thin Film using Flash DSC at Low Aging Temperatures. *Polymer* **2016**, *96*, 182−187.
(467) Koh, Y. P.; Simon, S. L. The Glass Transition and Enthalpy Recovery of A Single Polystyrene Ultrathin Film using Flash DSC. *J. Chem. Phys.* **2017**, *146*, 203329.
(468) Echeverría, I.; Kolek, P. L.; Plazek, D. J.; Simon, S. L. Enthalpy Recovery: Creep and Creep-recovery Measurements during Physical Aging of Amorphous Selenium. *J. Non-Cryst. Solids* **2003**, *324*, 242−255.
(469) Svoboda, R.; Pustková, P.; Málek, J. Relaxation Behavior of Glassy Selenium. *J. Phys. Chem. Solids* **2007**, *68*, 850−854.
(470) Matsuishi, K.; Nogi, K.; Ogura, H.; Onari, S.; Arai, T. Dynamics of Glass Transition of Bulk a-Se and Se Clusters Incorporated into Zeolites. *J. Non-Cryst. Solids* **1998**, *230*, 799−803.
(471) Svoboda, R.; Pustková, P.; Málek, J. Volume Relaxation of a-Se Studied by Mercury Dilatometry. *J. Non-Cryst. Solids* **2006**, *352*, 4793−4799.
(472) Cubeta, U. S. *Fast Scanning Calorimetry Studies of Molecular Dynamics in Crystals, Liquids, and Glasses*. The George Washington University, Ph.D. thesis, 2018.
(473) Ediger, M. D.; Angell, C. A.; Nagel, S. R. Supercooled Liquids and Glasses. *J. Phys. Chem.* **1996**, *100*, 13200−13212.
(474) Schawe, J. E. K. A. Comparison of Different Evaluation Methods in Modulated Temperature DSC. *Thermochim. Acta* **1995**, *260*, 1−16.
(475) Schawe, J. E. K. Principles for the Interpretation of Modulated Temperature DSC measurements. Part 1. Glass transition. *Thermochim. Acta* **1995**, *261*, 183−194.
(476) Birge, N. O.; Nagel, S. R. Specific-Heat Spectroscopy of the Glass Transition. *Phys. Rev. Lett.* **1985**, *54*, 2674.
(477) Birge, N. O. Specific-heat Spectroscopy of Glycerol and Propylene Glycol near the Glass Transition. *Phys. Rev. B: Condens. Matter Mater. Phys.* **1986**, *34*, 1631−1642.
(478) Mauro, J. C.; Loucks, R. J.; Sen, S. Response to "Comment on 'Heat Capacity, Enthalpy Fluctuations, and Configurational Entropy in Broken Ergodic Systems'" [J. Chem. Phys. 134, 147101 (2011)]. *J. Chem. Phys.* **2011**, *134*, 147102.
(479) Gulbiten, O.; Mauro, J. C.; Guo, X.; Boratav, O. N. Viscous Flow of Medieval Cathedral Glass. *J. Am. Ceram. Soc.* **2018**, *101*, 5−11.
(480) Garden, J. L. Macroscopic Non-equilibrium Thermodynamics in Dynamic Calorimetry. *Thermochim. Acta* **2007**, *452*, 85−105.
(481) Toll, J. S. Causality and the Dispersion Relation: Logical Foundations. *Phys. Rev.* **1956**, *104*, 1760−1770.
(482) Schawe, J. E. K.; Höhne, G. W. H. The Analysis of Temperature Modulated DSC Measurements by Means of the Linear Response Theory. *Thermochim. Acta* **1996**, *287*, 213−223.
(483) Reading, M. The Use of Modulated Temperature Programs in Thermal Methods. *J. Therm. Anal. Calorim.* **2001**, *64*, 7.
(484) Yang, G.; Gulbiten, O.; Gueguen, Y.; Bureau, B.; Sangleboeuf, J.-C.; Roiland, C.; King, E. A.; Lucas, P. Fragile-strong Behavior in the As_xSe_{1-x} Glass Forming System in Relation to Structural Dimensionality. *Phys. Rev. B: Condens. Matter Mater. Phys.* **2012**, *85*, 144107.
(485) Simon, S. L.; McKenna, G. B. The Effects of Structural Recovery and Thermal Lag in Temperature-nodulated DSC Measurements. *Thermochim. Acta* **1997**, *307*, 1−10.
(486) Simon, S. L.; McKenna, G. B. Quantitative Analysis of Errors in TMDSC in the Glass Transition Region. *Thermochim. Acta* **2000**, *348*, 77−89.
(487) Bechgaard, T. K.; Gulbiten, O.; Mauro, J. C.; Smedskjaer, M. M. Parametric Study of Temperature-modulated Differential Scanning Calorimetry for High-temperature Oxide Glasses with Varying Fragility. *J. Non-Cryst. Solids* **2018**, *484*, 84−94.
(488) Lucas, P.; King, E. A.; Gulbiten, O.; Yarger, J. L.; Soignard, E.; Bureau, B. Bimodal Phase Percolation Model for the Structure of Ge-Se Glasses and the Existence of the Intermediate Phase. *Phys. Rev. B: Condens. Matter Mater. Phys.* **2009**, *80*, 214114.
(489) Golovchak, R.; Jain, H.; Shpotyuk, O.; Kozdras, A.; Saiter, A.; Saiter, J. M. Experimental Verification of the Reversibility Window Concept in Binary As-Se Glasses Subjected to A Long-term Physical Aging. *Phys. Rev. B: Condens. Matter Mater. Phys.* **2008**, *78*, 014202.
(490) Shpotyuk, O.; Kozdras, A.; Saiter, J.-M.; Golovchak, R. Comment on "Molecular Origin of Aging of Pure Se glass: Growth of Inter-chain Structural Correlations, Network Compaction, and Partial Ordering,". *J. Chem. Phys.* **2018**, *148*, 157101.
(491) Bhageria, R.; Gunasekera, K.; Boolchand, P.; Micoulau, t. M. Fragility and Molar Volumes of Non-stoichiometric Chalcogenides: The Crucial Role of Melt/Glass Homogenization. *Phys. Status Solidi B* **2014**, *251*, 1322−1329.

DOI: 10.1021/acs.chemrev.8b00510
Chem. Rev. XXXX, XXX, XXX−XXX

(492) Černošková, E.; Qu, T.; Mamedov, S.; Černošek, Z.; Holubová, J.; Boolchand, P. Reversibility Window in As-quenched Ge-As-S Glasses. *J. Phys. Chem. Solids* **2005**, *66*, 185−189.
(493) Feng, X.; Bresser, W. J.; Boolchand, P. Direct Evidence for Stiffness Threshold in Chalcogenide Glasses. *Phys. Rev. Lett.* **1997**, *78*, 4422−4425.
(494) Georgiev, D. G.; Boolchand, P.; Micoulaut, M. Rigidity Transitions and Molecular Structure of As_xSe_{1-x} Glasses. *Phys. Rev. B: Condens. Matter Mater. Phys.* **2000**, *62*, R9228−R9231.
(495) Bhosle, S.; Gunasekera, K.; Boolchand, P.; Micoulaut, M. Melt Homogenization and Self-Organization in Chalcogenides-Part II. *Int. J. Appl. Glass. Sci.* **2012**, *3*, 205−220.
(496) Vempati, U.; Boolchand, P. The Thermally Reversing Window in Ternary Ge_x P_x S_{1-2x} Glasses. *J. Phys.: Condens. Matter* **2004**, *16*, S5121.
(497) Wang, Y.; Wells, J.; Georgiev, D. G.; Boolchand, P.; Jackson, K.; Micoulaut, M. Sharp Rigid to Floppy Phase Transition Induced by Dangling Ends in a Network Glass. *Phys. Rev. Lett.* **2001**, *87*, 185503.
(498) Taylor, H. E. The Dielectric Relaxation Spectrum of Glass. *Trans. Faraday Soc.* **1956**, *52*, 873−881.
(499) Kakiuchida, H.; Saito, K.; Ikushima, A. J. Dielectric Relaxation in Silica Glass. *J. Appl. Phys.* **1999**, *86*, 5983−5987.
(500) Simon, S. L.; McKenna, G. B. Interpretation of the dynamic heat capacity observed in glass-forming liquids. *J. Chem. Phys.* **1997**, *107*, 8678−8685.
(501) Reading, M. Comments on "A Comparison of Different Evaluation Methods in Modulated-Temperature DSC". *Thermochim. Acta* **1997**, *292*, 179−187.
(502) Guo, X.; Mauro, J. C.; Allan, D. C.; Yue, Y. On the Frequency Correction in Temperature-Modulated Differential Scanning Calorimetry of the Glass Transition. *J. Non-Cryst. Solids* **2012**, *358*, 1710−1715.
(503) Carpentier, L.; Bustin, O.; Descamps, M. Temperature-modulated Differential Scanning Calorimetry as a Specific Heat Spectroscopy. *J. Phys. D: Appl. Phys.* **2002**, *35*, 402.
(504) Alvarez, C.; Moura-Ramos, J. J. The Glass Transition Relaxation in a Side-chain Liquid Crystalline Polymer Studied by Modulated Temperature Differential Scanning Calorimetry. *Phys. Chem. Chem. Phys.* **2000**, *2*, 4743−4747.
(505) Yang, G.; Bureau, B.; Rouxel, T.; Gueguen, Y.; Gulbiten, O.; Roiland, C.; Soignard, E.; Yarger, J. L.; Troles, J.; Sangleboeuf, J.-C.; Lucas, P. Correlation between Structure and Physical Properties of Chalcogenide Glasses in the As_xSe_{1-x} System. *Phys. Rev. B: Condens. Matter Mater. Phys.* **2010**, *82*, 195206.
(506) Hutchinson, J. M.; Tong, A. B.; Jiang, Z. Aging of Polycarbonate Studied by Temperature Modulated Differential Scanning Calorimetry. *Thermochim. Acta* **1999**, *335*, 27−42.
(507) Golovchak, R.; Oelgoetz, J.; Vlcek, M.; Esposito, A.; Saiter, A.; Saiter, J.-M.; Jain, H. Complex Structural Rearrangements in As-Se Glasses. *J. Chem. Phys.* **2014**, *140*, 054505.
(508) Mauro, J. C.; Uzun, S. S.; Bras, W.; Sen, S. Nonmonotonic Evolution of Density Fluctuations during Glass Relaxation. *Phys. Rev. Lett.* **2009**, *102*, 155506.
(509) Fukawa, Y.; Matsuda, Y.; Kawashima, M.; Kojima, S. Determination of Complex-specific Heat and Fragility of Sodium Borate Glasses by Temperature-modulated DSC. *J. Therm. Anal. Calorim.* **2010**, *99*, 39−44.
(510) Bechgaard, T. K.; Gulbiten, O.; Mauro, J. C.; Hu, Y.; Bauchy, M.; Smedskjær, M. M. Temperature-modulated Differential Scanning Calorimetry Analysis of High-temperature Silicate Glasses. *Am. Ceram. Soc. Bull.* **2018**, *97*, 31−33.
(511) Matsuda, Y.; Fukawa, Y.; Ike, Y.; Kodama, M.; Kojima, S. Dynamic Specific Heat, Glass Transition, and Non-Debye Nature of Thermal Relaxation in Lithium Borate Glasses. *J. Phys. Soc. Jpn.* **2008**, *77*, 084602.
(512) Cole, K. S.; Cole, R. H. Dispersion and Absorption in Dielectrics I. Alternating Current Characteristics. *J. Chem. Phys.* **1941**, *9*, 341−351.
(513) Havriliak, S.; Negami, S. A Complex Plane Representation of Dielectric and Mechanical Relaxation Processes in Some Polymers. *Polymer* **1967**, *8*, 161−210.
(514) Alvarez, F.; Alegra, A.; Colmenero, J. Relationship between the Time-domain Kohlrausch-Williams-Watts and Frequency-domain Havriliak-Negami Relaxation Functions. *Phys. Rev. B: Condens. Matter Mater. Phys.* **1991**, *44*, 7306−7312.
(515) Boolchand, P.; Goodman, B. Glassy Materials with Enhanced Thermal Stability. *MRS Bull.* **2017**, *42*, 23−28.
(516) Selvanathan, D.; Bresser, W. J.; Boolchand, P.; Goodman, B. Thermally Reversing Window and Stiffness Transitions in Chalcogenide Glasses. *Solid State Commun.* **1999**, *111*, 619−624.
(517) Shatnawi, M. T. M.; Farrow, C. L.; Chen, P.; Boolchand, P.; Sartbaeva, A.; Thorpe, M. F.; Billinge, S. J. L. Search for a Structural Response to the Intermediate Phase in Ge_xSe_{1-x} Glasses. *Phys. Rev. B: Condens. Matter Mater. Phys.* **2008**, *77*, 094134.
(518) Zeidler, A.; Salmon, P. S.; Whittaker, D. A. J.; Pizzey, K. J.; Hannon, A. C. Topological Ordering and Viscosity in the Glass-Forming Ge-Se System: The Search for a Structural or Dynamical Signature of the Intermediate Phase. *Front. Mater.* **2017**, *4*, 32.
(519) Mauro, J. C.; Varshneya, A. K. Multiscale Modeling of Arsenic Selenide Glass. *J. Non-Cryst. Solids* **2007**, *353*, 1226−1231.
(520) Bhosle, S.; Gunasekera, K.; Boolchand, P.; Micoulaut, M. Melt Homogenization and Self-Organization in Chalcogenides-Part II. *Int. J. Appl. Glass. Sci.* **2012**, *3*, 205−220.
(521) Li, P.; Zhang, Y.; Chen, Z.; Gao, P.; Wu, T.; Wang, L.-M. Relaxation Dynamics in the Strong Chalcogenide Glass-former of $Ge_{22}Se_{78}$. *Sci. Rep.* **2017**, *7*, 40547.
(522) Gunasekera, K.; Bhosle, S.; Boolchand, P.; Micoulaut, M. Superstrong Nature of Covalently Bonded Glass-forming Liquids at Select Compositions. *J. Chem. Phys.* **2013**, *139*, 164511.
(523) Karpukhina, N.; Hill, R. G.; Law, R. V. Crystallisation in Oxide Glasses - A Tutorial Review. *Chem. Soc. Rev.* **2014**, *43*, 2174−2186.
(524) Komatsu, T. Design and Control of Crystallization in Oxide Glasses. *J. Non-Cryst. Solids* **2015**, *428*, 156−175.
(525) Rodrigues, A. M.; Cassar, D. R.; Fokin, V. M.; Zanotto, E. D. Crystal Growth and Viscous Flow in Barium Disilicate Glass. *J. Non-Cryst. Solids* **2018**, *479*, 55−61.
(526) Zanotto, E. D. Glass Crystallization Research - A 36-Year Retrospective. Part I, Fundamental Studies. *Int. J. Appl. Glass Sci.* **2013**, *4*, 105−116.
(527) Zanotto, E. D. Glass Crystallization Research - A 36-Year Retrospective. Part II, Methods Of Study And Glass-Ceramics. *Int. J. Appl. Glass Sci.* **2013**, *4*, 117−124.
(528) Höland, W.; Beall, G. *Glass-ceramic Technology*, 2nd ed.; The American Ceramic Society & John Wiley and Sons Inc.: USA, 2012.
(529) Zanotto, E. D. A. Bright Future for Glass-Ceramics. *Am. Ceram. Soc. Bull.* **2010**, *89*, 19−27.
(530) Montazerian, M.; Zanotto, E. D. A Guided Walk through Larry Hench's Monumental Discoveries. *J. Mater. Sci.* **2017**, *52*, 8695−8732.
(531) Montazerian, M.; Zanotto, E. D. Bioactive and Inert Dental Glass-Ceramics. *J. Biomed. Mater. Res., Part A* **2017**, *105*, 619−639.
(532) Montazerian, M.; Zanotto, E. D. History and Trends of Bioactive Glass-Ceramics. *J. Biomed. Mater. Res., Part A* **2016**, *104*, 1231−1249.
(533) Fokin, V. M.; Yuritsyn, N. S.; Zanotto, E. D. Nucleation and Crystallization Kinetics in Silicate Glasses: Theory and Experiment. In *Nucleation Theory and Applications*; Schmelzer, J. W. P., Ed.; Wiley: USA, 2005; pp 74−125.
(534) Zanotto, E. D.; Tsuchida, J. E.; Schneider, J. F.; Eckert, H. Thirty-year Quest for Structure-Nucleation Relationships in Oxide Glasses. *Int. Mater. Rev.* **2015**, *60*, 376−391.
(535) Schmelzer, J. W. P. Introduction. In *Nucleation Theory and Applications*; Schmelzer, J. W. P., Ropke, G., Priezzhev, V. B., Eds.; Joint Institute for Nuclear Research Publishing House: Dubna, Russia, 1999; p 1.

DOI: 10.1021/acs.chemrev.8b00510
Chem. Rev. XXXX, XXX, XXX−XXX

(536) Tammann, G. Uber die Abhangigkeit der Zajl der Kerne. *Z. Phys. Chem.* **1898**, *25*, 441−479.
(537) Fokin, V. M.; Zanotto, E. D.; Yuritsyn, N. S.; Schmelzer, J. W. P. Homogeneous Crystal Nucleation in Silicate Glasses: A 40 Years Perspective. *J. Non-Cryst. Solids* **2006**, *352*, 2681−2714.
(538) Marotta, A.; Buri, A.; Branda, F. Nucleation in Glass and Differential Thermal Analysis. *J. Mater. Sci.* **1981**, *16*, 341−344.
(539) Marotta, A.; Buri, A.; Branda, F.; Saiello, S. Nucleation and Crystallization of $Li_2O.2SiO_2$ Glass - A DTA Study. *Adv. Ceram.* **1982**, *4*, 146−152.
(540) Marotta, A.; Buri, A.; Branda, F.; Saiello, S. Nucleation in Glass-Forming Systems. A DTA Study. *Thermochim. Acta* **1985**, *85*, 231−234.
(541) Ray, C. S.; Day, D. E. Determining the Nucleation Rate Curve for Lithium Disilicate Glass by Differential Thermal Analysis. *J. Am. Ceram. Soc.* **1990**, *73*, 439−442.
(542) Xu, X. J.; Ray, C. S.; Day, D. E. Nucleation and Crystallization of $Na_2O{\cdot}2CaO{\cdot}3SiO_2$ Glass by Differential Thermal Analysis. *J. Am. Ceram. Soc.* **1991**, *74*, 909−914.
(543) Ray, C. S.; Day, D. E. An Analysis of Nucleation-Rate Type of Curves in Glass as Determined by Differential Thermal Analysis. *J. Am. Ceram. Soc.* **1997**, *80*, 3100−3108.
(544) Weinberg, M. C. Interpretation of DTA Experiments Used for Crystal Nucleation Rate Determinations. *J. Am. Ceram. Soc.* **1991**, *74*, 1905−1909.
(545) Kelton, K. F. Estimation of the Nucleation Rate by Differential Scanning Calorimetry. *J. Am. Ceram. Soc.* **1992**, *75*, 2449−2452.
(546) Fokin, V. M.; Cabral, A. A.; Reis, R. M. C. V.; Nascimento, M. L. F.; Zanotto, E. D. Critical Assessment of DTA-DSC Methods for the Study of Nucleation Kinetics in Glasses. *J. Non-Cryst. Solids* **2010**, *356*, 358−367.
(547) Xia, X.; Dutta, I.; Mauro, J. C.; Aitken, B. G.; Kelton, K. F. Temperature Dependence of Crystal Nucleation in $BaO{\cdot}2SiO_2$ and $5BaO{\cdot}8SiO_2$ Glasses Using Differential Thermal Analysis. *J. Non-Cryst. Solids* **2017**, *459*, 45−50.
(548) Ray, C. S.; Fang, X.; Day, D. E. New Method for Determining the Nucleation and Crystal-Growth Rates in Glasses. *J. Am. Ceram. Soc.* **2000**, *83*, 865−872.
(549) Ranasinghe, K. S.; Ray, C. S.; Day, D. E. A Generalized Method for Determining the Crystal Nucleation and Growth Rates in Glasses by Differential Thermal Analysis. *J. Mater. Sci.* **2002**, *37*, 547−555.
(550) Johnson, W. A.; Mehl, R. F. Reaction Kinetics in Processes of Nucleation and Growth. *Am. Inst. Min. Metall. Eng.* **1939**, *135*, 416−458.
(551) Avrami, M. Kinetics of Phase Change. I: General Theory. *J. Chem. Phys.* **1939**, *7*, 1103−1112.
(552) Yerofyeyev, B. V. Generalized Equation of Chemical Kinetics and Its Application to the Solid-State Reactions. *Dokl. Akad. Nauk USSR* **1964**, *52*, 511 (in Russian). .
(553) Kolmogorov, A. N. Statistical Theory of Crystallization of Metals. *Izv. Akad. Nauk. USSR* **1937**, *1*, 355 (in Russian). .
(554) Ranasinghe, K. S.; Wei, P. F.; Kelton, K. F.; Ray, C. S.; Day, D. E. Verification of an Analytical Method for Measuring Crystal Nucleation Rates in Glasses from DTA Data. *J. Non-Cryst. Solids* **2004**, *337*, 261−267.
(555) Cabral, A. A.; Ferreira, E. B.; Villas-Boas, M. O. C.; Zanotto, E. D. On the Determination of the Concentration of Crystal Nuclei in Glasses by DSC. *J. Am. Ceram. Soc.* **2013**, *96*, 2817−2823.
(556) Deubener, J.; Montazerian, M.; Krüger, S.; Peitl, O.; Zanotto, E. D. Heating Rate Effects in Time-Dependent Homogeneous Nucleation in Glasses. *J. Non-Cryst. Solids* **2017**, *474*, 1−8.
(557) Ranasinghe, K. S.; Ray, C. S.; Day, D. E.; Humble, G. Heterogeneous Nucleation on Platinum Doped $Li_2O{\cdot}2SiO_2$ Glass by Differential Thermal Analysis. *J. Non-Cryst. Solids* **2017**, *473*, 141−146.
(558) Gupta, P. K.; Baranta, G.; Denry, I. L. DTA Peak Shift Studies of Primary Crystallization in Glasses. *J. Non-Cryst. Solids* **2003**, *317*, 254−269.
(559) Uttormark, M. J.; Zanter, J. W.; Perepezko, J. H. Repeated Nucleation In an Undercooled Aluminum Droplet. *J. Cryst. Growth* **1997**, *177*, 258−264.
(560) Wilde, G.; Sebright, J. L.; Perepezko, J. H. Bulk Liquid Undercooling and Nucleation in Gold. *Acta Mater.* **2006**, *54*, 4759−4769.
(561) Yang, D.; Abyzov, A. S.; Zhuravlev, E.; Gao, Y.; Schmelzer, J. W. P.; Schick, C. Size and Rate Dependence of Crystal Nucleation in Single Tin Drops by Fast Scanning Calorimetry. *J. Chem. Phys.* **2013**, *138*, 054501.
(562) Heneghan, A. F.; Wilson, P. W.; Haymet, A. D. J. Heterogeneous Nucleation of Supercooled Water, and the Effect of an Added Catalyst. *Proc. Natl. Acad. Sci. U. S. A.* **2002**, *99*, 9631−9634.
(563) Maeda, M.; Wells, D.; Becker, N. C.; Hartley, P. G.; Wilson, P. W.; Haymet, A. D. J.; Kozielski, K. A. Development of a High Pressure Automated Lag Time Apparatus for Experimental Studies and Statistical Analyses of Nucleation and Growth of Gas Hydrates. *Rev. Sci. Instrum.* **2011**, *82*, 065109.
(564) Krüger, S.; Deubener, J. Stochastic Nature of the Liquid-To-Crystal Heterogeneous Nucleation of Supercooled Lithium Disilicate Liquid. *J. Non-Cryst. Solids* **2014**, *388*, 6−9.
(565) Krüger, S.; Deubener, J. The TTT Curves of the Heterogeneous and Homogeneous Crystallization of Lithium Disilicate − A Stochastic Approach to Crystal Nucleation. *Front. Mater.* **2016**, *3*, 42.
(566) Perepezko, J. H.; Hebert, R. J.; Tong, W. S.; Hamann, J.; Rösner, H. R.; Wilde, G. Nanocrystallization Reactions in Amorphous Aluminum Alloys. *Mater. Trans.* **2003**, *44*, 1982−1992.
(567) Sieber, H.; Park, J. S.; Weissmüller, J.; Perepezko, J. H. Structural Evolution and Phase Formation in Cold-rolled Aluminum-nickel Multilayers. *Acta Mater.* **2001**, *49*, 1139−1151.
(568) Krüger, S.; Deubener, J. Heterogeneous Surface Nucleation of Lithium Disilicate Glass: An Isothermal DSC Study. *J. Non-Cryst. Solids* **2015**, *417−418*, 45−51.
(569) Krüger, S.; Deubener, J. Lag Time to Crystal Nucleation of Supercooled Lithium Disilicate Melts: A Test of the Classical Nucleation Theory. *J. Non-Cryst. Solids* **2015**, *426*, 1−6.
(570) Krüger, S.; Deubener, J. Thermal analysis of Repetitive Single Crystallization Events in Glass-forming Liquids at Low Undercooling. *J. Non-Cryst. Solids* **2018**, *501*, 36−42.
(571) Reis, R. M. C. V.; Fokin, V. M.; Zanotto, E. D. Determination of Crystal Growth Rates in Glasses over a Temperature Range Using a Single DSC Run. *J. Am. Ceram. Soc.* **2016**, *99*, 2001−2008.
(572) Moesgaard, M.; Pedersen, H. D.; Yue, Y. Z.; Nielsen, E. R. Crystallization in Stone Wool Fibres. *J. Non-Cryst. Solids* **2007**, *353*, 1101−1108.
(573) Neuville, D. R., Cormier, L., Caurant, D., Montagne, L., Eds. *From Glass to Crystal. Nucleation, Growth and Phase Separation: From Research to Applications*, 1st ed.; EDP Sciences: Les Ulis, 2017.
(574) Illeková, E.; Šesták, J. Crystallization of Metallic Micro-, Nano-, and Non-Crystalline Alloys. In *Thermal Analysis of Micro, Nano- and Non-Crystalline Materials: Transformation, Crystallization, Kinetics and Thermodynamics*; Šesták, J., Šimon, P., Eds.; Springer: Netherlands, 2013; Chapter 13.
(575) Ray, C. S.; Huang, W.; Day, D. E. Crystallization Kinetics of a Lithia−Silica Glass: Effect of Sample Characteristics and Thermal Analysis Measurement Techniques. *J. Am. Ceram. Soc.* **1991**, *74*, 60−66.
(576) Ray, C. S.; Zhang, T.; Reis, S. T.; Brow, R. K. Determining Kinetic Parameters for Isothermal Crystallization of Glasses. *J. Am. Ceram. Soc.* **2007**, *90*, 769−773.
(577) Blaine, R. L.; Kissinger, H. E. Homer Kissinger and the Kissinger Equation. *Thermochim. Acta* **2012**, *540*, 1−6.
(578) Marques, L. E.; Costa, A. M. C.; Crovace, M. C.; Rodrigues, A. C. M.; Cabral, A. A. Influence of Particle Size on Nonisothermal Crystallization in a Lithium Disilicate Glass. *J. Am. Ceram. Soc.* **2015**, *98*, 774−780.

DOI: 10.1021/acs.chemrev.8b00510
Chem. Rev. XXXX, XXX, XXX−XXX

(579) Ozawa, T. Kinetics of Non-Isothermal Crystallization. *Polymer* **1971**, *12*, 150−158.
(580) Augis, J. A.; Bennett, J. E. Calculation of the Avrami Parameters for Heterogeneous Solid-State Reactions Using a Modification of the Kissinger Method. *J. Therm. Anal. Calorim.* **1978**, *13*, 283−292.
(581) Piloyan, G. O.; Ryabchikov, I. D.; Novikova, O. S. Determination of Activation Energies of Chemical Reactions by Differential Thermal Analysis. *Nature* **1966**, *212*, 1229.
(582) Borchardt, H. J. Initial Reaction Rates from DTA. *J. Inorg. Nucl. Chem.* **1960**, *12*, 252−254.
(583) Coats, A. W.; Redfern, J. P. Kinetic Parameters from Thermogravimetric Data. *Nature* **1964**, *201*, 68−69.
(584) Šesták, J. Applicability of DTA to the Study of Crystallisation Kinetics of Glasses. *Phys. Chem. Glasses* **1974**, *15*, 137−140.
(585) Šesták, J. On the Applicability of the P(X)-Function to the Determination of Reaction Kinetics under Non-Isothermal Conditions. *Thermochim. Acta* **1971**, *3*, 150−154.
(586) Ligero, R. A.; Vazques, J.; Villares, P.; Jimenez-Garay, R. A Study of the Crystallization Kinetics of Some Cu−As−Te Glasses. *J. Mater. Sci.* **1991**, *26*, 211−215.
(587) Vyazovkin, S.; Burnham, A. K.; Criado, J. M.; Pérez-Maqueda, L. A.; Popescu, C.; Sbirrazzuoli, N. ICTAC Kinetics Committee Recommendations for Performing Kinetic Computations on Thermal Analysis Data. *Thermochim. Acta* **2011**, *520*, 1−19.
(588) Vyazovkin, S.; Chrissafis, K.; Di Lorenzo, M. L.; Koga, N.; Pijolat, M.; Roduit, B.; Sbirrazzuoli, N.; Suñol, J. J. ICTAC Kinetics Committee Recommendations for Collecting Experimental Thermal Analysis Data for Kinetic Computations. *Thermochim. Acta* **2014**, *590*, 1−23.
(589) Henderson, D. W. Thermal Analysis of Non-Isothermal Crystallization Kinetics in Glass Forming Liquids. *J. Non-Cryst. Solids* **1979**, *30*, 301−315.
(590) Henderson, D. W. Experimental Analysis of Non-Isothermal Transformations Involving Nucleation and Growth. *J. Therm. Anal.* **1979**, *15*, 325−331.
(591) Matusita, K.; Sakka, S. Kinetic Study of The Crystallisation of Glass By Differential Scanning Calorimetry. *Phys. Chem. Glasses* **1979**, *20*, 81−84.
(592) Yinnon, H.; Uhlmann, D. R. Applications of Thermoanalytical Techniques to the Study of Crystallization Kinetics in Glass-Forming Liquids, Part I: Theory. *J. Non-Cryst. Solids* **1983**, *54*, 253−275.
(593) Málek, J. The Applicability of Johnson-Mehl-Avrami Model in the Thermal Analysis of the Crystallization Kinetics of Glasses. *Thermochim. Acta* **1995**, *267* (C), 61−73.
(594) Šesták, J. The Quandary Aspects of Non-Isothermal Kinetics Beyond the ICTAC Kinetics Committee Recommendations. *Thermochim. Acta* **2015**, *611*, 26−35.
(595) Koga, N.; Šesták, J.; Strnad, Z. Kinetics of Crystallization in the Soda-Lime-Silica System? Part 1. $Na_2O.CaO.2SiO_2$ and $Na_2O.CaO.3SiO_2$ Glasses. *Thermochim. Acta* **1992**, *203*, 361−372.
(596) Koga, N.; Šesták, J. Influence of Preliminary Nucleation on the Physicogeometric Kinetics of Glass Crystallization. In *Thermal Analysis of Micro, Nano- and Non-Crystalline Materials: Transformation, Crystallization, Kinetics and Thermodynamic*; Šesták, J., Šimon, P., Eds.; Springer: Netherlands, 2013; Chapter 10.
(597) Ozawa, T. Kinetics of Growth from Pre-Existing Surface Nuclei. *J. Therm. Anal. Calorim.* **2005**, *82*, 687−690.
(598) Everton, L. S.; Cabral, A. A. Determining the Kinetic Parameters for Isothermal Crystallization in a Lithium Disilicate (LS2) Glass by OM And DSC. *J. Am. Ceram. Soc.* **2014**, *97*, 157−162.
(599) Elder, J. P. The General Application of the Kissinger Equation in Thermal Analysis. *J. Therm. Anal.* **1985**, *30*, 657−669.
(600) Boswell, P. G. On the Calculation of Activation Energies Using a Modified Kissinger Method. *J. Therm. Anal.* **1980**, *18*, 353−358.
(601) Matusita, K.; Sakka, S. Kinetic Study on Crystallization of Glass by Differential Thermal Analysis: Criterion on Application of Kissinger Plot. *J. Non-Cryst. Solids* **1980**, *38*−*39*, 741−746.
(602) Matusita, K.; Komatsu, T.; Yokota, R. Kinetics of Non-Isothermal Crystallization Process and Activation Energy for Crystal Growth in Amorphous Materials. *J. Mater. Sci.* **1984**, *19*, 291−296.
(603) Ozawa, T. Nonisothermal Kinetics of Crystal Growth from Pre-existing Nuclei. *Bull. Chem. Soc. Jpn.* **1984**, *57*, 639−643.
(604) Kemeny, T.; Šesták, J. Comparison of Crystallization Kinetics Determined by Isothermal and Nonisothermal Methods. *Thermochim. Acta* **1987**, *110*, 113−129.
(605) Koga, N.; Šesták, J. Kinetic Modeling of Advanced Inorganic Glass-Ceramics Formation by Crystal Growth from Pre-Existing Nuclei. *J. Therm. Anal. Calorim.* **2000**, *60*, 667−674.
(606) Koga, N.; Šesták, J. Crystal Nucleation and Growth in Lithium Diborate Glass by Thermal Analysis. *J. Am. Ceram. Soc.* **2000**, *83*, 1753−1760.
(607) Koga, N.; Yamaguchi, K.; Šesták, J. Crystallization Kinetics of Lithium Diborate Glass by DTA. *J. Therm. Anal. Calorim.* **1999**, *56*, 755−761.
(608) Šimon, P.; Thomas, P. S. Application of Isoconversional Methods for the Processes Occurring in Glassy and Amorphous Materials. In *Thermal Analysis of Micro, Nano- and Non-Crystalline Materials: Transformation, Crystallization, Kinetics and Thermodynamics*; Šesták, J., Šimon, P., Eds.; Springer: Netherlands, 2013; Chapter 11.
(609) Vyazovkin, S. Is The Kissinger Equation Applicable to the Processes that Occur on Cooling? *Macromol. Rapid Commun.* **2002**, *23*, 771−775.
(610) Koga, N. Ozawa's Kinetic Method for Analyzing Thermoanalytical Curves: History and Theoretical Fundamentals. *J. Therm. Anal. Calorim.* **2013**, *113*, 1527−1541.
(611) Müller, R. The Influence of Grain Size on the Overall Kinetics of Surface-Induced Glass Crystallization. *J. Therm. Anal.* **1989**, *35*, 823−835.
(612) Sandu, C.; Singh, R. K. Modeling Differential Scanning Calorimetry. *Thermochim. Acta* **1990**, *159*, 267−298.
(613) Reis, R. M. C. V.; Zanotto, E. D. Simple Model for Particle Phase Transformation Kinetics. *Acta Mater.* **2018**, *154*, 228−236.
(614) Fernandes, R. G.; Ferreira, E. B. The Shape of Diopside Glass Particles Probed by the Non-Isothermal Crystallization Kinetics and Differential Scanning Calorimetry. *J. Non-Cryst. Solids* **2018**, *497*, 63−70.
(615) Scherer, G. W. Glass and Amorphous Materials. In *Mater. Sci. Technol.* Cahn, R. W., Haasen, P., Kramer, E. J., Eds.; VCH Publications: New York, 1991; Vol. *9*, Chapter 3.
(616) Uhlmann, D. R.; Yinnon, H. Glass Science and Technology. In *Glass Forming Systems*; Uhlmann, D. R., Kreidl, N. J., Eds., Academic: New York, 1983; Vol. *1*, Chapter 1.
(617) Ray, C. S.; Reis, S. T.; Brow, R. K.; Höland, W.; Rheinberger, V. A New DTA Method for Measuring Critical Cooling Rate for Glass Formation. *J. Non-Cryst. Solids* **2005**, *351*, 1350−1358.
(618) Weinberg, M. C.; Uhlmann, D. R.; Zanotto, E. D. "Nose Method" of Calculating Critical Cooling Rates for Glass Formation. *J. Am. Ceram. Soc.* **1989**, *72*, 2054−2058.
(619) Weinberg, M. C.; Zelinski, B. J.; Uhlmann, D. R.; Zanotto, E. D. Critical Cooling Rate Calculations for Glass Formation. *J. Non-Cryst. Solids* **1990**, *123*, 90−96.
(620) Barandiarán, J. M.; Colmenero, J. Continuous Cooling Approximation for the Formation of a Glass. *J. Non-Cryst. Solids* **1981**, *46*, 277−287.
(621) Whichard, G.; Day, D. E. Glass Formation and Properties in the Gallia-Calcia System. *J. Non-Cryst. Solids* **1984**, *66*, 477−487.
(622) Huang, W.; Ray, C. S.; Day, D. E. Dependence of the Critical Cooling Rate for Lithium-Silicate Glass on Nucleating Agents. *J. Non-Cryst. Solids* **1986**, *86*, 204−212.
(623) Havermans, A. C. J.; Stein, H. N.; Stevels, J. M. Critical Cooling Rates in Alkali Silicate Systems. *J. Non-Cryst. Solids* **1970**, *5*, 66−69.
(624) Cormier, L. Nucleation in Glasses − New Experimental Findings and Recent Theories. *Procedia Mater. Sci.* **2014**, *7*, 60−71.

DOI: 10.1021/acs.chemrev.8b00510
Chem. Rev. XXXX, XXX, XXX−XXX

(625) Mastelaro, V. R.; Zanotto, E. D. X-ray Absorption Fine Structure (XAFS) Studies of Oxide Glasses - A 45-year Overview. *Materials* **2018**, *11*, 204.
(626) Sosso, G. C.; Chen, J.; Cox, S. J.; Fitzner, M.; Pedevilla, P.; Zen, A.; Michaelides, A. Crystal Nucleation in Liquids: Open Questions and Future Challenges in Molecular Dynamics Simulations. *Chem. Rev.* **2016**, *116*, 7078−7116.
(627) Bras, W.; Clark, S. M.; Greaves, G. N.; Kunz, M.; Van Beek, W.; Radmilovic, V. Nanocrystal Growth in Cordierite Glass Ceramics Studied with X-ray Scattering. *Cryst. Growth Des.* **2009**, *9*, 1297−1305.
(628) Kleebusch, E.; Patzig, C.; Höche, T.; Rüssel, C. Effect of the Concentrations of Nucleating Agents ZrO_2 and TiO_2 on the Crystallization of $Li_2O-Al_2O_3-SiO_2$ Glass: an X-ray Diffraction and TEM Investigation. *J. Mater. Sci.* **2016**, *51*, 10127−10138.
(629) Hoell, A.; Varga, Z.; Raghuwanshi, V. S.; Krumrey, M.; Bocker, C.; Rüssel, C. ASAXS Study of CaF_2 Nanoparticles Embedded in a Silicate Glass Matrix. *J. Appl. Crystallogr.* **2014**, *47*, 60−66.
(630) Fernandez-Martin, C.; Bruno, G.; Crochet, A.; Ovono Ovono, D.; Comte, M.; Hennet, L. Nucleation and Growth of Nanocrystals in Glass-ceramics: An In Situ SANS Perspective. *J. Am. Ceram. Soc.* **2012**, *95*, 1304−1312.
(631) Cebe, P. Recent Developments in Thermal Analysis of Polymers: Calorimetry in the Limit of Slow and Fast Heating Rates. *J. Polym. Sci., Part B: Polym. Phys.* **2005**, *43*, 629−636.
(632) Drzeżdżon, J.; Jacewicz, D.; Sielicka, A.; Chmurzyński, L. Characterization of Polymers Based on Differential Scanning Calorimetry Based Techniques. *TrAC, Trends Anal. Chem.* **2019**, *110*, 51−56.
(633) Treviño-Quintanilla, C. D.; Krishnamoorti, R.; Bonilla-Ríos, J. Flash DSC Crystallization Study of Blown Film Grade Bimodal High Density Polyethylene (HDPE) Resins. Part 2. Non-isothermal kinetics. *J. Polym. Sci., Part B: Polym. Phys.* **2017**, *55*, 1822−1827.
(634) Li, Z.; Ye, X.; Wang, D.; Zeng, Y.; Zhou, H.; Guo, W. Novel Experimental Protocol Used To Determine The Nucleation Kinetics of Polymer Realized By Flash DSC: The Case of poly (l-lactic acid)/poly (d-lactic acid) blends. *Polym. Test.* **2018**, *66*, 251−255.
(635) Zhuravlev, E.; Schmelzer, J. W. P.; Wunderlich, B.; Schick, C. Kinetics of Nucleation and Crystallization in Poly(ε-caprolactone) (PCL). *Polymer* **2011**, *52*, 1983−1997.
(636) Supaphol, P.; Spruiell, J. E. Isothermal Melt- and Cold Crystallization Kinetics and Subsequent Melting Behavior in Syndiotactic Polypropylene: A Differential Scanning Calorimetry Study. *Polymer* **2001**, *42*, 699−712.
(637) Long, Y.; Shanks, R. A.; Stachurski, Z. H. Kinetics of Polymer Crystallization. *Prog. Polym. Sci.* **1995**, *20*, 651−701.
(638) Toda, A.; Androsch, R.; Schick, C. Insights into Polymer Crystallization and Melting From Fast Scanning Chip Calorimetry. *Polymer* **2016**, *91*, 239−263.
(639) Li, Z.; Zhou, D.; Hu, W. Recent Progress on Flash DSC Study of Polymer Crystallization and Melting. *Acta Polym. Sin.* **2016**, 1179−1197.
(640) Wang, J.; Li, Z.; Perez, R. A.; Mueller, A. J.; Zhang, B.; Grayson, S. M.; Hu, W. Comparing Crystallization Rates Between Linear and Cyclic Poly(Epsilon-Caprolactones) via Fast-Scan Chip-Calorimeter Measurements. *Polymer* **2015**, *63*, 34−40.
(641) Liu, S. J.; Tao, H. Z.; Zhang, Y. F.; Yue, Y. Z. A New Approach for Determining the Critical Cooling Rates of Nucleation in Glass-Forming Liquids. *J. Am. Ceram. Soc.* **2017**, *100*, 3875−3882.
(642) Turnbull, D. Formation of crystal nuclei in liquid metals. *J. Appl. Phys.* **1950**, *21*, 1022.
(643) Thompson, C. V.; Spaepen, F. On the approximation of the free energy change on crystallization. *Acta Metall.* **1979**, *27*, 1855−59.
(644) Kozmidis-Petrovic, A.; Šesták, J. Forty Years of the Hrubý Glass-Forming Coefficient via DTA when Comparing Other Criteria in Relation to the Glass Stability and Vitrification Ability. *J. Therm. Anal. Calorim.* **2012**, *110*, 997−1004.
(645) Hrubý, A. Evaluation of glass-forming tendency by means of DTA. *Czech. J. Phys.* **1972**, *22*, 1187−1193.
(646) Saad, M.; Poulain, M. Glass Forming Ability Criterion. *Mater. Sci. Forum* **1987**, *19*−*20*, 11−18.
(647) Weinberg, M. C. Assessment of Glass Stability Criteria. *Phys. Chem. Glasses* **1994**, *35*, 119−123.
(648) Lu, Z. P.; Liu, C. T. A New Glass-Forming Ability Criterion for Bulk Metallic Glasses. *Acta Mater.* **2002**, *50*, 3501−3512.
(649) Lu, Z. P.; Liu, C. T. Glass Formation Criterion for Various Glass-Forming Systems. *Phys. Rev. Lett.* **2003**, *91*, 1155051−1155054.
(650) Zhang, P.; Wei, H.; Wei, X.; Long, Z.; Su, X. Evaluation of Glass-Forming Ability for Bulk Metallic Glasses Based on Characteristic Temperatures. *J. Non-Cryst. Solids* **2009**, *355*, 2183−2189.
(651) Du, X. H.; Huang, J. C.; Liu, C. T.; Lu, Z. P. New Criterion of Glass Forming Ability for Bulk Metallic Glasses. *J. Appl. Phys.* **2007**, *101*, 086108.
(652) Fan, G. J.; Choo, H.; Liaw, P. K. A New Criterion for the Glass-forming Ability of Liquids. *J. Non-Cryst. Solids* **2007**, *353*, 102−107.
(653) Long, Z.; Xie, G.; Wei, H.; Su, X.; Peng, J.; Zhang, P.; Inoue, A. On the New Criterion to Assess the Glass-forming Ability of Metallic Alloys. *Mater. Sci. Eng., A* **2009**, *509*, 23−30.
(654) Yuan, Z. Z.; Bao, S. L.; Lu, Y.; Zhang, D. P.; Yao, L. A New Criterion for Evaluating the Glass-Forming Ability of Bulk Glass Forming Alloys. *J. Alloys Compd.* **2008**, *459*, 251−260.
(655) Weinberg, M. C. Glass-forming Ability and Glass Stability in Simple Systems. *J. Non-Cryst. Solids* **1994**, *167*, 81−88.
(656) Cabral, A. A.; Fredericci, C.; Zanotto, E. D. A Test of the Hrubý Parameter to Estimate Glass-Forming Ability. *J. Non-Cryst. Solids* **1997**, *219*, 182−186.
(657) Avramov, I.; Zanotto, E. D.; Prado, M. O. Glass-forming Ability versus Stability of Silicate Glasses. II. Theoretical Demonstration. *J. Non-Cryst. Solids* **2003**, *320*, 9−20.
(658) Cabral, A. A.; Cardoso, A. A. D.; Zanotto, E. D. Glass-forming Ability versus Stability of Silicate Glasses. I. Experimental Test. *J. Non-Cryst. Solids* **2003**, *320*, 1−8.
(659) Nascimento, M. L. F.; Souza, L. A.; Ferreira, E. B.; Zanotto, E. D. Can Glass Stability Parameters Infer Glass Forming Ability? *J. Non-Cryst. Solids* **2005**, *351*, 3296−3308.
(660) Ranasinghe, K. S.; Ray, C. S.; Day, D. E.; Rogers, J. R.; Hyers, R. W.; Rathz, T. Containerless Processing of a Lithium Disilicate Glass. *J. Mater. Sci.* **2007**, *42*, 4291−4297.
(661) Ferreira, E. B.; Zanotto, E. D.; Feller, S.; Lodden, G.; Banerjee, J.; Edwards, T.; Affatigato, M. Critical Analysis of Glass Stability Parameters and Application to Lithium Borate Glasses. *J. Am. Ceram. Soc.* **2011**, *94*, 3833−3841.
(662) Marques, T. V. R.; Cabral, A. A. Influence of the Heating Rates on the Correlation between Glass-Forming Ability (GFA) and Glass Stability (GS) Parameters. *J. Non-Cryst. Solids* **2014**, *390*, 70−76.
(663) Qiao, A.; Bennett, T. D.; Tao, H. Z.; Krajnc, A.; Mali, G.; Doherty, C. M.; Thornton, A. W.; Mauro, J. C.; Greaves, G. N.; Yue, Y. Z. A Metal-organic Framework with Ultrahigh Glass-forming Ability. *Sci. Adv.* **2018**, *4*, No. eaao6827.
(664) Zanotto, E. D.; Cassar, D. R. The Microscopic Origin of the Extreme Glass-forming Ability of Albite and B_2O_3. *Sci. Rep.* **2017**, *7*, 43022.
(665) *ASTM Standard Practices for Measurement of Liquidus Temperature of Glass by Gradient Furnace Method, Annual Book of ASTM Standards, C829-81*; American Society for Testing and Materials: Gaithersburg, MD, 1990.
(666) Beerkens, R. G. C.; Conradt, R. Round Robin Test on *Liquidus* Temperature of Soda-Lime-Magnesia-Silica Float Glass Samples: A Technical Report of the ICG Technical Committee (TC 18) on Properties of Glass Forming Melts. *Glass Technol.: Eur. J. Glass Sci. Technol., Part A* **2008**, *49*, 205−212.
(667) Rao, Q.; Piepel, G. F.; Hrma, P.; Crum, J. V. *Liquidus* Temperatures of HLW Glasses with Zirconium-Containing Primary Crystalline Phases. *J. Non-Cryst. Solids* **1997**, *220*, 17−29.

DOI: 10.1021/acs.chemrev.8b00510
Chem. Rev. XXXX, XXX, XXX−XXX

(668) Dreyfus, C.; Dreyfus, G. A Machine Learning Approach to the Estimation of the *Liquidus* Temperature of Glass-Forming Oxide Blends. *J. Non-Cryst. Solids* **2003**, *318*, 63−78.
(669) Wondraczek, L.; Beunet, L. *Liquidus* Prediction in Multi-component Lithium Alumosilicate Glasses. *J. Am. Ceram. Soc.* **2008**, *91*, 1309−1311.
(670) Verdonck, E.; Schaap, K.; Thomas, L. C. A Discussion of the Principles and Applications of Modulated Temperature DSC (MTDSC). *Int. J. Pharm.* **1999**, *192*, 3−20.
(671) Garidel, P.; Johann, C.; Blume, A. The Calculation of Heat Capacity Curves and Phase Diagrams Based on Regular Solution Theory. *J. Therm. Anal. Calorim.* **2005**, *82*, 447−455.
(672) Pedersen, A. S.; Pryds, N.; Linderoth, S.; Larsen, P. H.; Kjoller, J. The Determination of Dynamic and Equilibrium Solid/Liquid Transformation Data for Sn-Pb Using DSC. *J. Therm. Anal. Calorim.* **2001**, *64*, 887−894.
(673) Young, P. H.; Dollimore, D.; Schall, C. A. Thermal Analysis of Solid-Solid Interactions in Binary Mixtures of Alkylcyclohexanes using DSC. *J. Therm. Anal. Calorim.* **2000**, *62*, 163−175.
(674) Charsley, E. L.; Laye, P. G.; Palakollu, V.; Rooney, J. J.; Joseph, B. DSC Studies on Organic Melting Point Temperature Standards. *Thermochim. Acta* **2006**, *446*, 29−32.
(675) Höhne, G. W. H.; Hemminger, W.; Flammersheim, H. J. *Differential Scanning Calorimetry - An Introduction for Practitioners*; Springer Verlag: Berlin, 1996.
(676) Ferreira, E. B.; Lima, M. L.; Zanotto, E. D. DSC Method for Determining the *Liquidus* Temperature of Glass-forming Systems. *J. Am. Ceram. Soc.* **2010**, *93*, 3757−3763.
(677) Wakasugi, T.; Ota, R.; Fukunaga, J. Glass-forming Ability and Crystallization Tendency Evaluated by the DTA Method in the $Na_2O-B_2O_3-Al_2O_3$ System. *J. Am. Ceram. Soc.* **1992**, *75*, 3129−3132.
(678) Veit, U.; Houet, Y.; Laurent, D.; Rüssel, C. *Liquidus* Temperatures of Calcium Magnesium Alumosilicate Glass-forming Compositions Determined via Gradient Furnace and from the Melting Peak by Differential Thermal Analysis. *Thermochim. Acta* **2015**, *618*, 1−5.
(679) Deubener, J.; Allix, M.; Davis, M. J.; Duran, A.; Höche, T.; Honma, T.; Komatsu, T.; Krüger, S.; Mitra, I.; Müller, R.; et al. Updated Definition of Glass-ceramics. *J. Non-Cryst. Solids* **2018**, *501*, 3
(680) Marghussian, V. *Nano-Glass Ceramics: Processing, Properties and Applications*; Elsevier: Netherland, 2015.
(681) Mauro, J. C.; Ellison, A. J.; Pye, L. D. Glass: The Nanotechnology Connection. *Int. J. Appl. Glass Sci.* **2013**, *4*, 64−75.
(682) Zanotto, E. D. *Crystals in Glass: A Hidden Beauty*; John Wiley and Sons, Inc. and the American Ceramic Society: NJ, 2013.

DOI: 10.1021/acs.chemrev.8b00510
Chem. Rev. XXXX, XXX, XXX−XXX